

ASPECTS OF ARRAYS OF PARABOLOIDAL COLLECTORS
FOR UTILISATION OF SOLAR ENERGY

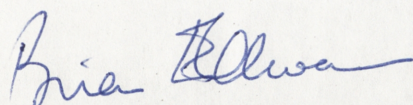
Brian Peter Edwards

March 1979.

being a thesis submitted for the
degree of Doctor of Philosophy at the
Australian National University.

Dept of Engineering Physics,
Research School of Physical Sciences,
THE AUSTRALIAN NATIONAL UNIVERSITY,
CANBERRA, A.C.T.

This thesis is entirely my own work,
except where indicated.


A handwritten signature in blue ink that reads "Brian Edwards". The signature is written in a cursive style with a long horizontal flourish at the end.

Brian Edwards.

Acknowledgements

I am indebted to my supervisor, Dr P O Carden, without whom this project would never have begun, and to Prof S Kaneff, who with Dr Carden provided excellent facilities for research and wasted no time in getting the project started. My appreciation goes to Dr Owen Williams for constructive suggestions, to Bob Whelan, Kazys, Keith, Lincoln and most importantly to Jens and Sue for the environment.

I especially acknowledge the contribution of my parents.

A handwritten signature in cursive script that reads "Brian Edwards". The signature is written in dark ink and is positioned in the lower middle section of the page.

Brian Edwards, March 1979.

ABSTRACT

Aspects of the collection of energy from solar radiation on a MW scale by arrays of paraboloidal collectors are considered in this thesis. Particular emphasis is placed on minimising the cost of the energy collected. The type of solar plant analysed has three main components: the paraboloidal collectors, each of which concentrate energy onto a small absorber at their respective foci; the central station, to which the collected energy is transferred; and a linking system which connects the collectors to the central station and transfers energy and control information. In the thesis three subsystems within the above scheme for energy collection are analysed. These subsystems are specific to the collectors themselves and to the linking system.

In the first analysis the spacing of the array of collectors is determined as a compromise between the cost of the linking system and the amount of energy collected, both of which increase with increasing separation. This procedure involves the calculation of the linking system costs and the calculation of the variation in the amount of energy collected due to one collector shading another. An easily implemented scheme for determining the cost effective spacing is provided. Analysis shows that a rectangular layout with relatively large East-West distances and links running over only short North-South distances will produce low costs.

The subject of the second analysis is the calculation of the efficiency of a cavity energy absorber at the focus of each paraboloid. The maximum possible efficiency is evaluated

as a function of three variables: the cavity absorber design, the tolerance in the contour accuracy of the reflecting paraboloid and the accuracy of the alignment of the paraboloid with the sun. Within this calculation it is necessary to evaluate the fraction of energy directed towards the absorber which actually enters the cavity aperture. A graph is presented so that this fraction can be easily calculated as a function of the tolerance in the contour accuracy of the paraboloid, the misalignment of the paraboloid, and the cavity aperture radius.

The aim of the third analysis is to investigate the variation of collector costs with the allowance for misalignment of the paraboloid and the sun, or sun following error. This analysis considers the relationships within the power plant which depend upon the sun following error. In analysing these relationships we consider the choice of the guidance and control scheme, the type of alignment method to be used, the collector rigidity and information transfer over the linking system. The properties of a cost effective guidance and control scheme are derived. Two specific contributions of this chapter are an analysis of the effect that wind induced deflections have on the design rigidity of the collector and the analysis of a computational alignment method which has the potential for lower costs than conventional methods.

Finally a hardware allotment for the controller at each collector is derived as a result of reliability considerations and the design and programming for a tracking servo to be

implemented in the controller is completed. The form of the communication link between the collectors and the central control is examined and it is shown that a fibre-optic communication network has the potential for lowest costs, principally due to its immunity to interference and induced damage from lightning.

CONTENTSPage No

1.0	PREFACE.	1
1.1	Publications.	3
1.2	Dept Of Engineering Physics Publications.	4
2.0	INTRODUCTION.	5
2.1	Research Into Solar Energy Utilisation.	5
2.2	The ANU Solar Ammonia Project.	7
2.3	Properties Of Collection Sites For Solar Energy.	9
2.4	Systems Under Study.	11
2.5	Solar Power Plant Design.	12
2.6	Study Objectives.	16
2.7	Method And Contents.	17
2.8	Study Conclusions.	19
3.0	SHADING AND SPACING IN PARABOLOIDAL ARRAYS.	21
3.1	Introduction.	21
3.2	System Under Study.	23
3.3	Cost Optimisation.	24
3.4	Shading Calculations.	26
3.4.1	General.	27
3.4.2	Direct Radiation Model.	31
3.4.3	Cloud Effects.	33
3.4.4	Procedure.	33
3.4.5	Results.	34

3.5	Costs Relevant To Determining Optimum Spacing.	38
3.5.1	Cost Of Energy Transfer.	38
3.5.2	Cost Of The Communication And Power Links.	42
3.5.3	Cost Of Energy Collectors.	42
3.5.4	Cost Of Land.	43
3.5.5	Total Costs.	43
3.6	Tradeoff Between Shading And Spacing.	44
3.6.1	Minimising Pipe Costs.	44
3.6.2	Procedure.	46
3.6.3	Situation Studied.	47
3.6.4	Results.	48
3.6.5	A Simpler Minimisation Process.	52
3.7	Rectangular Arrays.	55
3.7.1	Implications Of Square Array Analysis.	55
3.7.2	Analysis Of Rectangular Arrays.	57
3.7.3	North-South Spacing.	59
3.7.4	Electricity Costs For A Rectangular Array.	59
3.7.5	Further Calculations On Isolated N-S Rows.	64
3.8	Discussion And Conclusion.	65
4.0	CAVITY ABSORBER EFFICIENCY.	69
4.1	Introduction.	69
4.2	General.	70
4.3	Absorber Efficiency.	72
4.4	Radiation Field In The Absence Of Following Errors.	76

4.5	Influence Of Sun Following Errors On The Radiation Field.	81
4.6	Procedure.	82
4.7	Results.	83
4.7.1	Capture Ratio	83
4.7.2	Maximum Possible Cavity Efficiency.	85
4.8	Discussion Of Results.	89
4.8.1	Use Of Data.	90
4.8.2	Generality Of Assumptions.	90
5.0	GUIDANCE AND CONTROL SCHEME SELECTION.	93
5.1	Definitions.	93
5.2	Introduction.	95
5.3	Guidance And Control Scheme Properties.	97
5.3.1	Tracking Systems.	98
5.3.1.1	Tracking System Deficiencies.	101
5.3.2	Pointing Systems.	103
5.4	Sun Following Error Sources.	107
5.4.1	Speed Requirements.	107
5.4.2	Alignment.	110
5.4.2.1	Methods (a) And (b).	114
5.4.2.2	Method (c), Inferring Calibration Constants.	115
5.4.2.3	Comparison.	129
5.4.3	Disturbance Torques: Wind.	131
5.4.3.1	Wind Deflection Characteristics.	131
5.4.4	Disturbance Torques: Other Than Those Due to Winds.	145
5.4.5	Encoder Errors.	145
5.4.6	Mechanical Errors.	146

5.4.7	ACTUATOR DISPLACEMENT CALCULATIONS.	146
5.4.7.1	General Remarks.	147
5.4.7.2	Errors In Interpolation	148
5.4.7.3	Actuator Displacement Calculations	152
5.4.7.4	Approximating Functions.	154
5.4.7.5	Error Propagation And Accuracy.	156
5.4.7.5.1	Floating Point Calculations.	158
5.4.7.5.2	Fixed Point Actuator Displacement Calculations.	159
5.4.7.6	Results.	166
5.4.7.7	Time Required For Calculation.	166
5.4.7.8	Program Storage Requirements.	168
5.4.7.9	Data Rates Over The Communication Link.	171
5.4.8	Servo Lags.	174
5.4.9	Response Time.	176
5.4.10	Combination Of Error Sources.	178
5.5	Summary And Implications For Guidance and Control Scheme.	179
5.5.1	Location Of Guidance And Control Scheme Functions.	182
5.5.2	Assumptions Made In The Above Analysis.	187
5.5.3	Comparison With Central Receiver System: Some Comments.	188
5.6	Variation Of Costs With Error Specification.	188
5.6.1	Cost As A Function Of Collector Rigidity Specification.	189
5.6.2	Servo Errors.	192
5.6.3	Actuator Displacement Calculations.	193
5.6.4	Alignment.	194
5.7	Summary And Conclusion.	196
5.8	Recommendations For Further Work.	200

6.0	DESIGN AND IMPLEMENTATION OF LOCAL CONTROL.	201
6.1	Introduction.	201
6.2	Local Control Reliability And Maintenance.	201
6.2.1	Reliability And Costs.	201
6.2.2	Configuration Of Local Control.	204
6.2.3	Cost Of Repairs.	206
6.3	Tracking Servo Design.	209
6.3.1	Servo Design: General Remarks.	210
6.3.2	System Under Study.	211
6.3.3	Sampling: Qualitative Remarks.	213
6.3.4	Quantisation: Qualitative Remarks.	215
6.3.5	Saturation: Qualitative Remarks.	216
6.3.6	Servo Stability.	217
6.3.6.1	Proportional Control Only.	217
6.3.6.2	Integral And Proportional Control.	217
6.3.7	Calculations Required to Operate Servo.	222
6.3.8	Stability For Other Vibration Modes.	224
6.4	Communication Systems.	224
6.4.1	Information To Be Transferred.	226
6.4.2	Radio Communication.	226
6.4.2.1	Link Path Characteristics.	227
6.4.2.2	Error Performance.	228
6.4.3	Cable Systems.	229
6.4.4	Comparison Of The Two Communication Systems.	230
6.5	Summary.	231
6.5.1	Reliability And Maintenance.	231
6.5.2	Tracking Servo.	231

6.5.3	Communication Systems.	232
7.0	SUMMARY AND CONCLUSIONS	233
	- RECOMMENDATIONS FOR FURTHER WORK.	
7.1	Summary And Conclusions.	233
7.1.1	Shading And Spacing In Paraboloidal Collector Arrays.	233
7.1.2	Cavity Absorbers.	234
7.1.3	Guidance And Control.	235
7.1.3.1	Alignment Costs.	235
7.1.3.2	Effect Of Wind On Tracking Performance Of Collectors.	235
7.1.3.3	Tracking vs Pointing Schemes.	236
7.1.3.4	Calculations Of Actuator Displacements.	236
7.1.3.5	Cost Variation With Sun Following Error Budget.	237
7.1.4	Design And Implementation Of The Local Control.	237
7.2	Recommendations For Further Work.	238
7.2.1	Shading And Spacing.	238
7.2.2	Cavity Absorber.	238
7.2.3	Guidance And Control.	239
8.0	SYMBOLS.	240
9.0	REFERENCES.	249

APPENDICES

- A Program for calculating shading.
- B Analysis of Campbell Stokes Sunshine records for Griffith (N.S.W.), 1975.
- C Shading and Spacing in paraboloidal collector arrays.
-Solar Energy Vol 21, No 5, pp435-440.
- D Calibration constant determination.
- E Computer based sun following system.
-Solar Energy Vol 21, No 6, pp421-426.
- F Devices for feedback in Sun Tracking systems
(Dept of Engineering Physics Technical Publication,
En-Con TR-20.)
- G Aerodynamic Damping Coefficient of Collector.
- H A sun following scheme: Operation of the
Carden/McMurtrie/Whyte system.
(Dept of Engineering Physics Technical Publication,
En-Con TR-14)

1.0 PREFACE

The research reported here is part of a comprehensive study of the design of a solar power plant to generate electricity from solar radiation on a MW scale. At the initiation of the research in early 1975, the solar power plant studied at the A.N.U. involved an array of thousands of paraboloidal dishes, each concentrating sunlight onto its focus. In this plant the energy at each focus is transferred to a central generating facility by circulating ammonia which absorbs energy at each focus by dissociating: this energy is recovered at the central station during resynthesis of the ammonia. The project has been called the ANU solar ammonia system.

The writer claims originality in the work reported in the following respects:

1. The layout of the array of collectors and separations within the array have been determined for minimum energy cost as a function of collector costs and the costs of the links between the collectors and the central station. Most of this analysis has been published in (a) below.
2. The variation of the maximum possible efficiency of a cavity absorber is detailed as a function of the misalignment of the collector optical axis and the sun (or sun following error). Previously only reflector surface accuracy had been considered. Diagrams are presented which allow cavity absorber designers to include misalignment considerations

readily into their own calculations.

3. The reliability and maintenance costs of a microprocessor controller at each collector are detailed.

The consideration of the variation of collector costs with the specification for sun following error includes three significant original aspects (numbers 4,5,6 below):

4. The mathematical specification and performance details of a computational alignment method which is shown to involve lower costs than conventional manual alignment methods. This study is the topic of paper (b) below - the majority of the study has been published in (c) below.
5. An analysis of the effect that wind induced deflections have on the required rigidity of the collector. This analysis shows that the selection of guidance and control scheme bandwidth is important and that a bandwidth which accommodates the spectrum of the wind induced deflections allows a less rigid collector structure to be specified and thus allows cost savings. This study is the subject of paper (d).
6. The computer calculations necessary to direct a collector to any point in the sky are detailed with variations in accuracy and calculating machine type. The possibility of 8 bit microprocessor calculations is examined in detail. The errors involved in

calculating the positions at intervals and linearly interpolating between times are calculated. These last results have been published in (c).

1.1 Publications

(a) Edwards, B.P., 'Shading and spacing in paraboloidal collector arrays', Solar Energy Vol 21, No 5, pp435-439 (1978).

(b) Edwards, B.P., 'A computational alignment method for paraboloidal collectors'

Accepted for presentation at the 1979 International Solar Energy Society (ISES) Meeting, Atlanta, Georgia, May 1979.

(c) Edwards, B.P., 'Computer based sun following system', Solar Energy Vol 21, No 6, pp491-496 (1978).

(d) Edwards, B.P., 'Collector deflections due to wind gusts and control scheme design',

Accepted for presentation at the 1979 International Solar Energy Society (ISES) Meeting, Atlanta, Georgia, May 1979.

1.2 Dept Of Engineering Physics Publications

(e) Edwards, B.P., 'Heat exchangers', En-Con TR-10, May 1975, 19pp.

(f) Edwards, B.P., 'A suntracking scheme: Operation of the Carden/McMurtrie/Whyte system', En-Con TR-14, June 1977, 15pp.

(g) Edwards, B.P., 'Feedback devices for suntracking systems', En-Con TR-20, December 1978, 23pp.

2.0 INTRODUCTION

The collection of solar radiation offers one possibility for easing man's dependence on fossil fuels. A valuable approach to this collection is to use paraboloidal mirrors, each of which tracks the sun and concentrates direct radiation onto its focus. Within this scheme there are many problems to be considered and overcome before energy is available to a user in a suitable form and at the lowest possible cost.

Here we briefly review research into solar power plants and describe one solar power plant design, the ANU solar ammonia system. The work reported in this thesis is directly applicable to this system. The introduction concludes with a description of the objectives of the study and the study contents.

2.1 Research Into Solar Energy Utilisation: Background.

Research into solar energy utilisation is not a recent phenomenon, with an Austrian, C. Gunter, inventing a solar boiler using mirrors in 1845. Other notables in early research are J. Ericsson in 1876 and Frank Shuman who operated a plant with 50hp output in Cairo in 1913. Russian research in the 1950's and 1960's included designs of 1500kw plants similar to the current power tower concept.

Apart from the Russian effort, interest was in general sporadic until the 1974 fiscal year in the USA when comparatively large sums of money were invested in research. In this year both the Aerospace Corporation and Colorado State

University (with Westinghouse) performed analyses of the possibilities. These analyses recommended that the project closest to viability for electricity generation was the 'Central receiver' concept (Vant-Hull, 1976). In this concept, solar radiation is concentrated on a single absorber at the top of a tall tower by many plane mirrors arranged around the base of the tower. The advantages of the central receiver are most apparent for the American grid system where large electricity generating modules of 100MW size which possess little storage can be accommodated. The two initial studies also considered systems where concentration occurs at many points ('distributed systems') to be less attractive for the above application, principally due to the inefficiencies of transferring the energy from the many foci to a central location for electricity generation. For this reason less attention has been given to distributed systems.

Collection of energy from foci distributed over a large area (acres for each MW) has been made more attractive by recent research (Carden 1977) into thermochemical energy transfer. In this approach transfer of energy is accomplished at ambient temperature by the medium of the heat of a reversible reaction. Without this development, distributed systems tend to be limited in size and scope. Distributed systems which use thermochemicals for energy transfer can compete with the central receiver concept, particularly if advantage is taken of the possibility of long term (weeks) storage of energy which can be provided by the storage of the chemicals used. An added feature of the distributed system

with thermochemical transfer is that costs are not very sensitive to scale, and small (10MW) plants can produce electricity at moderate cost.

2.2 The ANU Solar Ammonia System.

This thesis forms part of a study of one possible solar based power generating system, the ANU Solar ammonia system (Carden, 1977). The essential features of this system are shown in figure 2.1. Paraboloidal collectors concentrate the direct beam solar radiation onto a small absorber in which dissociation of the ammonia takes place at near 700C. The resulting nitrogen/hydrogen mix heats the incoming ammonia in a counter flow heat exchanger, situated near the absorber. Thus both the ammonia and exiting gases are transferred at near ambient temperature. At the single central generating facility, the nitrogen/hydrogen mix is recombined to form ammonia, a process releasing heat, and the heat is used in a conventional steam generating facility for power production. Thus the energy is transferred from a number of collection sites in an array to a single generator by the transport of chemical energy, the so-called thermochemical energy transfer. System pressure is high around 300 atmospheres; this keeps pipe sizes and containers small and is compatible with the underground storage of the gases.

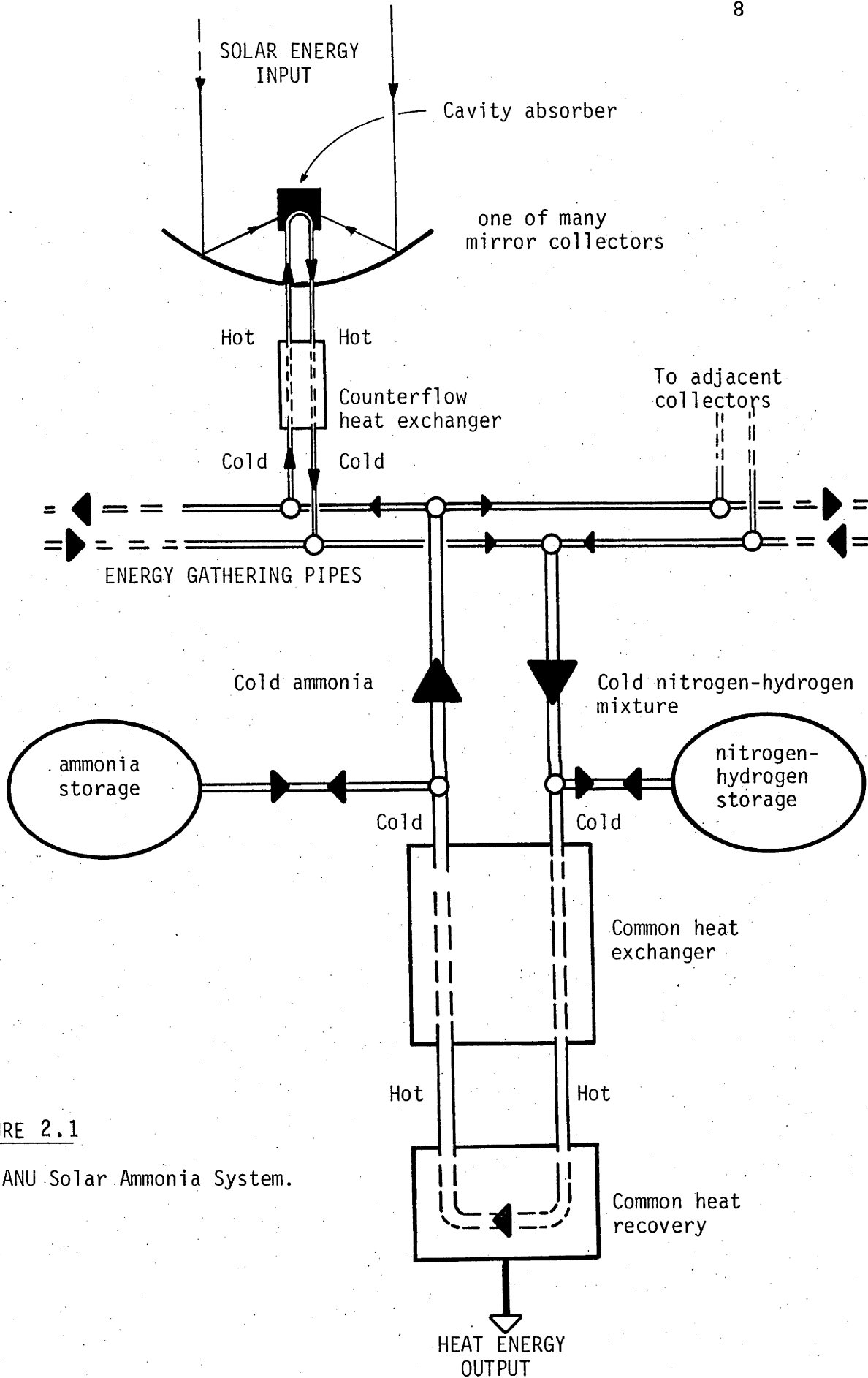


FIGURE 2.1

The ANU Solar Ammonia System.

2.3 Properties Of Collection Sites For Solar Energy.

This study is concerned with the collection of direct (or beam) radiation on a moderate scale of the order of megawatts. Such a scale corresponds to energy collection from an area of the order of tens of hectares. It is informative to consider the intensity of direct radiation which is principally a function of the elevation of the sun above the horizon. This intensity is given as a function of the time of day in figure 2.2. The total energy available over the year in the absence of clouds is only a weak function of latitude, and is typically 13GJm^{-2} . This figure is of course reduced by clouds, and the actual energy available in areas of Australia is given in figure 2.3. Clearly some areas are more suited to radiation collection than others and it is reasonable to site solar power plants in areas with good insolation characteristics. The existing electricity grids can be used for energy distribution if required. As can be seen from figure 2.3, the areas are likely to be arid, but in any case will certainly be rural.

The other important environmental property of collection sites is the wind. Wind can be responsible for damage to the structures which collect the energy (the collectors), whether by virtue of the sizes of forces produced by the winds, or due to abrasion caused by the particles transported in the wind. Further, the collectors can be deflected from their desired positions by wind forces. Collectors will need to be controlled to minimise problems caused by winds.

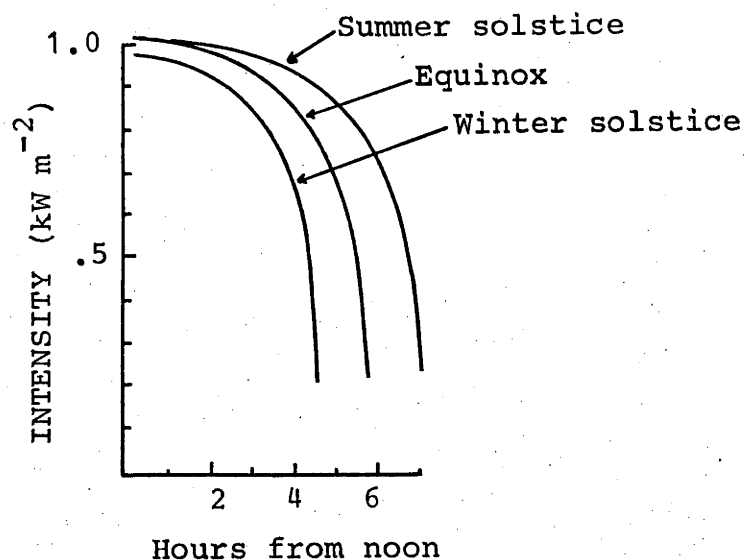


Figure 2.2 Intensity of direct radiation as a function of time of day, (Vant-Hull, 1976). Latitude 35N.

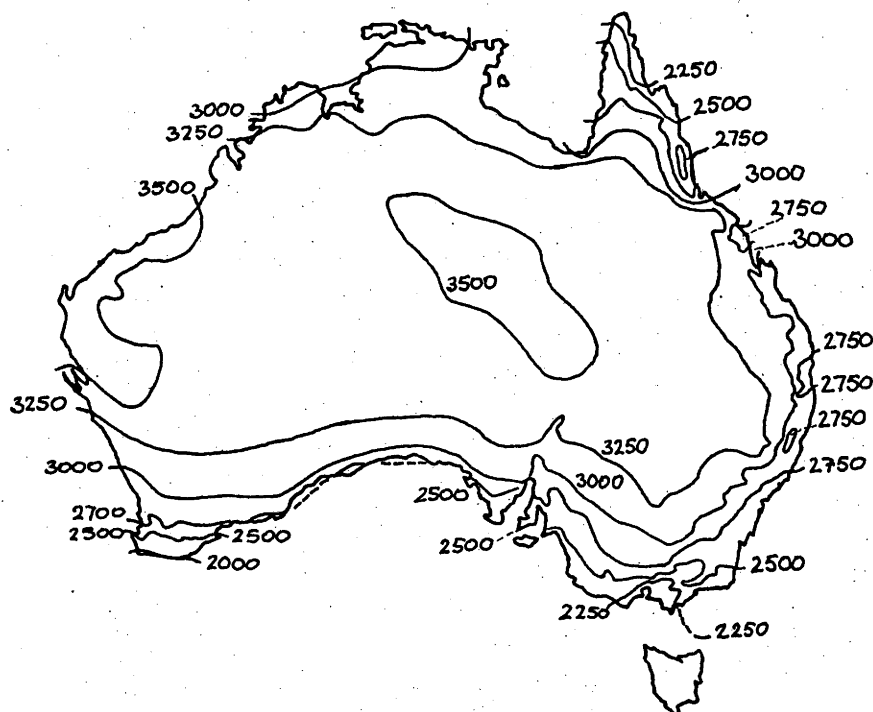


Figure 2.3 Expected hours of sunshine in Australia, (Climatological Atlas, 1976). The amount of direct radiation received per square metre can be estimated by multiplying the number of sunshine hours by 1kW .

2.4 Systems Under Study.

While this study is directly applicable to the ANU solar ammonia system, it is not specific to this system. In this section we describe the broader class of systems to which the study is applicable.

The concentration of direct radiation allows energy to be collected at high temperatures, which makes the task of converting heat to forms of work relatively efficient. Here we consider developing high temperatures using collectors which have a paraboloidal shape and reflect sunlight onto a small energy absorber. As such, these collectors require motion in two dimensions to align the optical axis of the collector with the sun. Thus each collector involves two actuators and a mount to translate the motion of the actuators into motion of the optical axis. Due to the large collection areas required, we consider a large number of collectors of the order of 1000's; each will require some form of control. Control elements may be located at the central station and at each collector.

To manoeuvre the collectors to face the sun, power is required and a network must exist between the central station and the collectors to provide this power. This network consists of a number of links between the collectors and the central station, the links being capable of also transferring the energy from each collector to the central station. Further, the links may also transfer information necessary for guidance and control between the collectors and the central station. Thus between each collector there will be a link

which can transfer energy, auxiliary power and also information.

Within these constraints there are an enormous number of systems which can be postulated, since many possibilities exist for the selection of each of the three elements, viz links, collectors and central station.

2.5 Solar Power Plant Design.

In general, solar power plants are technologically feasible; the barrier to implementation is the cost of the energy produced. Thus the designer must concentrate on energy costs. There are, however, a large number of studies to be completed before the most cost effective system can be derived. This task is complicated by the complex interrelationships between all facets of the solar plant. In figure 2.4 we illustrate the factors and interrelationships which have been studied in this thesis. It is not suggested that this list is exhaustive. The figure has been compiled with the premise that the collection of a fixed amount of energy is desired. Here we follow through a few of the relationships indicated to show the effects which need to be considered in selecting a solar plant which produces energy for minimum cost.

The level of insolation determines how many and thus the cost of the collectors required to produce a certain amount of energy.

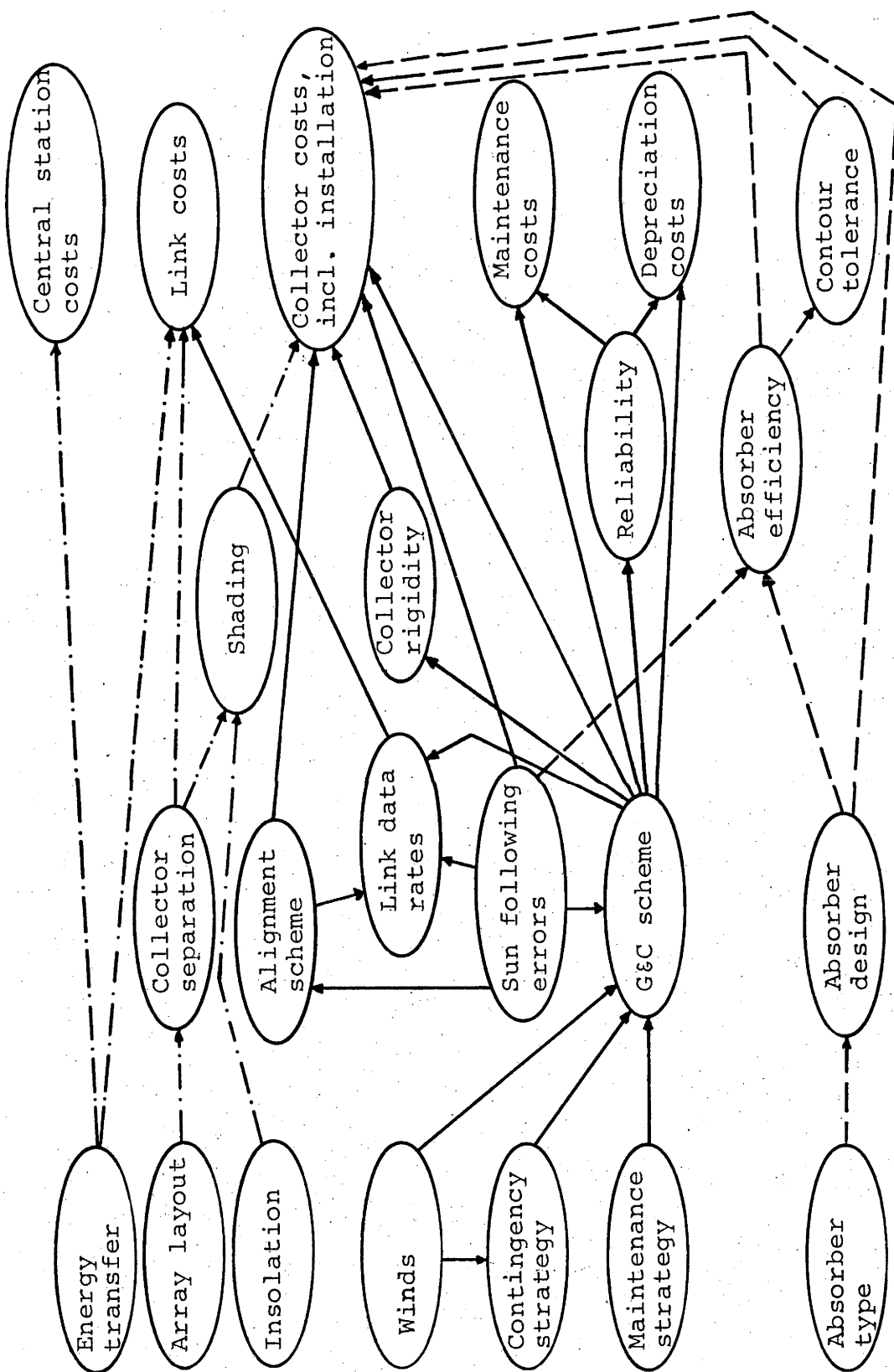


Figure 2.4 Interrelationships within the system being studied.
 The relationships are studied as follows:

- Chapter 3 — ····
- Chapter 4 — — — —
- Chapter 5 — — — —

Wind forces deflect the collector away from facing the sun during times of energy collection. This misalignment of the collector optical axis and the sun is called a sun following error. The frequency spectrum of these deflections, coupled with the sun following error tolerance and guidance and control scheme choice determine the design rigidity of the collector, and this is related to the collector cost.

Further, the characteristics of the wind determine what strategy is to be used to reduce wind damage, viz the contingency strategy. This strategy in turn determines facets of the guidance and control scheme.

The contour tolerance, which is the difference between the shape of the collector reflecting surface and a true paraboloid, determines the efficiency of the absorber at the focus and thus sets the cost of the collectors by determining how much energy is collected by each collector.

The sun following error has bearing on the design of the guidance and control scheme. The type of guidance and control scheme chosen will determine the amount of information flow over the link and thus will form part of the calculation of the link costs.

The layout of the collectors and the distances between them determine how much mutual shading will occur. This mutual shading reduces the energy collected thus increasing the number of collectors required, with attendant cost increases. Varying the spacing also increases the length of the links, and thus increases the link costs.

Other relationships exist as shown in the diagram.

2.6 Study Objectives.

The initial objective of the study was the design of a guidance and control scheme which would minimise costs. It was found, however, that certain pieces of information essential to the study were not available. Firstly, the layout of the collector array had been considered no further than to assume it would be square. This problem is important because the layout and spacing of the collectors determines both the type and cost of the communication system that can be used in the guidance and control scheme. Secondly, a feel for the allowable sun following error was necessary before analysis of the guidance and control scheme could proceed. An analysis of the collection efficiency variations with sun following error is conducted in chapter 4. Because of this lack of precise knowledge of the allowable sun following error, the initial objective was expanded to include not only a derivation of the components of a cost effective guidance and control scheme, but also the variation of guidance and control scheme cost with sun following error specification. This analysis is performed in chapter 5. With the addition of a study of hardware costs (collector structure, actuators etc) as a function of allowable sun following error, chapters 4 and 5 would provide the value of a cost effective sun following error specification. This value will be required for final design of the guidance and control scheme.

2.7 Method And Contents.

In the initial stages of a project it is customary to analyse the total plant as a series of smaller systems, where the boundaries of each smaller system are chosen to include all factors dependent on the particular variable. Variables which are yet to be determined by other analyses are included as independent variables. Analysis of each smaller system delineates cost variations as a function of the variable in question which allows a choice of the variable value to be made to minimise energy costs. Two steps are generally employed in this analysis. Firstly the variation in costs as a function of the variable is calculated and secondly the variation in energy collection is found as a function of the variable. The combination of the two pieces of information yields the value of the variable which will produce energy for the minimum cost.

In chapter 3 the variable in question is the distance between collectors. First the collection of energy as a function of the distance between collectors is studied. Energy collection is affected as collector separation varies due to the shading of nearby collector apertures. This variation is calculated for an array of paraboloidal collectors. Secondly the variations of the costs of the links between the collectors and the central station are analysed as a function of collector separation. The cost effective value of spacing is then determined from the combination of the information presented. This cost effective value of the spacing is evaluated as a function of site latitude, the cost

of the links per metre and the cost of each collector. Two layouts for the array of collectors are considered, and the cost advantages of an array based on a rectangular grid are shown. A simple method for determining the cost effective spacing is presented.

In chapters 4 and 5 the emphasis is placed on three other variables, namely the non-ideal orientation of the paraboloid with respect to the sun, or sun following error, the contour tolerance of the reflecting surface of the paraboloid and the losses of the absorber at the focus of the paraboloid.

In chapter 4 the energy collected by an isolated paraboloidal collector with a cavity absorber is evaluated as a function of the three variables. In this process the radius of the cavity is chosen so that the energy collection is a maximum. In this evaluation it was necessary to calculate the fraction of radiation which enters a cavity aperture as a function of cavity aperture size, sun following errors and paraboloid contour tolerance.

In chapter 5 the relationships depending on the sun following error are analysed. These relationships take in the choice of the guidance and control scheme, the choice of the alignment scheme, consideration of the rigidity of the collector and link data rates. The emphasis here is on the costs incurred as a function of the sun following error. The composition of the guidance and control scheme is considered in detail and the properties of a cost effective guidance and control scheme are derived. Two significant contributions of

this chapter are an analysis of the effect that wind induced deflections have on the design rigidity of the collector and an analysis of a computational alignment method which can be used in the guidance and control scheme.

Finally in chapter 6 the type of communication link is considered and the design of portions of the guidance and control system completed.

The appendices include two papers published in Solar Energy by the author during the course of the study. Further, the author found a lack of statistics on direct radiation; such statistics have a direct bearing on guidance and control scheme design. A remedy was effected by analysing data for Griffith N.S.W., the method and results of which are given in Appendix B. An example of the operation of the computational alignment method of chapter 5 on a collector mount is given in Appendix D.

Two appendices contain departmental technical reports which describe the author's work on feedback devices for sun following and the operation of a sun following scheme proposed by P.O.Carden(1978a).

2.8 Study Conclusions.

The study concludes that cost effective guidance and control schemes will possess elements of both tracking and pointing systems. When the sun is obscured, a pointing system is necessary to position the sun in readiness for solar energy collection. On the other hand, when the sun is shining cost

advantages are offered by a tracking system using a sun alignment sensor. This advantage is due to two factors; firstly the control loop of the tracking system includes deflections due to wind gusts and secondly alignment costs are reduced due to the tracking capability. Further the study concluded that collector arrays should be laid out on a rectangular grid with small North-South distances and large East-West spacings.

3.0 SHADING AND SPACING IN PARABOLOIDAL ARRAYS.

3.1 Introduction

Here we are concerned with the compromise between the decreasing costs of connecting collectors to the central station as separations decrease and the increase in energy collection as the separations increase due to lower mutual shading.

The nett cost of the energy collected from a paraboloidal array depends on both the collector cost and the amount of energy passing through each collector aperture. One way to decrease the cost of solar energy is to decrease the amount the aperture is shaded: if one increases the amount of energy collected by 1%, then all else remaining equal, the energy collected will be 1% cheaper. Terrestrial collectors suffer from shading by the earth during night, by clouds and also by adjacent collectors. In this chapter only shading of collectors by adjacent collectors is considered. The variations in losses due to shading as a function of spacing are evaluated for arrays based on a square grid, for isolated N-S rows of collectors, and for a specific array based on a rectangular grid. It is not realistic to increase the spacing between collectors sufficiently to completely eliminate shading caused by adjacent collectors, as several costs increase with increased spacing. These costs are dependent upon the links between the mirrors and the central control/power plant which in turn depend upon the system used to control the mirrors and the system used to collect the

energy from the mirrors. The costs of the links providing energy transfer, communication and power to the collectors are considered. It is assumed that a thermochemical energy transfer system will be used and the problem of appropriate pipe diameters for the energy transfer network is addressed following Williams(1978). The link costs are combined in conjunction with the shading calculations to evaluate optimum spacings. A simple method for determining optimum spacings is described and graphs provided to facilitate the determination.

Williams has noted that some change in technology is needed to reduce the installation costs for pipe networks. The effect of such a change is considered in this paper by varying parameter values in the link cost formulation, and studying the effects of such variations on the collector separation which produces minimum energy cost.

Optimum spacings for uniformly spaced square arrays are evaluated. The theory here indicates that a more cost effective array would be based on a rectangular grid. This rectangular array would have small N-S spacing and a large E-W spacing, with network links running N-S over short distances, with attendant low costs, while shading is low due to large E-W distances. Initial analyses of rectangular arrays are given which show the potential savings of the layout. Further, both uniform and non-uniform spacing is considered for an isolated row of N-S collectors and finally a simple procedure to determine cost effective spacing is described and graphs provided for ready implementation.

The optimum spacings evaluated are large, the optimum ratio of aperture area to land area occupied for a square array is 4-5. For a rectangular array, this optimum ratio being near 10. Previous work on distributed systems (Caputo 1975) made no attempt to determine optimum spacings and assumed ratios of 2-3.

In general in this chapter no hard costs are quoted, however, where estimates are given, these are derived from 1973 or 1974 documents and thus refer to 1973-1974 US dollars.

3.2 System Under Study

The system studied is an array of collectors with circular apertures, each collector being mounted on a fixed pedestal. The pedestals are laid out in a rectangular grid. Initially only square arrays are considered, ie. pedestals laid out on a square grid. Later, rectangular arrays are considered.

The energy transfer scheme used in this paper is the ammonia scheme of Carden(1977), where energy is transferred as chemical energy. System pressure is 300 atm and the mass fraction of dissociation occurring at the collectors is assumed to be 0.6. As in the study of Williams(1978), it is assumed that the thermal energy carried by the chemicals used for energy transfer cannot be recovered.

An advantage of this thermochemical transfer scheme is fast response to radiation input. Alternative schemes such as the transfer of sensible heat require a reasonable startup period during which the entire network of pipes must be heated (Caputo 1975). For the solar ammonia scheme, only the small receiver at each collector focus and the associated heat exchanger are heated during the startup period and thus energy is received at the central plant within a short period of the mirrors being illuminated. Hence early morning radiation is in fact useable energy, and does not simply make up heat leaks for this transfer scheme. It is assumed that storage is provided for the thermochemical reactants at the central plant and that the total plant produces a constant power output.

Another part of the collector array is the linking system for the distribution of power to the actuators on the collectors and communication links for control, in addition to the pipes required for energy transfer. In the present formulation, the costs of the three types of links in the array, namely power, energy transfer and communication, are combined into a single formulation representing the cost of the network.

3.3 Cost Optimisation.

The basic requirement for design is to minimise the cost of energy. Here we analyse the costs and energy flows, delineating the factors which must be evaluated before optimum spacings can be determined.

The costs associated with power production can be divided into several categories; the cost of the collectors, C_c , the cost of the links between the collectors, C_l , the cost of the central station generating and storage equipment, C_{gs} , and the cost of the pumping equipment required to circulate the chemicals. This final cost is the product of the maximum pumping power requirement, \dot{W}_{pm} , and the cost per unit power of the pumping equipment, I_p .

The output work (\dot{W}_e) is calculated as the difference between the work equivalent to the energy collected, expressed as if the collection was in fact continuous, \dot{W}_c , and the work required to circulate the chemicals. The latter is expressed as the product of the capacity factor of the pumping equipment, S and the maximum pumping power requirement (\dot{W}_{pm}). Thus:

$$\dot{W}_e = \dot{W}_c - S \dot{W}_{pm} \quad (3.1)$$

where the subscript m indicates a maximum value. For a typical solar power plant S assumes a value of around 0.2 (see later section 3.6.2).

The cost of the output electricity is given by the sum of the costs divided by the electrical output:

$$I_e = \frac{C_{gs} + C_l + C_c + I_p \dot{W}_{pm}}{\dot{W}_e} \quad (3.2)$$

In equation 3.2, storage and electricity generating costs are functions of spacing. It is assumed in later calculations that both of these costs are proportional to \dot{W}_e , and thus that:

$$I_e = \frac{C_l + C_c + I_p \dot{W}_{pm}}{\dot{W}_e} + I_{gs} \quad (3.3)$$

where I_{gs} is the appropriate constant of proportionality for generation and storage. None of the later figures include I_{gs} .

The energy collected (reflected in \dot{W}_c) is reduced by the shading and the losses due to shading need to be evaluated. This is performed in section 3.4. The costs which constitute the numerator in eqtn (3.2) are evaluated in section 3.5. To determine the optimum spacing, variables associated with the first term must be chosen to minimise costs. Such variables are the diameters of the pipes in the energy transfer network and the minimum cost of the energy transfer network is evaluated in section 3.6.1.

Information on all the terms in equation (3.2) is collated in section 3.6; optimum spacing is determined by minimising eqtn (3.2).

3.4 Shading Calculations

A brief description of the method used to calculate the shading is given and sections follow delineating the equations used. Results indicating the average fraction of aperture

which is illuminated are presented graphically.

3.4.1 General

In this section we calculate the variation in energy collection as a function of the separation between the collectors. The array studied is as shown in figure 3.1.

The shading of one mirror deep inside the array is representative of the shading of the whole array and thus it is necessary to calculate the amount of shading experienced by a single mirror only. This is accomplished by determining the boundary of the illuminated part (or parts) of the mirror, then the actual area illuminated can be calculated; see figure 3.2. This procedure is carried out for many points over a series of days for the whole year, and the average shading calculated. The mirror chosen as being representative of the field is called the shaded mirror.

The pseudo 3-dimensional plotting program HIDE(Williamson, 1972) has been modified to calculate the set of points which define the boundary. Details of the program are given in Appendix A. It is assumed that the shadow cast by each of the collectors is identical to the shadow cast by the aperture, i.e. the effect of the pedestal and support structure is not included.

A square array with 49 collectors was used in the calculations, with the shaded collector being the furthest from the sun in one corner of the array. This array was sufficiently large to include all collectors which might shade the collector in the corner of the array.

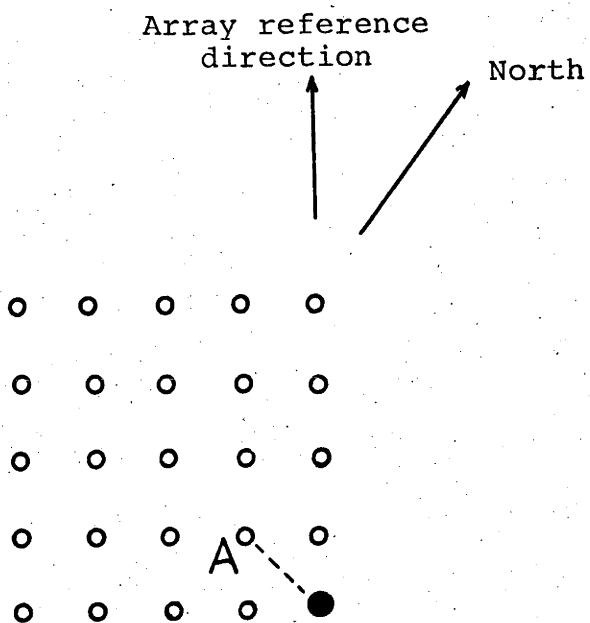


Figure 3.1 Layout of the rectangular array, indicating the collector under consideration (or shaded collector), black dot; the shading collectors, circles; and the array reference direction.

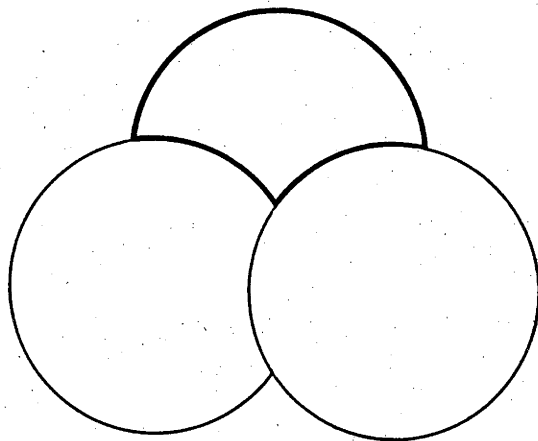


Figure 3.2 Diagram depicting the boundary (heavy line) surrounding the illuminated area of a collector shaded by two other collectors.

The energy available for collection each year per square metre, q_A , is a function of the shading each collector experiences because of the proximity of other collectors. The proximity is defined in terms of a ground cover ratio g , which is the ratio of the total aperture area to the area of ground occupied by the collectors. In terms of the aperture diameter (D) and the distance between collectors (L), the ground cover ratio is given by:

$$gL^2 = \pi D^2/4 \quad (3.4)$$

We use the illumination function $f(g)$ to relate the energy available for collection by a collector which is isolated and thus free from shading, ($q_A(0)$), and the energy available for collection by a collector in an array of spacing g . Thus:

$$f(g) = q_A(g)/q_A(0) \quad (3.5)$$

Only a fraction of the energy which passes through the collector is available for conversion from thermal energy to electrical energy at the central plant. A collection efficiency factor, η_c , quantifies this fraction, and includes the efficiency of the thermochemical energy transfer process, the quality of the alignment and optics, the reflectivity of the collector and so on. This factor does not include pumping losses and is not a function of spacing. The energy available to the central station (q_c) is therefore:

$$q_c = \eta_c f(g) q_A(0) \quad (3.6)$$

The annual work (W_c) produced by the power station is calculated from q_c using an estimate for the efficiency of the power station in converting heat to work of say 0.25. Thus:

$$W_c = 0.25 q_c N_c \pi D^2 / 4 \quad (3.7)$$

where N_c is the number of collectors.

Values for $f(g)$ have been calculated for the square array of figure 3.1. The orientation of the array, as determined by the direction of the array reference with respect to North, has been varied to determine the best orientation. The results are shown in figure 3.3 and discussed below in 3.4.5.

No energy collection is considered below 5 degrees elevation for two reasons. Firstly, direct radiation at these elevations is variable and not conducive to simple modelling, and secondly, the direct radiation from the sun decreases near the horizon and this reduces the relative importance of shading.

3.4.2 Direct Radiation Model

Vant-Hull(1976) has given several tabulations of the intensity of direct radiation in clear skies as a function of solar elevation. He considers the model of Allen(1964) to be appropriate for calculations for solar power stations as the other models he considered applied only to the relatively

contaminated atmospheres of urban environments and he notes that Allen's model is an adequate representation of clear skies at Inyokern. For a pressure of 760mm Hg the model is fitted by:

$$I = 1353. (1.0 - 0.232m_r^{0.427}) W m^{-2} \quad (3.8)$$

This assumes a water content of 14.4mm in the atmosphere. The relative air mass (m_r) is given as a function of solar elevation (θ) by:

$$m_r = (r^2 \sin^2 \theta + 2r + 1)^{0.5} - r \sin \theta \quad (3.9)$$

where $r=755.6$ for the chosen pressure of 760mm Hg. The equations used for the elevation and azimuth (ϕ) of the sun are (Brinkworth, 1972):

$$\sin(\theta) = \sin(\delta) \sin(B) + \cos(\delta) \cos(2\pi t) \cos(B) \quad (3.10)$$

$$\tan(\phi) = \sin(2\pi t) / (\cos(2\pi t) \sin(B) - \tan(\delta) \cos(B)) \quad (3.11)$$

where B is the latitude, t is the time in days, and δ , the solar declination is approximated by:

$$\sin(\delta) = 0.40 \sin(2\pi T) \quad (3.12)$$

where T is the time in years.

With these equations, the value of $q_A(0)$, with no energy collected when the elevation is less than 5 degrees, is equal to 13.6GJ m^{-2} and 13.3GJ m^{-2} for latitudes 25S and 35S respectively.

3.4.3 Cloud Effects

Since $f(g)$ is a ratio of two quantities, both of which will be affected similarly by cloud cover, $f(g)$ will be independent of cloud effects provided that the variation in cloud cover has no regular daily or seasonal variation. It is noted that Paltridge and Proctor(1976) assume that there is no regular daily variation, albeit tacitly, but this is not easily justified with available data. There are patterns of seasonal variation, which themselves vary across Australia. For example, Brisbane and places further North experience more clouds (in terms of the ratio of the duration of sunshine to the hours of daylight) in the summer months than in winter, while in Adelaide the reverse is the case. Data from specific sites will need to be examined before more exact calculations can be made. Thus the following calculations strictly apply only to areas where cloud cover is relatively constant throughout the year.

3.4.4 Procedure

At each instant the power available to each collector is the product of the instantaneous solar flux (from equation 3.8), and the fraction of the collector aperture illuminated

at the time, the latter being calculated by the program of appendix A, which requires knowledge of the angle of the sun as given by equations 3.10 and 3.11. This product is calculated at 40 points over each day and for twenty days equally spaced over half the year. The integration gives $q_A(g)$, and thus $f(g)$ from equation 3.5.

3.4.5 Results

The effect of changing the orientation of the array on the illumination function $f(g)$ is shown on polar scales in figure 3.3 for latitudes 25S and 35S. Shading is minimised with the direction of the array reference 45 degrees from North. The reduced dependence of $f(g)$ on array orientation at both larger ground cover ratios and higher latitudes can be explained in terms of the decreasing importance of sunrise and sunset in determining shading, relative to other times of the day.

Further information for this direction of the array reference is given in figure 3.4. Note that at small ground cover ratios, the effect of shading is pronounced near the equinox, which occurs when the sun rises in line with the collector 'A' in figure 3.1. The function $f(g)$ is plotted in figure 3.5 for the same array reference direction as in figure 3.4.

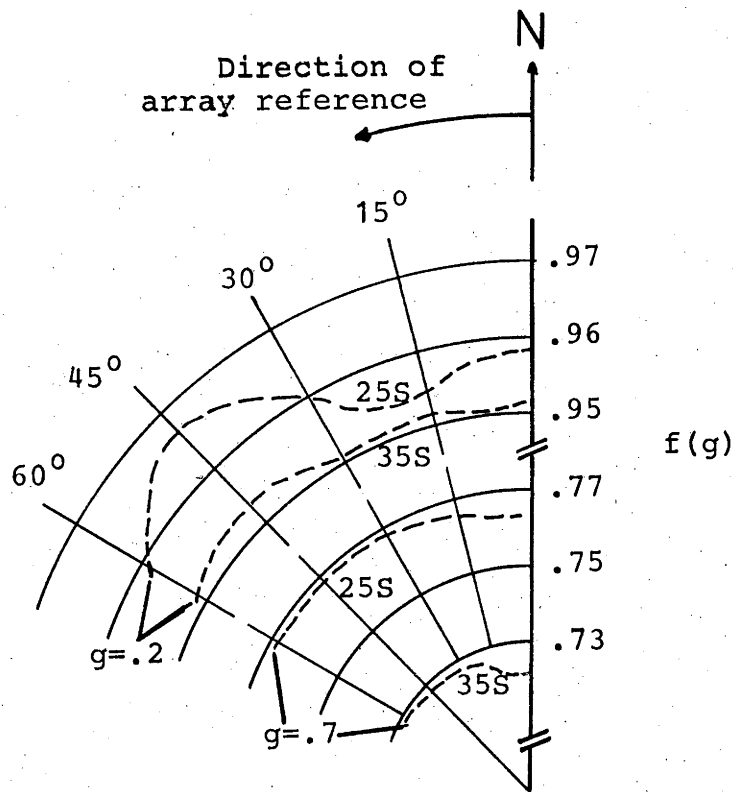


Figure 3.3 The function $f(g)$ as a function of the orientation of the direction of the array pattern. The function is the ratio of the annual energy entering an aperture for ground cover ratio g to the annual energy entering an aperture when g is zero. The orientation is expressed by the angle between North and the direction of the array reference indicated in figure 3.1.

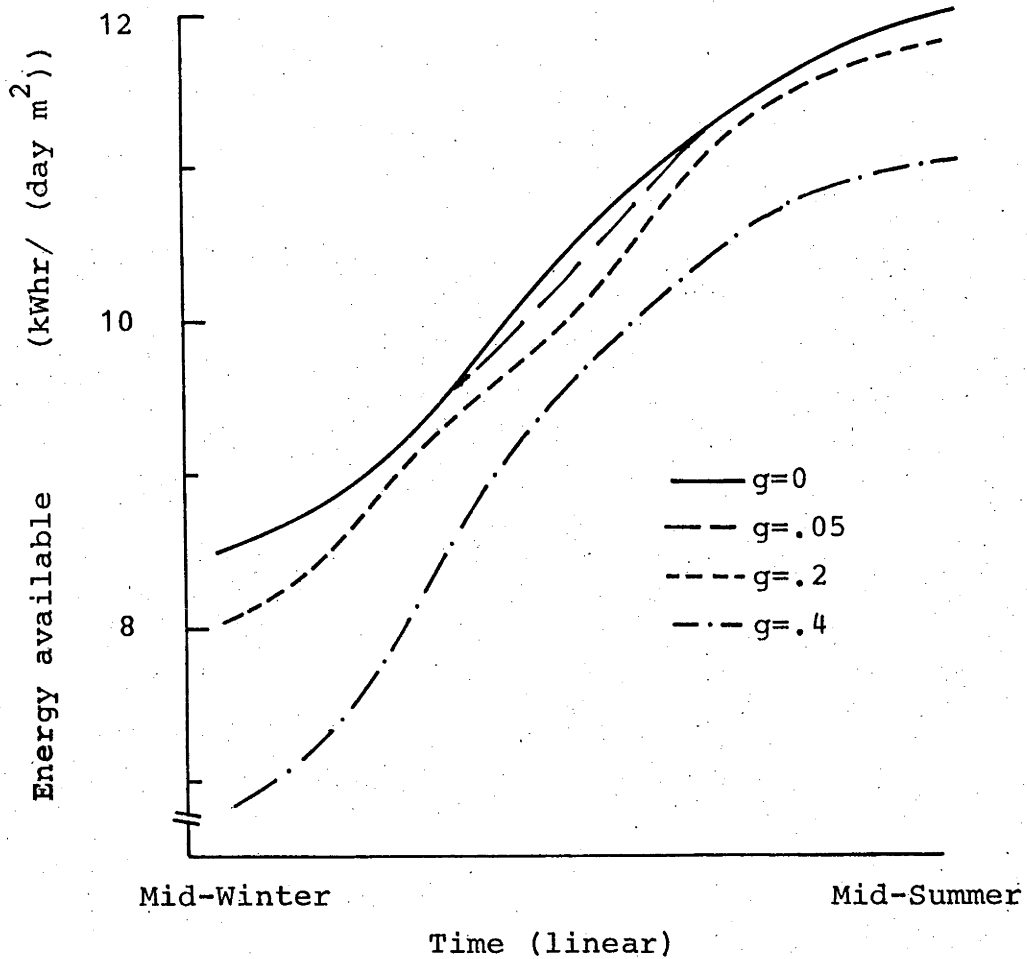


Figure 3.4 Energy entering a square metre of aperture per day as a function of the time of year. The array reference direction is 45 degrees West of North. The curves are for four different ground cover ratios. Latitude 35S.

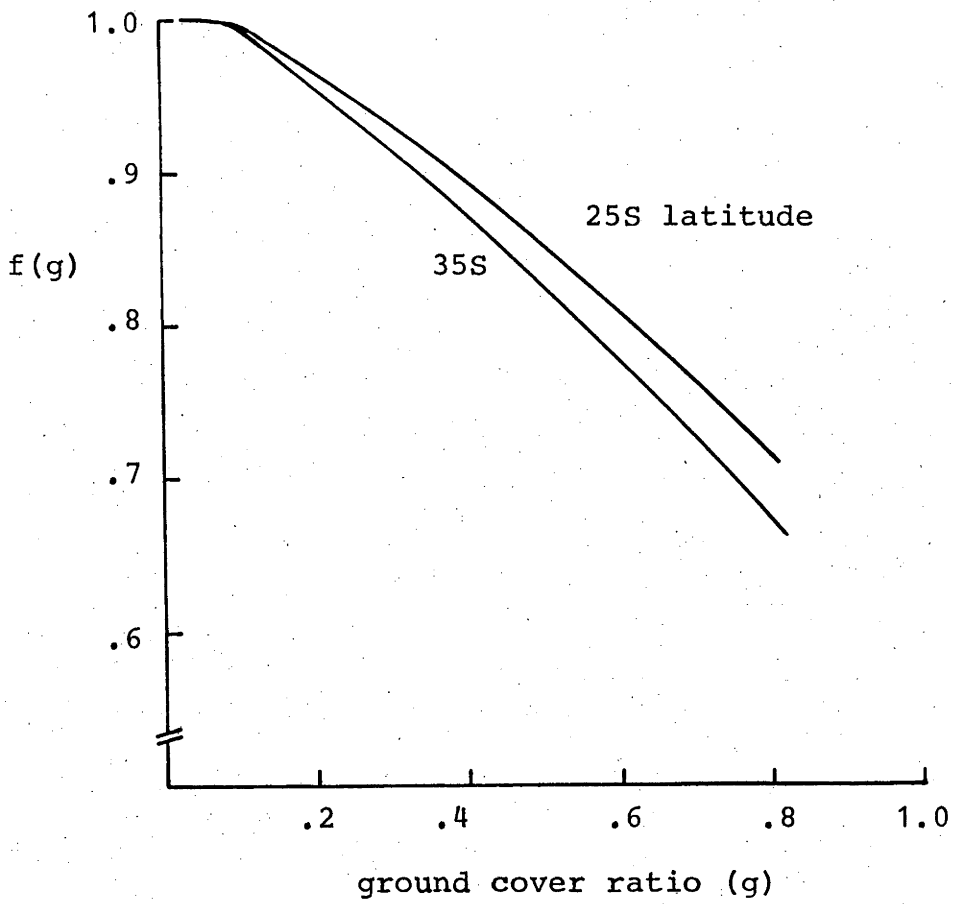


Figure 3.5 The function $f(g)$ vs g for an array reference direction 45 degrees West of North.

3.5 Costs Relevant To Determining Optimum Spacing.

Here we analyse those costs which constitute the numerator of the first term in eqtn 3.3, namely C_c , C_ℓ , and $I_p (W_{pm})$. These costs are the cost of the collectors and the final two terms are the cost of energy transfer, including the cost of communication and auxiliary power links. These are discussed in the ensuing sections. All costs are combined into a single formulation in the final subsection.

3.5.1 Cost Of Energy Transfer

Costing the hardware involved in pipe layouts presents few problems to the designer. Difficulties arise, however, when an attempt is made to include in the costing such intangibles as handling, hauling and storage of components. Several methods for costing pipe systems are outlined in the Chemical Engineer's Handbook (Perry, 1973), one of which is to cost by weight of material knowing that the installed cost of piping generally is in the region 850-1100\$/ton. Another method is to cost on the basis of each joint as joining is usually the significant cost. These methods are appropriate where knowledge of construction costs for a particular plant type such as an ammonia plant can be built up from records of plant construction costs.

In a novel system such as the thermochemical energy transfer system proposed for a solar energy plant, it is felt that a better costing method would explicitly account for each cost component, such as joints, pipe material and footings,

since costs for each vary. A notional pipe layout must be developed before such a costing exercise can be implemented: this is now discussed.

Since the most significant cost factor is joints, the first requirement of the pipe layout is that the number of joints is minimised. A minimum number of joints is two per collector, with a connection at each collector and a connection at a trunk pipe for each collector.

Such an approach will be feasible only if pipes are available in sufficient lengths to avoid intermediate connections. The availability of pipes in long lengths is dependent on both manufacturing processes and transportation costs, the latter being the limiting factor. There are several techniques for making pipes of any length, but whichever is chosen, the critical factor is the requirement that the pipes can be coiled for easy transport. This sets a limit on the diameter of pipe which can be used, estimated by Carden(1977) to be around 6mm OD for 300 atmosphere operation. Pipes of this size are suitable for the thermochemical energy transfer system and this enables us to consider joint costs as a fixed amount for each collector, involving two joints and thus independent of collector separation.

In summary, the cost of the energy transfer network is divided into three parts: a material cost term, proportional to the length and square of the diameter of the pipe; a connection term; and an installation term, which includes footings, or, in the case of buried pipes, excavation and filling costs which are proportional to pipe length. We

discuss these costs briefly below.

It is probable that pipes would be installed underground, a process which would involve digging a small trench with perhaps sand or aggregate fill. The majority of pipes would be small, around 1cm diameter or less and it is for this reason that installation costs are assumed to be independent of pipe diameter. Pipe material cost is estimated at 370\$/ton, as suggested by Caputo(1975). The connection term involves two welding connections, the cost of welded connections being given by Perry(1973). For 1cm pipes, this amounts to some 2 manhours per joint, or some \$20-32. This cost is not dependent on pipe lengths: pipe diameter is set by the collector diameter. Thus it is reasonable to include these costs as an adjustment to collector cost.

With the above provision for connection costs, the cost of installed pipe per unit length(c_m) is assumed to be given by an expression with a constant cost per unit length term and a cost term proportional to material volume, which for pipes will be proportional to length and the square of diameter. Thus:

$$c_m = B_1 + B_2 d^2 \quad (3.13)$$

where B_1 and B_2 are cost parameters and d is the internal diameter of the pipe. This expression is the cost per unit length of one pipe; two such pipes are required in the thermochemical scheme considered here. Thus the cost per unit length of network link installation is approximated by $2B_1$ if

$B_2 d^2$ is small. In all later calculations the convention is observed, that B_1 is half the cost per unit length of link. The cost of the links is the cost of each link summed over all link segments in the array. The subscript k is used to denote the k th segment, and thus:

$$C_\ell = \sum L_k (c_m)_k \quad (3.14)$$

where the calculation of c_m takes into account the need for two pipes of possibly different sizes.

The cost of energy transfer is given by the sum of the cost of the pipe links (C_ℓ) and the cost of the equipment required to circulate the energy transfer fluid. The cost of pumping equipment is the product of the maximum pumping power requirement (\dot{W}_{pm}), and the capital cost of pumping equipment per installed watt (I_p). Thus the cost of the energy transfer network may be expressed:

$$C_{et} = C_\ell + \dot{W}_{pm} I_p \quad (3.15)$$

where the second term is the cost of the pumping equipment.

The pumping power can be calculated using the Fanning (or Darcy) equation (Perry, 1973) where:

$$W_p = \Delta P \frac{\dot{m}_t}{\eta_p \rho} \quad (3.16)$$

where \dot{m}_t is the total mass flow rate through the circulating pump, η_p is the efficiency of the pumping equipment, ρ the density of the pumped fluid, and ΔP the pressure drop across

the pump, which is given by:

$$\Delta P = (8 \sum f L_k \dot{m}_k^2 / d_k^5) / (\pi^2 \rho) \quad (3.17)$$

where f is the friction factor, \dot{m}_k the mass flow rate through the k th pipe segment and the summation extends along a single trunk line.

3.5.2 Cost Of The Communication And Power Links.

Dubberley(1977) has provided tables of costs for the installation of telephone line equipment. Just as for pipe costs, it is assumed that termination and connection costs are included by adjusting the collector cost. These tables indicate that the cost of a communication network is related only to the total length of line and is directly proportional to the total length. Costs are estimated to be of the order of 1\$/m. Costing of power cables(Perry, 1973), is also carried out per unit length, with direct burial costs of around \$30/metre. The cost of both these items can be included in (3.13) simply by adjusting B_1 . As for pipes, the cost of installation is of the order of 10 times the material cost.

3.5.3 Cost Of Energy Collectors.

The collectors are costed at c_c dollars per square metre of aperture. The collector cost c_c is assumed to include the connection costs for pipes and cables as mentioned in the

previous two sections.

3.5.4 Cost Of Land.

At a land cost of \$250 per acre, land costs amount to only 1% of total costs. The cost of land at suitable sites is unlikely to approach such a figure, and thus land costs have been ignored in this study.

3.5.5 Total Costs.

The total costs which are relevant to determining optimum spacing is therefore:

$$C = C_{et} + N_c c_c \pi D^2 / 4 \quad (3.18)$$

where N_c is the number of collectors, D the collector diameter and c_c the cost of collectors per square metre suitably adjusted to include connection costs. In determining C_{et} in eqn 3.15 B_1 must be adjusted to include power and communication costs. Although B_1 now includes the cost of direct burial of pipes and power and communication cables, one can expect cost savings from installing all items together in the same trench. It would be expected further that B_1 would not be the simple sum of cost estimates of the three independent items.

Estimating appropriate values for c_c and B_1 is not straightforward. In the present calculation, c_c is assumed to be $50\$/m^2$, a value which would ensure economic viability.

Several factors are in favour of a low value for B_1 . Firstly, installation conditions would be close to ideal, over a rural, or arid surface. Secondly, hazards facing the laid pipes and cables, such as traffic and digging, can be well controlled. This factor will favour low burial depths. Finally, relatively large lengths are involved, with half a kilometre of piping required for each thermal MW (see later section 3.6.3). It seems possible, therefore, that the costs of directly buried cable, estimated by Perry(1973), at 30\$/m, may be reduced. In later calculations we assume that a reasonable value for B_1 is 10\$/m, which is equivalent to a cost per unit length of link of 20\$/m.

3.6 Tradeoff Between Shading And Spacing.

In this section the first term in eqtn 3.3 is minimised. The procedure to minimise the cost of energy transfer is outlined in the first section and later sections present optimum spacing as a function of the parameters in the cost formulation. Finally a simple method for determining optimum spacing is described and graphs for implementation provided.

3.6.1 Minimising Pipe Costs.

If spacing is uniform, shading losses are the same for all collectors and thus each collector gathers equal energy and the mass flow rates through all collectors are the same.

The determination of the distribution of pipe sizes in the network is identical to the method used by Williams. Flow rates are determined by fixing the degree of dissociation desired at the collectors and a pipe size distribution is evaluated subject to the requirement of minimum cost and pressure drop equality across parallel paths. Williams evaluated the distribution of pipe sizes with respect to the smallest pipe in the network and the cost of the network was evaluated in terms of both the smallest diameter and a set of dimensionless parameters $(l(N_c), v(N_c), \Delta Pr(N_c))$ (Williams, 1978), which are respectively the pipe length per collector, the average pipe inner volume and the total pressure drop, all normalised to the appropriate variables for the smallest pipe segment. The parameter $l(N_c)$ is very nearly unity.

In the present study, the cost determining equation (3.2) differs slightly from the cost equation used by Williams (1978) and in this case for minimum costs the smallest pipe diameter in the network should be chosen as:

$$d_0^7 = \frac{H \Delta Pr(N_c) \dot{m}^3 (I_p + SI_e)}{v(N_c) B_2} \quad (3.19)$$

where H is a constant determined by the thermochemical cycle used and \dot{m} is the mass flow rate through a single collector. The expression for the minimum cost of the network is identical to that given by Williams, with the replacement of

his cost per installed watt by $(I_p + S I_e)$. The expression for the minimum cost of energy transfer is:

$$C_{et} = 2B_1 L l(N_c) + \gamma (v(N_c) B_2)^{5/7} L \Delta Pr(N_c)^{2/7} (\dot{q}_{in})_m^{6/7} \quad (3.20)$$

$$\text{where } \gamma = 1.71 \left[1 + \left(\frac{f'/\rho'}{f/\rho} \right)^{2/7} \right] \left[\frac{f(I_p + S I_e) M^3}{\delta^3 \eta_p \rho^2 \Delta H^3} \right] \quad (3.21)$$

where the apostrophe identifies return pipe properties, δ is the fractional degree of dissociation, $\Delta H/M$ is the enthalpy change between reactant and product per unit mass and $(\dot{q}_{in})_m$ is the maximum power absorbed by each collector.

Note that adjusting B_1 to include the other components of the total network will not affect the calculation of this minimum cost.

3.6.2 Procedure.

The total costs for energy transfer were calculated using equations 3.20 and 3.21 using values for the friction factor f (in the range .02-.03), and pump efficiency (.75), as calculated by Williams. The cost of electricity was calculated using equation 3.1, with $f(g)$ as calculated in section 3.2. The values of the variables $l(N_c)$, $v(N_c)$, $\Delta Pr(N_c)$ are given for a square array by Williams.

In determining the pump capacity factor S , we assume that the flow rate is controlled so that the amount of dissociation in the focal receiver is held constant. Thus the compositions of the feed and return pipes are held constant. The capacity factor of the pump can be calculated from the time variation of the power input to the cavity. We assume the mass flow rate is proportional to the product (\dot{q}_{in}) of the instantaneous illumination function and the instantaneous solar flux. Using the Fanning (or Darcy) equation for pressure drops (Perry 1973), the pumping power is proportional to the cube of the mass flow rate and thus:

$$S = \int \dot{q}_{in}^3 dt / (\dot{q}_{in})_m^3 \quad (3.22)$$

where $(\dot{q}_{in})_m$ is the maximum value of \dot{q}_{in} . S was evaluated at the same time as $f(g)$ was calculated, and is likewise a function of spacing. Typically, S is in the range .15-.2.

The electrical output, \dot{W}_e , is calculated from eqn 3.1, using eqns 3.6 and 3.7, and:

$$\dot{W}_e = 0.25 \eta_c f(g) q_A(0) N_c \pi D^2 / 4 / 3.15E07 - \dot{S} W_{pm} \quad (3.23)$$

3.6.3 Situation Studied.

In the following figures for square arrays, an array of collectors with a total aperture area of approximately 150,000 square metres is coupled to a storage facility and the

combination supplies the central boiler with $42 \eta_c MW_t$ continuously. The value of η_c was taken as .65 and thus the available thermal energy from this array is $27MW_t$. The collector diameter used was 5m and so approximately 7500 collectors are involved.

3.6.4 Results.

The cost of the electrical output (excluding the costs of the central station equipment C_{gs}) is given as a function of ground cover ratio in figure 3.6. The worth of evaluating optimum spacing (g_o) is demonstrated in the figure. The effect of B_1 and collector cost on both cost of the work and g_o is shown in figures 3.7 and 3.8.

Increasing collector cost is coupled with lower ground cover ratios and greater utilisation of the collector area (higher $f(g)$). Increasing B_1 leads to higher ground cover ratios as the costs of connecting mirrors increases. Note that a reduction in B_1 from 32\$/m to 10\$/m involves a corresponding increase of 5% in $f(g)$ and this increase in energy collected lowers energy costs.

The resulting spacings are surprisingly large. Previous reports, eg Caputo (1975), consider ground cover ratios of 0.46 to be acceptable. The consideration of shading is thus shown not to be an idle proposition, as costs vary considerably with spacing. Excluding I_{gs} the resulting cost of $0.96\$/W_e$ can be compared with a total cost of $2\$/W_e$ which would ensure viability.

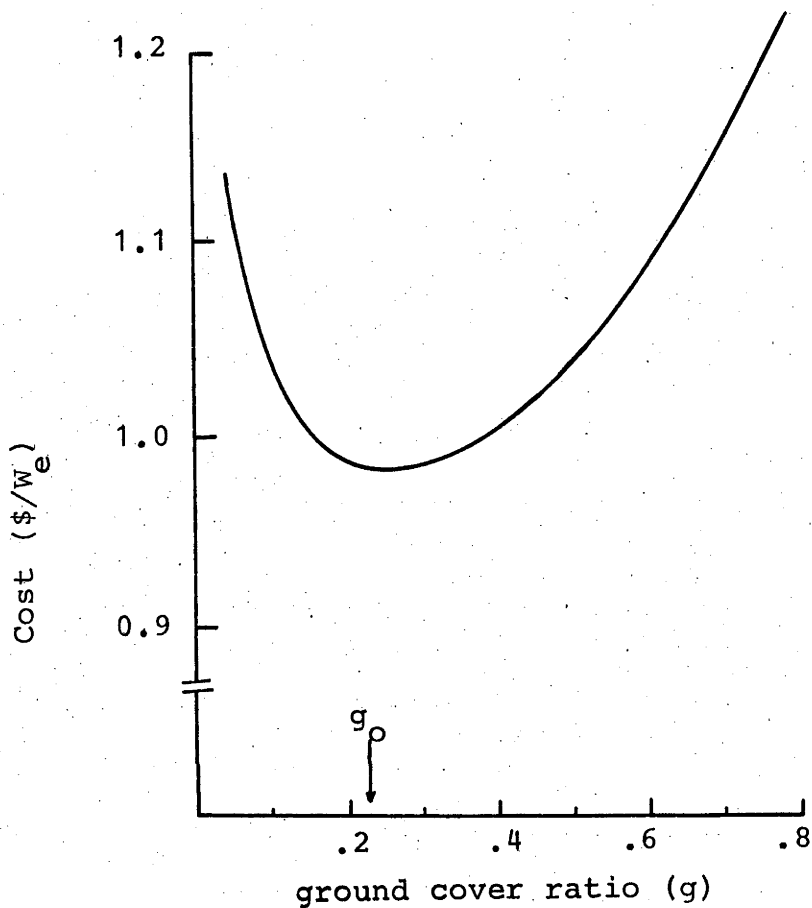


Figure 3.6 Variation of costs with spacing. Capital costs due to the collectors and the network linking the array. The optimum spacing (g_0) is arrowed.
 $c_c = 50 \$m^{-2}$; $B_1 = 10 \$m^{-1}$; $B_2 = .663 \times 10^4 \$m^{-3}$;
 $D_c = 5m$.

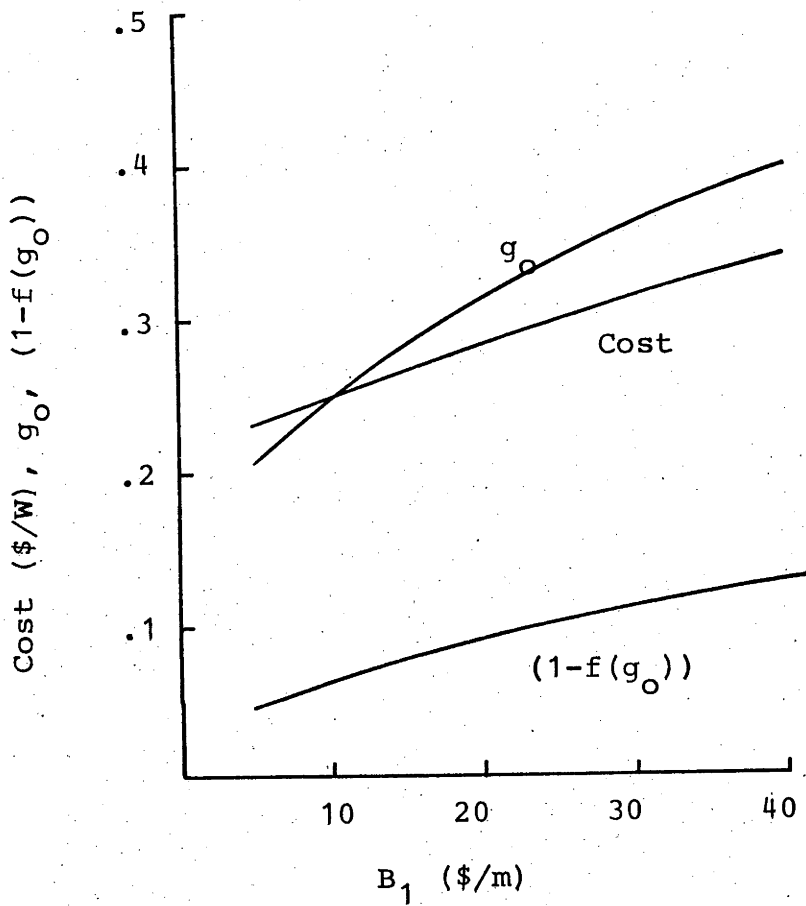


Figure 3.7 Variation of costs with B_1 . Capital costs of both the network links and the collectors per thermal watt. $B_2 = .663 \times 10^{-3} \m^{-3} ; $c_c = 50 \$m^{-2}$; $D = 5m$. The cost per electrical watt is greater by a factor of four.

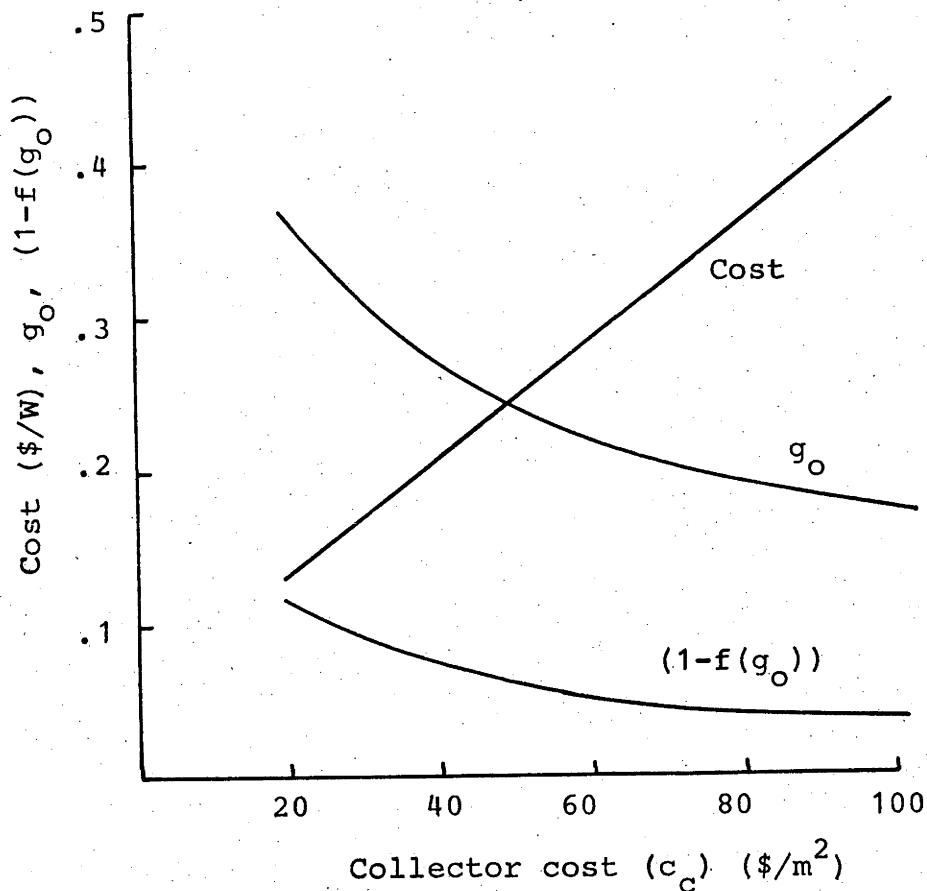


Figure 3.8 Variation of costs with c_c . Capital costs due to both the network costs and collector costs.
 $B_1 = 10\$/m^{-1}$; $B_2 = .663 \times 10^4 \$/m^{-3}$; $D = 5m$.
 The cost per electrical watt is greater by a factor of four.

A note on C_{gs} .

It is possible that the storage costs will not be related to \dot{W}_e as assumed. However, if this is the case, then a linear approximation to storage costs as a function of \dot{W}_e can be made and the constant term in this linear approximation included by adjusting c_c . The portion of the approximation proportional to \dot{W}_e can be included in I_{gs} as above.

3.6.5 A Simpler Minimisation Process.

Increasing the spacing between collectors reduces shading, increases the amount of energy collected and thus the flow rate. In general the pipe capacity varies with the collector separation. A simpler calculation can be made if we assume that the cost of the links per metre is not a function of spacing and that the variation of mass flow rate with spacing can be ignored. If this is the case, then ignoring I_{gs} , the minimisation of (3.3) is equivalent to minimising:

$$I_e = 0.25 (\sum 2B'_1 L_k + N_c c_c \pi D^2 / 4) / (W_c / 3.15E07) \quad (3.24)$$

where $2B'_1$ is an effective cost per unit length of the links between collectors and the constant is the number of seconds in a year, converting a yearly energy W_c into an average power.

In this case, one can determine the spacing for each network link individually, if the cost of the link per metre is known. For this formulation, spacing is a function of the

dimensionless variable $B_1'/(Dc_c)$. Suitable values for g_0 as a function of $B_1'/(Dc_c)$ are given in figure 3.9. We note that as B_1' approximates the cost per unit length of pipe and two pipes are required in a thermochemical energy transfer link, equation (3.24) gives the costs for a network whose link cost is $2B_1'\$/m$.

Applicability of equation 3.24.

Differentiating equation (3.3) leads to the condition that

$$(\dot{W}_c)_k \gg \frac{\dot{m}_v}{\dot{m}_k} (\dot{W}_p)_k \quad (3.25)$$

which must be true for (3.24) to be applicable. In this equation, $(\dot{W}_c)_k$ is the contribution to \dot{W}_c due to the kth collector, $(\dot{W}_p)_k$ the contribution to pumping power due to the kth link segment and \dot{m}_k the flow rate through the kth segment. \dot{m}_v is the varying portion of \dot{m}_k , ie the part of \dot{m}_k determined by the energy collected by the kth collector, itself principally determined by L_k . The right hand side of this inequality is the pumping power expended due to friction in the kth segment reduced by the ratio of variable to total flow rate. The left hand side is the contribution to the total work produced by the kth collector. The only situation in which this inequality might not be true would be if \dot{m}_k swamped \dot{m}_v , since pumping power increases as the square of \dot{m}_k .

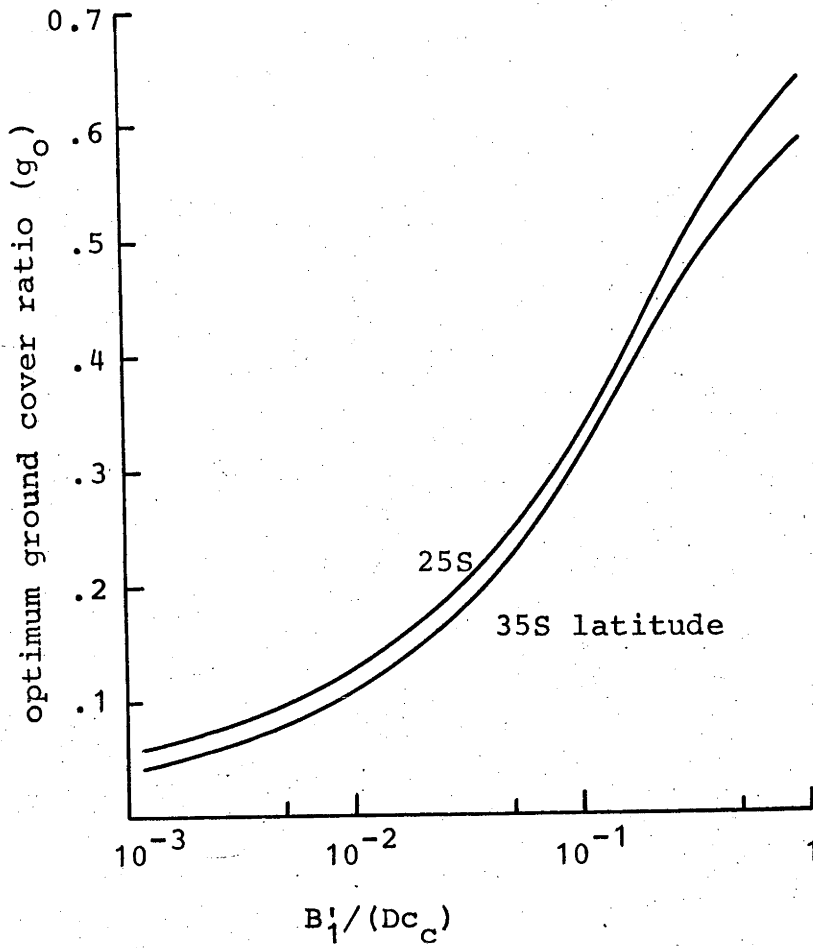


Figure 3.9 Ground cover ratio (g_0) required to minimise installed costs for the alternative network cost formula eqtn 3.24.

Estimation of B_1' .

The calculation of the optimum spacing by this simple method relies on an estimate of B_1' , which can be derived from the derivative of (3.3), ignoring the terms which include derivatives of mass flow rate with respect to L_k . We have:

$$B_1' = B_1 + B_2 d_k^2 + (I_p + SI_e) (\dot{W}_{pm})_k \quad (3.26)$$

In general B_1 is the dominant term and an estimate for the final terms suffices.

3.7 Rectangular Arrays.

Here we determine the cost reductions possible if an array with asymmetric spacing is used. In the following section we semi-quantitatively discuss the advantages of rectangular arrays and the possible costs are analysed more thoroughly in ensuing sections. The minimisation of costs for a rectangular array is more complex than that for a square array because of the additional spacing variable and only initial calculations are presented.

3.7.1 Implications Of Square Array Analysis.

The question arises as to whether there is a layout which allows more economic energy collection than the above layout. Williams studied a pipe layout for a square array and considered it reasonable because the cost of piping per collector is very nearly proportional to the length of piping. It is probable that for most arrays the length of the

pipe/communication network is nearly proportional to the pipe length between collectors, the trunk lines having only a small effect. To collect energy as efficiently as possible, we must therefore minimise the pipe length between collectors and minimise the shading. The latter requires long distances between collectors which shade each other, but these two apparently conflicting requirements are compatible, as the parameter which principally determines shading is the East-West distance and the pipes can be run over a short North-South distance. Thus an array with North-South rows of collectors relatively far apart in the East-West direction may satisfy both requirements. Analysis of such a layout requires the formulation of cost estimates for piping for such an array. Neither Williams(1978) nor Caputo(1975) considered piping costs in the light of shading. The following calculation gives some insight into the possible savings of such a scheme.

For a square array at latitude 35, a ground cover ratio of .13 would give an illumination factor of .98 (figure 3.5). The pipe and communication costs for this layout would be approximately proportional to the pipe length per collector(L), which for g of .13 is 2.46D metres. A rectangular layout was assumed with the North-South distance between mirrors (where the pipes would be run) being 1.48D. To attain the same illumination factor of .98, the East-West distance was set at 4.44D. The pipe length per collector for this layout is only 1.48D. Thus a simple layout change has reduced the costs derived from B_1 by 40%. Whether the costs

due to B_2 have increased enough to nullify this advantage depends upon the values of B_1 and B_2 . For the values given by Williams (1978) ($B_1=32\$/m$, $B_2=6630\$/m^3$), costs due to B_1 are dominant.

In the next section we consider in more detail the analysis of a rectangular array.

3.7.2 Analysis Of Rectangular Arrays.

To determine the optimum spacing within a rectangular array completely, one would need to generate shading information and also network cost (C_ℓ) information as a function of two variables; the N-S and the E-W separation.

No attempt is made to solve this problem completely, rather an iteration of the optimisation is completed by firstly ignoring E-W shading and optimising N-S spacing, and secondly calculating shading as a function of E-W spacing for a particular N-S separation. The spacing variable used for the N-S separation is the ratio of separation to collector diameter.

A calculation of the costs for the array considered in 3.6.3 was performed with the layout of the array changed to rectangular, in order to compare directly with figure 3.6. To allow strict comparison, it was assumed that the site available for the power station was in fact square and two arrays of the form shown in figure 3.10 fed thermochemicals to a central location. Pipe costs for the array were evaluated according to Williams and the N-S spacing in the array was chosen using the simplified method of section 3.6.5.

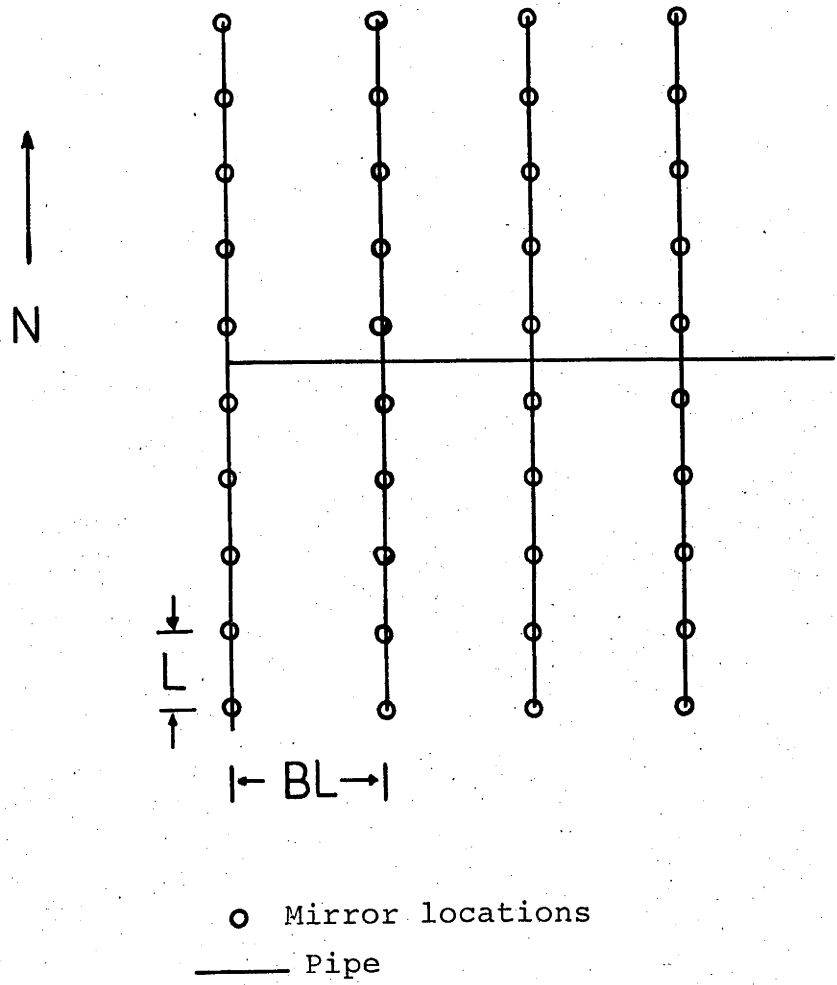


Figure 3.10 Layout of pipes considered for rectangular array.

3.7.3 North-South Spacing.

Shading for an isolated row of N-S collectors was calculated using the program of appendix A. In this case the spacing variable chosen was the ratio of collector separation to collector diameter, L/D . The illumination function for this array, $f(L/D)$ is shown in figure 3.11. A row of 11 collectors located in the Southern Hemisphere was used in the calculations, with the shaded collector being the southernmost of the row.

Using equation 3.24, a figure similar to figure 3.9 can be generated, as shown in figure 3.12. It is assumed that a separation of $1.05D$ is necessary for logistic purposes and optimum separations are not shown below this value.

3.7.4 Electricity Costs For A Rectangular Array.

In this calculation the ground cover ratio is varied by holding the N-S separation constant and varying the E-W spacing, labelled BL in figure 3.10. The area occupied is maintained square by adjusting the number of collectors in each N-S row. Pipe costs were generated as a function of B from eqtns (3.20) and (3.21). The illumination function was calculated as a function of B for specific N-S separations as shown in figure 3.13.

The combination of this information gives costs as shown in figure 3.14, as a direct comparison with the data in figure 3.6. For the middle line at a ground cover ratio of .384, the rectangular array reduces to a square array and costs are similar. At higher ground cover ratios the asymmetry of the

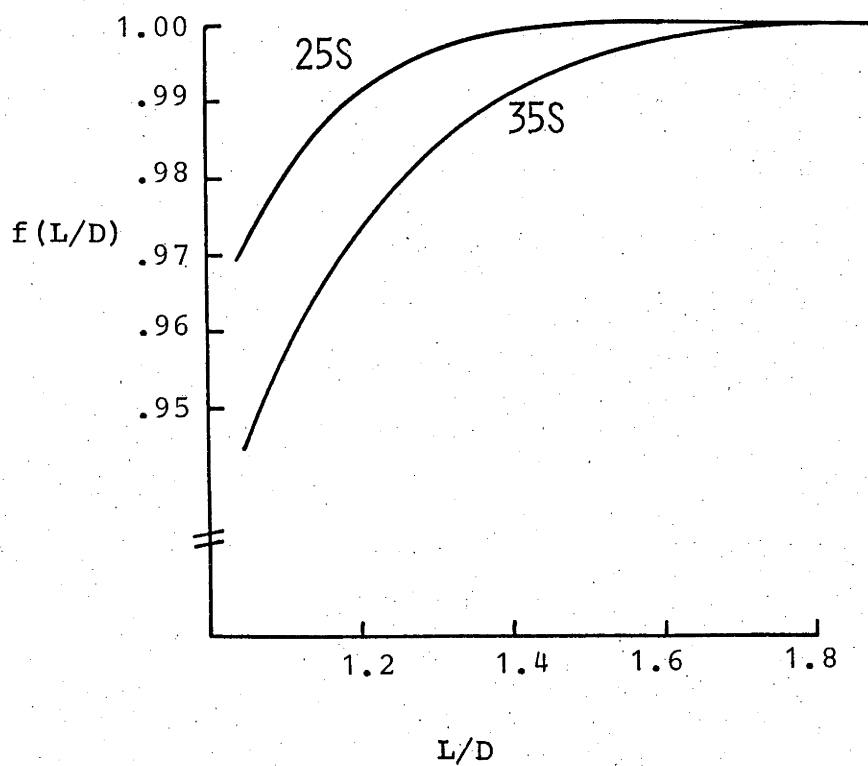


Figure 3.11 Variation of shading for an isolated N-S row of collectors. The illumination function for a row, $f(L/D)$, is the yearly average of the fraction of the collector aperture illuminated.

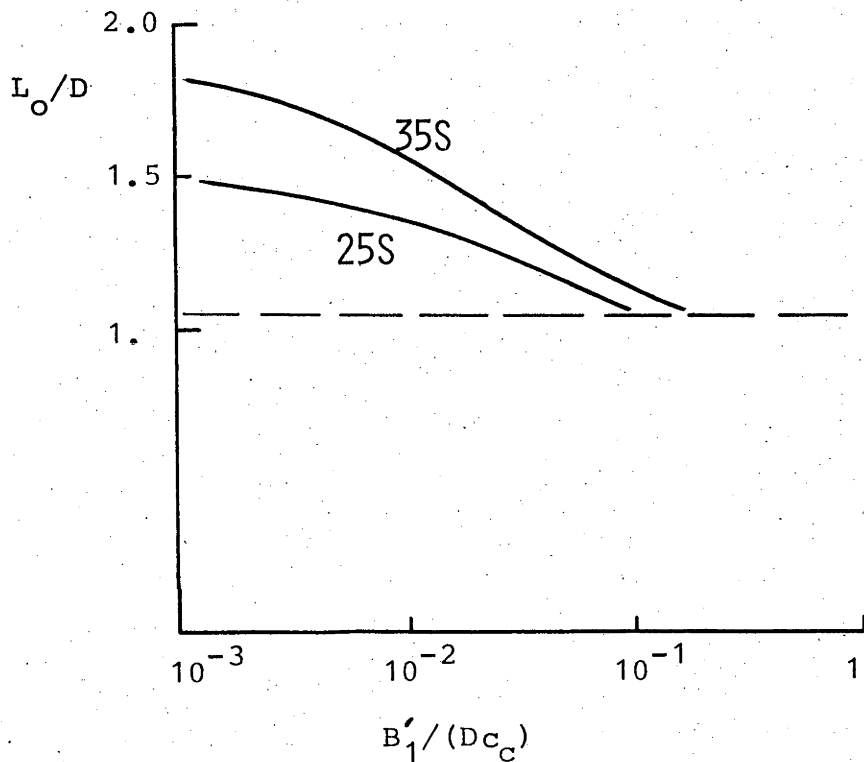


Figure 3.12 Spacing to minimise energy cost for an isolated row of collectors. It is assumed that a minimum separation of $1.05D$ is required for logistic purposes. The subscript o indicates an optimum value for L .

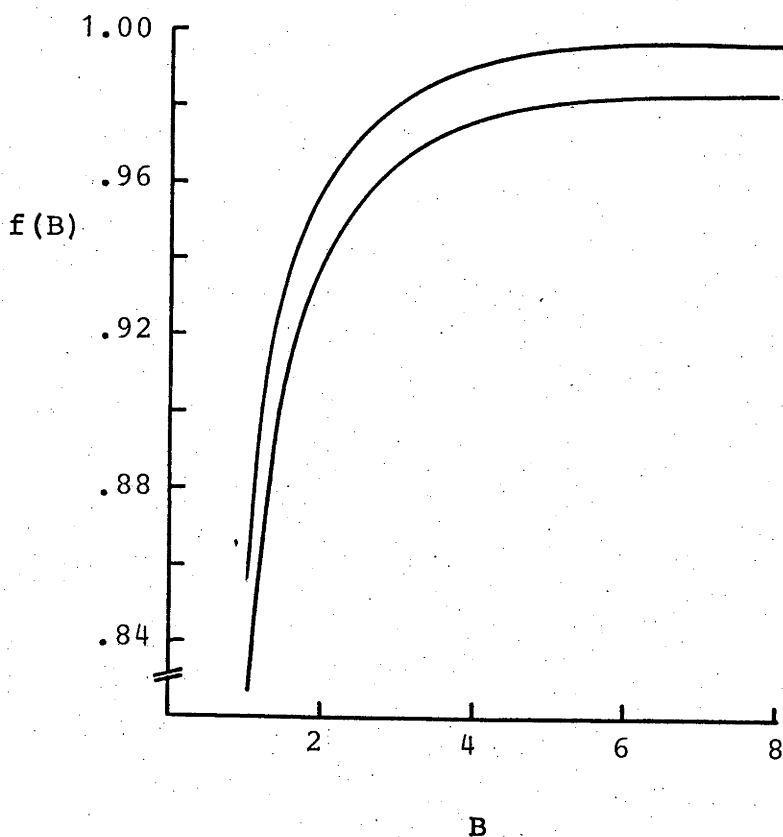


Figure 3.13 Shading variation with E-W spacing.
 Upper line; N-S separation is 1.27D for 25S latitude, and 1.43D for 35S. Information for both latitudes is essentially coincident.
 Lower line; 35S latitude with N-S separation 1.28D.
 B is the ratio of the E-W separation to the N-S separation.

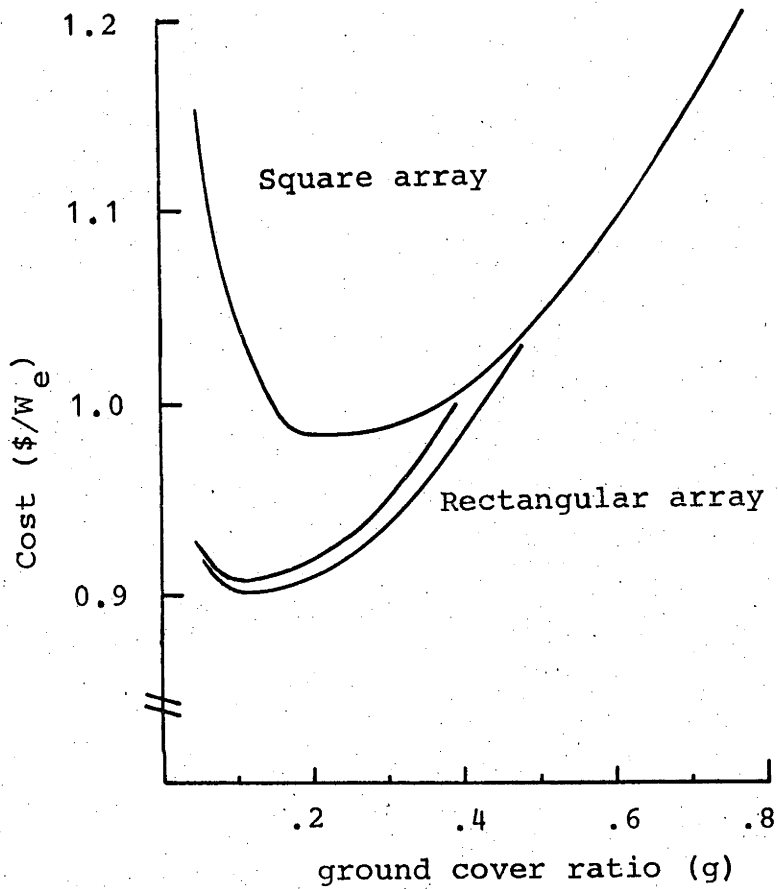


Figure 3.14 Variation of costs with spacing for rectangular arrays. Parameter values are identical to those of figure 3.6.
 Upper line; costs for square array.
 Middle line; costs for rectangular array, N-S separation 1.43D.
 Lower line; costs for rectangular array, N-S separation 1.28D.

array involves larger N-S distances than E-W distances: this is not desirable since costs are larger than for a square array. Clearly from the figure the rectangular array has a cost advantage which is not lessened by the knowledge that the pipe layout chosen is not necessarily optimum and only the initial stages of an optimisation have been performed.

The bottom line of figure 3.14 is calculated using a North-South separation of $1.28D$ which is the optimum separation in an isolated North-South row of collectors with the parameter values of figure 3.6, calculated from figure 3.12. Only a small cost penalty is paid if the non-optimum N-S separation of $1.43D$ is used and this result has been foreshadowed by the information in figures 3.6 and 3.14, where the slope of the curve is low on the side where spacings are larger than the optimum.

We note that the minimum costs predicted by this procedure occur at even lower ground cover ratios than were found for square arrays: this is a consequence of the relatively small costs involved in E-W trunks.

Since the size of the E-W trunk will vary considerably from one segment to another, further savings can be expected by adjusting each E-W segment length individually using the procedure of section 3.6.5.

3.7.5 Further Calculations On Isolated N-S Rows.

The diminished number of variables in a N-S row allows the possibility of performing a complete minimisation by allowing separation between collectors to be non-uniform,

while still considering the complete equation 3.3. The analytical method for minimising pipe costs of Williams is applicable only for uniform spacing, ie L_k independent of k . In this case, however, both L_k and d_k are chosen to minimise costs. The cost penalty of using uniform spacing for this array is derived.

The array considered is a simple row of collectors, oriented N-S. In specific calculations, an array of 10, 5m diameter collectors was considered. B_1 was taken as 10\$/m, and collector cost set at 50\$/m². I_e in equation 3.3 was minimised for two cases, firstly with the collector separation non-uniform and secondly with uniform spacing. The decrease in cost achieved with variable separation along the row of collectors was less than .01%, and this negligible reduction can be expected as long as costs due to B_2 remain second order. The resultant spacings and pipe diameters are shown in figure 3.15. The accuracy of eqtn 3.24 was checked using an estimate for B_1' of:

$$B_1' = B_1 + 2B_2 d_k^2 \quad (3.27)$$

The spacing calculated using (3.27) and figure 3.11 coincided with the data of figure 3.15.

3.8 Discussion And Conclusion

This chapter has demonstrated the importance of the cost per unit length of the links between collectors in an array,

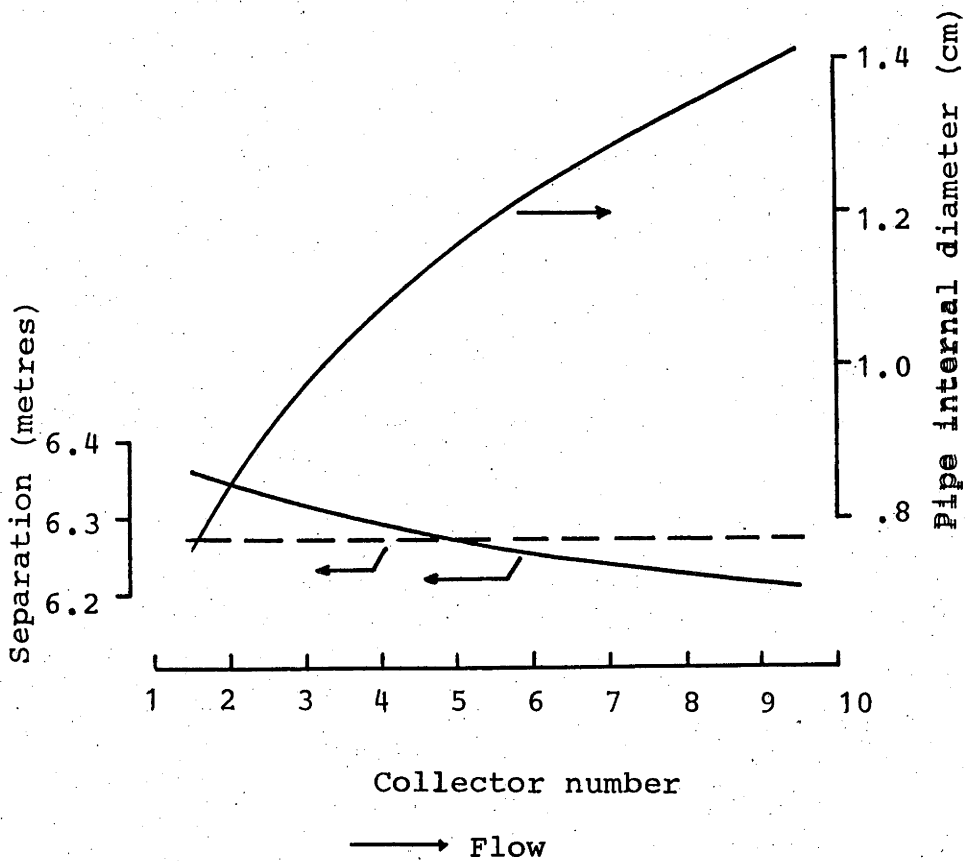


Figure 3.15 Minimum energy cost pipe diameters and collector separations for an isolated row of 10 collectors. The pipe segment from collector 9 to collector 10 carries the most flow in the array. Pipe diameters were the same for both equal and unequal collector separation. $D=5\text{m}$; 35S latitude; $B_1=10\$/\text{m}$; $c=50\$/\text{m}$, $B_2=6630\$/\text{m}^3$.

be they pipes, cables or both. This value determines the optimum spacing and network costs can contribute significantly to the total cost of electricity. A simple technique for evaluating the optimum spacing has been described and graphs relating the estimated cost per unit length to the optimum spacing via the collector diameter and cost have been given.

Ground cover ratios are significantly smaller than previously accepted values (Caputo 1975). Rectangular arrays are shown to have potential for lower costs than square arrays and in one case analysed, costs due to collectors and links were reduced by 8%. Optimum ground cover ratios for rectangular arrays were smaller than those for square arrays and in the case analysed, the ground cover ratio was .1 for the rectangular array and .23 for the square array.

As stated by Williams (1978), a different installation technique is required to overcome the high cost of pipe installation as estimated by Black and Veatch (1974). This cost was presumably determined by the number of footings and pipe joints, as telephone cable installed in trenches costs only 1\$/m (Dubberley, 1977), while installed .5 inch pipe costs 32\$/m (Black and Veatch, 1974). There is an advantage in being able to reel out the pipes in unlimited lengths, with minimal attention to footing, as is done for cables, and this would be possible if tubes up to 6mm OD were employed. Carden (1977) has shown that such tubes are appropriate for thermochemical systems employing high pressure gases and liquids. Using the same trench, or footing, for both pipes and cables would also save money.

This optimisation has application to any distributed system where energy is to be transferred to a central point with negligible energy is lost in transit. For example, Caputo(1975) suggests a scheme where a Brayton engine and generator is located at each collector and energy is transferred in the form of electricity to the central plant by Aluminium cables. He estimates that these cables cost 32\$/m(1974\$US) to buy and install, of which 90% is installation cost. The optimum ground cover ratio for this situation can be determined from figure 3.9 with B_1' at 16\$/m.

4.0 CAVITY ABSORBER EFFICIENCY.

4.1 Introduction

The efficiency with which the absorber at the focus of a paraboloidal dish collects the energy reflected to it is an important parameter. In this chapter we examine this efficiency as a function of sun following errors, paraboloid contour errors and absorber design. This information is necessary to determine the values of the above three variables which will produce energy for minimum cost. The value of the sun following error is particularly important as it in turn determines the rigidity of the collector structure and the sophistication of the servo equipment controlling the collector orientation. Thus this study is essential before one can determine an allowable sun following error and set reasonable standards for the manufacture of the collectors.

Previous authors, eg Lof and Duffie(1963), do not appear to have considered the influence of sun following errors on radiation collection and the inclusion of this effect is an important extension of their work. The present study has benefited from the experiments of Weiss(1978) who has determined the radiation, convection and conduction losses from a specific type of cavity absorber. His data is used as a guide to reasonable values of losses from cavity absorbers.

Experimental and theoretical studies of the radiation field in the focal plane of a paraboloid have been published in a series of papers in the Russian journal *Geliotekhnika*, eg Zakhidov and Vainer(1974). These studies have been used

herein as the basis for determining the radiation field in the focal plane. The amount of energy captured by a cavity absorber of a specific size has then been calculated and the losses subtracted. The 'absorber efficiency' is then assessed as the ratio of the energy absorbed to the energy directed at the absorber. The size of the cavity is chosen to maximise the absorber efficiency. In these calculations account is taken of the collector surface accuracy and sun following errors in determining the radiation field and hence the energy captured by the absorber. Data is given which relates absorber efficiency to collector surface accuracy, the sun following error, and the magnitude of absorber losses.

4.2 General.

The energy absorber is the interface between a radiation field and an energy absorbing fluid and as such must take into account the characteristics of both. The temperature profile of enthalpy changes of a thermochemical working fluid is shown in figure 4.1 for the ammonia/nitrogen-hydrogen system (Carden and Williams 1978). Most of the energy is absorbed over one high temperature region and a small fraction absorbed at moderate temperatures. An absorber design that provides energy with this particular temperature distribution would be optimal. A simple solution to the problem of providing a large amount of energy at a high temperature involves the use of a cavity and only this option is considered here.

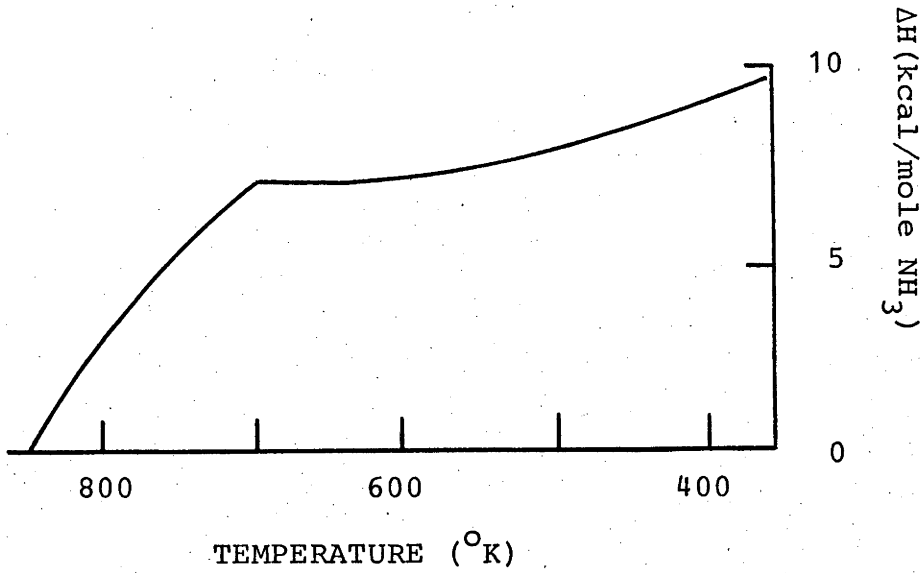


Figure 4.1 Temperature profile of enthalpy changes of a thermochemical working fluid (Carden and Williams, 1978), for the ammonia/nitrogen hydrogen system.

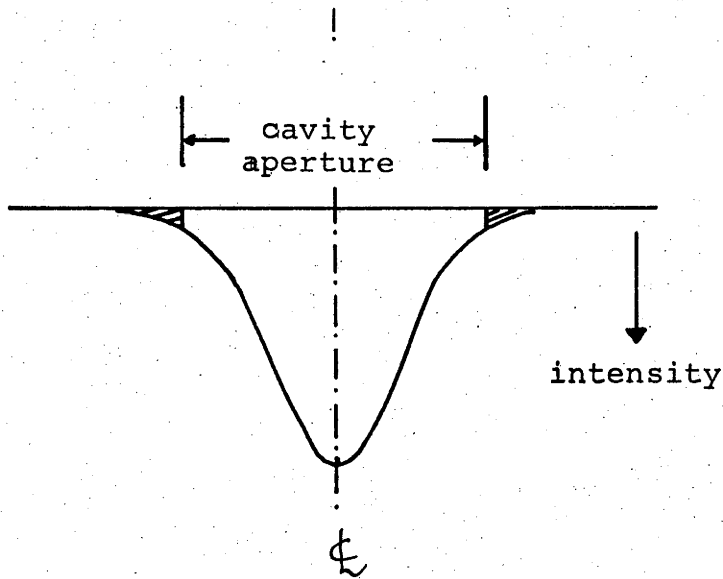


Figure 4.2 Radiation flux crossing focal plane and sizing of cavity to maximise absorption. Hatched area indicates energy not absorbed by the cavity.

The radiation intensity in the focal plane is axisymmetric and is approximated by a Gaussian profile, as shown in figure 4.2. The angular diameter of the sun and errors in the collector surface determine the half width of the profile. The effect of sun following errors, provided they are isotropic, is to produce a distribution which when averaged over time is also Gaussian, but with a larger half width.

The cavity must be sized so that not all the radiation is collected, as increasing the absorber aperture to include the radiation in the wings of the Gaussian profile involves extra losses which are greater than the extra radiation collected. The resulting situation is depicted in figure 4.2, where the hatched region is the radiation not absorbed due to the size of the cavity aperture. However, it is not necessary that this is a loss since the thermochemical working fluid requires some low temperature heat. This requirement could be met by placing absorbing tubes operating at low temperatures outside the cavity in the hatched region of figure 4.2.

4.3 Absorber Efficiency

The coordinates used in the following discussion are shown in figure 4.3. The energy striking the absorber is given by:

$$\dot{Q}_{in} = \eta \pi \left(\frac{p \sin U}{1 + \cos U} \right)^2 I_0 \quad (4.1)$$

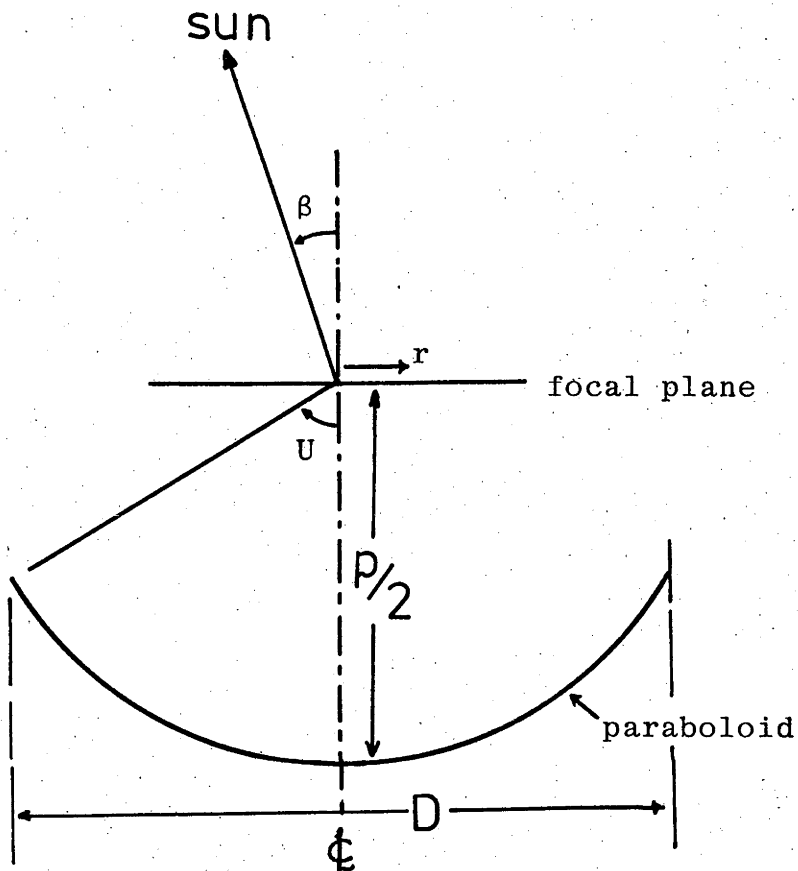


Figure 4.3 Coordinates used in paper.
 U is the rim angle of the paraboloid
 p is the focal parameter, equal to twice the focal length.
 r is the radius in the focal plane
 β is the misalignment angle
 D is the collector diameter.

where the aperture diameter D has been expressed in terms of U and p , ρ is the reflectivity of the mirror surface, I the direct solar intensity, U the angle between the mirror axis and a line from the rim to the focus (the rim angle), and p is the focal parameter, which is twice the focal length. The capture ratio η indicates the fraction of the energy directed towards the absorber which actually enters the cavity aperture.

The power which can be extracted from the absorber is expressed as:

$$\dot{Q} = \eta(\text{eff}) \pi \left(\frac{p \sin U}{1 + \cos U} \right)^2 I \rho \quad (4.2)$$

where $\eta(\text{eff})$ is an effective capture ratio and includes the capture ratio η and the magnitude of absorber losses.

Weiss(1978) has studied the losses of the cavity shown in Figure 4.4. For this cavity operating at 973K, losses are 20W for each square cm of cavity aperture. This figure is useful as a guide to the expected magnitude of cavity absorber losses. The following calculations assume no specific cavity design, only that cavity losses are proportional to cavity aperture area, the constant of proportionality being \dot{q}_ℓ . This assumption is justified later in 4.8.2.

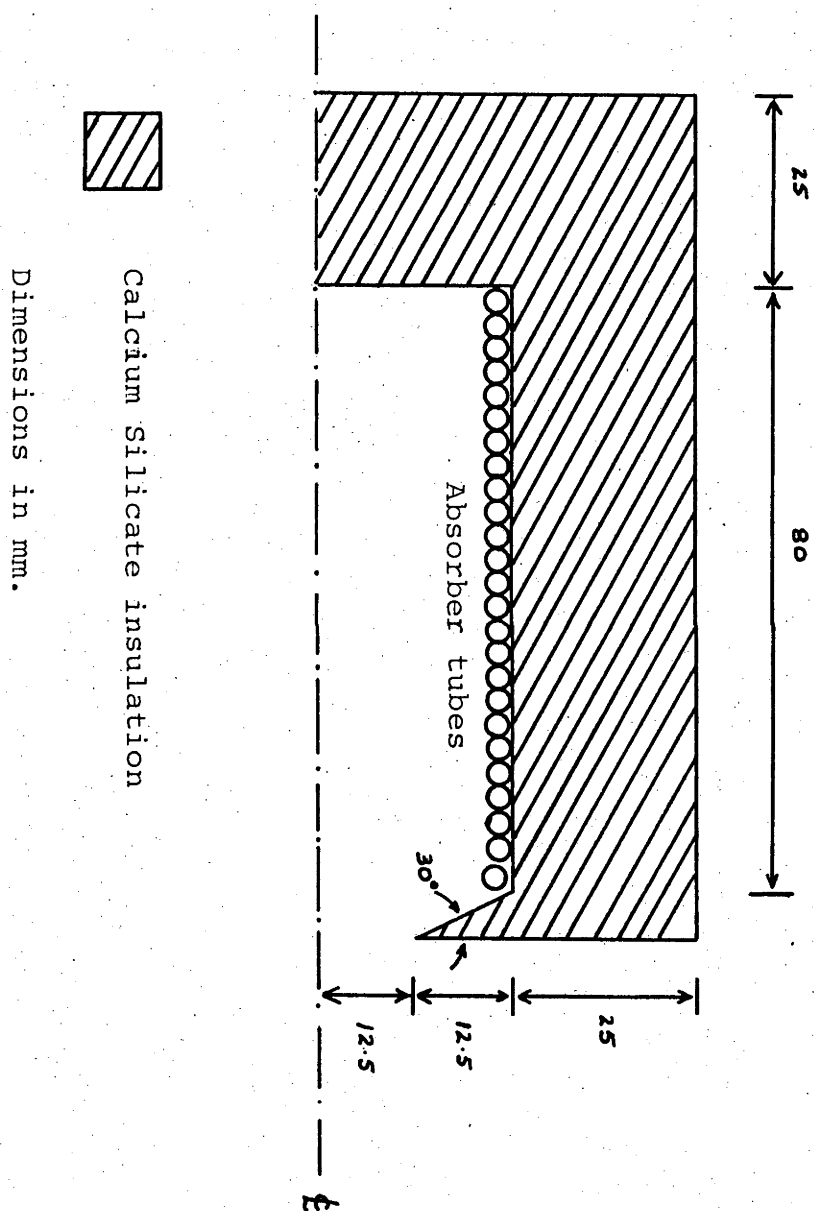


Figure 4.4 Cavity design studied by Weiss(1978).

The total losses of the cavity are given by \dot{Q}_ℓ , and thus from (4.1) and (4.2):

$$\eta(\text{eff}) = \eta \left(1.0 - \frac{\dot{Q}_\ell}{Q_{\text{in}}} \right) \quad (4.3)$$

The evaluation of $\eta(\text{eff})$ is hindered only by the complexity of the capture ratio η . This is evaluated in two parts: firstly, the radiation flux field in the focal plane is calculated as a function of the contour errors in the reflective surface in section 4.4 and secondly, the sun following errors are incorporated by averaging the radiation field over time for the expected distribution of sun following errors in section 4.5. The capture ratio is expressed as a function of the cavity aperture radius.

4.4 Radiation Field In The Absence Of Following Errors

The calculation of the radiation field follows the work of Teplyakov and Poluektov(1968), and is based on the similarity of the field in two generalised coordinates, the generalised radius R , related to the radius r in the focal plane and the generalised misalignment angle B . The derivation of these coordinates is covered fully by Teplyakov and Poluektov(1968) and will not be reproduced here. The coordinates are derived in terms of r , the angle β by which the paraboloid is misaligned, an accuracy parameter h and the focal parameter, p , (see figure 4.3). The relationships

are: (1)

$$R = hr/p \quad (4.4)$$

$$B = h \beta$$

The parameter h was introduced into radiation field calculations as a mathematical convenience. The source of the parameter is a calculation of the radiation distribution in the focal plane (see for example Teplyakov and Poluektov, 1968) in which it is assumed that the beam reflected from each part of the mirror surface has a Gaussian intensity distribution, namely:

$$I(a) = h/\pi \exp(-h^2 a^2) \quad (4.5)$$

where a is the angle from the centre of the beam and the centre of the beam is assumed to pass through the focus. These assumptions are chosen to simulate the real situation where the intensity distribution across the beam corresponds to that of the sun, though the reflecting surface is not perfect and thus the centre of the beam does not necessarily pass through the focus. Thus it is seen that the assumptions

(1): These Soviet papers appear to confuse the reader with units, for example h commonly has dimensions of (1/deg), and thus R commonly is also in (1/deg). B is usually given in units of radians, when radians/degree is intended.

of this method do not correspond with reality. However, the mathematical consequences of this assumption, as far as the radiation field in the focal plane is concerned, agree well with experimental and other theoretical calculations.

The radiation field in the focal plane is derived by Zakhidov (1965) using the above assumptions, integrating the flux from each element of the paraboloid for each element of the cavity aperture. The derived expression is:

$$E(r) = (180h/\pi)^2 I \rho \sin^2 U \exp(-(180/\pi)^2 (1+\cos U)^2 R^2) \quad (4.6)$$

where $E(r)$ is the radiation intensity at radius r . From the exponential term it can be seen that the larger the rim angle, the larger the width of the Gaussian profile, while the more accurate the mirror (larger h and thus R), the narrower the Gaussian profile. The leading constants ensure that the integral of the expression equals the energy input.

In a practical application a value for h is not known and for an operational paraboloid a value for h is obtained by comparing eqn (4.6) with an experimental determination of the radiation field of the paraboloid.

The relationship between h and a measurable property of the collector, the rms contour errors, is given in figure 4.5.

Zakhidov and Vainer (1974) calculate the radiation distribution in the focal plane using the more realistic assumptions that slope errors are distributed according to a Gaussian distribution, reflection is perfect at the mirror surface and that the sun has finite size and the limbs of the

sun are darker than the centre.

Their results are obtained by numerical integration and cannot be expressed analytically. Because of the simplicity of (4.6), Zakhidov and Vainer compared the formula with their own calculations and found it reasonable provided slope errors were present. The radiation distribution was not well approximated by (4.6) for meridional(radial) errors of less than 12 minutes, which corresponds to equal meridional and sagittal(hoop) errors of less than 8 minutes, both situations corresponding to an h of 3.6. The relationship between the accuracy parameter h and the rms sagittal and meridional slope errors is shown in figure 4.5 (Zakhidov and Vainer 1974).

Further confirmation of the appropriateness of (4.6) is given by Zakhidov(1977) who reports that experimental investigations confirm that the formula (4.6) is a satisfactory representation of the irradiance distribution in the focal plane. Teplyakov(1973) reports its appropriateness for rim angles from 40-70degrees. The formula is not appropriate for larger rim angles (Baum and Mamedniyazov, 1977). With this justification, in the following we assume 4.6 is a reasonable approximation.

The capture ratio for a cavity of radius r is given by:

$$\eta = \frac{\int_0^r E(s) ds}{\int_0^\infty E(s) ds} \quad (4.7)$$

and thus, from eqtns 4.6 and 4.7:

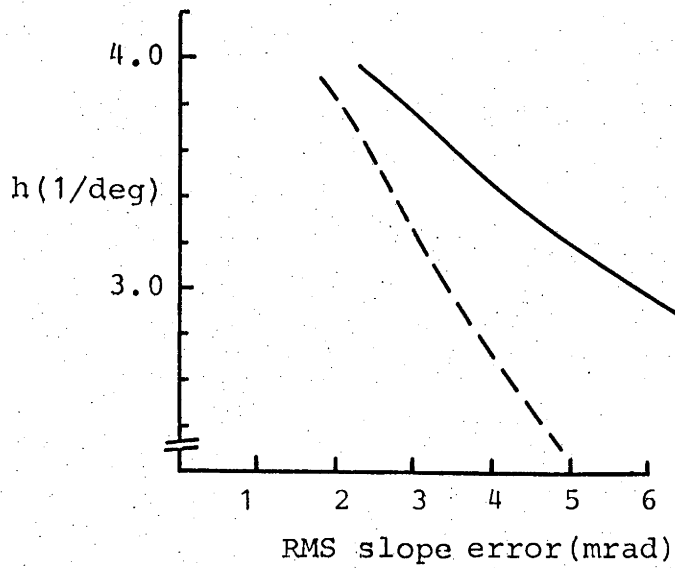


Figure 4.5 Variation of h as a function of the rms slope errors (Zakhidov and Vainer (1974)).
Unbroken line: no sagittal (hoop) errors.
Dashed line: isotropic slope errors.

$$\eta = 1.0 - \exp\left(-\left(\frac{180}{\pi}\right)^2 (1+\cos U)^2 R^2\right) \quad (4.8)$$

4.5 Influence Of Sun Following Errors On The Radiation Field.

Zakhidov and Teplyakov(1966) have included sun following errors by approximating the effect of a dynamic focal radiation pattern with an effective static radiation pattern. The effective pattern is assumed to be Gaussian and is described by the usual equation with an accuracy parameter $h(B)$ in place of h . The value of $h(B)$ is calculated by evaluating the average maximum intensity at the focal spot and comparing with the intensity when no misalignment is present, given by:

$$I(\max) = \left(\frac{180h}{\pi}\right)^2 I_{\rho} \sin^2 U \quad (4.9)$$

The average intensity in the dynamic situation is given by Zakhidov and Teplyakov(1966) as:

$$I(\max) = I_{\rho} \sin^2 U \left(\frac{180h}{\pi}\right)^2 \frac{1}{T} \int_0^T \exp\left(-\left(\frac{180 B(t)}{\pi}\right)^2\right) dt \quad (4.10)$$

There are many causes of misalignment errors, including structural deflections due to winds and thermal effects, servo errors and so on. The combination of these independent errors will produce sun following errors which are distributed in a

near Gaussian relation and so we assume here that $B(t)$ is drawn from a Gaussian distribution of standard deviation σ . Thus by evaluating (4.10) and comparing with (4.9):

$$h(B)^2 = \frac{h^2}{2\sigma^2} \left[\left(\frac{180}{\pi} \right)^2 + \frac{1}{2\sigma^2} \right]^{-1} \quad (4.11)$$

With this value for h , equation (4.8) can be used to estimate the capture ratio in the presence of sun following errors.

The influence of sun following errors on the radiation field has also been considered by Teplyakov and Poluektov (1968), who suggest a relationship between the capture ratio at zero misalignment and the capture ratio at a specific misalignment, based on both experimental and theoretical calculations. The average capture ratio was evaluated using this relationship and the same variation of B with time as was used to generate eqtn (4.11). Agreement was to within 5% over the range of B up to .05 (rad/deg) and for R over the suitable range of .02-.03 (1/deg).

4.6 Procedure.

The aim is to evaluate the efficiency $\eta(\text{eff})$ of the absorber as a function of contour tolerance (related to h), sun following errors (β), cavity losses (Q_c), and cavity radius. To calculate $\eta(\text{eff})$, via eqtn 4.3, requires that the capture ratio η be calculated. This is given in eqtn 4.9 as a function of R , itself a function of h and r . In considering the effects of sun following errors, we use $h(B)$ from 4.11 instead of h .

The cavity radius can be chosen to maximise $\eta(\text{eff})$, given values of the other variables h , σ_β , and \dot{q}_ℓ . A range of cavity designs is considered by taking \dot{q}_ℓ as 5, 10 and 20W for each square cm of absorber aperture. These losses were used in equation 4.5 to evaluate $\eta(\text{eff})$. It should be noted that a black body at 973K emits energy at the rate of $5\text{W}/\text{cm}^2$ and this sets a reasonable lower limit for the losses.

4.7 Results

4.7.1 Capture Ratio

The majority of the chapter is devoted to calculating the capture ratio and this quantity is made available for general use by expressing equation 4.8 in the form:

$$\eta = 1.0 - \exp(-A^*/A) \quad (4.12)$$

where the concentration ratio A is the ratio of collector aperture area to cavity aperture area. A^* is the concentration ratio which would produce a capture ratio of 0.63. From equation 4.8, A^* is given by:

$$A^* = (180/\pi)^2 \sin^2 U h^2(B) \quad (4.13)$$

With $h(B)$ given by (4.11) and a collector rim angle of 60 degrees, the variation of A^* with both collector surface accuracy h and standard deviation of sun following errors σ_β is given in figure 4.6. This diagram and equation 4.12 can

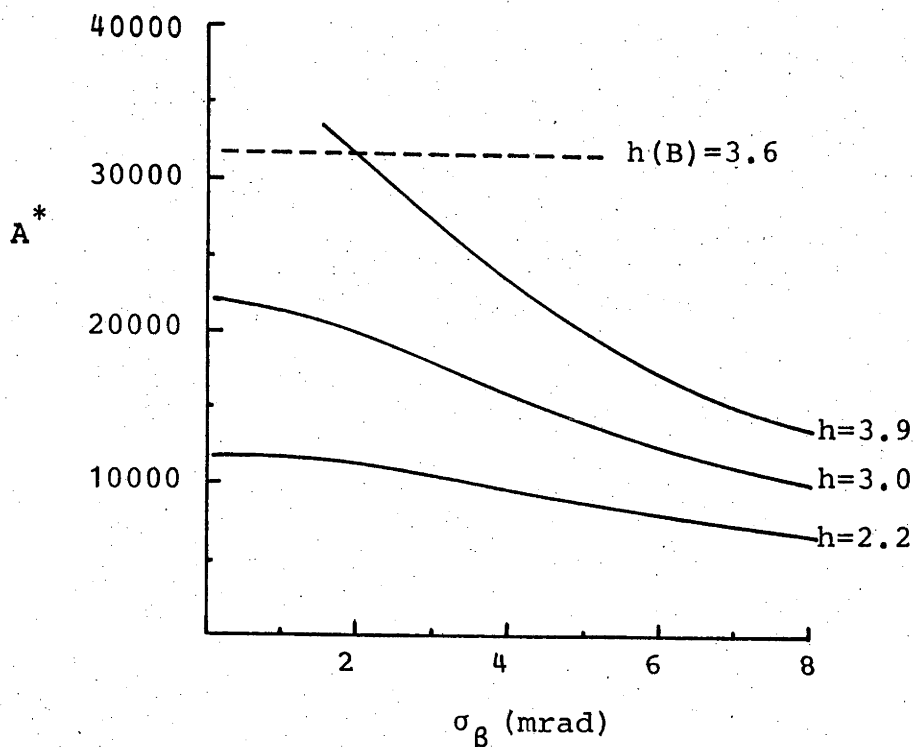


Figure 4.6 Variation of the concentration ratio A^* as a function of sun following errors and collector surface accuracy. A cavity/collector system with a concentration ratio of A^* will have a capture ratio of 0.63. Other capture ratios can be calculated using equation 4.12. The horizontal line drawn indicates the limit of the approximations used.

give the capture ratio with little calculation for any concentration ratio and any combination of σ_β and h . The limit of applicability of the equations used in determining figure 4.6 as suggested by Zakhidov and Vainer(1974) is indicated by the horizontal line at $A = 31000$ which is equivalent to $h(B) = 3.6$.

4.7.2 Maximum Possible Cavity Efficiency.

The value of $\eta(\text{eff})$ is shown as a function of the absorber generalised radius in figure 4.7 for a relatively accurate mirror with $h = 3.9$ which corresponds to isotropic surface errors of 1.7mrad. As in all following examples, the collector rim angle is 60 degrees. As expected, the choice of the absorber radius for maximum power absorption becomes more critical as the accuracy of sun following increases. Although the approximately 0.5% difference in ultimate performance between a collector which follows to 2mrad accuracy and one which follows to 1mrad accuracy may appear trivial, this 0.5% will reflect directly into installed capital costs.

The maximum possible $\eta(\text{eff})$ was calculated as a function of the accuracy of the mirror surface (h), the losses of the cavity (\dot{q}_ℓ) and the standard deviation of sun following errors (σ_β). These values of $\eta(\text{eff})$ are presented in figure 4.8. The radius of the cavity aperture required to achieve these values of $\eta(\text{eff})$ is shown in figure 4.9. Also shown as an ordinate in figure 4.9 is the concentration ratio of the collector/cavity system as defined below in equation 4.12.

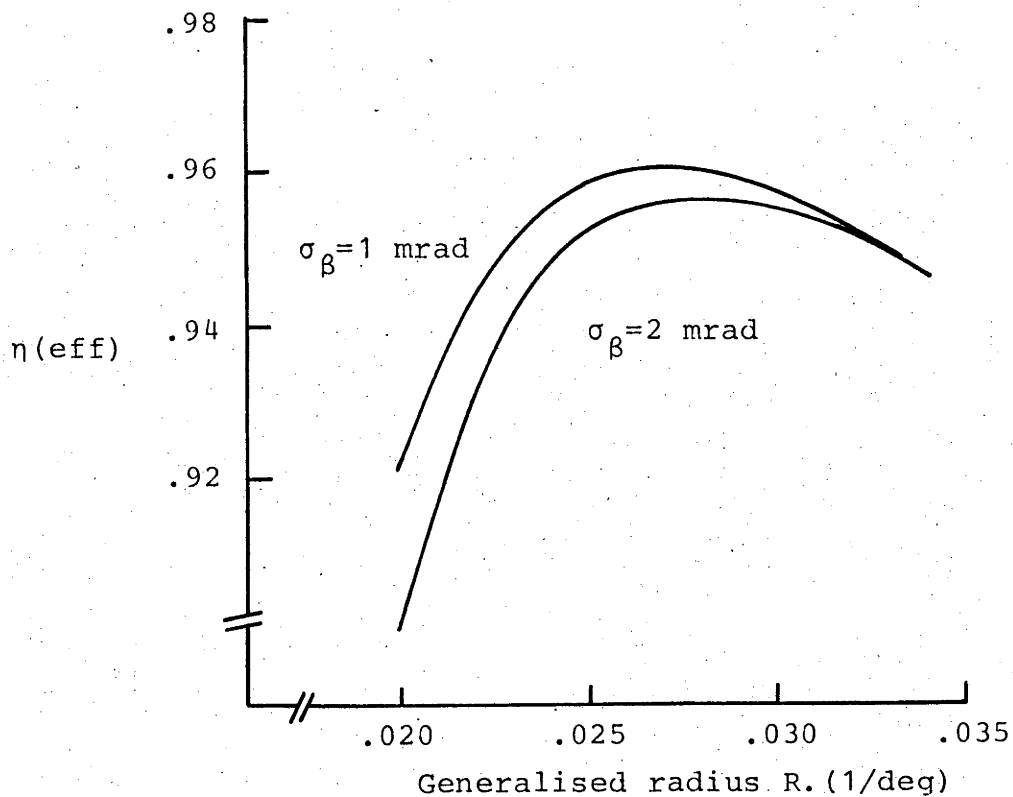


Figure 4.7 Variation of the effective capture ratio with generalised radius R . Precision parameter $h=3.9$, Collector rim angle 60° . σ_β is the standard deviation of the sun following errors. Cavity losses 20 W/cm^2 , surface reflectivity 85% , solar intensity 1 kW/m^2 .

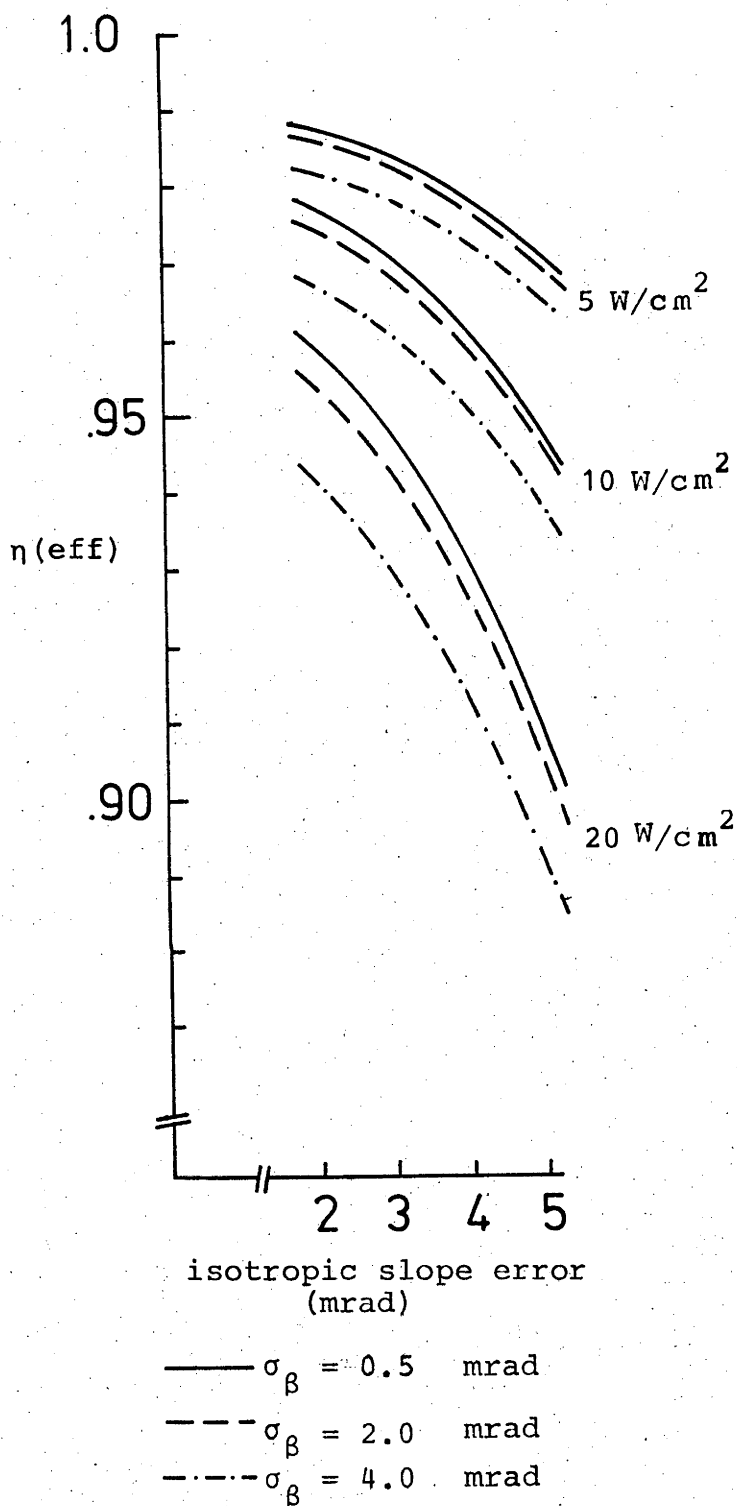


Figure 4.8 Variation of the maximum possible effective capture ratio as a function of the standard deviation of sun following errors, σ_β , the paraboloid surface accuracy, and the absorber losses which are rated per unit area of cavity aperture. Collector rim angle 60 degrees.

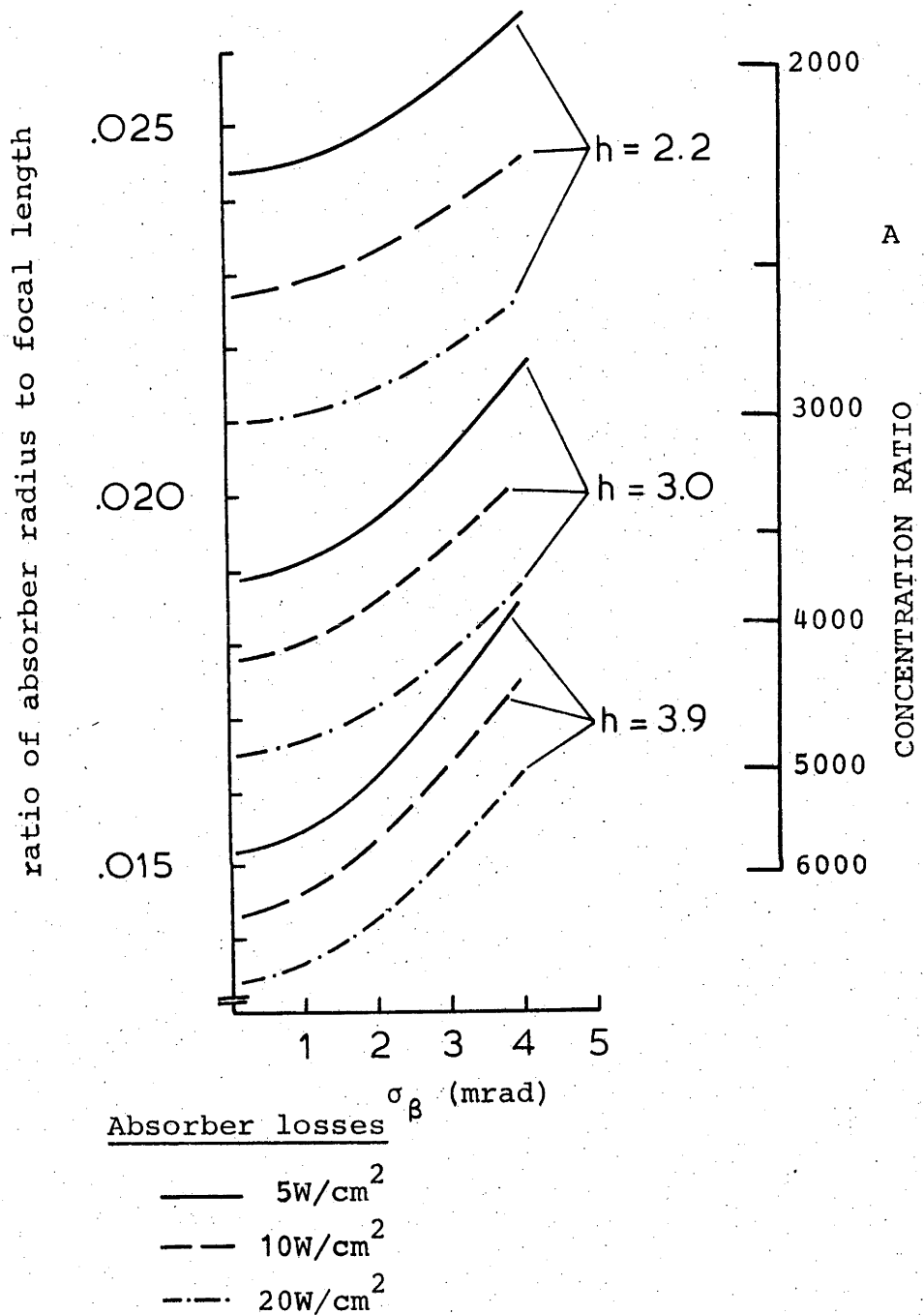


Figure 4.9 Variation of the ratio of the absorber aperture radius to the focal length as a function of the absorber losses, the paraboloid surface accuracy, and the standard deviation of the sun following errors. Absorber losses are rated per unit area of absorber aperture. A is the concentration ratio of the cavity.

4.8 Discussion.

Discussion of Results

Firstly, referring to figure 4.9, there is no obvious point at which increasing the accuracy of the collector surface will yield no benefit. It is, however, possible that this result is a corollary of the assumption that the radiation field has a Gaussian shape, which was observed not to hold for very accurate concentrators. According to Zakhidov and Vainer(1974), the data displayed for collector surface errors of 1.74 mrad and sun following errors of 2mrad, is at the limit of the approximation used.

Secondly, the information contained in Figures 4.8 and 4.9 is the starting point for determining the allowable sun following errors, the appropriate surface accuracy specification and the absorber design. Combining the information of figures 4.8 and 4.9 with estimates of the cost of the collector structure and guidance system as a function of sun following error will determine the cost effective sun following error specification. Similarly, information on the cost of the absorber, which will be a function of the absorber losses, can be used to determine appropriate absorber design criteria. The collector surface accuracy can be similarly handled.

4.8.1 Use Of Data.

1. Cavity designers with an awareness of cavity losses and collector parameters such as h and σ_{β} will be able to determine the maximum possible efficiency for their design from figure 4.8 and the cavity radius to achieve that efficiency from figure 4.9.

2. Cavity designers who wish to perform their own radius choice may use the information from figure 4.6 and equation 4.12 to determine the capture ratio for input to their own calculations.

4.8.2 Generality Of Assumptions.

The main assumption quoted is that losses are proportional to the area of the cavity aperture. There are three main losses which can be considered here. Firstly radiation losses through the cavity aperture which will most likely be proportional to cavity aperture area. Secondly, conduction losses through the insulation around the cavity which will depend on insulation design and may or may not be proportional to cavity aperture area. Finally, losses due to the shading of the paraboloid by the cavity also may or may not be proportional to cavity aperture area, depending on the way the cavity design is scaled. The results of the chapter, however, may be applied to any function which represents losses by expressing the loss relation as a linear function of

area, namely,

$$\dot{Q}_l = \dot{q}_1 + \dot{q}_2 \pi D^2 / (4A) \quad (4.12)$$

where $\pi D^2 / (4A)$ is the cavity aperture area and \dot{q}_1 and \dot{q}_2 are chosen so that at the optimum aperture area both the magnitude and gradients of the true and approximate loss functions agree. The additive constant \dot{q}_1 will not affect the position of the minimum, and is easily included in the calculation of $\eta(\text{eff})$. With the above conditions and with η being a simple exponential function of area, it can be shown that the minimum calculated using the above approximation will not differ from the minimum calculated with the true function.

Influence of the cavity shading the paraboloid.

The effect of the shading of the central region of the paraboloid can be considered via equation 4.6, with the resultant radiation field in the focal plane being the difference between the radiation field of a paraboloid of rim angle U , and a (fictitious) paraboloid of rim angle U' , where the angle U' delineates the shadow cast by the cavity on the paraboloid. Inspection of the formula 4.6 indicates that the resultant focal plane distribution will be reduced only near the centre. That is, the shadow of the cavity will fall near the focus and as long as the cavity is not unusually small, the energy entering the cavity will be reduced by the amount of radiation blocked by the cavity, adjusted for reflectivity

losses. This loss can be accommodated in the above calculation by increasing \dot{q}_ρ (the losses per unit area of cavity aperture) by an amount proportional to ρI (reflectivity times solar intensity). The constant of proportionality depends on the ratio of the size of the cavity to the size of the cavity aperture. For the design of figure 4.2, losses would be increased by $16\rho I$ per unit cavity aperture area. This adjustment to \dot{q}_ρ would enable the maximum efficiency and optimum cavity size to be obtained from figures 4.8 and 4.9.

5.0 GUIDANCE AND CONTROL SCHEME SELECTION.

5.1 Definitions

Sun sensor: A sun sensor is a device which gives information on the position of the sun relative to its own null axis. The quality of information available on the relative position varies with the types of sun sensor. For example, the information from one sensor may be limited simply to an indication of whether the null axis is leading or lagging the sun. Another sensor may be able to provide the magnitude of the relative direction of the sun, regardless of the position of either the sun or the null axis. Other sensors may yield information falling between these two extremes, with, for example, the magnitude of the relative direction given up to a certain magnitude but beyond that magnitude only the sign of the direction is indicated.

Tracking: Tracking is the process of following the sun in a closed loop relation using real time information from the sun sensor.

Pointing: Pointing is the process whereby the collector is aimed at a point in the sky by calculating appropriate actuator displacements which correspond to the position in the sky and displacing the actuators to those positions. Encoders are used at the actuator axes to determine the actuator position.

Guidance and control scheme: The word scheme is used here in contrast to system (tracking and pointing). A guidance and control scheme is a scheme to control the collectors to perform functions appropriate to the solar power plant operation. These functions include following the sun during energy collection periods and stowage during inclement weather. Guidance and control schemes may utilise either or both of the above systems.

Sun following error: The angle between the optical axis of the collector and the direction of the sun. The sun following error usually varies with time, in which case the term generally refers to an rms value.

5.2 Introduction.

In this chapter an attempt is made to delineate the costs which vary with the sun following error. This information constitutes an essential part of the optimisation which determines an appropriate sun following error specification for the collector array. The main preoccupation here is with the necessary step of determining a guidance and control scheme which can achieve a sun following error specification at the lowest cost.

In particular it is shown that the selection of an economical guidance and control scheme relies principally on two considerations:

Firstly the use of control loops which can compensate for structural deflections, thus allowing less rigid collector structures to be specified, resulting in a cost saving. This compensation is most easily achieved using a tracking system.

Secondly, it is shown that alignment costs for guidance and control schemes which do not have a sun sensor are large and that, in contrast, alignment of collectors capable of tracking can be accomplished cheaply.

It is shown that a guidance and control scheme relying only on tracking would not be appropriate and that a rudimentary pointing system must be incorporated to achieve effective guidance and control.

First a general discussion on the abilities of pointing and tracking systems, with emphasis on the causes of sun following error in each is presented. The sources of sun following error are considered in detail and the implications

on costs of sun following error specifications are examined. In some cases this requires detailed analyses of possible methods and equipment. It is shown that a guidance and control scheme relying solely on pointing is comparatively uneconomic, principally due to the ability of the tracking system to easily compensate for a large proportion of deflections due to wind gusts. This reduces the required rigidity of the collector, which results in a large advantage. A further advantage of a guidance and control scheme incorporating tracking over a scheme incorporating pointing only is in the costs of alignment. Alignment methods are analysed and costs projected for both schemes. An alignment method which can be used only in conjunction with a sun sensor is costed.

The results of this analysis for paraboloidal collectors are compared with the proposed guidance and control schemes for the heliostats used in the USA central receiver approach.

The design and implementation of the guidance and control scheme is discussed and it is shown that the system could be economically configured in a microprocessor-based module at each collector. There are two locations of 'intelligence' in the guidance and control scheme; at the collector and at the central control. A section is devoted to discussing where each guidance and control function should be performed.

Finally the variation of costs with error specification is discussed and it is shown that the primary consideration is the capital cost of the collector structure, the guidance and

control costs being relatively minor in extent.

5.3 Guidance And Control Scheme Properties.

The obvious function of a guidance and control scheme is to align the optical axis of the collector with the sun when energy collection is desired. An equally important function is to extend the useful life of the collector where possible. Conditions which may damage the collector include strong winds, in which wind loadings may cause structural failure and wind borne particles may damage the mirror surface. There will be a particular orientation, a stow position, which will reduce drag coefficients and thus alleviate wind loads and there will be some position(s) which reduces abrasion. The cost of collectors is such that collector damage must be reduced to low levels and a capability to assume a stow position seems essential.

It is improbable that the control at each collector (or 'local control') would itself have sufficient intelligence to anticipate strong winds and thus determine when to stow, or even to indicate which stow position to assume. Thus each collector must be capable of receiving a command to stow from the central supervisory machine or 'central control'. This communication link, once established, may be used for other purposes, such as maintenance and performance monitoring.

A guidance and control scheme based on a pointing system alone can perform all of the required guidance and control functions, but could not be based on a tracking system alone,

as some pointing system is required, at least for stowage. In its simplest form this pointing system could employ limit switches as position encoders.

In the discussion which follows, the details of tracking and pointing systems are examined particularly with respect to the causes of sun following errors. The discussion is based on one dimensional simplifications to avoid confusion, with the necessary modifications for extension to two dimensions being presented in later sections.

5.3.1 Tracking Systems.

The principal elements of a one dimensional tracking system are shown in figure 5.1. The servo takes information from the sun sensor and adjusts the power to the actuators in an attempt to null the sensor output. It is customary for the sun sensor to be tightly coupled to the collector optical axis, as is shown. The air damping force can be included under the heading of disturbance torques but has been explicitly illustrated here to show that the collector structure is damped. Disturbance torques include the wind loads, dead loads, thermal loads and acceleration loads.

The spring shown in the diagram represents the rigidity of the collector structure. This rigidity with the damping determines the magnitude of the displacements caused by the disturbance torques.

The causes of sun following error can be seen in the diagram and are discussed in the ensuing paragraphs.

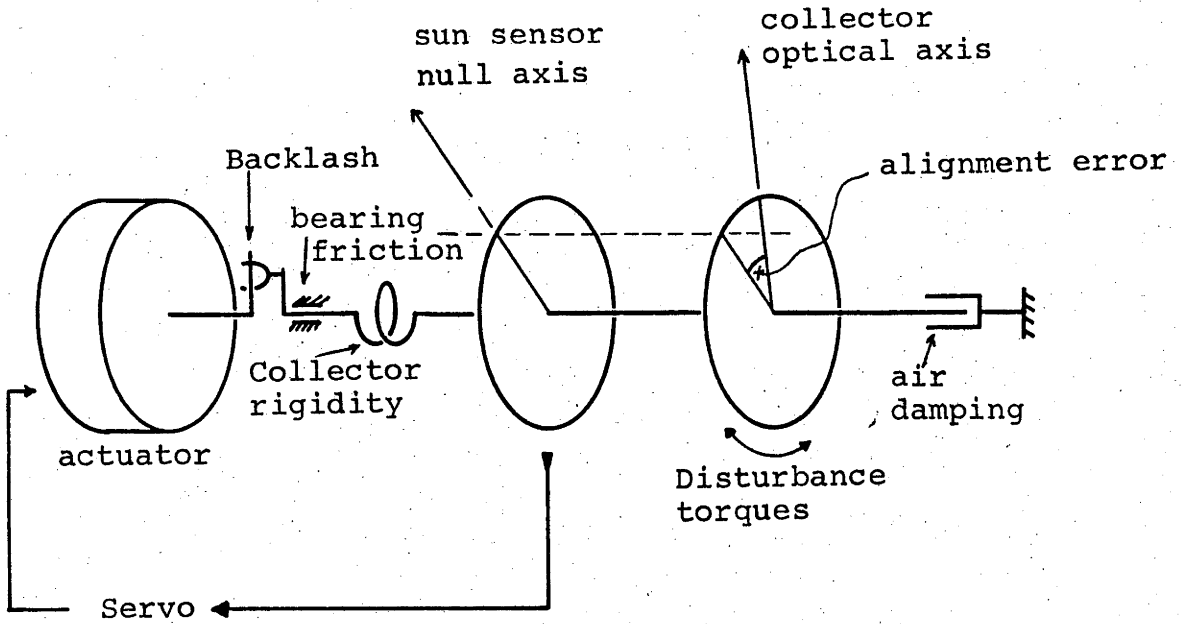


Figure 5.1 Schematic of tracking system. One dimensional simplification based on rotary motion.

Error sources

1. The difference in direction between the sensor null axis and the collector optical axis is designated an alignment error. This error is not random with respect to time, but may still vary due to drift phenomena in the sun sensor, caused by temperature variation or ageing.
2. Servo lags may occur due to the required motion of the null axis, eg velocity lags.
3. The nature of the information from the sun sensor may introduce errors. An example of this occurs if the sun sensor has relay-like properties at the null point, giving one signal above the point and another signal below. In such a case the sun following error will oscillate around zero with a certain amplitude - this effect is illustrated in chapter 6.

The servo may be unable to null the sensor output because of the characteristics of the disturbance torques.

Examples of this kind include:

4. The possibly non-linear nature of friction may make it difficult to control the output shaft at precisely the desired speed, as instanced by the hunting experienced when motors are operated near stall. This results in an oscillation of the sun following error. This is treated under the heading of mechanical errors.

5. The displacements produced by the disturbance torques may be varying with a frequency which is beyond the bandwidth of the servo. For example, for stability reasons the servo bandwidth must be less than the lowest natural frequency of the collector structure and the collector may be displaced at that frequency by disturbance torques. The only disturbance torque that is important here is the torque due to the wind forces - this problem is treated under the heading disturbance torques.

5.3.1.1 Tracking System Deficiencies.

In general, sun sensors give no information on the relative position of the sun when it is not shining. Thus, after a prolonged period without direct radiation, a collector controlled by a tracking system is unlikely to be aligned with the sun. A certain time will accordingly elapse between the beginning of the sunshine burst and the resumption of energy collection, called the response time(τ).

An exact figure for the resulting lost hours of sunshine over the year would require knowledge of the strategy followed by the collector when the sun stops shining. Simple strategies might be to continue at the same speed for ten minutes and then stop, or perhaps stop as soon as the sun stops shining. Calculation of losses would require knowledge of the sequence of sunshine bursts, information which is not generally available.

An estimate can, however, be made which serves as a guide to the amount of losses. Data on sunshine for Griffith(N.S.W.) (Appendix B) was used for this purpose by the author and it was found that for this location, 70% of the total sunshine hours are contained in bursts immediately following periods without sunshine which are longer than 7 hours. After such a time it is certain the position of a collector guided by a tracking system as defined will bear no consistent relative position to the sun. For Griffith, the beginnings of the sunshine bursts are distributed evenly in time throughout the day. If we assume that the collector's position at the start of these sunshine bursts is similarly evenly distributed and uncorrelated with the sun position for the 70% of hours mentioned, then the mean relative angle that the collector must travel to align itself with the sun can be calculated. The largest angle will be in azimuth and the mean angle, given the above assumptions, is $\pi/3$ rads. With a maximum speed of 1rad/sec the response time will be some 1000secs. The resulting uncollected sunshine following 7hr periods without sunshine amounted to 3% of total sunshine hours for Griffith (Appendix B). This represents a considerable amount of energy.

To eradicate these losses a pointing system can be incorporated in conjunction with a tracking system. Losses due to response time for such an arrangement are discussed further in a later section.

5.3.2 Pointing Systems.

A single axis rotary pointing system is illustrated in figure 5.2. In this diagram the encoders have been placed tightly coupled to the actuator shaft rather than to the collector optical axis as this is generally the economic solution.

The position servo compares the requested position with the position recorded by the encoder and adjusts the power to the actuators in an attempt to maintain both requested and recorded positions equal.

The disturbance torques are identical to those for the tracking system.

Sources of sun following error in this case are:

1. The lack of correspondence between the actual encoder zero position and the controller's conception of the zero position. This aspect is treated under the heading of alignment errors.
2. The displacements produced by the disturbance torques. In contrast to the tracking case, all disturbance torques are important here.
3. The accuracy of the requested position information delivered to the position servo which is treated under the heading of actuator displacement calculations.
4. The error in the information from the encoder, which includes possible linearity errors in the encoder and in the case of a digital device the error introduced by representing an analogue quantity by a digital

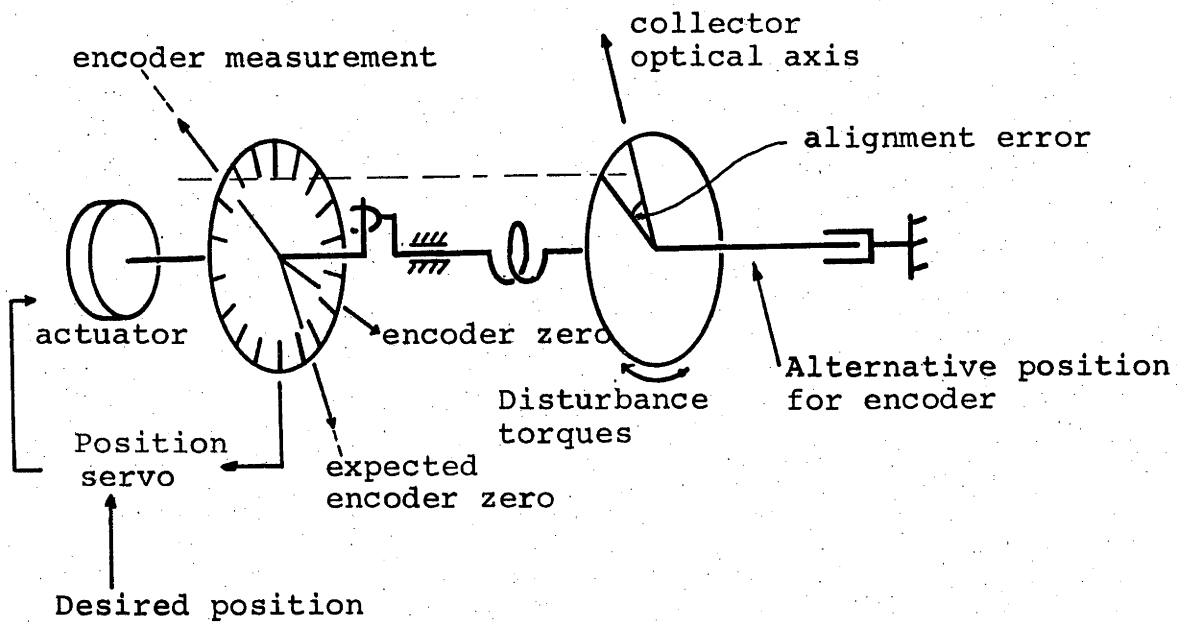


Figure 5.2 Schematic of pointing system.

quantity. This error cause is treated under the heading of encoder.

5. Finally, the position servo may be unable to maintain correspondence between the desired position commands and the actuator position as recorded by the encoder. This may occur due to friction nonlinearities and velocity requirements in the same manner as for tracking systems.

The significant difference between this system and tracking systems is that the disturbance torques are outside the servo loop. Disturbance torques can be included by increasing the sophistication of the servo loop as shown in figure 5.3. In operation, an additional feedback loop in the system inputs disturbance torque values and estimates the displacements which these torques will cause: this is achieved by employing an empirical or theoretical model of the collector. The desired position is then adjusted to compensate for these displacements. This process of compensation can substantially reduce the errors caused by disturbance torques.

The frequency with which these compensating corrections are calculated and transmitted to the collector determines the error sources for which compensation can be used. For example, dead load and thermal load distortions vary on a time scale of hours, and can be easily reduced with only a few corrections each day. These corrections would be the same for each collector in the field and thus the cost of the

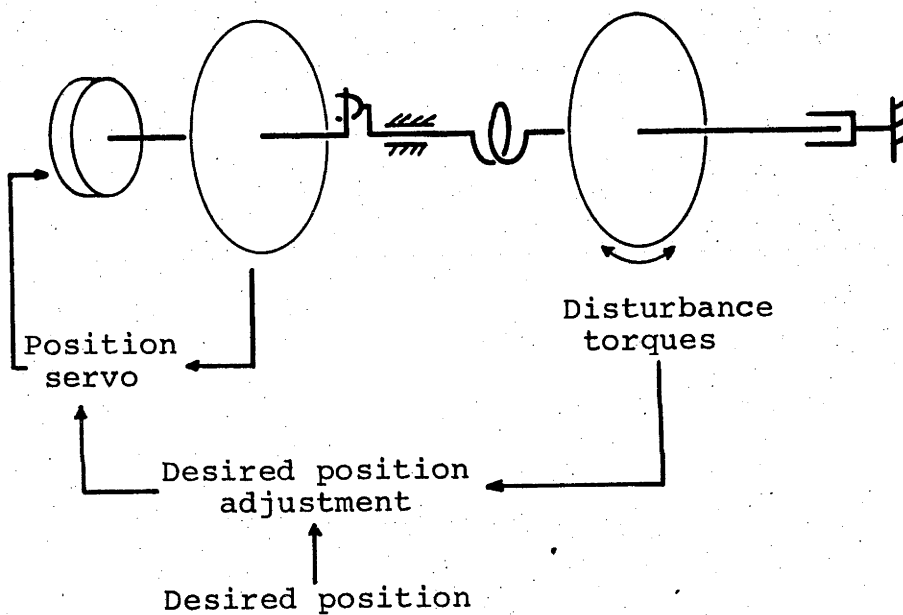


Figure 5.3 Schematic of pointing system with sophistication increased by additional loop which, given values for the disturbance torques, compensates for the resultant deflections. Disturbance torques can be calculated from meteorological data, or measured on a particular collector.

calculation per collector would be trivial. In contrast, deflections due to wind loads vary on shorter time scales and compensation may prove more complicated.

The basic information required for operating a pointing servo can be calculated either by the central control or by the local control, or the calculation can be shared. In any case, information relevant to pointing will need to pass between the two controls and this information transfer may use the communication link already in use for the issue of stow commands, provided that large data rates are not required.

5.4 Sun Following Error Sources.

In the following section we consider each of the causes of sun following errors in detail. The errors caused by alignment, disturbance torques and the calculation of the actuator displacements are considered in detail, because these errors have the most effect on the design of the guidance and control scheme. The reduction of errors due to mechanical faults are matters of component selection and are considered only briefly. The section concludes with a brief note on the method which should be used to combine the error sources to produce an overall picture of sun following errors.

5.4.1 Speed Requirements

The optimum choice of actuator maximum speed will be a matter of compromise: on the one hand if the speed is too low, then sun following errors may occur. On the other hand

if actuator speed is too high the actuators will be unnecessarily powerful and expensive. This section is concerned with the range of speeds required of the actuators on the collector. Requirements depend upon the type of mount used and in this study we consider mounts whose operation parallels a frame of reference in which the fixed axis is in the N-S plane, inclined to the equatorial plane at an angle B (the effective latitude) and the secondary or rotational axis is orthogonal to the fixed axis. Such a situation is shown in Figure 5.4. For an appreciation of the motion required of the collector, we consider the motion of the sun to be that of an artificial sun which rotates around the earth's axis at a fixed rate. The formulae which convert from the solar hourangle (kt) and declination (δ) to the local coordinates (θ, ϕ) are (Brinkworth, 1972):

$$\sin\theta = \sin(B)\sin(\delta) + \cos(B)\cos(\delta)\cos(kt) \quad (5.1)$$

$$\tan\phi = \sin(kt)/(\sin(B)\cos(kt) - \tan(\delta)\cos(B)) \quad (5.2)$$

By analogy with the alt-azimuth system, the coordinate θ is called the elevation, and the coordinate ϕ the azimuth angle. The speed requirements for the elevation actuator are never greater than the sun's speed in hourangle (k), but are much more severe for the azimuth actuator. The maximum requirement here is given by:

$$\dot{\phi}(\max) = k \cos(\delta)/\sin(B-\delta) \quad (5.3)$$

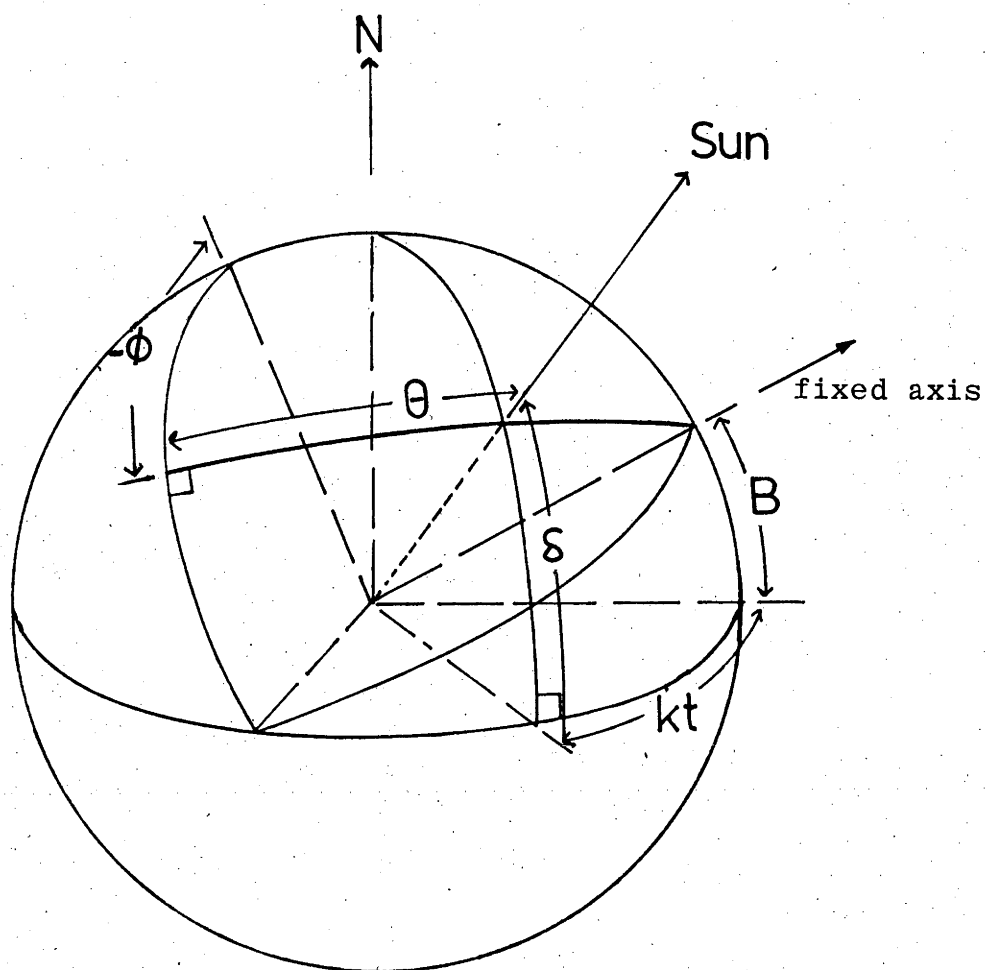


Figure 5.4 Coordinate system.

kt, δ - hourangle and declination of the sun.

B - inclination of the fixed axis to the equatorial plane.

θ, ϕ - actuator displacement coordinates of the tracker.

with the value of δ determined by that of B.

For this reason azimuth and elevation speeds are plotted in figure 5.5 in terms of the parameter $(B-\delta)$, (with δ held constant at 23.5 degrees), and B varying. The azimuth maximum speed requirement (Figure 5.6) increases as $(B-\delta)$ decreases and equation (5.3) indicates that for an alt-azimuth system at latitude 30S, a maximum speed of 1rad/sec would be adequate for following the sun. Similarly at latitude 25S, by leaning the principal axis South through 5 degrees and making the effective latitude 30S, the same maximum speed would be adequate.

5.4.2 Alignment

The collector acts as a well behaved operator or function, transforming the input which is the displacements of the actuators, into an output, a pointing direction. The form of this 'collector function' is determined by the type of mount used, (eg alt-az), the type of actuators used and a series of parameters called calibration constants. Only the calibration constants vary from collector to collector. These calibration constants include parameters such as the zero points of the actuator displacements and constants which specify the orientation of the fixed axis of rotation. Alignment is defined as the process which determines these constants and is equivalent to determining the frame of reference which corresponds to the collector mount.

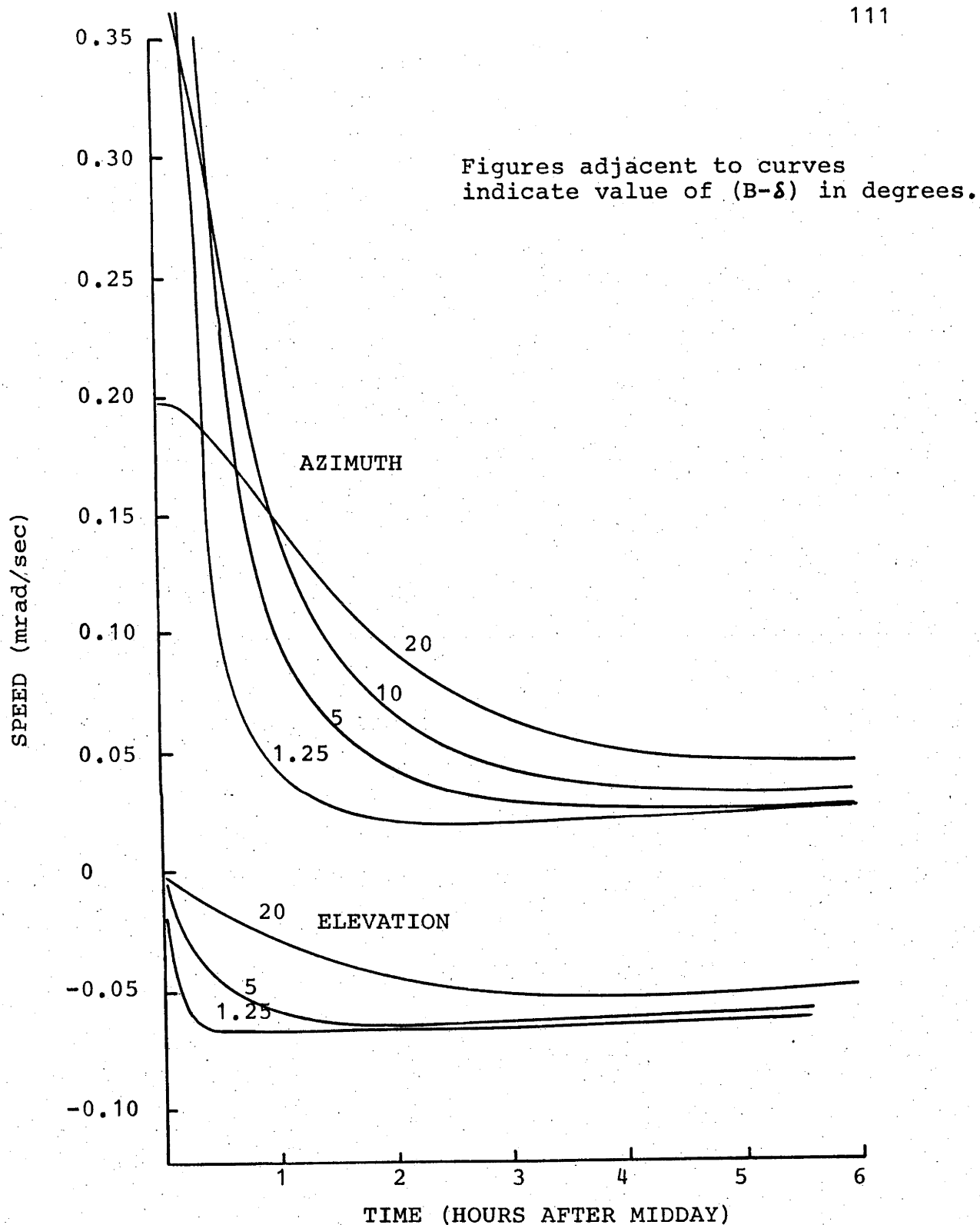


Figure 5.5 Variation of the azimuth and elevation speeds over a day.

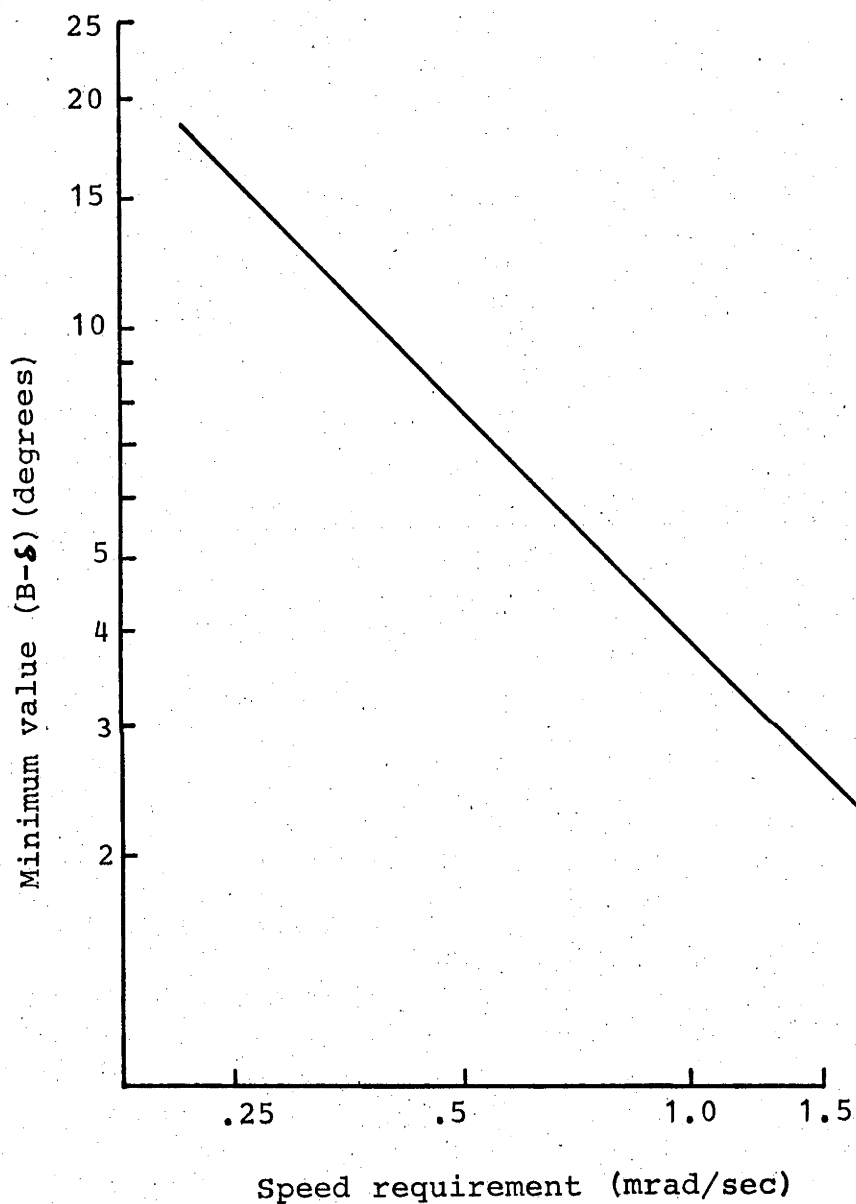


Figure 5.6 Variation of the maximum speed required of the azimuth drive with the value of $(B-\delta)$. B is the angle of fixed axis relative to the equatorial plane, measured in the vertical N-S plane. δ is the declination of the sun.

The calibration constants include the angle between the sun sensor null axis and the optical axis as shown in figure 5.1. For a tracking system, the two dimensional equivalent of this sun sensor alignment error is the only calibration constant. For pointing systems, the number of calibration constants is larger, as indicated in figure 5.2; moreover each of the errors shown recur for each of the axes of rotation. For pointing systems, the calibration constants are all dependent on field installation and foundation subsidence, whereas the sun sensor alignment error, once established during the construction of the collector, is independent of installation. It would be most appropriate to measure the sun sensor alignment error on the assembly line, where it can be measured more cheaply than in the field. The following discussion refers to calibration constants other than the sun sensor alignment error. The drift of the sun sensor alignment error is not considered here.

Alignment may be an expensive process, particularly if it needs to be performed frequently. The frequency with which alignments must be carried out is determined by a number of factors, including the type of foundation and site characteristics. It is probable, however, that reducing the frequency of alignments necessary will require a more substantial and thus expensive foundation. Here we consider three possible methods of determining the constants:

(a) Carry out adjustments to make all calibration constants identical to a set of given values.

(b) Measure the constants after installation.

(c) Mathematically infer the calibration constants by analysing the behaviour of the collector.

It is shown that the third alternative is the cheapest if the collector needs to be aligned more than one or two times in its lifetime.

5.4.2.1 Methods (a) And (b).

Methods (a) and (b) are considered together as both involve the same process, in that a manual process is required to align the collector as often as is required. Whether the result of the measurement is recorded or adjustments made makes little difference to the cost of the process.

A procedure for measuring the pointing direction of the fixed axis would require a special instrument which could be attached to the collector frame and a measurement would require the provision of a reference direction. Due to the characteristics of the field of collectors, it would not be feasible to set up datum points and magnetic compasses would not be appropriate because of the abundance of metal in the vicinity. A north seeking gyroscope, a compact and portable direction reference, accurate to 30" of arc, could be used in this application. Such an instrument is currently priced at around \$5000, and its cost is accordingly not relatively great. To determine the alignment of the collector

completely, a further two axis measurement of the initial pointing direction of the collector would be required. Surveying equipment could align a mount to 1 minute of arc, or 0.3mrad.

For method (a), where it is desired to align the collector to a specific position, probably two or three measurements, coupled with appropriate adjustment would be required. It should be noted that these adjustment means must be substantial enough to take the full loadings of the collector and therefore their presence will increase the collector cost. Adjustment of the zero points of the actuator encoders would also be accomplished simultaneously. It is improbable that such a measurement would involve less than half a man hour labour and thus the cost of the alignment may be \$15 or more.

5.4.2.2 Method (c), Inferring Calibration Constants.

This method of determining alignment relies on the fact that just as with a knowledge of the collector function and calibration constants one can determine the output (a pointing direction) from the input (the actuator displacements), similarly with knowledge of the output and the input, one can determine the calibration constants.

This method has been proposed for solar collectors by Carden (1978a). For astronomical telescopes this approach has been extant since at least 1965 (IAU, 1965). The method can be used only if each collector is equipped with a sun sensor. The method involves calculating the calibration constants, the output being the pointing direction of the sun sensor null axis. This approach cannot determine the error between the sun sensor null axis and the optical axis of the collector.

In order to generate a sequence of input data points and corresponding output data points, the central control interrogates the collector for sun sensor information and actuator displacement encoder information, the latter being one of the input points. The time of interrogation enables the sun's position to be calculated. The information from the sun sensor gives the position of the sun sensor null axis relative to the sun, which, coupled with the position of the sun, gives the position of the sensor null axis. Thus the output data points are determined. In principle it is not necessary for the collector to follow the sun during this process. However, here we study the simpler case where the sun sensor is near null at the time of each interrogation. We assume the sun sensor is maintained near null by a tracking system.

Analysis.

The mathematical process uses a set of input points (actuator displacements) and a corresponding set of output points (the position of the sun) and functions as follows:

The i th set of pointing coordinates are calculated using the collector function described in 5.4.2. In this 2-dimensional case it is easier to consider the function as two functions, one for each coordinate. The functions are common to all collectors in contrast to the calibration constant vector G which is specific to each collector.

The vector G relates the actuator displacement vector X_i to the corresponding pointing direction (θ, ϕ) via the two functions $\hat{\theta}$ and $\hat{\phi}$. The relationships are:

$$(\theta, \phi) = (\hat{\theta}(X_i, G), \hat{\phi}(X_i, G)) \quad (5.4)$$

In addition, from the known position of the sun and from the sun sensor error data, the actual pointing coordinates θ_i and ϕ_i are determined. For a sequence of n sets of coordinates we may determine the root mean square error between the actual and calculated pointing directions as:

$$S^2 = \frac{1}{n} \sum_{i=1}^n (\theta_i - \hat{\theta}(X_i, G))^2 + (\phi_i - \hat{\phi}(X_i, G))^2 \cos^2 \theta_i \quad (5.5)$$

and define the best estimate available for G as the value of G , namely $G^\#$, which minimises S .

Choice of algorithm to compute $G^\#$.

Algorithms for the minimisation of general functions can of course be applied to the minimisation of sums of squares, though intuitive arguments (Brent, 1973) show that, given a good initial approximation, an improved estimate will be found with fewer calculations if each term in the summation is inspected, rather than considering only the sum S . Lill (1976) describes several algorithms and reports that the most suitable choice lies between Gauss-Newton algorithms and Levenberg-Marquardt algorithms, the former being faster but less reliable, particularly if the initial estimate is poor. Further, the former is more sensitive to scaling difficulties, which are discussed in the next section. Brown and Dennis (1972) survey a plethora of least squares minimisation routines and illustrate that the Gauss-Newton method is the fastest-if it finds a minimum, while the Levenberg-Marquardt algorithm is the most reliable, though its speed is not exceptional. The Levenberg-Marquardt algorithm was used in the work in this study.

Form of the functions $\hat{\theta}, \hat{\phi}$.

The speed of the minimisation program is dependent on the form of the functions $\hat{\theta}$ and $\hat{\phi}$ and it is appropriate to arrange $\hat{\theta}, \hat{\phi}$ so that the speed is high. The properties of $\hat{\theta}$ and $\hat{\phi}$ which are important in this respect are outlined below.

Firstly, the scaling of the calibration constants in the vector G is important. An intuitive idea of scaling is that similar changes in each of the constants in G cause similar changes in the value of S . Kowalik and Osbourne (1965) report

that scaling is crucial to the success of some minimisation methods and is always important as far as speed is concerned. Secondly, the function chosen must allow reasonably close initial estimates and this in turn depends upon the choice of coordinates. As an illustration of this point, consider the coordinates of a position which is nominally the North Pole. Coordinates based on longitude and latitude would not allow a good initial estimate for the longitude of the position and a better coordinate system would be a polar one based on an axis in the equatorial plane.

For these reasons the orientation of the fixed axis of the collector has been defined here in coordinates based on the polar axis of the earth, rather than in terms of altitude and azimuth deviations from the local vertical, which is the nominal position of the fixed axis. Thus the polar coordinates of the fixed axis correspond to latitude and longitude of the collector when the fixed axis is vertical.

Calibration constants considered.

As well as the constants describing the fixed axis orientation, others considered were the position of the fiducial mark (or zero point) for both actuator displacement encoders and the gain of the displacement encoders. These last mentioned calibration constants would be necessary if for example a belt drive were employed between the encoder shaft and the collector axis. Variations in the driving or driven pulley diameter may cause one encoder on a particular

collector to give a reading of say 100 for a collector motion of 1 rad, while on another collector an encoder may read 102 for the same displacement. Another calibration constant which could have been considered, (but was not considered here) concerns a constant describing the orthogonality of the axes of rotation.

Accuracy of calibration constant determination.

The accuracy of the estimate $G^\#$ is of only incidental interest, the important factor being the angular difference between the coordinates of a position on the sky and the pointing direction of the collector, as aimed using the estimate $G^\#$. An rms average of this angular difference is used as a measure of the usefulness of $G^\#$ - the angular difference is formulated in the following paragraph by considering the method used for aiming the collector.

We define two functions $\hat{\theta}^{-1}$ and $\hat{\phi}^{-1}$ which are the inverse functions to $\hat{\theta}$ and $\hat{\phi}$ and which transform sun positions into actuator displacements, ie:

$$x_i = (\hat{\theta}^{-1}(\theta, \phi, G), \hat{\phi}^{-1}(\theta, \phi, G)) \quad (5.6)$$

To aim the collector at a specific point (θ_i, ϕ_i) in the sky the actuator displacements corresponding to this position are calculated using the best estimate $G^\#$. The point on the sky with which these calculated actuator displacements corresponds will not in general be the same as the original

point because G is not necessarily equal to $G^\#$. This point will be given by:

$$\theta_i^\# = \hat{\theta}(\hat{\theta}^{-1}(\theta_i, \phi_i, G^\#), \hat{\phi}^{-1}(\theta_i, \phi_i, G^\#), G) \quad (5.7)$$

$$\phi_i^\# = \hat{\phi}(\hat{\theta}^{-1}(\theta_i, \phi_i, G^\#), \hat{\phi}^{-1}(\theta_i, \phi_i, G^\#), G)$$

The pointing errors introduced due to the inaccuracy of $G^\#$ are thus calculated by a summation of the form:

$$(S^\#)^2 = \frac{1}{n} \sum (\theta_i - \theta_i^\#)^2 + (\phi_i - \phi_i^\#)^2 \cos^2(\theta_i) \quad (5.8)$$

This average is the contribution to sun following error of a pointing system using this method of alignment.

The position of the sun is known to high accuracy and the estimation of G is determined by the accuracy of the data points X_i . The ratio of $S^\#$ to the rms error in either coordinate of X , $\sigma(X)$, is designated the 'error ratio'. It is assumed that the rms errors in both coordinates of X are identical. The error ratio is therefore defined by:

$$r = \frac{S^\#}{\sigma(X)} \quad (5.9)$$

The error $\sigma(X)$ is the rms difference between the actuator displacement encoder positions recorded and the positions which would have been recorded in a perfect system where the encoders are tightly coupled to the optical axis and

the optical axis is perfectly aligned with the sun. Thus the error is the sum of the mechanical, servo and torque disturbance errors and the encoder errors for a tracking system, all calculated for one axis only. The distribution of the combination of all these errors will tend to be Gaussian, regardless of the distribution of the individual errors, in accordance with the Central Limit theorem.

The error ratio was assessed from a series of simulation runs, which were conducted as follows.

A set of sun positions was calculated, spaced evenly in time over the sunshine hours of one day of the year. Corresponding to this set, a set of actuator displacements was calculated using a specific set of calibration constants G . To simulate errors, random numbers from a Gaussian distribution with a fixed rms value of $\sigma(X)$ were then added to the actuator displacements to obtain the X_i . Different sets of random numbers were used in each simulation with rms errors of both .7 and 7mrad. Using a minimisation routine, $G^\#$ was calculated by minimising S . Knowing the true G , it is then possible to calculate the contribution to sun following error due solely to the inaccuracy of $G^\#$ as given in equation 5.8. The error ratio is then calculated with equation 5.9. Each simulation used a different set of random numbers though each set was drawn from a single distribution of known rms value. The expected value for the error ratio is estimated by the rms value of the error ratio encountered in the simulations. The maximum error ratio which occurred in the simulations was noted to give a guide to the variations to be expected. As

expected, no variation in the error ratio was observed between the two different $\sigma(X)$ values used.

From basic statistics, one appreciates that the difference between $G^\#$ and G will depend on both the number of points used in the sum S and also on the spatial variation in the input and output points. In particular, a set of points distributed evenly in time over the summer solstice sunshine hours will determine G with more accuracy than a set of points drawn from the winter solstice due to the restricted motion of the sun on the winter solstice. Further, the error ratio depends upon the day used to calculate $S^\#$. This effect is particularly severe if the day used to gather the points is the winter solstice and $S^\#$ is calculated for the summer solstice.

All these effects have been considered in obtaining the results from 40 simulations shown in Table 5.1. These results are based on sun position data for two days, the winter solstice and the summer solstice. Using this data and the method already described, the calculated approximation to the set of calibration constants was calculated using a set of N data points taken at equal intervals over the one day. As $G^\#$ is an approximation, the pointing directions generated using $G^\#$ differ from those generated by the actual calibration constant set and this difference, quantified as the error ratio, depends upon the day of the year used to calculate the difference. In the table, five sample days of the year have been used, marked (1) through (5). These are defined below the table.

TABLE 5.1 ERROR RATIO

Four Calibration Constants (two determining the orientation of the fixed axis and two determining the zero points of the position encoders).

Winter Solstice data					Summer Solstice data					
	(1)	(2)	(3)	(4)	(5)	(1)	(2)	(3)	(4)	(5)
N										
10	.59	.66	.88	1.2	1.3	.60	.59	.58	.58	.57
20	.42	.47	.66	.91	1.1	.38	.38	.37	.37	.38
40	.30	.34	.48	.64	.76	.27	.26	.26	.27	.27
80	.22	.25	.33	.44	.50	.20	.20	.20	.20	.20

Six Calibration Constants (as for four calibration constants, but also including two actuator gain constants).

Winter Solstice data					Summer Solstice data					
	(1)	(2)	(3)	(4)	(5)	(1)	(2)	(3)	(4)	(5)
N										
10	.73	.94	1.9	3.3	4.1	.76	.71	.67	.68	.71
20	.52	.63	1.2	2.3	2.7	.51	.48	.45	.46	.47
40	.38	.48	1.0	1.9	2.2	.42	.40	.37	.33	.33
80	.27	.35	.71	1.4	1.6	.28	.27	.26	.25	.24

* Indicates the day for which the pointing error due to the difference between the true calibration constant set G and the calculated set G was evaluated.

- (1) Winter solstice.
- (2) Winter solstice + 46 days.
- (3) Winter solstice + 91 days.
- (4) Winter solstice +137 days.
- (5) Summer solstice.

--All calculations for latitude 35degrees and a near alt-az mount.

The error ratio calculated using the summer solstice day for data collection and the same day for the calculation of $s^{\#}$ is shown in figure 5.7.

Cost of calibration.

For the simulation runs, programming was based on the Brown and Dennis (1972) modification of the Levenberg-Marquardt algorithm which uses derivatives calculated by finite difference methods. Average execution time for calculating the calibration constants using a DEC-10 KA processor is illustrated in figure 5.8 and is typically 3 seconds or less for a 10 point calibration. On this basis and estimating the cost of processor time for the DEC-10 at \$100/hr, the computation for each calibration is \$.1/collector for a 10 point calibration. Processor time cost is in general related to computer speed and one can expect cost studies for both faster and slower machines to yield somewhat similar values.

The cost of computation is not the only expense, as the data for the calibration must also be gathered and stored. The storage required is small, with at most 160 bytes being required for each collector. Total storage requirements are not determined by multiplying this figure by the number of collectors, as not all data needs to be stored at one time. Costs here will be minimal and the computation of calibration constants can be scheduled so that the facilities of the central machine will not be stretched by the storage requirement. Thus the central machine cost is not increased

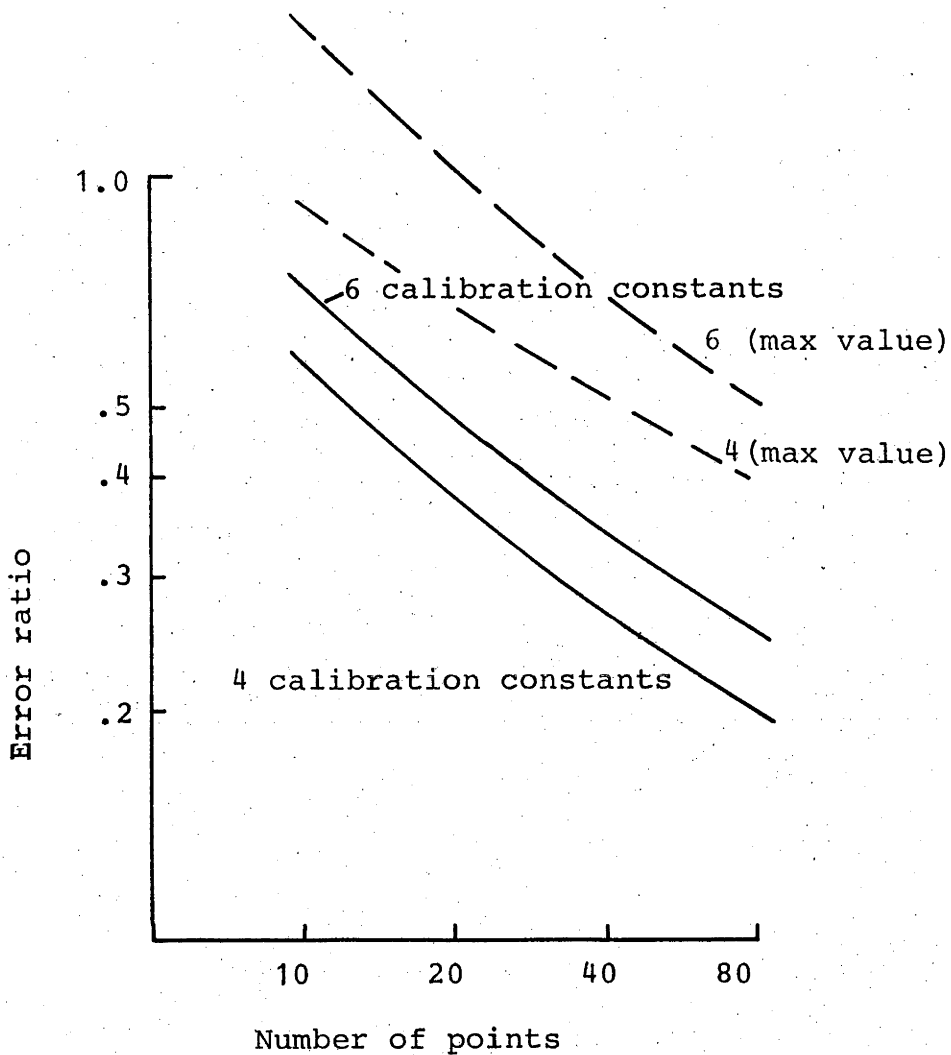


Figure 5.7 Ratio of the pointing error on the day of the summer solstice because of errors in the calculated calibration constants to the rms error in the actuator displacement values, (or error ratio). The values shown are averages calculated from 40 simulation runs, and as such have possible errors of 15%. The error ratio depends on the number of calibration constants which need to be calculated, as shown.

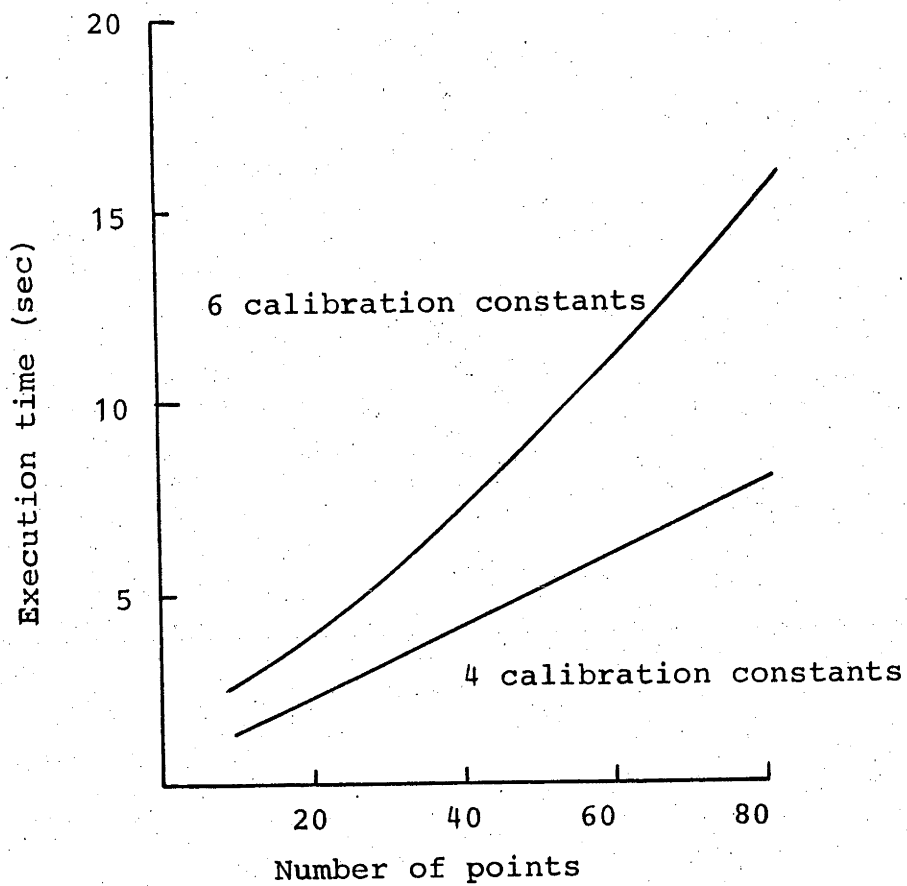


Figure 5.8 Average execution time to calculate the calibration constants. DEC-10 KA processor.

by this requirement and no cost should be ascribed to the alignment method.

Data collection will require the provision of a return communication link from each collector to the central machine and possibly special data handling facilities if the data rate requirement is high. An estimate for the data rate is made in the following paragraph.

Data rates for alignment.

We assume that the central controller can interrogate each collector with a series of requests with one request for sensor data and one for encoder information. The collector returns a data word with an identifying set of bits to indicate which collector is replying. Here we assume this identifier is 14 bits long, which is sufficient for individual identification of 10 000 collectors. The sensor data is assumed to require 12 bits and the two pieces of information for the two encoders are assumed to require 10 bits each, which gives an rms error in each axis of near 7mrad. We further assume that the information is returned in two words, one for the sensor and one for the encoders. Thus 60 bits need to be returned for each interrogation. If it is desired to collect information for an alignment of all 10 000 collectors on one day and interrogation occurs at regular intervals of t seconds, then information will return with a data rate of:

$$R = (60) * 10\ 000 / t \quad (\text{bits/sec}) \quad (5.10)$$

The interrogation interval t depends on the number of points used in determining G . For a 10 point alignment, t is 4320 seconds and thus from (5.10) the data rate of returning information will be only about 140bits/sec. Such a data rate would not require any special data handling facilities. Thus the cost of the alignment can be estimated from the execution times in figure 5.8. A study of the data rates of an alternative data collection scheme for alignment is given by Edwards(1978b), reproduced in Appendix E.

A note on data transmission cost.

Facilities for data transmission do not display a monotonic increase in cost with data rate and in general costs increase in steps, at particular data rates. For simple two wire transmission over cables equivalent to telephone lines, costs would be invariant up to data rates around 3kHz, in outdoor environments. Thus no cost increase for data transmission can be expected provided data rates are kept below this figure.

5.4.2.3 Comparison

At the beginning of this section three methods for alignment were suggested, viz:

(a) Carry out mechanical adjustments to make all calibration

constants identical to a set of given values.

(b) Measure the constants after installation.

(c) Mathematically infer the calibration constants by analysing the behaviour of the collector.

The basic difference in cost between methods (a) and (b) on the one hand and (c) on the other is that the former is characterised by low initial costs of the instruments required for measuring alignment, but involve high costs for each alignment, while the latter is characterised by the relatively high initial costs for the sun sensor and data gathering equipment, but low subsequent costs. Thus the former is more economical if the total number of alignments per collector over the collector's lifetime is low, whereas the latter is more economical if the number of alignments is high.

The breakeven point between the two groups is the number of alignments per collector for which costs are the same regardless of which method is used. The breakeven point is probably as low as one or two alignments per collector, which is not many for the entire life of the solar plant. For any greater number, method (c) would be more economic.

A further advantage of method (c) is that, due to the availability of information from the sun sensor, alignments will be performed no more often than is necessary, in contrast to methods (a) and (b), where alignments must be performed routinely if a sun sensor is not available.

5.4.3 Disturbance Torques: Wind.

Here we analyse the deflections of the collector structure caused by wind gusts which may cause sun following errors. This involves the calculation of the wind forces and the aerodynamic admittance of the structure, both of which are functions of frequency. The spectrum of the deflections may then be evaluated as a combination of the above information. The errors may be reduced by introducing feedback into the guidance and control system and therefore knowledge of the spectrum is important for the selection of an appropriate guidance and control scheme bandwidth. Data on this spectrum is presented and the implications for the design of the guidance and control scheme outlined below.

5.4.3.1 Wind Deflection Characteristics.

Each degree of freedom of the structure can be described by a certain rigidity, resonant frequency and damping factor. The resultant response of the structure to winds will be the sum of the component responses for the respective degrees of freedom. On the other hand the resultant sun following error will depend upon the collector design as well as being a complex function of such quantities as the strength and direction of the wind relative to the collector. Here we analyse a single degree of freedom of the structure to gain insight into the size and spectrum of the wind deflections.

It should be noted that some of the variables upon which calculations of wind effects are based are not known accurately. Among these in particular are variables which

describe the turbulence of the wind. Consequently the following calculations themselves are not precise.

In evaluating a spectrum of the collector displacements we use a spectral density function $S_v(f)$ of variable v at frequency f , whose importance can be seen from the equation:

$$d(\overline{v^2}) = S_v(f) df \quad (5.11)$$

where $d(\overline{v^2})$ is the contribution to the variance of v from frequency components in the range f to $f+df$. The variance of v is thus given by:

$$\overline{v^2} = \int_0^{\infty} S_v(f) df \quad (5.12)$$

Wind forces may be expressed similarly, with the mean wind force \overline{F} being a function of the spectral density function ($S_F(f)$) of the wind force, namely:

$$\overline{F^2} = \int_0^{\infty} S_F(f) df \quad (5.13)$$

The relationship between the two spectral density functions above can be derived simply (Davenport 1975) and the influence of the ratio of the size of the wind disturbance to the size of the collector is included using an 'aerodynamic admittance function', χ^2 , which is a function of the frequency, a characteristic dimension of the collector (L) and the mean wind velocity (\overline{V}) (Vickery, 1970). The spectrum of the wind force is expressed in terms of the velocity spectrum

(Davenport, 1975):

$$S_F(f) = \frac{4\bar{F}^2}{\bar{V}^2} S_V(f) \chi^2\left(\frac{fL}{\bar{V}}\right) \quad (5.14)$$

The function χ^2 is given graphically by Vickery(1970). For low values of fL/\bar{V} , χ^2 approaches unity, implying that the object fully accepts the force. At high values of fL/\bar{V} , χ^2 approaches zero, indicating the force has little affect on the object.

We assume that the wind forces produce moments in the structure which cause angular deflections and the deflections are assumed to be proportional to the wind force. It is possible to design structures whose response to a specific wind force is not an angular displacement, however, certain assumptions, such as uniform wind force over the collector, are required for design. Gradients in the wind force across the collector are likely and these will cause angular displacements. Further, designs which prevent(or reduce) angular deflections will of necessity be more complex and thus more costly.

The deflections are calculated as the product of the spectral density function of the force and the following transfer function between force and displacement for a single vibration mode of the collector with resonant frequency f_0 , damping coefficient ζ and rigidity k .

$$\frac{1}{k^2} |H(f)|^2 = \frac{1/k^2}{\left[1 - (f/f_0)^2\right]^2 + 4\zeta^2 (f/f_0)^2} \quad (5.15)$$

The deflections of this mode are related to the force spectrum using the mean deflection (\bar{x}) of the collector under force \bar{F} where:

$$\bar{x} = \bar{F}/k \quad (5.16)$$

The standard deviation (σ_x) of the deflections at frequencies above the frequency of the steady wind is obtained from 5.14, 5.15 and 5.16:

$$\sigma_x^2 = \frac{4\bar{x}^2}{V} \int \chi^2 \left(\frac{fL}{V} \right) |H(f)|^2 S_V(f) df \quad (5.17)$$

Strictly speaking the integration limits should be 0^+ , (thus not including the steady component), and infinity. In practice the lower frequency limit is the frequency of the mean wind (around .001Hz) and the upper limit is just above the resonant frequency of the structure in question.

If all deflections are related to the mean deflection at 1m/s, \bar{x}_1 , then:

$$\sigma_x^2 = 4 \bar{x}_1^2 \bar{V}^2 \int \chi^2 \left(\frac{fL}{\bar{V}} \right) |H(f)|^2 S_V(f) df \quad (5.18)$$

The variation with frequency of the various terms is shown in figure 5.9. Heuristically, the result of the integration is split into two parts, the contribution to σ_x

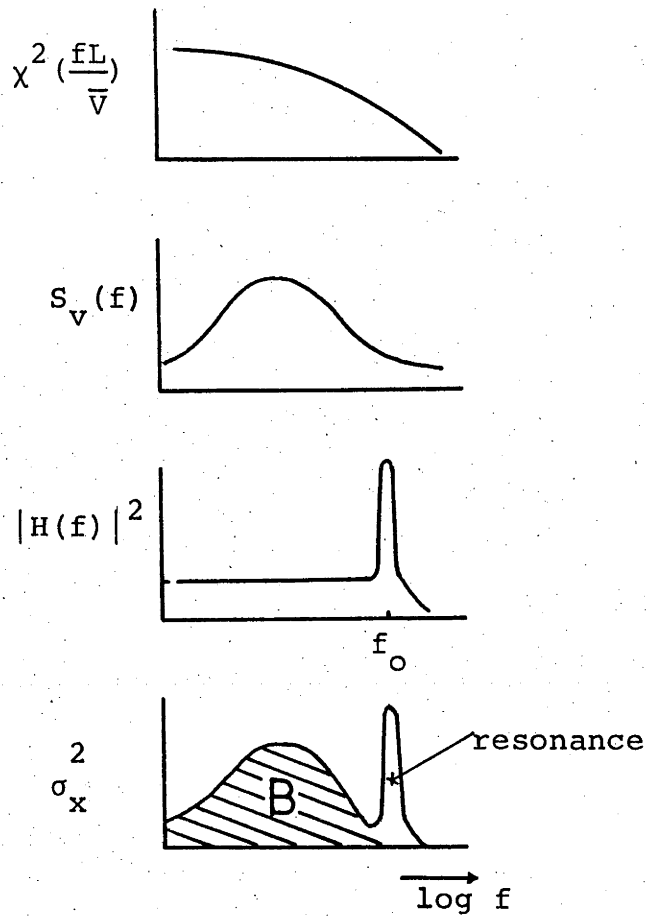


Figure 5.9 Diagrammatic explanation of the integration in equation 5.18, and subsequent partitioning into two parts, the resonant contribution, equation 5.19, and 'B' effect contribution, equation 5.20.

from the deflections near resonance ($\sigma_x(\text{res})$) and the contribution to σ_x from the non-resonant deflections ($\sigma_x(\text{B})$) as shown in figure 5.9. These are calculated from:

$$\sigma_x^2(\text{res}) = \chi^2 \left(\frac{f_0 L}{\bar{V}} \right) S_V(f_0) \frac{\pi f_0}{\zeta} \bar{x}_1^{-2} \bar{V}^2 \quad (5.19)$$

The extra term being the integral of $H(f)$ for frequencies near f_0 (Davenport, 1975).

The non-resonant deflections are called B (for background) effects and $H(f)$ is unity for these frequencies.

$$\sigma_x^2(\text{B}) = 4 \bar{x}_1^{-2} \bar{V}^2 \int \chi^2 \left(\frac{fL}{\bar{V}} \right) S_V(f) df \quad (5.20)$$

The deflections of importance are those which occur during solar energy collection. To calculate a mean we need to know how many hours of sunshine occur at each mean wind speed. Data is sparse here, and we rely upon Vant-Hull et al(1975), who give the results of a correlation between mean wind speed(\bar{V}) and direct sunshine at Inyokern, in the form of the fraction of sunshine hours lost if equipment is closed down for mean winds above a given speed. This data is reproduced in figure 5.10. The shape of this curve is approximately exponential, with decay constant, \bar{V}_k , of near 3m/s. This suggests that the fraction(dt) of sunshine hours with winds in the velocity range \bar{V} to $\bar{V}+d\bar{V}$ is given by:

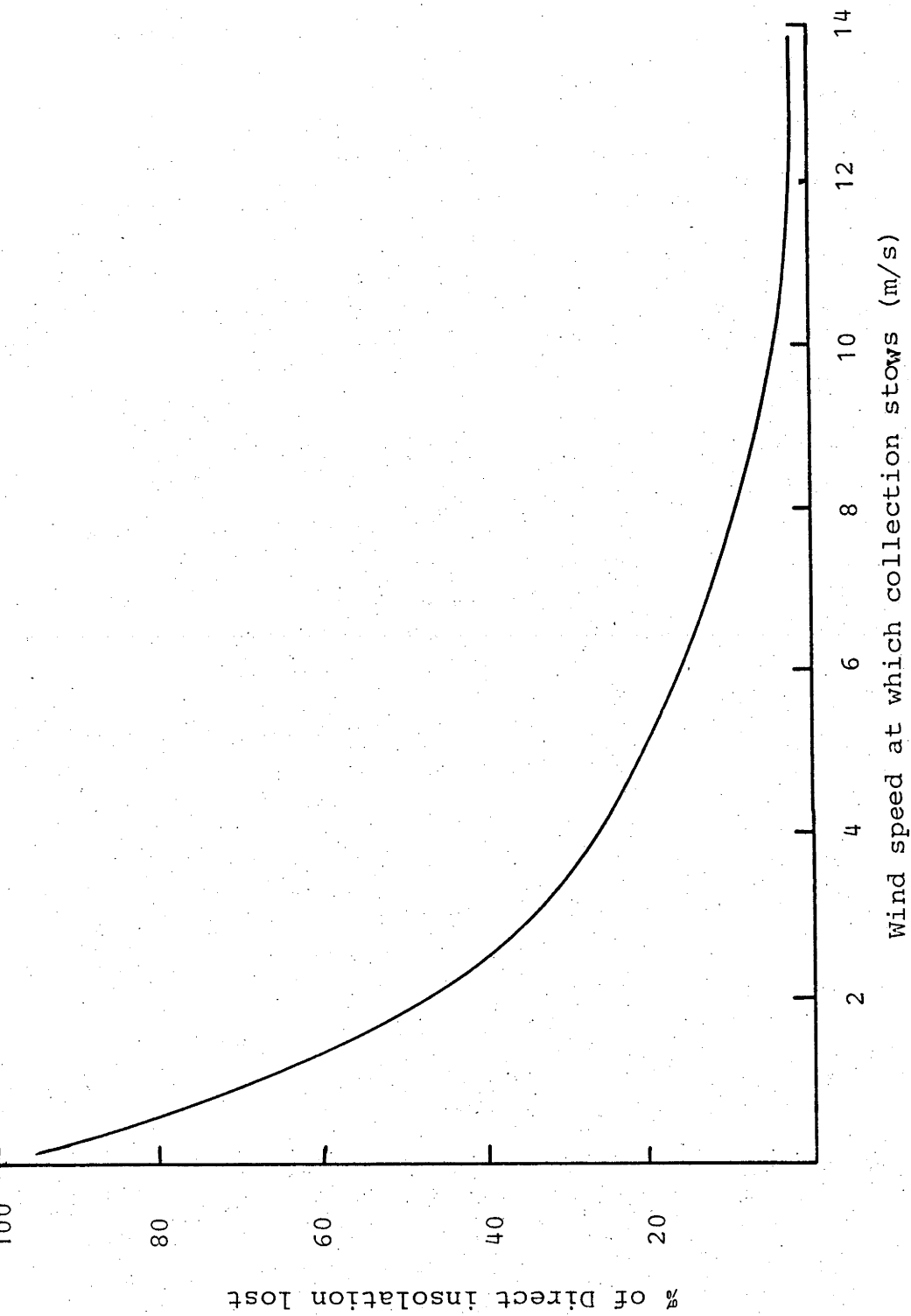


Figure 5.10 Direct insolation loss due to shutdown of collector at specific mean wind speed for Inyokern, a typical solar power plant site in the desert near Los Angeles (Vant-Hull, 1975).

$$dt = 1/\bar{V}_k \exp(-\bar{V}/\bar{V}_k) d\bar{V} \quad 0 < t < 1 \quad (5.21)$$

An appropriate mean for the two $\bar{\sigma}_x$ values, averaged over the sunshine hours is thus given by:

$$\sigma_x^2(\text{res}) = \left| \bar{x}_1^2 \int_0^{\bar{V}_s} \chi^2\left(\frac{f_0 L}{\bar{V}}\right) S_V(f_0) \frac{\pi f_0}{\zeta} \frac{\bar{V}^2}{\bar{V}_k} \exp(-\bar{V}/\bar{V}_k) d\bar{V} \right. \quad (5.22)$$

$$\sigma_x^2(\text{B}) = 4 \bar{x}_1^2 \int_0^{\bar{V}_s} \frac{\bar{V}^2}{\bar{V}_k} \left(\int_0^{\infty} \chi^2\left(\frac{fL}{\bar{V}}\right) S_V(f) df \right) \exp(-\bar{V}/\bar{V}_k) d\bar{V} \quad (5.23)$$

where \bar{V}_s is the wind speed above which the collectors will be stowed and thus not collecting energy. In the following calculations, \bar{V}_s was 10m/s.

In calculating $\bar{\sigma}_x(\text{B})$ and $\bar{\sigma}_x(\text{res})$, the velocity spectrum of the winds $S_V(f)$ was approximated by (Simiu and Lozier 1975):

$$\frac{f S_V(f)}{k' \bar{V}^2} = \frac{4.0 b^2}{(1+b^2)^{4/3}} \quad (5.24)$$

where $b = (1200 \text{ metres}) f/\bar{V}$, and k' is the surface drag coefficient, which was assumed to be .04, an urban value. The function $\chi^2\left(\frac{fL}{\bar{V}}\right)$ is taken from the graphs provided by Vickery(1970).

The mean square deviation for the resonance deflections ((5.22) and (5.23)) is plotted as a function of resonant frequency and damping ratio in figure 5.11.

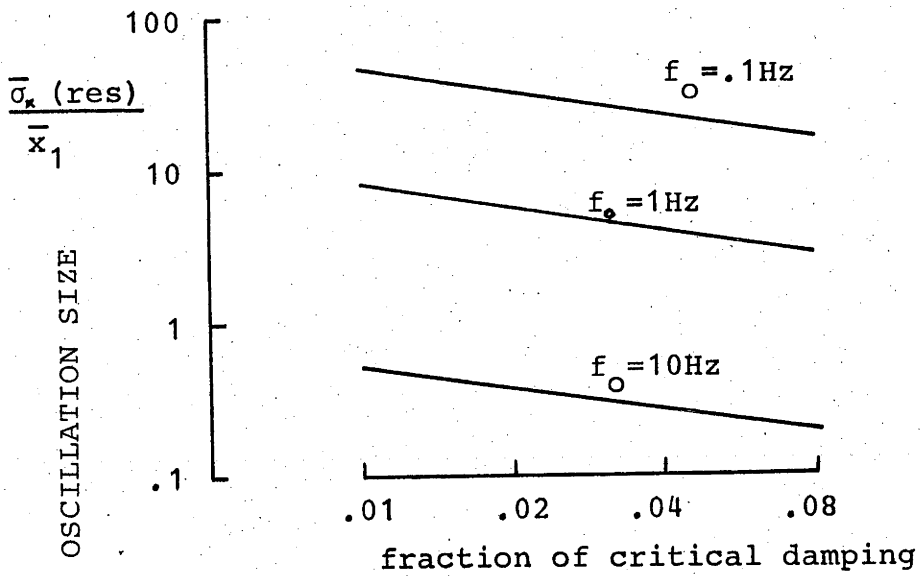


Figure 5.11 Resonance structural deflections as a function of resonant frequency (f_o) and damping. \bar{x}_1 is the mean deflection in a 1m/s wind.

The B effects are functions of frequency, the spectrum being plotted in figure 5.12. Practically all the B deflections occur in the frequency range .001Hz to .1Hz.

For a design value of $\bar{\sigma}_x$ of 1mrad, the specification for the structural rigidity of the collector, \bar{x}_1 , is plotted for varying resonant frequencies in figure 5.13. The compensation process has been described in section 5.3.2. Briefly, it requires that the servo respond quickly enough to prevent deflections from causing sun following errors. Unless damping is very low, a servo possessing this property of compensation will allow less rigid collector structures to be specified, provided that resonant frequencies are above 0.1Hz.

If we assume that the mode of deflection illustrated in figure 5.14 is dominant, we can derive an expression for the resonant frequency in terms of the design specification \bar{x}_1 , viz.:

$$(2\pi f)^2 = F / (\rho t \bar{x}_1 D/2) \quad (5.25)$$

where F is the force on the collector per square metre in 1m/s wind,

ρ is the density of the collector material,

t is the effective collector thickness,

and D is the collector diameter.

This resonant frequency information can be combined with figure 5.11 to give \bar{x}_1 as a function of $\bar{\sigma}_x$, which is shown in figure 5.15. Also shown are the minimum strength requirements, (with the deflection mode of figure 5.14), to

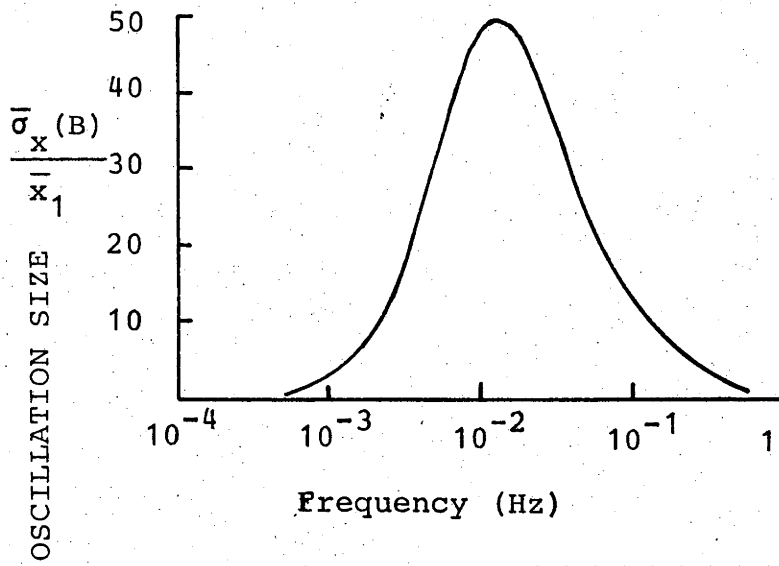


Figure 5.12 Spectrum of 'B' effects. Data is from a histogram with eight logarithmic steps per decade.

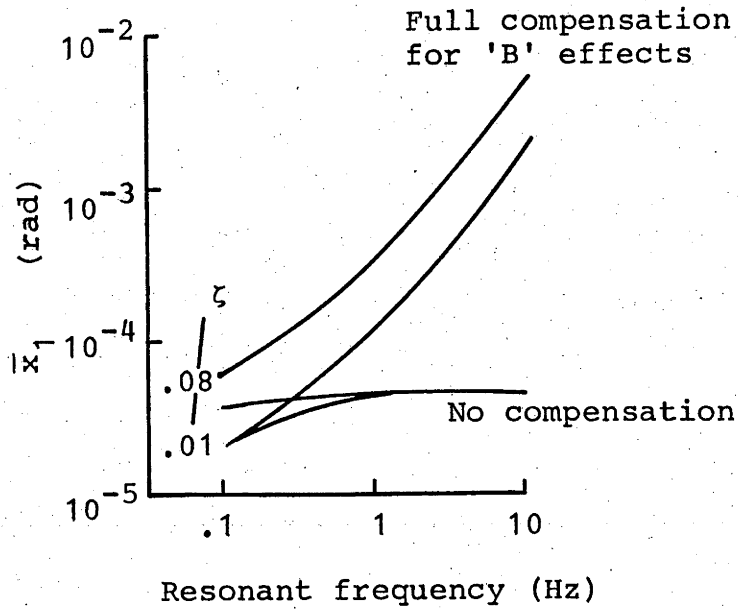


Figure 5.13 Required design deflection in 1m/s wind, \bar{x}_1 , as a function of collector resonant frequency and servo type for resultant rms wind induced deflections of 1mrad. ζ is the damping coefficient of the structure. Compensation is the process whereby the servo controlling the collector can compensate for the 'B' effect deflections, thus reducing sunfollowing errors.

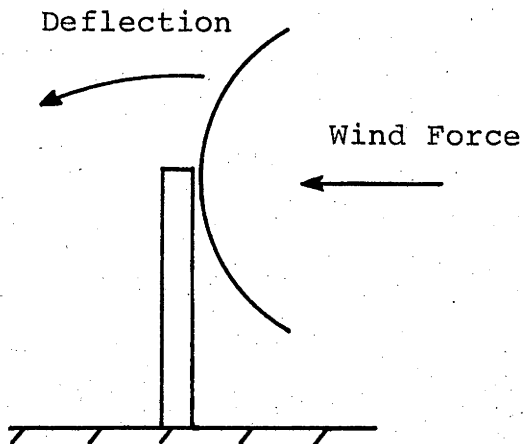


Figure 5.14 Deflection mode of collector assumed in text.

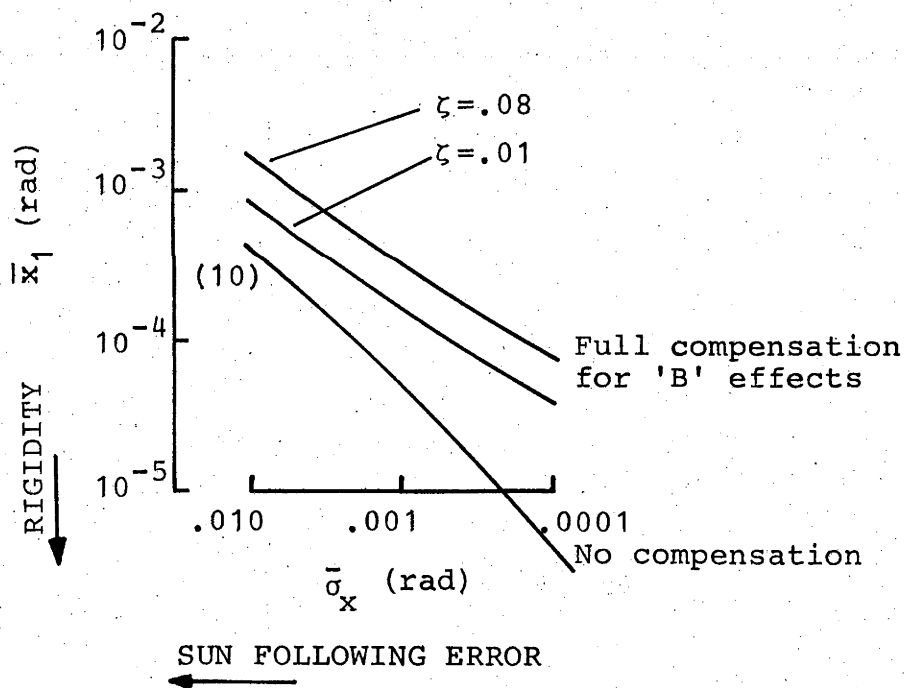


Figure 5.15 Design rigidity of collector structure expressed as deflection in 1m/s steady wind, x_1 . $\bar{\sigma}_x$ is the resultant standard deviation of deflections averaged over all sunshine hours.

(10)--Required rigidity to withstand steady 10m/s wind when unstowed.

ζ is the structure damping ratio.

withstand 10m/s winds while unstowed. Stow positions can be designed so that these minimum strengths are adequate for extreme (50m/s) winds.

Compensation has been described as the process whereby the controlling servo adjusts the collector position so that deflections due to the disturbance torques do not produce sun following errors. Clearly compensation for deflections at frequencies outside the bandwidth of the servo is not possible and thus no compensation can be used for resonant deflections. If the resonant frequency is less than .1Hz, then resonant deflections dominate the total deflections and compensation can at best have only a small effect on sun following errors. However, if the resonant frequency is greater than .1Hz, then the bandwidth of the servo is very important in determining resultant sun following errors. In figure 5.15 the resonant frequencies resulting from equation 5.25 are between 0.4 and 2Hz. In this case servo systems with bandwidths approaching the resonant frequency will be able to compensate for a large fraction of wind gust deflections. Such a servo possesses the operational equivalent of rigidity, whose costs are negligible, while the alternative of increasing rigidity by the required factor of 3 or so would be expensive. The costs associated with increasing rigidity are discussed in section 5.6.1.

5.4.4 Disturbance Torques Other Than Those Due To Winds.

Here we include structural loadings such as may be caused by the acceleration of the collector, loads due to the weight of the collector and loads due to thermal stresses in the collector. Only under very unusual conditions does the sun's motion include appreciable accelerations and this loading is ignored. For pointing systems using the extra loop in the pointing system of figure 5.3, errors due to dead and thermal loadings can be reduced by calculating appropriate corrections to the desired direction to compensate for the loadings. This process of compensation for errors can reduce these errors to near zero. The servo of a tracking system would have no difficulty with any of these loads, which vary slowly.

5.4.5 Encoder Errors.

The error between the actual shaft displacement and the information recorded by the encoder is the encoder error. If the encoders yield digital outputs with a minimum change of $(\Delta\epsilon)$, this is equivalent to an rms error of $(.29\Delta\epsilon)$. It is assumed that this error dominates other possible encoder problems such as linearity. The encoder error in the two axis situation considered here is the resultant of the errors for each of the two encoders, which, if identical, will be approximated by $1.4(.29\Delta\epsilon)$. The approximation is due to the fact that the cosin expression in the exact equation for combining the two errors, eqtn 5.26, has been ignored.

5.4.6 Mechanical Errors.

The effects of non-linear friction on servo performance have already been commented on. Other mechanical causes of error include backlash and axis wobble, the latter occurring when the axis of rotation does not exactly coincide with the axis of the axle being rotated. The impact of these errors is unknown until a hard design is formulated.

In the case of a tracking system, backlash and axis wobble are unlikely to cause sun following errors provided the relatively constant disturbance torques, such as dead loads, exceed the varying disturbance torques, such as wind loads. For a pointing system all mechanical error causes must be considered. These errors are not considered further in determining the composition of the guidance and control scheme.

5.4.7 ACTUATOR DISPLACEMENT CALCULATIONS.

A necessary input to the pointing system is the calculation of the actuator displacements corresponding to the desired pointing direction. This calculation can be carried out to any desired accuracy. We now analyse at length the method of calculation and present the cost of the calculation in terms of computer time as a function of the maximum error in the calculated actuator displacements. The impact of different computing machines on the times taken is considered. Results are presented in a set of graphs in section 5.4.7.7: in the case of 8 bit microprocessor calculations, detailed programming is outlined and storage requirements for the

programs given.

The calculations required to operate the additional loop of figure 5.3 are not considered here, but these would include the calculation of deflections due to dead loads and so on. In general, these calculations are identical for each collector and would not add to the cost of the calculation significantly provided that they are performed by the central control.

5.4.7.1 General Remarks

The calculation of the actuator displacements has two distinct parts. First the sun's position must be calculated - if the compensating loop of figure 5.3 is used then appropriate corrections must be applied. The second calculation yields the actuator displacements corresponding to the sun's position using the calibration constants for each collector. Only this second calculation must be repeated for each collector and this dominates the computation required - it is the only calculation considered here.

Regardless of whether the calculations are performed at the central or at the local control, some information must pass between the two controls. The data rate of the required information is considered in section 5.4.7.9.

The task is considerably simplified if the actuator displacements are calculated at intervals and linearly interpolated for times in between.

In this situation there are two error causes. The first is that caused by assuming the sun's path with time to be a series of straight line segments and the second is due to the errors in calculating the actuator displacements corresponding to the sun's position.

The first cause is a function of both the latitude of the alt-az mount and the length of the straight line segments. The error decreases with decreasing length or increasing latitude. Data on this error is presented in a pair of graphs, figures 5.16 and 5.17.

In analysing the second error source we consider calculation of the actuator displacements using four calibration constants only. Using the six calibration constants as outlined in section 5.4.2.2 ('Form of functions..') would make little difference to the results, adding two multiplications only to the effort required.

5.4.7.2 Errors In Interpolation

The path of the sun was assumed to be given by the equations derived for a uniformly rotating earth, with the declination of the sun varying sinusoidally with time, as given by Brinkworth(1972). Equations 5.1 and 5.2 were used to calculate the sun's position.

The strategy for calculating a path closely approximating the sun's in either coordinate is as follows: for the first segment, the path is an unconstrained linear least squares approximation to the sun's path. For subsequent

segments a linear least squares approximation is used with the constraint that the starting point must coincide with the endpoint of the previous interval.

This error is affected by the length of the segment and the curvature of the sun's path. Investigation shows that the latter cause is most severe when the sun is closest to being directly in line with the fixed (azimuth) axis. Using a precision sufficiently high to eliminate any discretization errors in the calculation itself, errors for pointing using the above strategy were calculated. The errors in both coordinates are combined to give a pointing error ($\Delta\theta_1$) by the formula:

$$(\Delta\theta_1)^2 = (\Delta\theta)^2 + (\cos\theta \Delta\phi)^2 \quad (5.26)$$

where $\Delta\phi$ and $\Delta\theta$ are the errors in azimuth (ϕ) and altitude (θ) respectively.

The variation of rms error over the year with variations in both segment length and latitude is shown in figure 5.16. Although the length of the segment has most effect on $\Delta\theta_1$, the phase relationship between the succession of segments and the functions describing θ and ϕ with time is also important. Thus in figure 5.16, $\Delta\theta_1$ vs segment length is represented by a zone in some cases rather than by a specific curve, the exact position within the zone being dependent on the phase. The maximum rms error over a single segment is shown in figure 5.17. This maximum rms error occurs at the summer solstice, around midday. Clearly this error is very small, even at

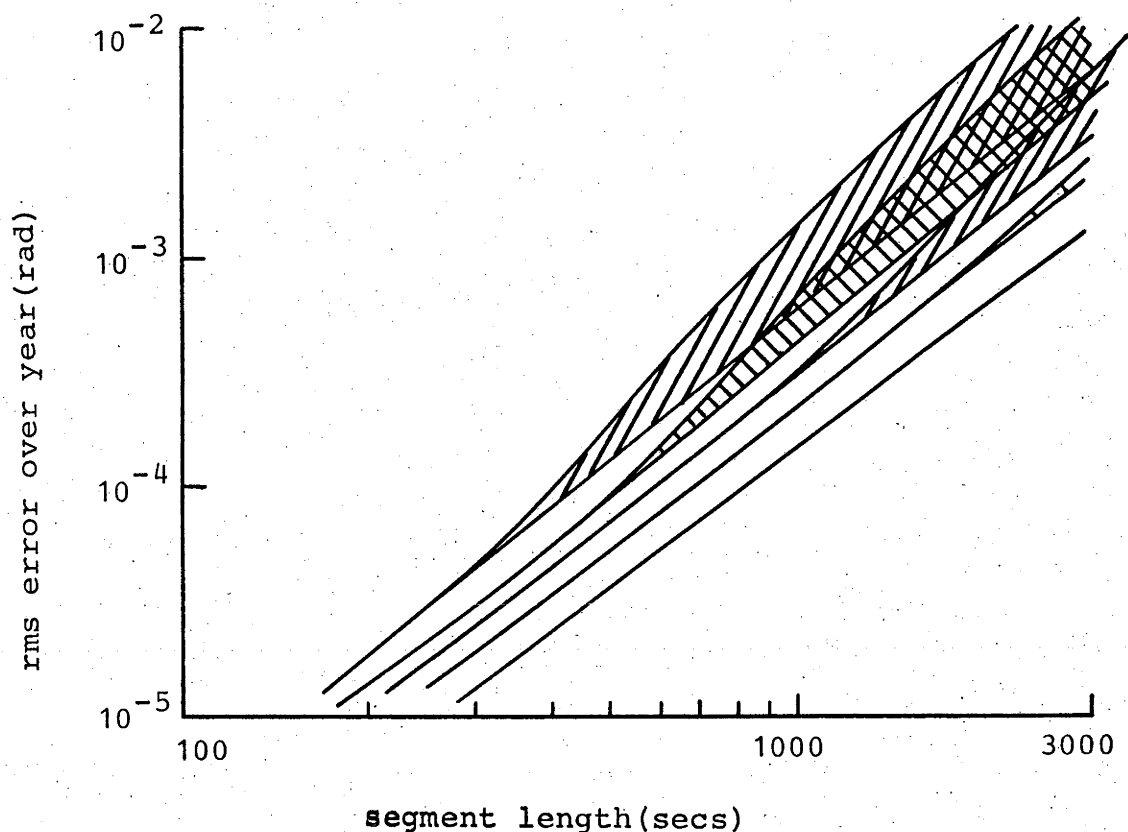


Figure 5.16 Errors due to approximating the sun's path as a series of straight line segments. Rms error calculated over all sunshine hours, for an azimuth-altitude collector at latitudes 24.75, 26, 28.5, 33.5, and 43.5 degrees respectively from top to bottom. The hatched area indicates the variation due to the phase relationship between the succession of straight line segments and midday.

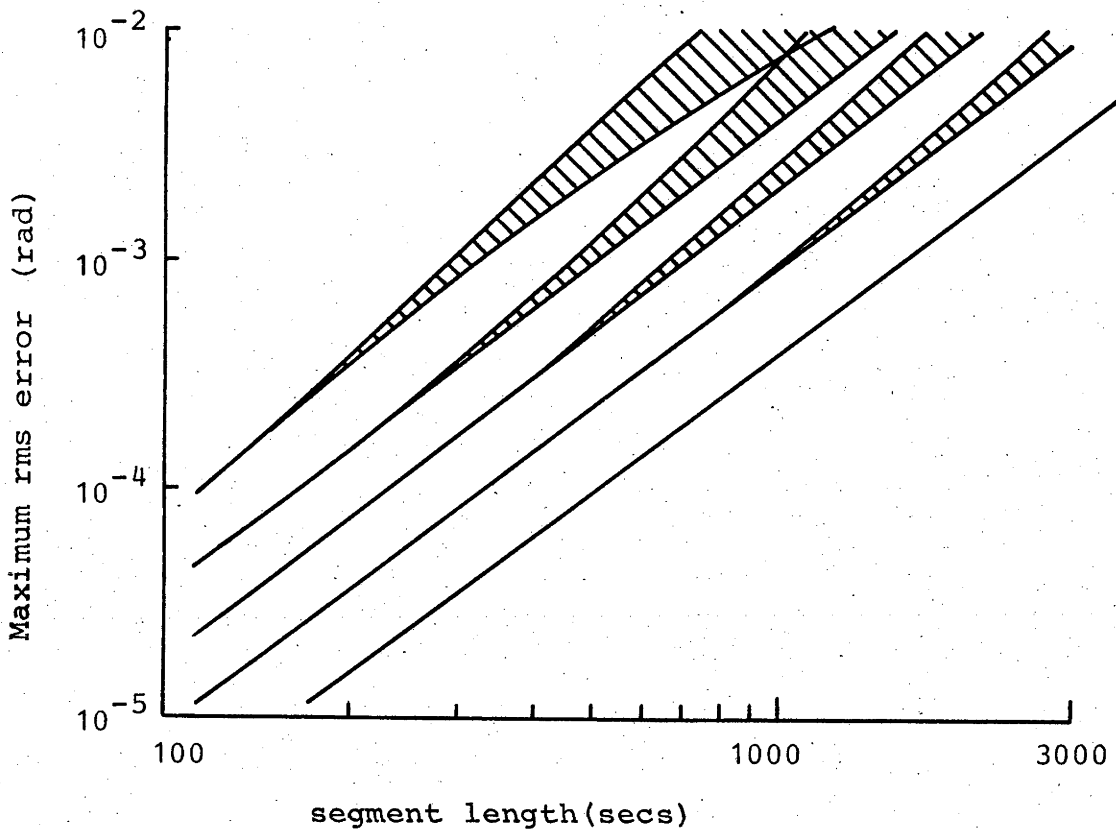


Figure 5.17 Maximum rms error over a year for a single segment due to approximating the sun's path as a series of straight line segments, for an azimuth-altitude collector considered at latitudes 24.75, 26, 28.5, 33.5, 43.5 degrees respectively from top to bottom. The hatched area indicates the variation due to the phase relationship between the succession of straight line segments and midday.

segment lengths of 1000 seconds.

5.4.7.3 Actuator Displacement Calculations.

The time to calculate the actuator displacements corresponding to a position in the sky depends upon the allowable error between an exact calculation of the displacements and an approximate calculation. In this section we relate this allowable error to the number of multiplications or divides in the calculation and assume that the time taken will be proportional to the total number of multiplications or divisions. For convenience we use the word multiplication to represent either multiplication or division as both operations are equally complex.

For floating point calculations, a graph relating pointing error to the number of multiplications is derived. Tests on two typical machines (PDP-11 and DEC-10) were made to determine the average time taken for each multiplication for this application. Thus the computation time to derive the actuator displacements can be calculated as a function of the accuracy of the computation. A separate section on the possibility of calculating the actuator displacements using a fixed point computation, as would be suitable for microprocessor calculation, is also given. Specific programming for an 8 bit calculation is shown and storage requirements and execution time are estimated. Requirements for 16 bit calculations using an 8 bit microprocessor are estimated by extrapolation.

No apologies are made for the nature of the estimation as the computation time required will vary quite markedly depending on machine features such as architecture and particularly on whether the machine has a hardware floating point multiplication instruction. The total time required will certainly be proportional to the number of multiplications for microprocessors without hardware multiplication, where the multiplication time dominates all other operation times. This will also be the case for machines with software based floating point multiplication routines, where multiplication routines also take a relatively long time. The assumption that time is proportional to the number of multiplications is possibly less true for machines with hardware floating point multiplication capability, where the multiplication time is of the order of the addition time. However, the actuator displacement calculation involves a reasonably constant mix of multiplications, additions and so on, accordingly the proportionality is still reasonable.

The actuator displacements θ and ϕ are given by the usual equations which transform the sun's position in equatorial coordinates into nominal alt-azimuth coordinates, using the calibration constants of the collector.

A number of equations can be derived, of which the most useful are:

$$\sin \theta = \sin B \sin \delta + \cos B \cos \delta \cos kt \quad (5.27)$$

$$\cos \phi = (\cos \delta \cos kt \sin B - \cos B \sin \delta) / \cos \theta \quad (5.28)$$

$$\sin\phi = \cos\delta \sin kt / \cos\theta \quad (5.29)$$

$$\tan\phi = \sin kt / (\sin B \cos kt - \tan\delta \cos B) \quad (5.30)$$

$$\cos\phi = (\sin\delta - \sin B \sin\theta) / \cos B \cos\theta \quad (5.31)$$

The calibration constants are included with B being the 'latitude' of the fixed axis and kt including the longitude of the fixed axis. The encoder zero errors can be included by adjustment of θ and ϕ .

For each computation of the actuator displacements equations (5.27) and (5.30) or (5.31) require the least multiplications/divisions. Equations (5.28, 5.29, 5.31) exhibit greatly reduced accuracy for ϕ near $\pi/2$ due to the error propagating properties of division in fixed point operations. Equation (5.30) is to be preferred, since the tangent of an angle determines the angle with more precision than any other trigonometric function.

In general, machines compute functions such as sin and cos by computing an approximation to the function - such an approximation could be a polynomial. The accuracy of the approximation increases with the number of terms and multiplications in the approximating function.

5.4.7.4 Approximating Functions.

In designing approximating functions it is customary to utilise an approximation which is valid over a range smaller than the possible values of the argument. The range of the argument is reduced by using standard identities. Also, usually only the inverse tan function is approximated and the

other functions calculated from it. Further only one of sin and cosin is approximated and one calculated from the other. Here we review the range reduction formulas used and particular points about the approximating functions required to calculate θ and ϕ .

The tan function is approximated over the range $(0, \pi/4)$, and the range is reduced to this by the relation:

$$\tan(x) = 1/\tan(\pi/2-x) \quad (5.32)$$

The atan (or arctan) function is similarly approximated over the reduced range $(0,1)$ and range reduction uses the same formula, resulting in, on average for evenly spread x , half an extra multiplication for each evaluation of the atan or tan function.

The asin function is calculated via the atan function using the formula:

$$\text{asin}(x) = \text{atan}(x/\sqrt{1-x^2}) \quad (5.33)$$

Thus a square root, an atan calculation and two extra multiplications must be performed for an asin calculation.

The square root function is economically calculated using a linear approximating function and iterative Newton-Raphson improvement. Range reduction to $(.25,1)$ is accomplished using the formula:

$$\sqrt{(2^{2b}x)} = 2^b\sqrt{x} \quad (5.34)$$

Only binary 'shifts' are involved, which correspond to movements of the decimal point in the decimal system. Thus the formula is easy to implement in the binary system. The linear approximation to the square root function is accurate to seven bits (or 2.1 decimal digits) and requires one multiplication only. Each iterative refinement requires one multiplication also and doubles the number of significant digits in the result.

Suitable approximations for the above functions are given by Hastings(1955) and Hart(1968) for various levels of approximation. In figure 5.18 the error with which the functions are represented is displayed with the abscissa being the number of multiplications required to achieve that error. Error here is defined in the same sense as Hart(1968), being the maximum relative error between the function approximation and the function.

5.4.7.5 Error Propagation And Accuracy.

Here we investigate the propagation of computation error through the calculation of the actuator displacements and estimate the accuracy of calculations as a function of the number of mathematical operations.

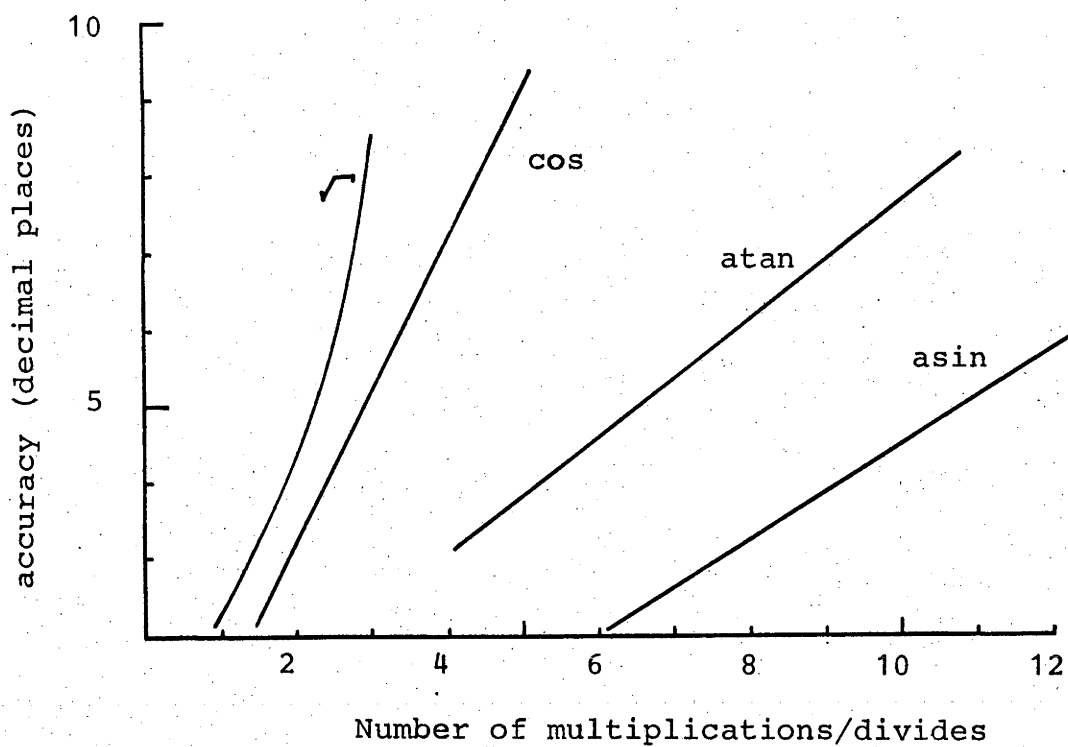


Figure 5.18 Accuracy (in decimal digits) of approximating functions represented with the number of multiplies or divides in the approximating function as the abscissa.

5.4.7.5.1 Floating Point Calculations.

In calculating the values of θ and ϕ , it is assumed that all approximating functions used have similar accuracies. The maximum possible error in the result of a floating point multiplication is simply twice the error in the multiplicands. Addition does not change the relative error, but subtraction does, particularly if the result is small.

If each approximating function has peak possible error f , then by inspecting formula 5.27 it seems reasonable to assume that θ will be calculated with a maximum possible error of $4f$. We ignore here the problems which arise if the argument of the asin function is near zero due to subtraction, or near 1, the latter resulting in error magnification due to the shape of the asin curve. Likewise in the calculation of ϕ , large errors may result for the denominator near zero. This problem will occur over only a small region of the sky (as is incidentally, the case for $\sin\theta$ near 1) and should not influence energy collection greatly. Thus the ϕ calculation (5.30) is assumed to involve peak errors of around $4f$ also. The resulting peak pointing error is the resultant of the errors in θ and ϕ , and is approximated by $5.6f$, being $\sqrt{2}$ ($4f$).

A range of possible accuracies for θ and ϕ was considered by selecting sets of approximating functions of equal accuracies from figure 5.18. The total number of multiplications required to achieve the error ($5.6f$) was calculated. Results are presented later together with the fixed point calculations (figure 5.21).

5.4.7.5.2 Fixed Point Actuator Displacement Calculations.

The errors introduced in eight bit fixed point calculations of the actuator displacements were analysed rigorously using function approximations specific for the task. Preliminary estimates by the author showed that the microprocessor at the local control could perform all tasks in a fraction of the time available and thus functions were calculated from approximate expressions rather than by looking up values in stored tables. This method would reduce storage requirements at the expense of increasing calculation times.

Storage of constants.

To ensure maximum possible accuracy, angles are stored with 377(octal), the maximum number possible in eight bit format, representing $\pi/2$ rads. Numerical values other than angles are stored without sign and in this case 377(octal) represents unity. The sign of the numbers and the quadrant of the angles are calculated by comparison operations, eg azimuth is in the first quadrant if the numerator and denominator of its tan are positive.

Error propagation in fixed point.

We define the function δ , such that $\delta(A)$ is the absolute error in the representation of A.

For fixed point calculations,

$$\begin{aligned} (\delta(AB))^2 &= (B^2 + A^2)g^2 \\ (\delta(A/B))^2 &= (1/B^2 + A^2/B^2)g^2 \end{aligned} \quad (5.35)$$

where g is the absolute error in representing a fixed point number (a constant for a fixed point machine).

We see here an important facet of fixed point division, namely that the magnitude of the denominator determines the error in the result, with a small denominator producing large errors.

Errors in calculating functions increase with the number of operations and also with the number of coefficients which cannot be represented exactly in the machine. Thus functions requiring minimal mathematical operations and small numbers of stored coefficients are doubly efficient.

Functions: General

The solutions derived by Hart(1968), and Hastings(1955) were derived for floating point operations. Error propagation in fixed point calculations is markedly different from the floating point case, particularly in division if the denominator approaches zero. For this reason functions represented as the ratio of two polynomials must be selected with care.

Functions used.

$$\cos(\pi/2 X) = 255/256 + X^2(-57/256 + 57/256 X^2) - X^2$$

(derived from Hart(1968))

(5.36)

This approximation requires three multiplications and has a maximum error of 2.6/256.

$$\text{atan}(X) = X(162/256 + X^2(-47/256 + 13/256 X^2))$$

(derived from Hastings(1955))

(5.37)

This approximation requires 4 multiplications and has a maximum error of 1.4/256 over the range $0 < X < 1$.

The form of the function $\text{asin}(X)$ over the full range $(0,1)$ makes implementation of an approximation difficult in fixed point calculations. All the suggested approximations of Hart(1968) do not yield sufficient accuracy, due to computation errors. To overcome this problem a standard tactic is to obtain an approximation to $\text{asin}(X)$ over a smaller range, say $(0, \sin \pi/4)$, and use the transformation:

$$\text{asin}(X) = \pi/2 - 2 \text{asin} \sqrt{(1-X)/2}$$

(5.38)

Unfortunately this transformation involves considerable loss of accuracy in fixed point and the method is of little value here. Another tactic is to use a relationship between

the atan function and the asin function, but again the transformation introduces too much error. Over the range $(0, \sin\pi/4)$, the asin function can be approximated by:

$$\text{asin}(X) = (163/256 X)/(1 - 50/256X^2)$$

(derived from Hart(1968))

(5.39)

This approximation has a maximum error of $2.6/256$ over the range $(0, \sin\pi/4)$. In later calculations if an asin value was required from outside this range, the value was generated by adding a random error of $2/256$ to a relatively accurate determination of the asin value.

There is no doubt an approximation for the rest of the range could be found. As a last resort, a trial and error routine based on the cos function could be used.

Actuator displacement calculation in 8 bit fixed point.

For the system of number storage assumed, eqtn 5.30 will be unworkable if $\tan\phi$ is greater than unity. There are two alternatives to avoid this problem. One possibility is to invert 5.30 and evaluate $(\pi/2-\phi)$ via the atan function. Alternatively, equation 5.31 can be used. Economy of programming suggests the former is the more appropriate and this is followed here.

The difference between the calculation of (θ, ϕ) by 8 bit fixed point computation and accurate (27 bit floating point) calculations is called the computation error. The computation error in (θ, ϕ) due to 8bit fixed point calculations is shown in figure 5.19. At low values of $(B-\delta)$ there is a large computational error in the calculation of ϕ via equation (5.30) as both numerator and denominator are small compared to unity.

The calculation time is dominated by the time required for multiplication and division, and the calculations described here required 31 such operations. Typical microprocessors take .5ms for each such operation; thus a calculation would require at most 15ms.

Interest here is in using 8 bit computations to guide a sun follower into position before the sun appears, ie a pointing system. When the sun does appear a tracking system would operate and reduce the sun following error to acceptable levels. The time between the appearance of the sun and the consequent reduction of sun following error to low levels determines the effectiveness of the pointing system and this response time is determined by the computational error in θ and ϕ . There will be two errors, one in θ and one in ϕ , the larger of the two errors will determine the response time. An overall picture of the expected response time due to computation errors is thus given by the mean daily value of the maximum of the two errors. This is plotted in figure 5.20. The mean, maximum computation error over the year was 16mrad for 30 degrees latitude and 10mrad for 40 degrees

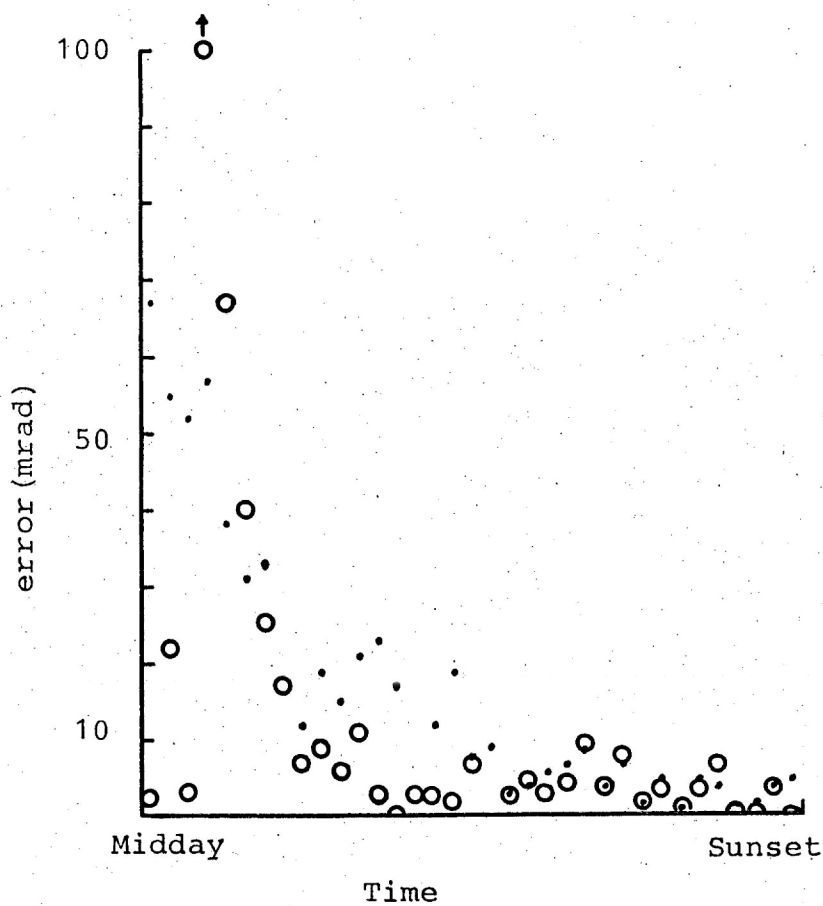


Figure 5.19 Computation errors for 8 bit fixed point calculations of the sun's position. Calculations are for an altitude azimuth mount at 30degrees latitude, the solar declination is 23.5 degrees.

- Error in azimuth.
- Error in altitude.

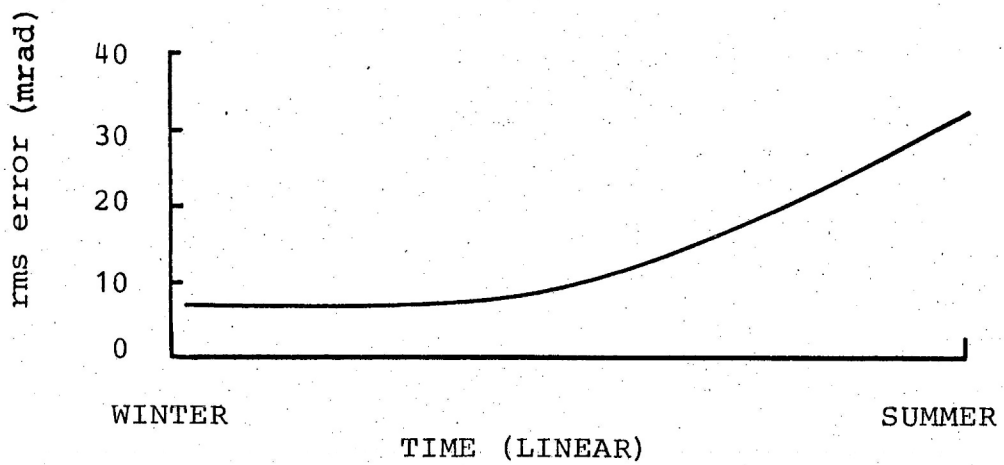


Figure 5.20 Daily error in the calculation of the sun's position by 8 bit fixed point computer as a function of the time of year. Latitude 30 degrees.

latitude.

5.4.7.6 Results

The accuracy of calculation as a function of the number of multiplication operations is displayed in figure 5.21 for floating point operations. Also shown in figure 5.21 is the expected maximum error in calculating θ and ϕ by fixed point calculations. This has been estimated from figure 5.19. The accuracy of 16 bit fixed point calculations is estimated from the slope of the floating point line and the results of the 8 bit calculations.

5.4.7.7 Time Required For Calculation.

The calculation of θ and ϕ was programmed for a DEC-10 and a PDP-11 machine, chosen as being representative of two broad classes of machines; the former is equipped with hardware floating point multiplication instructions and can calculate a product in some 6-10 μ s, while the latter calculates a product without such equipment and takes some 300 μ s. For the evaluation of the actuator displacements, the DEC-10 took on average some 40 μ s for each multiplication, while the PDP-11 took 350 μ s.

Integer (fixed point) calculations on an 8 bit microprocessor are totally dominated by the multiplication time, which, for an 8 bit multiplication is about 500 μ s and for a 16 bit multiplication, some 2ms. The time to calculate θ and ϕ as a function of accuracy and machine type is given in

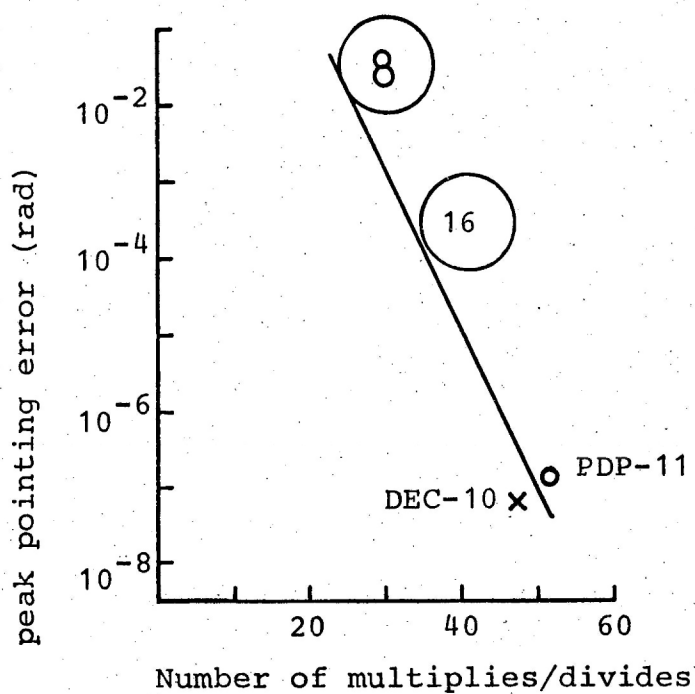


Figure 5.21 Peak pointing error between accurate calculations of actuator displacements θ and ϕ and approximate calculations, as a function of the number of multiplies or divides in the approximate calculations. The unbroken line is data for floating point calculations, with the maximum accuracy of typical machines shown. 8 and 16 are the results for 8 or 16 bit fixed point computation.

figure 5.22.

5.4.7.8 Program Storage Requirements.

Program storage requirements are trivial for the central machine; however, they may be critical if the calculation is to be performed by a microprocessor where memory size is important. To gain an estimate of the program size for an 8 bit microprocessor, a program to calculate θ and ϕ in 8 bit fixed point computation was coded for the Intel 8080. (The programs were not run).

The following notes are pertinent to the program and place the storage estimates in perspective.

1. All subroutines stored and restored the general purpose registers B through L of the 8080.
2. The program was written to minimise the time taken to write the program, not storage requirements.
3. In general, values were recalculated rather than stored in read/write memory.
4. No provision was made for calculating an elevation less than zero.
5. The evaluation of ϕ requires care to be taken at several points. In particular, juggling is required to ensure that the subtraction in the denominator of eqtn 5.30 does not underflow, with the further problem that $\sin(\delta)$ may be negative. If the numerator is larger than the denominator, $\cot(\phi)$ is evaluated, and ϕ determined via the atan function.

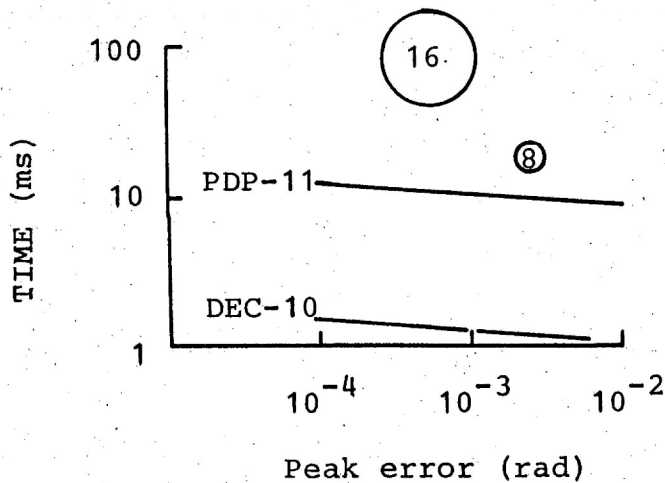


Figure 5.22 Execution time to calculate θ and ϕ as a function of peak error and machine type. 8 and 16 refer to 8 and 16 bit fixed point calculations on an 8 bit microprocessor. PDP-11 used here has software floating point operations, in contrast to the DEC-10 which has hardware multiply and divide operations.

6. It was assumed that the argument for the asin function always fell in the range (0.,0.707) so that eqtn (5.39) was used in the implementation.

The program storage requirements for each of the basic units of the programming were as follows: (Storage requirements are expressed in bytes.)

Read only memory (ROM) requirements (bytes):

Divide	27
Multiply	27
cos	37
sin	11
asin	30
tan	13
atan	40
θ calculation	50
ϕ calculation	95
Total	330

Read or write memory (RAM) requirements:

Constants from RAM: declination, time, latitude.

Constants to RAM : θ, ϕ .

-----say 9 bytes.

The extrapolation to estimate memory requirements for 16 bit calculations uses the rule of thumb that twice the storage will be required. Thus it is estimated that 700 bytes would be needed.

5.4.7.9 Data Rates Over The Communication Link.

Here we analyse the expected data rates over the link between the central control and the field of collectors. We assume that all collectors are attached to a single medium, so that individual instructions must be accompanied by some identification. This party line structure could be a single frequency radio link or a cable network. The rates are considered in two sections, depending on whether the central control carries out the complete actuator displacement calculation or only the sun position calculations.

Case 1. Central control calculates sun position only.

The solar position can be transmitted as the hourangle and declination of the sun in equatorial coordinates and the local control with the aid of the calibration constants calculates the corresponding actuator displacements. The hourangle of the sun can easily be transmitted via the power line frequency, as the difference between local mean solar time and the sun's hourangle varies slowly, on a time scale of months. The local control can count the oscillations of the power line variations in exactly the same manner as a digital clock; a single command to each collector advising when to

set the hourangle to zero would complete the effective transmission of the sun's hourangle. The declination of the sun varies approximately sinusoidally, so to transmit declination accurate to 10mrad, a command informing the local control of the sun's declination would need to be transmitted every 3 days. To transmit declination accurate to 1mrad the interval would have to be 7hours. Clearly the data rates would be negligible and transmission of the calibration constants to the collector would not place any significant extra demands on the communication link.

Case 2. Central control performs all calculation.

In this case the obvious compromise is between calculating the actuator displacements frequently, with correspondingly low interpolation errors, but high data rates, and calculating the displacements at relatively large intervals, but with low data rates.

We calculate the data rates assuming that the method of data transfer involves the central control giving speed commands at regular intervals t_c , called the command time (Carden 1978a). The local control maintains the desired speed for this time without accumulating errors. Thus a parallel interpretation of the command is that after t_c seconds the actuator will have displaced through t_c times the requested speed.

The speed command is represented by $(n_m + 1)$ bits, being the magnitude and direction of the speed. The minimum speed change is given by (Carden 1978a) as:

$$\Delta\omega = \omega_m / 2^{n_m} \quad (5.40)$$

where ω_m is the maximum speed, assumed to be $\pi/3600$ rads/sec.

In guiding an actuator from position A' to position B' in an attempt to duplicate the best straight line approximation of the sun's path from A to B, a speed is chosen to minimise the errors between the two paths. Due to the discretisation of the speed commands, (A-A') and (B-B') will both come from a distribution uniformly spread over an interval determined by the length of the command interval and the minimum speed change, centred on A and B respectively. The width of the distribution is given by:

$$\max |A-A'| = \max |B-B'| = \Delta\omega t_c / 2 \quad (5.41)$$

The rms difference between the paths AB and A'B' is calculated from 5.41 and is given by:

$$\Delta\theta_2 = .47 \Delta\omega t_c / 2 \quad (5.42)$$

This information can be combined with figure (5.16), to give the portion of the rms pointing error which is caused by the method of calculation of the actuator displacement and the information transmission scheme. It is assumed that the

errors in the calculations by the central control are sufficiently small to be ignored.

The data rate of the commands is given by:

$$R_m = N_c (\log_2 N_c + 2n_m + 2) / t_c \quad (5.43)$$

where $\log_2 N_c$ is the number of bits required to give a unique address to each of N_c collectors. Data rates for speed command communication assuming unique commands to each collector are given in figure 5.23 for 10 000 collectors. Latitude 28.5 is the lowest latitude at which a collector with a maximum azimuthal velocity of ω_m (defined below eqtn 5.40) can follow the sun at all times. Clearly, even for small pointing errors due to the transmission technique, data rates are small. The command time and the number of bits in the speed command have been chosen to minimise the data rate R_m for a particular error contribution.

5.4.8 Servo Lags.

The size of velocity and acceleration lags depends on a combination of the design of the servo and the velocities and accelerations of the object being followed.

If a collector mount corresponds to the equatorial frame of reference, the actuator velocities and accelerations are such that simple servo designs result in negligible lag errors. Non-negligible lag errors arise only if an alt-azimuth mount is used and the fixed or azimuth axis at some time goes close to intersecting the sun's position. This

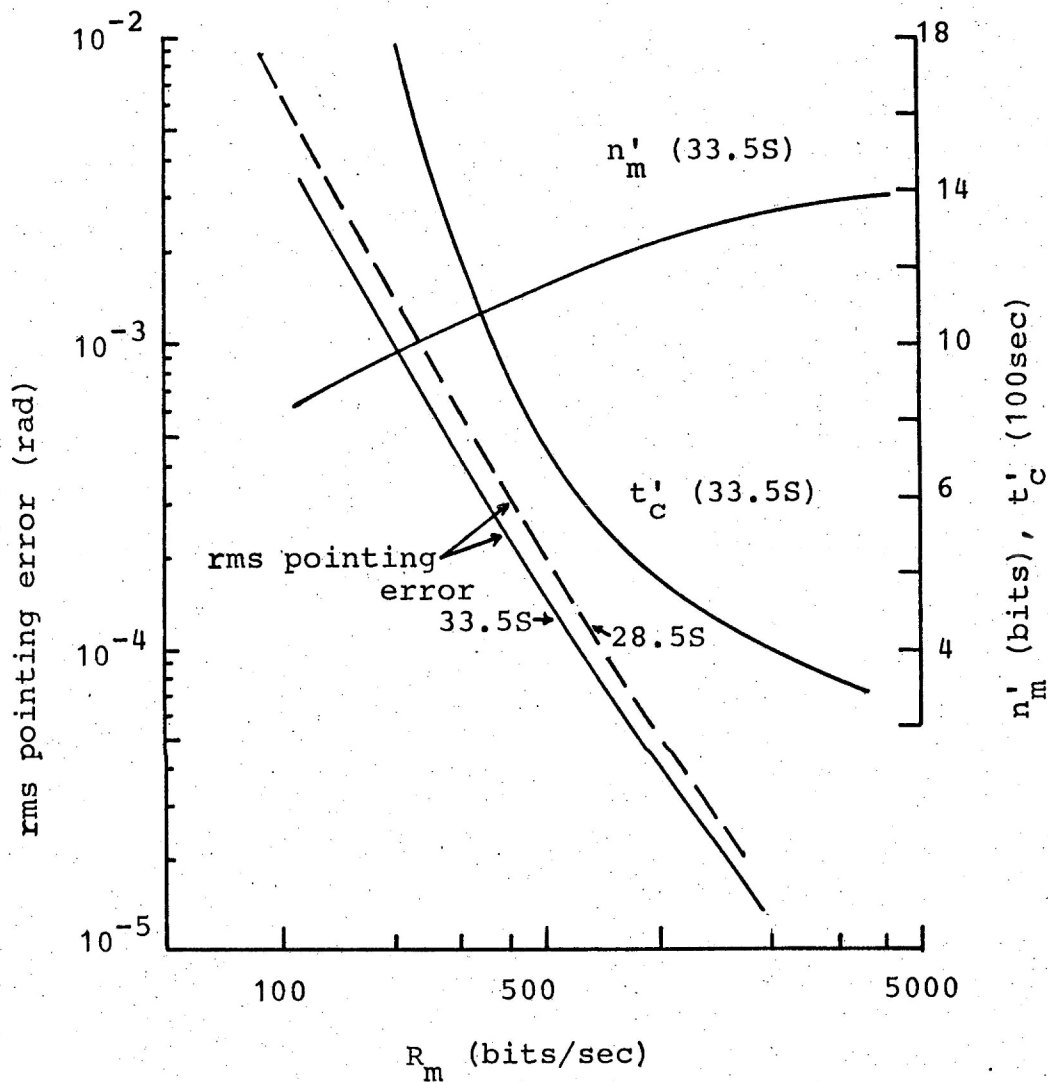


Figure 5.23 Rms pointing error over a year as a function of data rate R_m of the speed commands. The error indicated is the combination of errors due to approximating the sun's path as a series of straight line segments and using digital speed commands. t'_c and n'_m are the values of t_c and n_m which minimise the error for a particular R_m .

problem occurs for alt-az mounts at latitudes between 27S and 27N. The problem can be avoided by leaning the fixed axis towards the equatorial axis. In any case, the region where high velocities and accelerations are encountered is small and lags can be ignored.

5.4.9 Response Time.

As reported in section 5.3.1.1, guidance and control schemes using tracking systems for sun following fail to collect some 3% of the available sunlight due to the misalignment of the collector at the beginning of the sunshine burst. This misalignment and thus the amount of uncollected energy can be reduced by incorporating a pointing system to guide the collector when the sun is not shining. The sun following errors associated with the pointing system and the maximum velocity capability of the actuators determine the response time, but each axis must be considered individually and the maximum of the two response times thus calculated is the important value. A measure of the response time can be approximated simply as the mean sun following error divided by the maximum actuator velocity.

The relationship between the amount of uncollected energy and the response time is determined for Griffith and is used as a guide. For Griffith, 98% of the sunshine hours occur in 1000 bursts all of which are longer than 10 minutes. Thus a response time of τ seconds will result in a total of 1000τ seconds of uncollected sunshine which can be related to the total sunshine hours for Griffith of 2800. Table 5.2

shows the relationship between the sun following error, response time and collection losses for this site. The sun following error at the start of the sunshine burst is called the initial sun following error; in calculating this value for a particular pointing scheme it should be noted that it should be the arithmetic mean of the maxima of the errors in the two axes.

TABLE 5.2

τ (sec)	Initial Sun Following Error (rad) (a)	Collection Losses (%) (aa)	Value (\$/m ²) (#)
0	0	0	0
10	.009	.1%	.05
100	.09	1.0%	.5

(a) based on a maximum speed of ω_m (8.7×10^{-4} rads/sec)

(aa) based on 1000 sunshine periods/year and total sunshine of 2800hrs/yr.

(#) based on the viable cost structure of 50\$/m².

Thus increasing collection by reducing the response time is a worthwhile practice. There are two obvious ways of reducing τ ; one can either increase the maximum speed capability of the collector, or one can reduce the sun following error at the time the sun appears.

The former method will reduce the smoothness of operation under normal sun following conditions due to the limited dynamic range of the actuators and more powerful and therefore more expensive motors will be required.

Hence the preferred solution is to reduce the initial sun following error. An accurate pointing system is not, however, required as a mean pointing error of 45mrad involves collection losses of only .5%.

It is made clear in Appendix B that, at least for Griffith, each sunshine burst begins at positions which are isotropically spread over the sky and thus a pointing system capable of anticipating the the sun's position at sunrise only would not be very effective.

5.4.10 Combination Of Error Sources.

We detail here the method which should be used to combine the error estimates for the previously analysed sources into a single figure, because the justification of the method is not immediately obvious.

For each individual collector, the errors which are random in time can be combined by summing the squares and the effect of the errors which are not random with time, such as alignment errors for both tracking and pointing systems, can be included by addition. Such an approach neglects the objective of calculating a suitable average sun following error from which the amount of energy collected by the array of collectors can be calculated. The alignment error causes, while not being randomly distributed around zero in time, are randomly distributed around zero for the whole field, each collector having a different value. An rms value for this error estimated for the whole array of collectors can be combined with the other errors to give an rms average value of the sun following error which will enable a calculation of the amount of energy collected to be made.

There are several other errors which may not be randomly distributed around zero and these are considered as follows.

1. Servo lag errors. The characteristics of the motion of the sun are such that simple servo designs eliminate such errors. (see chapter 6 for a servo design.)
2. Disturbance torque errors. In the simple pointing system illustrated in figure 5.2, disturbance torque errors produced by thermal and dead loads may be strictly additive. The improved system of figure 5.3 will not be capable of reducing these errors to zero, as there will be further errors in the error correction process. However, these further errors will be random around zero.

Thus all errors may be combined simply as an rms average which will enable an estimate of the energy collection of the array to be made.

5.5 Summary Of Implications For The Guidance And Control Scheme.

Here we outline the principal conclusions of the above analysis.

(A) If the sun is shining use a tracking system.

The importance of servo bandwidth is shown in figure 5.15, where the required rigidity (\bar{x}_1) of the collector structure is shown as a function of rms deflection ($\bar{\sigma}_x$) over

the sunshine hours. Collectors controlled by servos with bandwidths of .1Hz allow collector structure rigidity to be 3-10 times less than collectors controlled by servos with a bandwidth of only .001Hz.

Using the sun sensor in a feedback path local to the collector could easily achieve such a bandwidth and would be a simple solution. However, the sun sensor is in an environment which is not conducive to perfect reliability, in contrast to the components of a pointing scheme and it is possible that the reliability of the sun sensor may introduce losses in collection. However, this reliability as calculated later in chapter 6, introduces only 0.0015% collection losses.

An alternative which avoids the use of a sun sensor would be to operate a pointing system when the sun is shining. For a pointing system to be competitive, the costs associated with the pointing system must not exceed the equivalent of .0015% of the sunshine hours. For a pointing system to collect equivalent energy to a tracking system, there are three alternatives, as follows.

1. Operate the pointing system using an array of wind sensors to provide compensation for the deflections due to winds, using the servo loop of figure 5.3. Corrections to the desired position would need to be calculated at least every second and these corrections would need to anticipate deflections produced by the wind in two directions. Also, the corrections may be different for each collector. The cost of this compensating process is constrained to be less

than .0015% of the cost of the collectors, or roughly \$2000 for a square kilometre of collectors. This constraint is severe and appears impossible to meet.

2. Operate the pointing system at low bandwidth and increase the rigidity of the collectors. A factor of three (figure 5.15), is required, which is certain to cause additional costs greater than .0015% of the cost of the array.

3. Operate the pointing system at low bandwidth and provide additional collectors to gather the energy lost due to the increased deflection of collectors. The standard deviation of the deflections and thus that of the sun following errors increases by a factor of about six and additional losses (see figure 4.4) amount to .5% even for efficient absorbers.

None of the above alternatives seem remotely viable, especially considering that the reliability of the additional components of the pointing system has not been considered.

(B) Pointing systems.

If it is desired to reduce losses due to response time below around 3%, a pointing system must be incorporated in the guidance and control scheme. The magnitude of the collection losses due to response time is shown in table 5.2. Losses due to response time can be reduced by utilising a pointing system, but, as shown in the table, a high accuracy pointing system is not required.

(C) Alignment method (c) should be used.

The dual usage of the sun sensor for both tracking and alignment makes this computational method even more economic in comparison with the manual methods (a) and (b).

5.5.1 Location Of Guidance And Control Scheme Functions.

The results of these deliberations is a guidance and control scheme of the form shown in figure 5.24. The communication link is available for maintenance and diagnostic procedures and is used for the alignment process when necessary.

Ignoring for a moment contingency operation such as stowage and maintenance, a diagram of the required sun following functions is shown in figure 5.25. Three processes are required for this system, a tracking process, an alignment process and a pointing process.

The tracking process operates when the sun is shining with a feedback loop encompassing the sun sensor, local control and actuators. The design of the tracking servo is considered in detail in chapter 6.

The pointing process operates when the sun is not shining and the power to the actuators is adjusted so that the position encoders record the requested actuator positions as calculated to correspond to the sun's position. The accuracy of this process need not be high, which will make rudimentary and thus cheap position encoders possible.

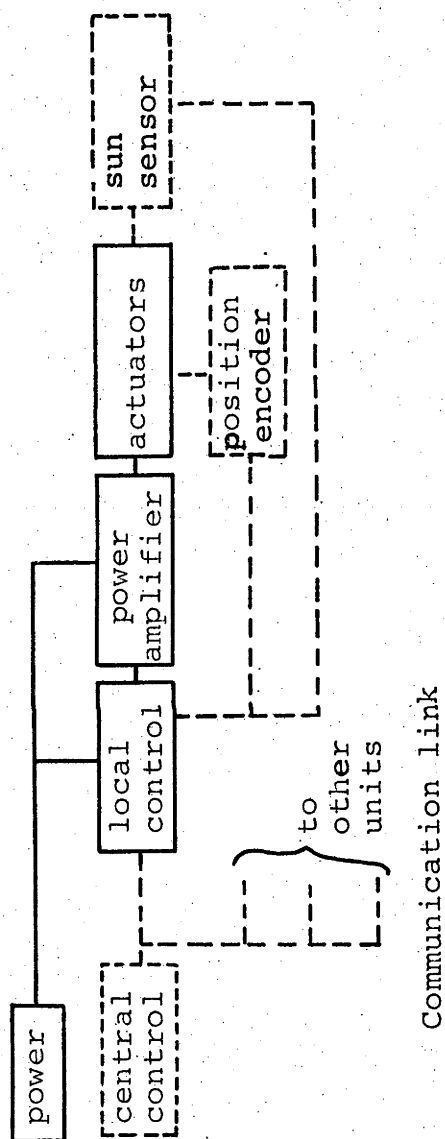


Figure 5.24 Outline of guidance and control scheme items. Dashed lines are used to indicate non-continuous operation, for example the sun sensor is not used if the sun is not shining.

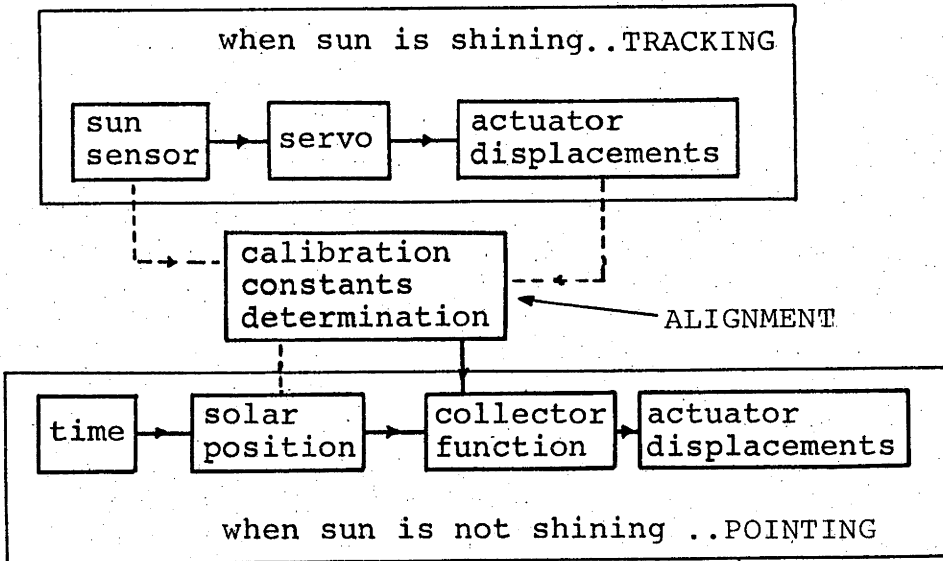


Figure 5.25 Functions required of guidance and control scheme for energy collection. Contingency operations ignored in this diagram.

There are two basic locations of 'intelligence' in the solar power plant: at the central supervisory machine and at each collector. In the following paragraphs we discuss briefly each of the above processes, with particular emphasis on where each process should be based.

The tracking process requires that the servo take information from the sun sensor and adjust the power to the actuators appropriately. A reasonable bandwidth of .1Hz is required, but the nature of the sun's motion and the collector characteristics make simple servo designs feasible. Thus it seems reasonable to base this process at each collector. The implementation of the servo is detailed in chapter 6.

The theory of the alignment process has been described in section 5.4.2. The program to implement the alignment process on the DEC-10 used some 10000 36bit words and thus this process cannot be based at each collector and must be performed by the central machine.

The pointing process involves several calculations, including the calculation of the sun's position and the calculation of the actuator displacements. The complexity of the calculations depends upon the required accuracy. Calculating the sun's position is relatively complex: it is reasonable that the central machine perform this calculation, which is identical for all collectors. The decision on where to base the calculation of actuator displacements is not as clear and depends upon the tolerable losses due to response time.

For example, fixed point calculations at each collector carried out to 8 bit accuracy would be capable of reducing collection losses to .2% and would leave the central machine free to concentrate on other tasks. Furthermore, the same calculations based on 16 bits would make losses due to response time negligible, though requiring more memory at each collector. However, this memory requirement is not stringent, as current production one chip microprocessors have 2048 bytes of ROM as standard whereas the 16 bit program requires only 700 bytes.

On the other hand, should the actuator displacement calculations be based at the central machine, the calculations can be carried out with peak errors of less than 1mrad at a rate of 80/sec by a machine with no floating point multiplication hardware. Such errors will introduce no losses due to response time. Intervals between calculations of 200 seconds would introduce little additional error and thus 10 000 collectors could readily be handled by a single machine.

A disadvantage of the central machine approach is that the reliability of the single machine affects the whole collector array. Another disadvantage is the additional load on the communication link, although this seems a minor consideration.

The independence of calculating the actuator displacements at each collector is an important asset; this approach is favoured and this is further discussed in section 5.6.3.

5.5.2 Assumptions Made In Above Analysis.

Several assumptions have been made in the above analysis and the validity of these should be checked before final judgement passed. These assumptions are:

1. The resonant frequencies of the collector are sufficiently high to ensure dominance of the 'B' induced deflections over resonant deflections.
2. The spectral density function of the wind velocity in the collector field is adequately described by equation 5.24.
3. The initial cost of the sun sensor is not considerable.
4. Frequent attention to the sun sensor (eg re-alignment) is not necessary.
5. Stow positions are found that enable a collector to survive extreme winds without increasing collector strengths above the strength equivalent to the deflection specification.

Point 4 is important, particularly for the central receiver concept, where the sun sensor will be resting on a foundation which may subside relative to the target.

5.5.3 Comparison With Central Receiver System: Some Comments.

It is interesting to compare the guidance and control scheme described above with the various schemes proposed for the heliostats of the power tower projects. Sun sensors for the power tower project, when employed, are more expensive, as each sensor must be aligned with the central receiver in the field. Of the four heliostat proposals (Vant-Hull 1976), two have guidance and control systems utilising pointing systems only, while two are equipped with sun sensors. The two with sun sensors are of conventional design, with a single broad mirror face of some 40m^2 . The two pointing schemes include the Boeing proposal, where the heliostat is protected by an inflated plastic dome and the Honeywell proposal (Fourakis et al 1977), which uses a low profile heliostat consisting of several segments in a venetian blind formation. Both of these concepts have reduced vulnerability to wind gusts.

5.6 Variation Of Costs With Error Specification.

Data which relates the cost of achieving a specific error budget as a function of that error budget is essential to the design of an economical solar power plant. Here we ignore those budgets which rely upon a specific hardware configuration. These ignored budgets include the sun sensor accuracy, position encoder accuracy and mechanical errors. Thus only the costs of achieving deflection budgets, servo lags, calculation of the sun's position and alignment will be considered.

5.6.1 Cost As A Function Of Collector Rigidity.

Energy losses dependent on the deflections of the collector can be reduced by increasing the collector rigidity, which in turn will increase the cost of the collector.

It is possible to get only an order of magnitude estimate here; this is obtained as follows: The solar energy collector is composed of a series of structural members and a change of specification for a wind load deflection requires that the structural members be resized.

We estimate the variation of collector cost with wind deflection specification by considering the variation in mass of a pipe with a deflection specification. This variation in mass is then related to the collector cost. We note here that gravitational effects on the mass of the pipe are of no relevance as only higher frequency wind deflections are of importance.

The strength of the structure is increased by varying the pipe cross section. This variation can be accomplished in a number of ways, for example the gauge of the pipe can be increased by holding the outer diameter (or inner diameter) constant. Other alternatives are to hold the pipe gauge constant and vary the pipe diameter, or to hold the ratio of pipe wall thickness to pipe diameter constant and vary the diameter. In resizing the pipe, the factor S is the ratio of the original pipe deflection to the new pipe deflection under an identical load. The factor M is the ratio of the mass of the new pipe to the mass of the old pipe. For the first two alternatives, the relationship between M and S is calculated

readily as:

$$M = (1 - \sqrt{1 - S + S k_o^4}) / (1 - k_o^2) \quad (5.44)$$

where k_o is the ratio of the inner diameter to the fixed outer diameter of the original pipe. The equation is unchanged if the resizing is accomplished by fixing the inner diameter, providing k_o is redefined as the ratio of the outer diameter of the original pipe to the fixed inner diameter. Representative values of the two ratios are shown in figure 5.26. As k_o approaches unity (a thin wall pipe), the derivative of the above expression with respect to S goes to unity, for S near 1. For k_o greater than 1, a pipe being resized by increasing the outer diameter, the derivative approaches 0.5. The most economical way to resize pipes is to use thin wall pipes and increase both inner and outer diameter. If the wall thickness is held constant, then the derivative is $1/3$. If the ratio of the wall thickness to pipe diameter is held constant and the diameter varied, then the derivative is $1/2$.

Not all structural members can be thin wall pipes and due to other constraints, such as bearings, resizing probably cannot be accomplished in the most ideal manner. Thus it seems reasonable to assume that the mass of the collector will increase at least as fast as $1/2$ the deflection decrease.

To relate this increase in mass to an increase in collector cost, we assume that the collector cost will increase, but only due to the cost of the additional metal.

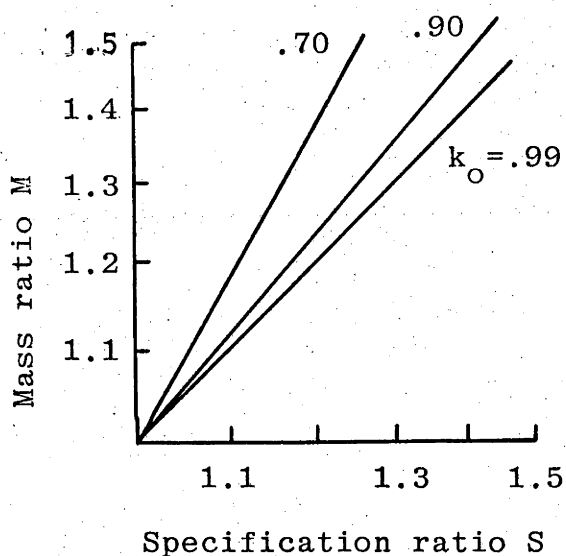


Figure 5.26 Variation of the increase in mass of a pipe with a decrease in deflection, as described by the ratio of the two pipe masses, and the ratio of the deflections of the two pipes under the same load. The ratio of the inner diameter to the outer diameter of the weaker of the two pipes is given by k_o .

This is equivalent to assuming that the other components of collector cost, namely, handling, welding and so on, do not increase. Carden(1978b) has shown that cars and bicycles, items which have an equivalent technology to paraboloid collectors, cost about 3000\$ for each tonne of metal. This is roughly 8 times the cost of the bulk metal and thus a 16% decrease in deflection specification, accompanied by a corresponding increase of approximately 8% in mass, will result in a 1% increase in collector cost. Stated another way, an order of magnitude estimate is that cost will vary as one-sixteenth of the deflection specification, where cost increases as deflections decrease.

5.6.2 Servo Errors.

Apart from the problems encountered when tracking near the zenith, sun following is basically a simple task. Servos with no velocity errors and negligible acceleration errors can be configured easily. As is shown in chapter 6, the digital control loop introduces relay-like oscillations into the sun following error; however, low oscillation amplitudes can be realized easily. Higher performance servos in general require compensating filters and should more performance be required the incremental cost of programming additional filtering stages will be very small.

5.6.3 Actuator Displacement Calculations.

If relatively low accuracy is required, it is feasible that the microprocessor situated at each mirror should perform the calculations. This is also an economic method, as the microprocessor can perform the calculations in the time it is idle and the only costs involved will be those of programming and memory requirements. Eight bit fixed point calculations have been shown to involve a mean error of some 16mrad for 30degree latitude calculations and 10mrad mean error at 40 degree latitude. This is equivalent to response time losses of the order of .1-.2%.

The incremental step in accuracy to be taken would be to use 16 bit calculations, which would be ultimately accurate to perhaps .05mrad. This ultimate accuracy would be achieved only if the calculations accounted for atmospheric refraction and the influence of dead and thermal loads. This would increase the complexity of the calculation substantially and may force the use of the central machine if this accuracy is demanded. However, 16 bit calculations using the same formula as shown in section 5.4.7.3 would be substantially more accurate than the eight bit calculations. The errors in the calculations would be solely due to the ignored effects, which, for refraction, would amount to 3mrad at 5 degrees elevation, increasing to 9mrad at the horizon. Ignoring refraction corrections would lead to response time losses of .002% at 30-40 degree latitudes. Dead loads similarly would be most important near the horizon, but the effect can be gauged only in the presence of a specific design.

The cost increment between .2% and .002% losses would be non-negligible only if the extra programming and memory requirements forced the use of a larger microprocessor chip.

The variation in costs with accuracy if the central machine calculates the actuator displacements has been shown in figure 5.22. A floating point hardware multiplication and division facility on the central machine, costing perhaps \$5000, would mean the central machine could perform the calculations for 10 000 collectors in a fraction of the time it has available.

5.6.4 Alignment.

Alignment would be carried out by method (c) of section 5.4.2.2 and the accuracy of this process is the product of two factors; the error ratio and the rms error in the actuator displacements. This latter error, as explained in section 5.4.2.2, is the sum of the mechanical, servo and torque disturbance errors for the tracking system and the encoder error, all calculated for one axis only. If the latter is constant, then alignment accuracy can be increased by using more data points in the calibration process. In this case, as suggested in a section 5.4.2.2, costs are principally determined by the execution time - this is given in figure 5.27 as a function of the error ratio. The value of this time is estimated at \$100/hour and thus full scale in the figure represents some .4\$/alignment.

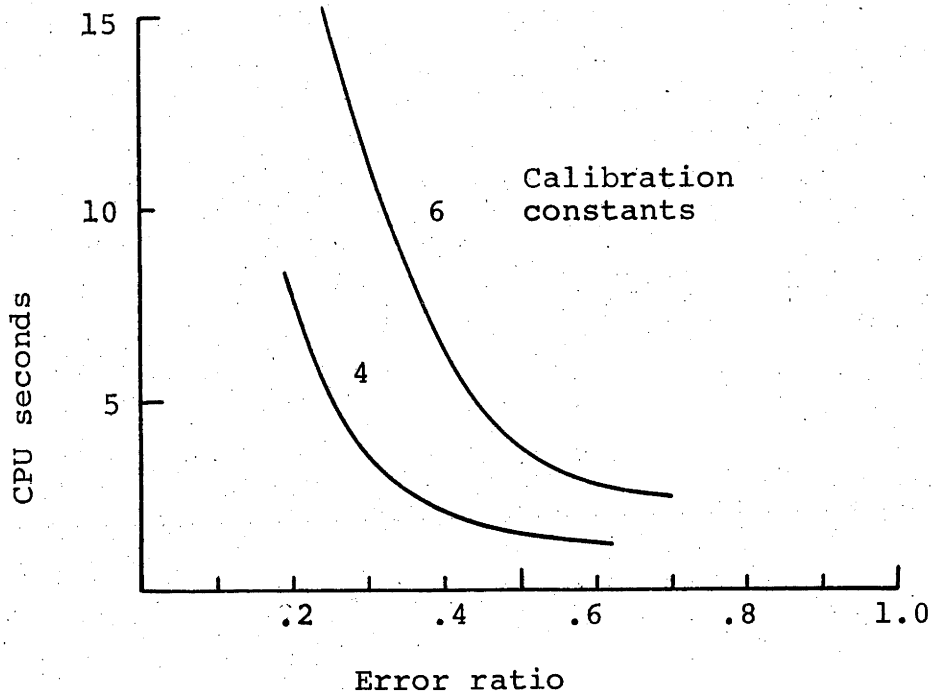


Figure 5.27 Variation of the costs of alignment with accuracy of alignment, as described by the computer time necessary to perform the alignment. The accuracy of the alignment is given by the product of the error ratio and the rms error in each of the points used in the mathematical process. This rms error will probably be dominated by the encoder accuracy.

5.7 Summary And Conclusions.

(a) Deflections due to wind gusts.

Assuming a standard urban wind spectrum, the spectral characteristics of wind-induced structural deflections have been calculated and averaged over the range of wind speeds to be encountered while collecting solar radiation. The relationship between the rigidity of one collector vibration mode and the sun following error specification has been presented. Providing resonant frequencies are above .1Hz, servo loops which can compensate for deflections at non-resonant frequencies are worthwhile. Further, bandwidths of around .1Hz are capable of compensating for a large fraction of these deflections. This saves costs by reducing the required rigidity of the collector structure as shown in figure 5.15.

(b) Alignment Costs.

Three different schemes for alignment have been analysed. It has been shown that a cheap method for alignment is to infer calibration constants mathematically. This mathematical process has been analysed fully and the aspects of operation detailed, in particular the necessary

programming. The accuracy of the process was presented in Table 5.1. To perform the process information must be gathered - data rates have been estimated and are small. The cost of this process may be considered to be in two parts, a one time initial cost which is some fraction of the cost of the sun sensor, communication link and central computer (a fraction because all items have multiple uses) and a recurring amount of computer time which has been estimated at 10 to 20 cents per alignment. The amount of computer time involved depends on the required accuracy, as shown in figure 5.27.

(c) Tracking vs Pointing systems.

It has been shown that for following the sun when energy collection is desired, a tracking system is more appropriate than a pointing system. This is because the bandwidths and compensation process mentioned in the previous paragraph are easily obtainable within such a system. A guidance and control scheme using tracking only has been shown to have the deficiency that time is taken between the emergence of the sun and the resumption of accurate tracking. This deficiency is responsible for collection losses which have been estimated at 3% of total sunshine. Thus a pointing system is, however, still required for anticipating the sun's position, though the sun following error requirements of the pointing system are not particularly stringent.

(d) Calculations of actuator displacements.

The costs, in terms of computer time, of calculating the actuator displacements to any desired accuracy have been evaluated, and have been indicated in figure 5.22. These costs vary significantly with accuracy only for unsophisticated machines such as an eight bit microprocessor. The errors associated with calculating the actuator displacements at intervals and linearly interpolating have been evaluated and have been indicated in figures 5.16 and 5.17. Both fixed point calculations, (relevant to microprocessor calculations) and floating point calculations have been considered. In the case of fixed point calculations program storage has been assessed at 350 bytes for 8 bit calculations.

If actuator displacements are calculated by the central control, the rate of data outflow to the collectors is estimated at 300Hz for 10000 collectors. This data rate will place no burden on available facilities.

(e) Cost variation with sun following error budget.

Here factors which are not strongly dependent on the actuators and other hardware have been analysed. The principal cost is the cost of achieving a specified deflection for a given load. Other costs due to error sources, such as alignment costs, actuator displacement calculations and the servo, change little with error specification. The cost of the other principal hardware components, the position encoders

and sun sensor, was not considered.

(f) Response time.

Losses due to response time have been related to the sun following error at the time the sun appears. A typical sun following error of 10mrad at this time will result in 0.1% of the sunshine not being collected.

(g) Location of guidance and control scheme functions.

It has been made clear that the tracking function should be under local control, while the alignment process should be handled by the central control. The location of the pointing process is determined by the specified losses due to response time. If these losses are allowed to be 0.2% or greater, then the local control is certainly capable of pointing tasks. If lower losses are desired (and thus higher accuracies), the central control may be required to perform the calculations.

(h) Speed requirements of collector actuators.

The speed requirements of the collector actuators have been discussed and it has been shown that a maximum speed of 1mrad/sec is adequate for an altitude azimuth mount at latitudes outside the tropics.

5.8 Recommendations For Further Work.

Further Wind Tunnel Analysis.

Neither underdesigned nor overdesigned solar energy plant will collect energy for the lowest possible cost. It has been shown that structural rigidity is an important cost component of the collectors and that wind gusts are the most important cause of structural deflections. It is clear that a comprehensive wind tunnel analysis is required to determine the deflections of the collectors with the upstream presence of other collectors, a situation not considered in existing radar and radio telescope dish studies.

Actuator Design.

There are a number of omissions in the above studies, principally caused by the lack of a specific actuator design. This has a large bearing on encoder selection, another expensive component. For, as an example, if permanent magnet DC motors were used, back emf measurements could be integrated to give position information. Such an approach, if sufficiently accurate, would seem to be very cheap.

6.0 DESIGN AND IMPLEMENTATION OF LOCAL CONTROL.

6.1 Introduction

In this chapter the design and implementation of the control local to each collector, (or local control), are discussed. The chapter is in three sections; the first concentrating on the hardware configuration of the local control and reliability and maintenance costs, the second is concerned with the design of the tracking function at the local control and the third section considers the communication link design.

6.2 Local Control Reliability And Maintenance.

We explore here the influence of reliability on the configuration of the local control, concluding with a notional hardware allotment for the local control and calculating reliability and maintenance costs for that allotment.

6.2.1 Reliability And Costs.

The environment in which local control components operate determines their reliability and conversely, reliability considerations determine where components should be located.

Reliability calculations involve the consideration of a basic failure rate, generally calculated at a temperature of 25-35C, which is then multiplied by a factor to obtain the failure rate at the operating temperature. The dependence of

failure rate on temperature is shown in figure 6.1 for transistors, thyristors and bipolar and MOS integrated circuits. It is obvious that for linear and power devices in particular, reliability is a strong function of temperature. Similarly, temperature cycling has a strong effect on reliability (Derr et al (1976)). Repair and maintenance costs are directly proportional to failure rate so that it is essential that components be placed in as benign an environment as possible. In the case of the sun sensor, there is little choice and the device must be exposed. Thus temperatures for this device will be similar to those found on parked cars and may be 80C (Derr et al (1975)). However, the power amplifiers and local control may be placed inside the concrete pedestal (if one is used), or even a short distance underground in the foundation. This would restrict temperatures and minimise temperature cycling.

We note also the importance of using already established IC components. The US military standardisation handbook on reliability prediction, MIL-HDBK-217-B (US Dept of Defence, 1974), recommends the multiplication of failure rates by a factor of ten if an unestablished electronic component is used. This indicates the value of the experience of production and constitutes a warning against the use of custom made IC's.

A strategy to reduce the costs involved with failures is to configure low reliability items separate from high reliability items, using plug-in modules. Such a practice saves unnecessary handling of intact components. It is shown

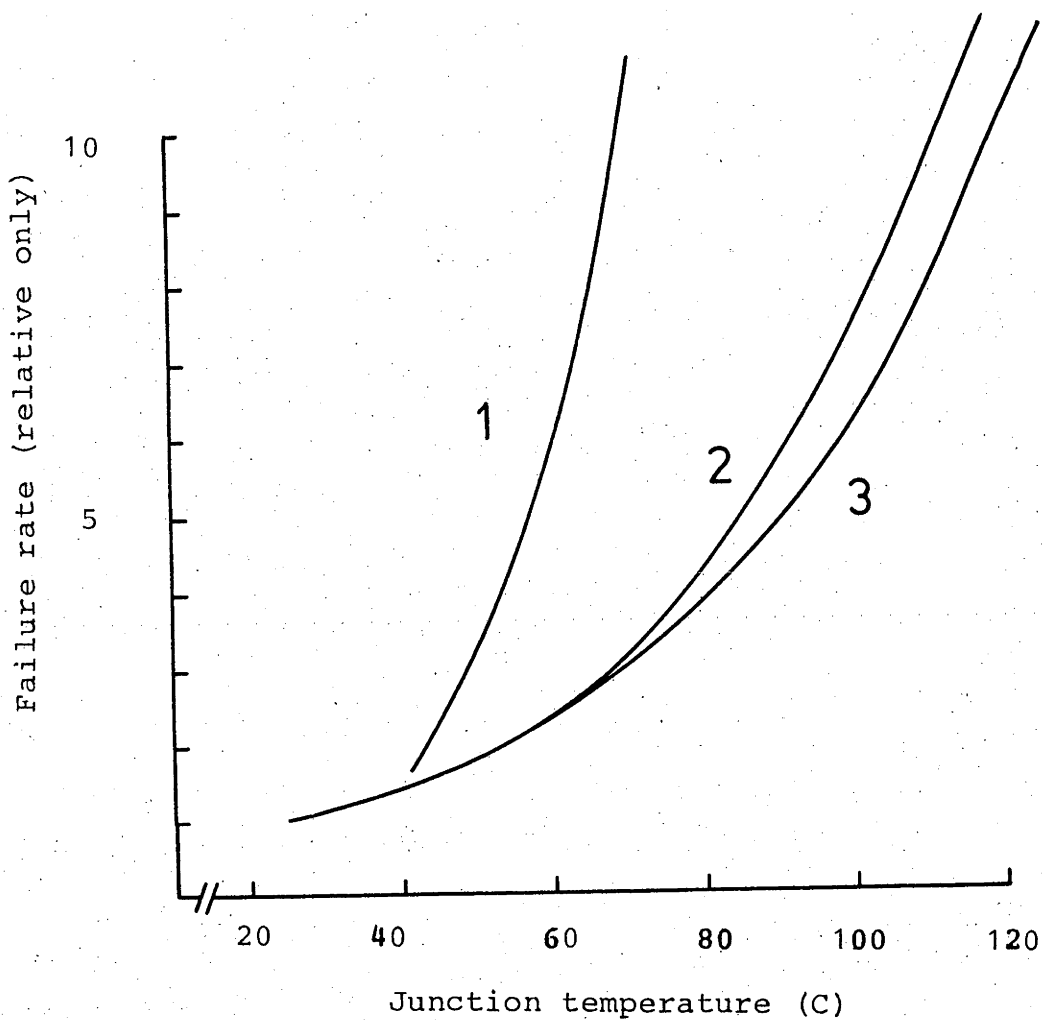


Figure 6.1 The relative reliability of semiconductor components is plotted here as a function of the junction temperature.

Curve 1. Discrete transistors (Peattie et al, 1974)

2. Bipolar digital IC's (Peattie et al, 1974)

3. MOS digital IC's (Derr et al, 1975)

The data in curve 1. approximates thyristor reliability data given by GE (1972).

later, however, that the cost of repairs is affected by the cost of components to second order only and the cost of the connectors for the above approach seems unjustified.

Basic failure rates for microprocessor-size digital IC's and small (around 30 transistor) linear IC's are of the same magnitude, around 10^{-7} /hr (MIL-HDBK-217B). The microprocessor, however, possesses many advantages including versatility and a history of production and usage. The versatility of the device allows high volume production which reduces costs and increases reliability. Use of this device as the basis of the local control seems mandatory.

6.2.2 Configuration Of Local Control.

A notional hardware allotment for the control at each mirror is shown in figure 6.2. It is suggested that the cheapest form of A-D conversion is achieved with the microprocessor controlling a successive approximation scheme. An alternative would be an analog to time interval converter, with the microprocessor calculating times via timing loops. The only cost variable, once such a system has been decided on is the programming (and thus memory) requirements which for economy must lie within the limits of commercially available units.

It is assumed in later calculations that the power amplifying element is a thyristor.

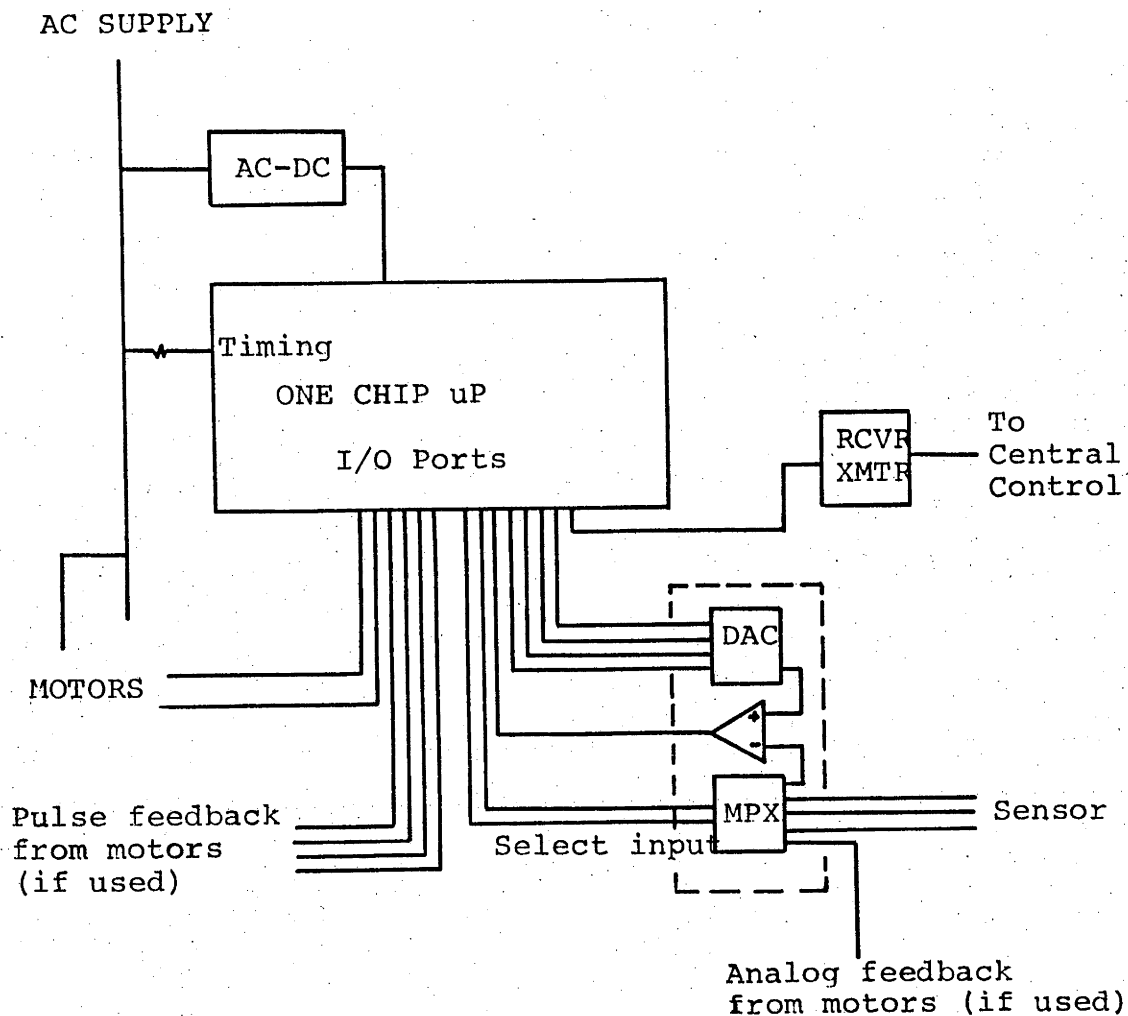


Figure 6.2 Notional configuration of the local control.

DAC Digital to analog converter

MPX Multiplexer

RCVR Receiver

XMTR Transmitter

uP Microprocessor

6.2.3 Cost Of Repairs.

The reliabilities of the four modular components of the local control are shown in Table 6.1. Actuator and actuator feedback device failures are not considered. The repair policy includes producing all spare parts at the time of construction and subsequent storage of these spares and precludes salvage of replaced parts. A plant lifetime of 20 years is assumed.

TABLE 6.1

Item	Failure rate (per million hrs)	Cost (\$)	Required number of spares
Sensor 4 phototransistors(a)	.4	5	700
2 thyristors(p/a)(b)	3.	1	5300
local control(d)	.5	4	900
Voltage regulator(c)	.1	1	180
XMTR/RCVR(c)	.1	1	180
DAC/MPX(c)	.1	1	180

(a) based on twice the failure rate of commercial transistors (Peattie et al, 1974), at 80C ambient.

(b) Lucas et al (1975).

(c) Based on reliability of single linear IC. (Lauffenburger, 1976).

(d) Derr et al (1975).

The failures due to these components amount to some .037 failures/year/unit. The cost of the repairs is made up of 5 components, viz:

1. The cost of the new part less the salvage value of the replaced part (salvage value assumed zero above).
2. The value of the time of the repair technician.
3. The value of the energy not collected due to the downtime.
4. The value of the test equipment.
5. The cost of holding supplies of the replacement parts.

It is not the intention of the author to engage in complex economic calculations which could not be justified in this instance and the following calculations use standard methods (eg Grant and Ireson, 1960) to calculate the cost of repairs to the local control. The calculations are based on reducing all costs, regardless of the time of payment, to equivalent costs at the time of construction. This is sometimes referred to as present worth calculations. An example of this method is the time of construction worth of a repair, scheduled for one year from construction, costing \$110. The present worth of this repair would be \$100 if the interest rate was 10%p.a. Formula for other circumstances can be derived simply and are given by Grant and Ireson(1960).

The five components of repair costs for the local control are itemised as follows.

1. As per Table 6.1. The average cost per repair is \$1.7.
2. The present worth of each repair is calculated on the basis of continuous cash outflow, amounting to a total of \$25 outflow in 20years for each repair. The present worth of such an outflow at 12%p.a. is around \$9.40.
3. Two items are involved here, firstly the 'delay maintenance time', due to the non recognition of failure, and secondly the 'active maintenance time', which is the time between the recognition of the failure and the completion of the repair. A field of 10 000 units would be experiencing of the order of one failure per day(at the

above failure rates) and it is probable that repairs would be scheduled for a specific time. We assume that the total downtime is 12hrs of sunshine for each repair. For a 20m^2 aperture collector the value of this sunshine is around \$.13.

4. Test equipment for such a simple unit would involve no more than \$600, or \$.1/repair.
5. The number of spares required over the service life of the solar power plant is itemised in Table 6.1. The volume occupied by these items is largely dependent on the bulkiness of the sensor assembly and it is estimated that all items could easily be contained within 2m^3 . We estimate the value of this space by assuming it is part of a larger building, and construction costs for a small building are estimated at $60\text{\$m}^{-3}$. Thus the value of the storage space is only .02\$ for each repair and inaccuracies in the above calculation will have little effect on the total repair costs.

TABLE 6.2 Summary of present worth costs of repairs.

Repair costs (a)	1.	1.
	2.	5.6
	3.	.02 'Active'
		.05 'Delay'
	4.	.06
	5.	.02

Total Present Worth \$ 6.75

(a) On average each unit requires .6 of a repair.

This is the cost of repairs for the local control of one collector over 20 years. For a 20m^2 collector, this is an effective addition to capital cost amounting to about $.3\$/\text{m}^2$.

We note that the cost of components affects the cost of repairs only to second order and that the value of the energy not collected due to downtime is trivial. This latter point indicates that scheduling repairs for one day each week would not be unreasonable.

The crucial component for maintenance costs is the power amplifying thyristor; increasing the reliability of the thyristors by using more expensive items would be worthwhile. Increasing the reliability of other components would decrease maintenance costs only to second order.

6.3 Tracking Servo Design.

In this section we concentrate on the design of the sun tracking servo loop and it is shown that adequate servo performance is achieved readily. In particular the relationship between the size of the oscillations in the sun following errors due to the servo, the level width of the digitised sun sensor information and the servo bandwidth are discussed.

6.3.1 Servo design: General Remarks.^a

Here we consider the design of the servo loop controlling the actuator velocity from information on the sun following error.

There are two fundamental design requirements for the sunfollower servo; firstly it must have a low response time, as the interval between the sun's appearance and when accurate tracking is achieved represents wasted energy and secondly the servo must maintain low sun following error, preferably with the sun following error oscillating around zero.

These requirements are met here by operating the servo loop in two phases, as follows: If the sun following error data is saturated, that is does not vary with changing sun following error[#], then the calculated velocity is a maximum. The gain is a slight function of the number of levels in the digital representation of the sun following error, due to the fact that lack of saturation is obvious to the controller only when the sun following error is in the second outermost level.

^a Most calculations involving a speed use the rotational velocity of the earth ($7.3E-05$ rads/sec) as a reference, and the symbol 'k' is used to denote this speed. Other terms used include the 'unity gain frequency', which is the frequency at unity gain for the open loop transfer function. The 'gain margin' is the gain required to produce unity gain at the frequency where the phase angle is precisely -180 degrees.

[#]footnote on next page

If the sun following error data is not saturated, then the calculated velocity includes both proportional and integral control. The servo loop will be operated by the microprocessor located at each collector and this introduces problems due to quantisation of the information and sampling. These problems are considered semi-quantitatively in the following sections. Next, Bode diagrams (Thaler and Brown, 1960) of the proposed servo loops are plotted to indicate permissible gain constants. The response of the servo loop is simulated by computer calculations to show the expected performance. Finally, the time required of the microprocessor to perform servo calculations is estimated and the stability of the proposed servo loop to other modes of vibration is considered.

6.3.2 System Under Study.

The system under study is shown in figure 6.3. In operation, the sun following error is sampled to an accuracy of n_s bits and a speed of accuracy n_m bits is calculated to maintain low sun following errors. The type of actuator used is not specified. Here we merely assume that the response of

The saturation of the sun following error information depends upon the design of the sun sensor. Here we consider the design of Carden (1978a), where the sun sensor saturates at plus or minus half the sun's diameter and in between the output signal is proportional to the sun following error.

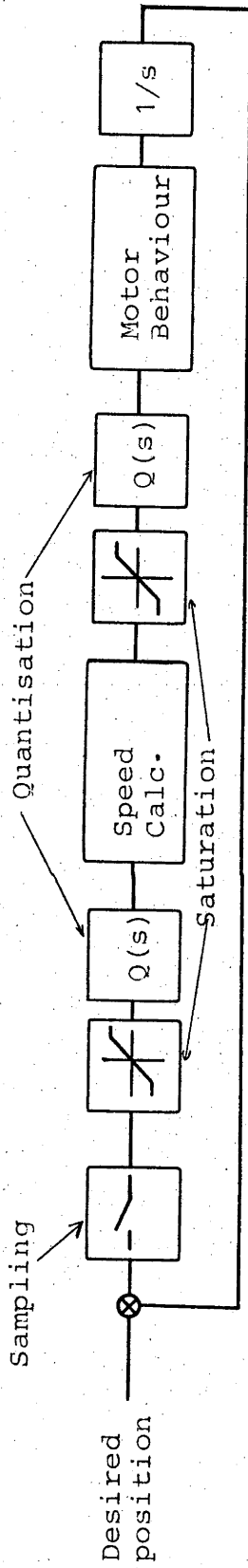


Figure 6.3 Tracking servo loop considered in section 6.3.

the collector to a velocity command is described by a transfer function of the form:

$$K(s) = f_0^2 (s^2 + 2f_0 \zeta s + f_0^2)^{-1} \quad (6.1)$$

where f_0 is a natural frequency of a mode of the structure, and ζ is the damping coefficient.

6.3.3 Sampling: Qualitative Remarks.

The effects of sampling can be considered by using the approximate transfer function in figure 6.4 (Thaler and Brown (1960)). If the sampling frequency is ten times the unity gain frequency of the servo used, sampling will produce an additional phase lag of a maximum of twenty degrees, the maximum occurring at the unity gain frequency. This frequency must necessarily be less than the lowest natural frequency of the collector structure and in the following examples, it is assumed that the lowest natural frequency is 0.1 Hz and the interval between sampling is accordingly 1 second. The resultant bandwidth can compensate for a large portion of the deflections caused by the winds, as outlined in chapter 5.

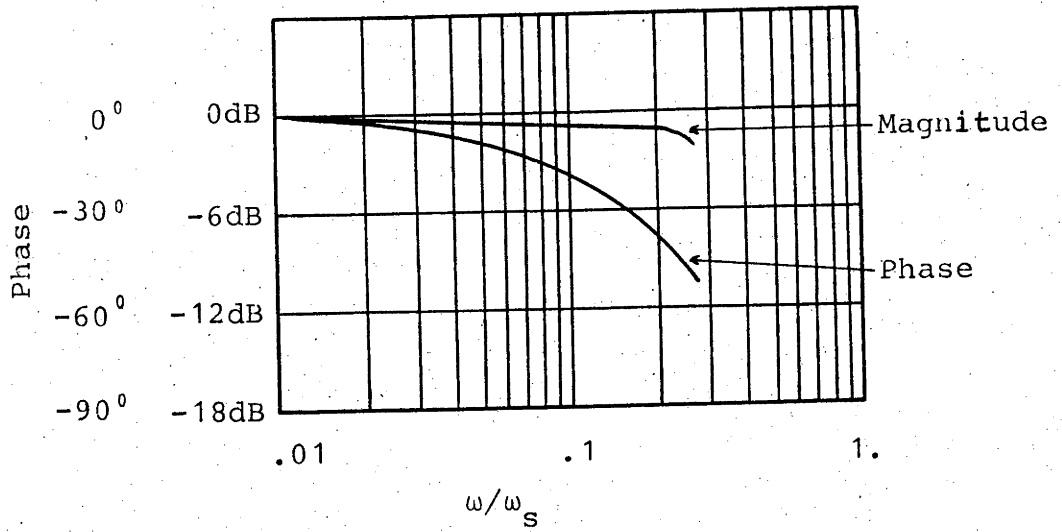


Figure 6.4 Approximate transfer function for a sample and hold circuit(Thaler and Brown, 1960).
 ω_s is the sampling frequency in rads/sec.

6.3.4 Quantisation: Qualitative Remarks.

Both the output velocity instruction and the input sun following error data will be quantised, that is, the data will be represented by one of a relatively small set of numbers. The level width is the maximum change in the actual data which can occur without the quantised information changing.

The accuracy of the output velocity will be limited to eight bits and there will be no difficulty in realizing this accuracy. Analog to digital conversion, however, is an intrinsically more difficult operation and there is merit in providing high accuracy tracking with sun following error data which has large quantisation errors.

Quantisation can be effected in two ways. If an odd number of levels is contemplated, then a zone will exist in which no sun following error will be recorded, though sun following error exists. With such a system it would be impossible to reduce the magnitude of sun following error oscillations below the width of each level.

An even number of levels does not suffer from such a problem and provided that the amplitude of sun following error oscillations remains smaller than the width of a level, the transfer function of the quantisation process will be identical to that of a relay. For a level width of $\Delta\epsilon$, the transfer function is (Thaler and Brown, 1960):

$$Q(s) = 2 (\Delta\epsilon) / (\pi A) \quad (6.2)$$

where A is the amplitude of the input sinusoid. Oscillations occur when the gain margin of the servo has been reduced to identically zero: this occurrence is a function of the gain margin of the unquantised system and the size of each level. In the basic systems considered the gain margin increases as the unity gain frequency decreases. Thus for a fixed A as the level width increases the response time increases. Specific calculations on this are presented later.

Quantisation does not, however, affect gain only for sun following errors in the lowest levels. In the second lowest level gain varies from .5 to 1.5. The range of gain encountered in each level decreases as the magnitude of the sun following error increases. Thus to avoid sun following error oscillations into the second level, it is preferable that the gain margin be at least 1.5, or 3.65dB.

6.3.5 Saturation: Qualitative Remarks.

Saturation reduces the overall gain and may create phase margin problems. The proportional control system is stable to all gain reductions. The integral and proportional scheme suggested, however, is more vulnerable and it is proposed that the integral and proportional scheme be used only for unsaturated values of the sun following error. Saturation of velocity is not a problem as in general the sun's velocity is always less than the saturation value. In the calculations, saturation occurred for sun following error at .005rads (the sun's semidiameter in round figures), and at .001 rads/sec for

the output velocity command.

6.3.6 Servo Stability.

In this section we calculate the conditions necessary for the stability of the two operating modes of the servo.

6.3.6.1 Proportional Control Only.

The magnitude and argument of the transfer function

$$|G(s)| = K_0/s \quad K(s) \quad (6.3)$$

is shown in figure 6.5. In this figure, f_0 has been set at .1Hz and accordingly the damping ratio for such a low resonant frequency is fairly high and here is set at 0.3 (see Appendix G for the relation between resonant frequency and damping ratio). The gain K_0 is unity in the figure, but needs to be less than .3 to maintain a 50 degree phase margin and this maximum feasible gain involves a velocity error of .2mrad at an output velocity of k .

6.3.6.2 Integral And Proportional Control.

The velocity error mentioned above can be avoided by the use of integral control. The transfer function is in this case:

$$|G(s)| = K_1 (s/(K_1/K_0) + 1)/s \quad K(s) \quad (6.4)$$

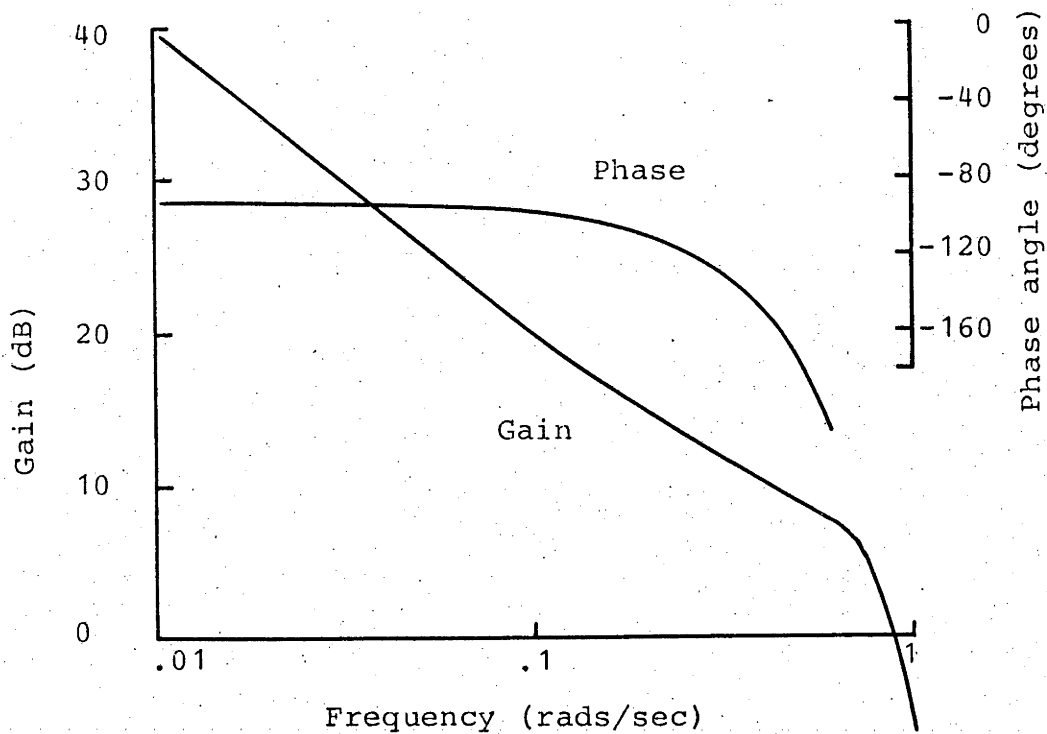


Figure 6.5 Open loop transfer function of servo with proportional control, and proportional gain constant, $K_0=1$. Natural frequency of collector structure, .1Hz, damping coefficient .3.

where K_1 is the integration gain, and K_0 the proportional gain. The frequency (K_1/K_0) must be smaller than the natural frequency of the collector to produce a reasonable phase margin. Here we choose $K_1/K_0 = .05$. The gain and phase plots for this system are shown in figure 6.6. The effects of sampling at 1 second intervals have been included.

If K_1/K_0 is maintained constant, (and thus the phase diagram remains unchanged), then the magnitude of the sun following error oscillations A , the level width ($\Delta\epsilon$) and the integration constant K_1 can be related by the expression:

$$A = 36 (\Delta\epsilon) K_1 \quad (6.5)$$

Hence for an eight level system, with oscillations around $.1(\Delta\epsilon)$, the required K_1 is $.0025$, and thus K_0 is $.05$. The response of this system to a step error input was simulated digitally and is shown in figure 6.7. A 32 level system, with the same oscillation amplitude of $.13\text{mrad}$, allows K_1 to be $.01$, and $K_0 = .2$. The response of this system is also shown in figure 6.7. The transfer function of this latter system has already been plotted in figure 6.6.

As expected, the servo possesses relay like oscillations and the magnitude of the oscillation is controlled by the gain constants and the level width. The gain constants also determine the bandwidth and to maintain low amplitude oscillations with large level widths, the bandwidth must be reduced. This is contrary to the design specifications, which require that the bandwidth be maintained as high as possible.

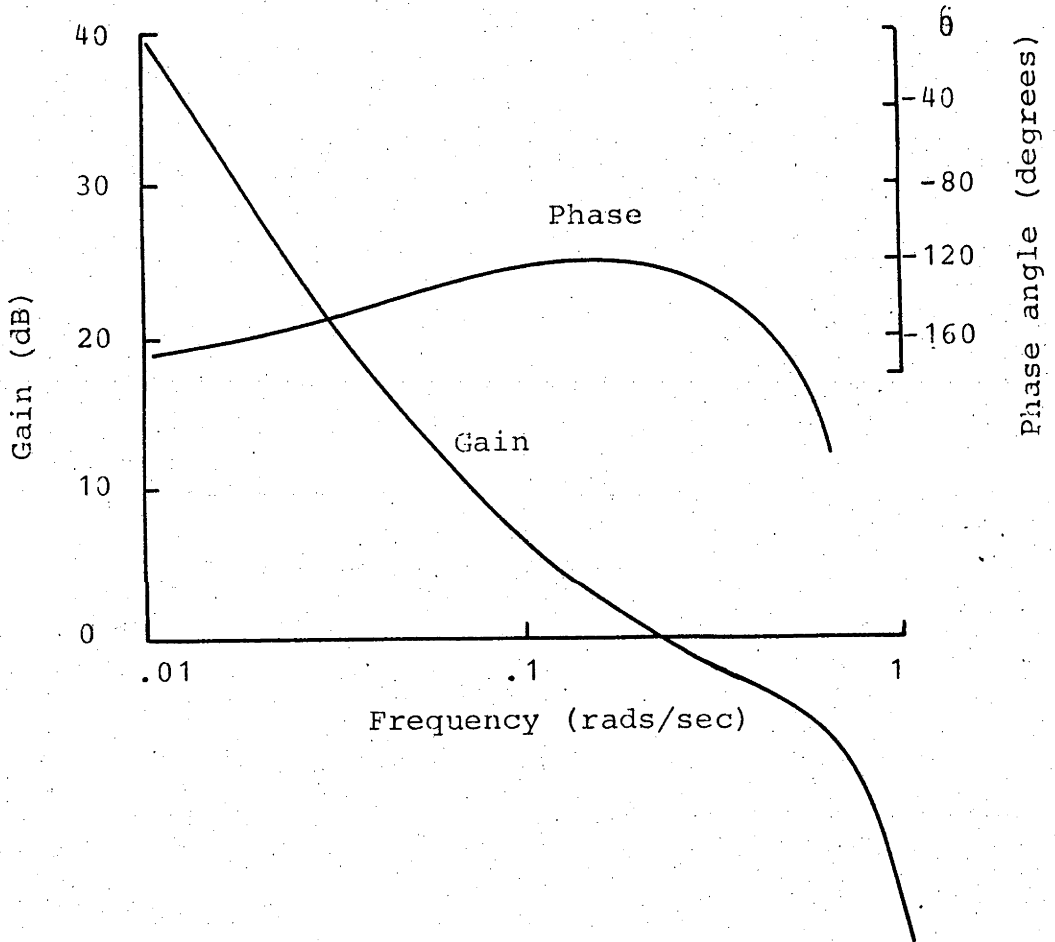


Figure 6.6 Open loop transfer function of servo with proportional and integral control. Proportional gain constant, $K_0=.2$, and integral gain constant, $K_1=.01$. Natural frequency of collector structure, $.1\text{Hz}$, damping coefficient $.3$.

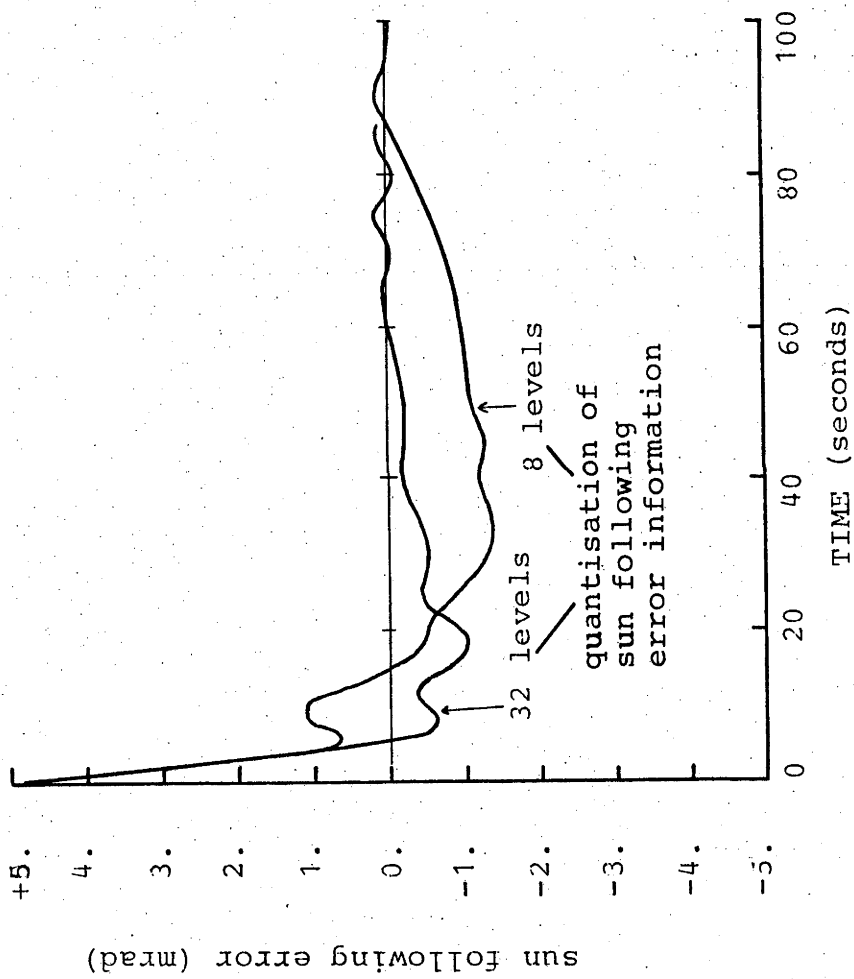


Figure 6.7 Simulation of transient response of servo. Sun velocity = -7.3×10^{-5} rads/sec. Initial follower velocity = $.001$ rads/sec. Initial sun following error = $.005$ rads. The levels indicated are the number of levels into which the sun following error information is

For the .1Hz resonant frequency considered here, K_0 can be no greater than 0.2 and with this figure set and K_1/K_0 set, the oscillation amplitude is proportional to level width. For the case studied in figure 6.7, the 32 level system is very near the bandwidth limit, while the 8 level system shown has reduced bandwidth, though it attains the same oscillation magnitude. Thus the level width should be as small as possible, but this should be compromised with the costs of A-D conversion which increase as the level width decreases. Thus design would hold the level width as large as is reasonable. For the case above where the rms servo error is .08mrad, 32 level sun sensor information is appropriate. Other cases are easily found as they are strictly proportional. For example, if the design servo error was .16mrad, the number of levels corresponding to this error at the above bandwidth is 16.

6.3.7 Calculations Required To Operate Servo.

A microprocessor based controller situated at each collector would be required to control two of the above servo loops simultaneously. The flowchart of operations is shown in figure 6.8. Analog to digital conversion would be most cheaply achieved with a successive approximation method, with the microprocessor controlling each approximation and specific programming for the 8080 shows that around .15ms is required for a four bit conversion. The computation required for each axis as shown in figure 6.8, would require about 0.3ms and the initial computation about .2ms. Thus perhaps 1ms is required

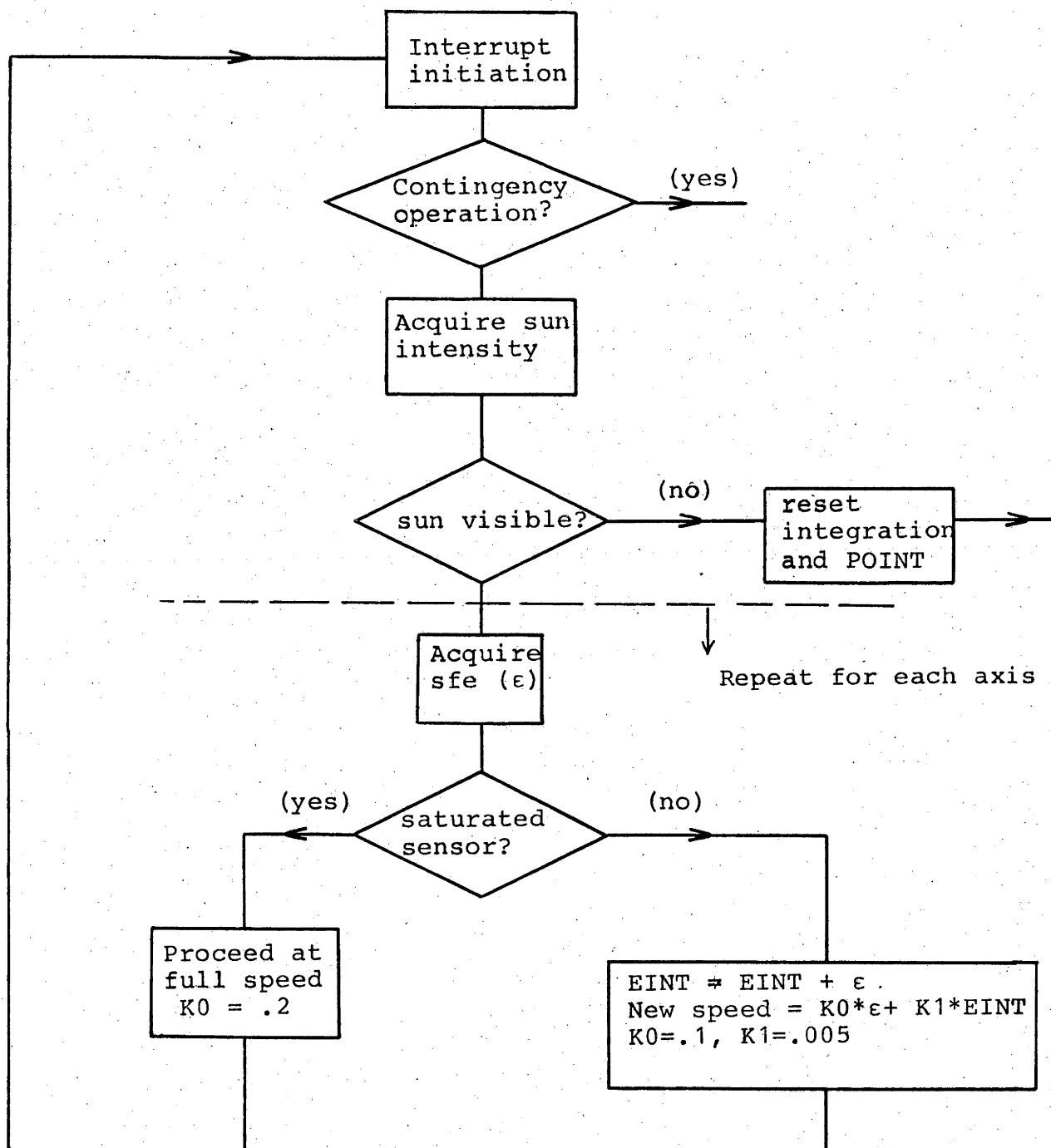


Figure 6.8 Sun follower tracking control flow chart. Constants are for quantisation of the sun sensor information into 16 levels. 'sfe' is an abbreviation for sun following error.

to perform the servo operations each second and this will be no substantial burden on the microprocessor.

6.3.8 Stability For Other Vibration Modes.

The stability of the servo control in conjunction with other modes of vibration is considered qualitatively as follows: There is no need to alter the bandwidth of the system, as .1Hz is sufficient to compensate for the majority of wind gust deflections. The wind gust deflection calculations show that a natural frequency below this figure would not be desirable. Modes of vibration with higher natural frequencies will have correspondingly lower damping ratios and while this will not decrease the phase margin, it is possible that the gain margin will be changed. However, it can be shown (see Appendix G) that the contribution to the damping ratio due to aerodynamic damping is inversely proportional to the resonant frequency. Aerodynamic damping will constitute a large fraction of the damping for a welded steel structure and this relationship ensures that the gain is never greater than -4dB at all frequencies above the unity gain frequency and this will ensure stability.

6.4 COMMUNICATION SYSTEMS.

As stated previously, it is essential that each collector have a stowage capability for protection from wind damage. There is no possibility that each collector would

itself have sufficient 'intelligence' to anticipate strong winds and thus determine when to stow. Hence each collector must be capable of receiving a stow command from the central controller. Further uses for a communication link would be to transmit information on the sun's position to each collector to allow the collector to anticipate the sun's position. Also, a communication link which allows transmission from each collector to the central station would be required to operate the economical alignment scheme detailed in chapter 5. There are two possible communication systems which could be used, either a radio system or a cable system. These two possibilities are considered in the following sections. A radio/cable combination system is not considered, as costs would not be reduced below that of a cable system. A comparison between the two schemes does not require costing estimates for the equipment at the central station, as this is distributed over a large number of collectors and the cost of the central equipment per collector will be small in comparison to the cost of the equipment at each collector.

Of particular interest is the possibility of a radio link, as this would obviate the need to lay cables and connect them to each mirror. A crucial consideration here is whether a radio system can communicate with sufficient reliability in stormy conditions when stow commands must be received. The consequences of collectors not stowing when required to do so could be disastrous. The reliability of transmission will be a function of the radiated power which is limited by legislation. This security of transmission is examined.

6.4.1 Information To Be Transferred.

Firstly, if data to enable pointing was transmitted, data rates would be low. These data rates depend upon the required pointing accuracy and in the first instance, transmitting pointing data which assumed all collectors were truly alt-azimuth, with accurate fiducial marks, would require only 20-30 bits of data in 700secs (Edwards 1978b). Individual attention for each collector increases this data rate by roughly the number of collectors in the array.

Data rates for other uses of the communication link have been calculated elsewhere (see appendix E, sections 5.4.2.2, 5.4.7.9), and are not more than 500 bits/sec for 10 000 collectors.

6.4.2 RADIO COMMUNICATION.

Several radio bands are available in Australia for the 'remote control of radio devices' (as it is expressed by the Australian telecommunication authorities). These are centred around the following frequencies, 27MHz, 41MHz, 2.4GHz and 5.8GHz. We consider the 27MHz band as most appropriate for collector communications and noise levels and other quantities are referenced to this frequency. Australian legislation forbids emitted power exceeding one watt.

6.4.2.1 Link Path Characteristics.

Transmission distances would be less than one kilometre, over a 'plain' of metal collectors. Line of sight transmission could not be guaranteed and the collectors would produce scattering and multipath transmission. Noise levels could be expected to be suburban (a power station is nearby) and thus of the order of -130dBW (ITT 1973) for a 10kHz bandwidth. Noise levels during a thunderstorm are much more severe and amount to some -100dBW for a 10kHz bandwidth, when the storm is 10km distant (Oetzel and Pierce, 1969). Thunderstorm noise is, however, fortunately distributed in bursts with a mean length of about $.5\text{sec}$ and a mean time between bursts of $2-5\text{secs}$ (Jayant 1967).

Receiver/Transmitter characteristics.

As usual the requirement here is for low cost. The transmitter cost will be of little consequence, however the receiver simplicity is vital for low cost. IC technology will have no difficulty in providing the required gain and demodulation, however a number of off-chip components will be required to provide selectivity. The number of off-chip components will probably determine the cost. The output of the receiver will be sampled by the local or central control and thus some logic will be available for error detection and correction.

Modulation and Detection.

The method chosen here is FSK (frequency shift keying) with non-coherent detection. This is the best method which can be employed without phase sensitive detection, a method which could not be implemented due to the possible multiple signal paths. The full benefits of the low data rates can be exploited only by a highly selective receiver, a situation which is not compatible with receiver costs. The error rate for a non-coherent FSK system is around 1 in 10 million for a 15dB signal to noise ratio. Because of the selectivity problem, in later calculations we assume the receiver bandwidth is 10kHz, regardless of the actual data rate. Synchronisation of the received waveform would most easily be achieved with reference to the AC power line.

6.4.2.2 Error Performance Of Radio Communication.

Calculations show that a 1mW transmitter could provide a 30dB S/N ratio at a receiver 1km away under suburban interference conditions. The noise induced errors at this margin are negligible. Communication errors will become appreciable only when a thunderstorm is within 10km of the receiver. Errors under these conditions will reach one in a thousand bits transferred. It is possible that a stop command may need to be transferred under these conditions. If the receiver is equipped with an error detection capability, such a command may be received correctly if the command is retransmitted until the transmission does not coincide with a

burst of noise from the thunderstorm. A 'slave' receiver, the output of which is available to the central transmitter, could determine when a noise free transmission has occurred.

6.4.3 CABLE SYSTEMS.

The production of fibre optic cables is expanding rapidly and costs are already around \$.5/m, with promise of \$.1-.2/m with larger production runs (Electronics, Nov 1977). This is of the same order as conventional cables used for telephone signal transmission, however, the cost of a fibre optic system will be cheaper as no electromagnetic interference suppression will be needed and repeaters will be unnecessary. Electromagnetic interference would be particularly severe for metallic cables with an effective kilometre of aerial and delicate semiconductor equipment attached (see for example Bennison et al (1973)).

The layout of collectors will be determined by the pipe network, which is the most expensive of the links between collectors. The layout problem has been considered (in chapter 3) and the collectors are certain to be arranged relatively close together in North-South rows, with the East-West separation between rows relatively large. Communication links are routinely configured with either 'star' connectors, or a series of 'T' or 'access' connectors. Although some fibre optic connectors are already qualified for military use in the USA, connector technology is in general embryonic. Star connector based systems offer the lowest

signal losses, but the configuration does not combine well with the layout of the collectors. Low loss 'T' connectors are being developed rapidly (eg Auracher 1977, Muska 1975): the first author describes a cheap system where some 20-30 connectors can be used on a single line with a consequent maximum power loss of only 50dB between the source and each detector. Such a power loss allows bit error rates of better than one in one hundred million (Kao 1976) at 100kHz bandwidth.

6.4.4 Comparison Of The Two Communication Systems.

Only very rough estimates can be made as to cost and feelings of the author are that installation costs will be comparable. It has been shown that lack of message integrity of radio transmission is not a factor. The relative complexity of the parts required for radio transmission and reception balance against the installation and connection of the cables in the field, though simple equipment is required for cable transmission and reception. The advantages of the cable system are as follows.

1. Low error rate due to both high bandwidth capability and immunity to electromagnetic interference. This is particularly important considering the possible climates when stowage commands are issued.
2. Immunity to electromagnetic induced damage.

3. Equipment simplicity leads to high reliability.
4. Two way communication easily implemented.
5. The prospect of 10 000 radio transmitters in a small area is daunting, should two way communication be required.

6.5 Summary.

In the design and implementation of the local control the following aspects have been considered.

6.5.1 Reliability And Maintenance.

The reliability and maintenance costs of the local control at each collector have been examined. On average each unit will require .6 of a repair to the electronic component over its 20year life. This is an effective addition to capital costs of $.3\$/m^2$ for a $20m^2$ collector.

6.5.2 Tracking Servo.

The design of the tracking servo has been detailed. The program is small and occupies less than one thousandth of the microprocessor time. The servo reduces velocity lags to zero.

6.5.3 Communication Systems.

The possible disadvantage of radio communication systems, namely lack of transmitted information integrity under thunderstorm conditions has been examined. Given current legislation on emitted power, this is not a problem. The arguments presented favour the use of a fibre optic communication system.

7.0 SUMMARY AND CONCLUSIONS - RECOMMENDATIONS FOR FURTHER WORK.

7.1 Summary And Conclusions.

In this study of aspects of paraboloidal arrays emphasis has been placed on minimising costs. Factors which have been identified as important in cost reductions have been discussed in the concluding sections of each chapter and are further summarised in the following sections.

7.1.1 Shading And Spacing In Paraboloidal Collector Arrays.

A program to calculate the amount of shading experienced by a collector in an array of collectors has been described. The amount of shading for square arrays and North-South rows of collectors has been presented graphically in figures 3.5 and 3.11 (pp 37,60). The cost of links between the collectors has been evaluated and collector separations to minimise costs have been presented for both square arrays and rows of collectors. A method for calculating the cost effective separations with little calculation has been derived and justified, and graphs have been provided for this purpose. (figures 3.9 and 3.12, pp 54,61).

Costs of linking collectors to the central station have been shown to be dominated by the total length of the links. It has been shown that the total link length can be reduced while maintaining low shading losses by utilising a rectangular array with large East-West distances and small link distances in the North-South direction. The cost advantage of such an array has been demonstrated for a small

collector array producing 27MW_t (figure 3.14, p 63).

The cost optimum spacings have been calculated in terms of the ground cover ratio. Typical cost optimum values are 0.2 for square arrays and 0.1 for rectangular arrays.

There is no doubt that the rectangular array has the potential for lower costs than a square array. An all up cost for links of $\$20/\text{m}$ will maintain link costs at $12\$/\text{m}^2$ (aperture), which is a reasonable target. A square array with the same link costs per metre will have total link costs of $16\$/\text{m}^2$.

7.1.2 Cavity Absorbers.

The variation of the maximum possible efficiency of cavity absorbers has been given as a function of cavity losses, the contour tolerance of the paraboloid and sun following errors in figure 4.8 (p 87). Information is presented in two graphs, with the cavity aperture area necessary to achieve maximum efficiency given in figure 4.9 (p 88). This contribution includes a simple presentation of data (figure 4.6 p 84) to enable easy calculation of the capture ratio, (the fraction of the energy directed at the cavity which actually enters the cavity aperture).

Considering the simplicity of cavity absorbers, absorption efficiencies are reasonable. If the cavity is designed so that its losses are dominated by radiation through the cavity aperture, efficiencies in excess of 96% are assured. If sun following errors are less than 4mrad , the figure will increase.

7.1.3 Guidance and Control Schemes.

Causes of sun following errors other than those dependent on actual hardware choices have been examined. The principal conclusions which have emerged in this study relate to the properties of the guidance and control scheme which will minimise plant costs. These are summarised as follows:

7.1.3.1 Alignment Costs.

Three different methods for alignment have been analysed and it has been shown that a cheap method for alignment results from mathematically inferring the calibration constants. The cost of this process may be considered in two parts; a one time initial cost which is some fraction of the cost of the sun sensor, communication link, and central computer (a fraction because all items have multiple uses) and an amount of computer time which has been estimated to cost 10 to 20 cents for each alignment. This computation time depends on the specified accuracy as shown in figure 5.27 (p195). Costs are certain to be lower with this method than for manual methods of alignment.

7.1.3.2 Effect Of Wind On Tracking Performance Of Collectors.

The spectral distribution of deflections of a collector has been calculated assuming a standard wind spectrum. The process of compensation, where an 'intelligent' servo loop positions the collector so that the wind induced deflections actually return the collector to near the desired position,

has been described. It has been shown that if the collector has no resonant frequencies below 0.1Hz, compensation for deflections which occur at other than resonant frequencies is worthwhile. Further, bandwidths of around 0.1Hz are capable of compensating for the majority of wind induced deflections. Compensation thus allows cost savings by reducing the required rigidity of the collector structure (fig 5.15 p143).

7.1.3.3 Tracking Vs Pointing Schemes.

It has been shown that for following the sun when energy collection is desired, a tracking system is more appropriate, because the bandwidths and compensation process mentioned previously are easily obtainable within such a system. A pointing system is, however, still required for anticipating the sun's position, though the sun following error requirements for the pointing system are not particularly stringent (10 or 20mrad) (Table 5.2, p177).

7.1.3.4 Calculations Of Actuator Displacements.

The costs, in terms of computer time, of calculating the actuator displacements corresponding to a position on the sky to any desired accuracy have been evaluated, as shown in figure 5.21 (p167). These costs vary significantly with accuracy only for unsophisticated machines such as an eight bit microprocessor. The errors associated with calculating

the actuator displacements at intervals and linearly interpolating at other times have been evaluated and are shown in figures 5.16 and 5.17 (pp150,151).

7.1.3.5 Cost Variation With Sun Following Error Budget.

Factors which are not strongly dependent on the type of actuators have been analysed. The major cost variation is due to the cost of achieving a specified rigidity. Other costs due to error sources, such as alignment costs, actuator displacement calculations and the programming for the tracking servo, change little with error specification. The cost of the other principal hardware components, the position encoders and sun sensor, has not been considered.

7.1.4 Design And Implementation Of The Local Control.

The influence of reliability on the configuration of the local control has been considered and the reliability and maintenance costs for a notional hardware allotment have been calculated. These costs have been shown to add only $0.3\$/m^2$ to the capital costs of the solar power plant.

A design of the suntracking servo loop was completed, and it has been shown that adequate servo performance can be easily achieved and that a microprocessor based controller would need to dedicate only one-thousandth of its time to servo calculations for a single two axis collector.

The possible disadvantage of radio communication, namely lack of transmitted information integrity under thunderstorm conditions has been examined. Given current legislation on emitted radio power, this disadvantage has been shown not to prevent the use of radio communication. However, the arguments that have been presented favour the use of fibre optic based communication systems, principally because of the immunity to lightning.

7.2 Recommendations For Further Work.

Further development of cost effective paraboloidal arrays would benefit from the following studies.

7.2.1 Shading And Spacing.

The costs involved with shutoff valves and other safety features of the link network must be evaluated. Also, the optimum layout of trunk pipes within the energy transfer network must be evaluated, although this layout cannot be determined until more accurate formulations of the installed cost of pipes are obtained.

7.2.2 Cavity Absorbers.

Cost studies of cavity designs as a function of cavity losses would, when combined with the data of chapter 4, give the cost-effective value of collector losses as a function of contour surface tolerance and sun following errors. Such a

procedure would resolve a variable in the solar power plant design.

7.2.3 Guidance And Control.

Future work in guidance and control should involve principally wind tunnel testing to determine the validity of derived theory. Tests should evaluate the spectrum of deflections at other than resonant frequencies and determine the effectiveness of stowage positions in reducing wind forces. Further, the buffeting of the collector structure due to upstream collectors ought to be considered. This last problem is particularly important for stowage positions which rely on the collector acting like a wind vane to minimise forces. Buffeting presents sudden wind shifts which may occur too quickly for the collector to move into alignment with the wind.

A study should be initiated to determine the collector support structure and actuator details. Once this information is available, a complete list of structure vibration modes can be assembled. Resonant frequencies and damping ratios for each mode can then be evaluated. Eventually, information relating collector cost to the accuracy of sun following error will be obtained and this information may then be combined with the information in chapter 4 to evaluate cost effective values of the variables.

8.0 SYMBOLS

General

The subscript o is used to denote an optimum value, usually optimum with respect to cost.

The subscript m is used to denote a maximum value, but may mean 'material'.

A dot above a value denotes differentiation with respect to time.

Small letters in general denote intensive quantities, for example q represents energy per square metre of aperture.

The subscript k refers to the kth segment in an array.

The section where further information on the symbol may be found is given in brackets.

Particular

a angle from the centre of a beam in the Gaussian reflected beam approximation (4.4).

A amplitude of sinusoidal input variation (6.3).

A concentration ratio (4.6).

B angle between fixed axis and equatorial plane, measured in N-S plane. Corresponds with latitude for a true alt-az mount.

- B_1, B_2 parameters in pipe cost formulation (3.5).
- B generalised sun following error, $B=h\beta$ (3.4).
- B effects..background wind deflections (5.4.3).
- C Cost (3.3).
- c_m cost per unit length of pipes (3.5).
- C_{et} Cost of energy transfer network (3.5).
- C_ℓ Cost of the links, not counting pumping power (3.5).
- c_c collector cost, $\$/m^2$.
- C_D Drag coefficient.
- d Pipe internal diameter.
- D Collector aperture diameter.
- $E(r)$ Irradiance in the focal plane of paraboloid, as function of radius r (4.4).
- $f(g)$ Illumination function, the ratio of energy collected by paraboloid in array of spacing g to isolated paraboloid (3.4).

- G Vector of calibration constants (5.4.2.2).
- $G(s)$ Open loop transfer function (6.3).
- g Ground cover ratio, ratio of aperture area to land area occupied (3.4).
- h Precision parameter defining accuracy of paraboloid surface (4.4).
- I_e Investment cost of electricity, \$/W (3.3).
- I_p Investment cost of pumping equipment, \$/W (3.3).
- K_0 DC gain constant in servo loop (6.3).
- K_1 Integral gain constant in servo loop (6.3).
- $K(s)$ Transfer function of collector structure (6.3).
- k Earth's rotational velocity.
- L Distance between collectors (3.4).
- $l(N_c)$ Dimensionless pipe network variable, the ratio of the average distance between collectors to the length of the smallest diameter pipe in the array (3.6).

m_r Relative air mass (3.4).

\dot{m} Mass flow rate (3.5).

N_c Total number of collectors.

n_s Number of bits in sun following error information for one axis.

n_m Number of bits in magnitude of speed command for one axis.

$\Delta Pr(N_c)$ Dimensionless variable relating the pressure drop as seen by the circulating pump to the pressure drop across the pipe segment with the smallest diameter (3.6).

p Parabola focal length parameter, equal to twice the focal length (4.3).

$Q(s)$ Transfer function of relay (6.3).

Q Energy collected by an aperture (4.3).

\dot{Q}_{in} Power input to cavity absorber (4.3).

\dot{Q}_l Power losses from cavity absorber.

q Energy collected by an aperture per square metre of aperture (4.3).

- q_A Energy available to be collected by an aperture, per square metre (3.4).
- q_C Energy available at central station (3.4).
- q_{in} Power input to cavity, proportional to instantaneous product of illumination function and solar flux (4.3).
- r Error ratio, ratio of difference between pointing directions generated by true calibration constant set and directions generated by calculated set, to the possible rms error in each of the original points (5.4.2.2).
- r Parameter in the calculation of direct radiation using Allen's clear air model (3.4).
- r Radius.
- R Data rate (5.4.2.2).
- R_m Data rate due to motor speed commands (App H).
- R_s Data rate due to sun sensor information (App H).
- R Generalised radius, equal to hr/p (3.4).

- S Pump capacity factor (3.3).
- T Traverse time.
- T Time in years.
- t Time.
- t_c Command interval, time between speed adjustments.
- U Parabola rim angle (4.3).
- V Wind velocity.
- \bar{V}_s Wind velocity at which collector will be stowed.
- \bar{V}_k Decay constant in describing curve which correlates winds with sunshine data.
- $v(N_c)$ Dimensionless pipe volume variable, ratio of average pipe inner volume to pipe inner volume of smallest diameter pipe (3.6).
- \dot{W} Power, usually referred to work forms.
- \dot{W}_e Electrical power output of station (3.3).
- \dot{W}_p Pumping power requirement (3.3).

X Variable in function representation of fixed point functions.

X Vector of actuator displacements (5.4.2.2).

GREEK

β Sun following error (4.4).

$\Delta(A)$ Absolute error in representation of A.

δ Solar declination.

$\Delta\epsilon$ Level width in representing analogue information in digital form (6.3.1).

ζ Damping coefficient.

η_c Efficiency in converting radiation energy to thermochemical energy.

η Efficiency in converting radiation energy to thermal energy at the central boiler (3.4).

$\eta(\text{eff})$ Efficiency of cavity receiver at absorbing radiation (4.3).

- η Capture ratio of cavity, ratio of energy which enters cavity to energy directed towards it (4.3).
- θ Altitude or elevation.
- $\Delta\theta$ Error in altitude.
- $\Delta\theta_i$ Error in angle of one sort or another.
- $\Delta\theta_f$ Error in estimation of position of sun for fast fix (App H).
- $\Delta\theta_s$ Error in estimation of position of sun for slow fix, also possible error in digitised sun sensor information (App H).
- $\hat{\theta}, \hat{\phi}$ Functions relating actuator displacements to equatorial coordinates (5.4.2.2).
- ϕ Azimuth angle.
- $\Delta\phi$ Error in azimuth.
- I Solar flux.
- ρ Reflectivity of a surface.
- σ Standard deviation of a quantity.

- τ Response time.
- ω Angular speed.
- $\Delta\omega$ Smallest speed change possible due to digitisation of speed commands.
- ω_m Maximum speed possible, usually taken as .87mrad/sec.
- Ω Solar diameter, around 9.3mrad.

9.0 REFERENCES

- Auracher, F and Witte, H.H.(1977), 'Optimised layout for a data bus system based on a new planar access coupler', Appl. Optics 16, 12, pp3140-3142.
- Baum, I.V. and Mamedniyazov, S.O.(1977), 'Comparitive analysis of models of irradiance field formation in wide aperture optical systems', Geliotekhnika 13, 5, pp26-36.
- Bennison, E. et al(1973), 'Lightning surges in open wire, coaxial and paired cables', IEEE transactions on communications, Vol COM-21, 10, pp1136-1143.
- Bevington, P.R.(1969), 'Data reduction and error analysis for the physical sciences', McGraw-Hill.
- Bider, M.(1958), 'Uber die Genauigkeit der Registrierungen des Sonnenscheinautographen Campbell-Stokes', Archiv fur Meteorologie, Geophysik und Bioklimatologie, Series B, v 9(2), pp199-230.
- Blaylock, R.B. et al(1964), 'Wind tunnel testing of antenna models', N.Y. Academy of Science, Annals, 116, pp240-274.
- Bokris, J.O'M(1975), 'Energy, the solar hydrogen alternative', Australian and New Zealand Book Co, Sydney.
- Bradshaw, P and Wong, F.Y.F(1972), 'The reattachment and

relaxation of a turbulent shear layer', J.Fluid Mech
52,1,pp113-135.

Brent, R.(1973), 'Algorithms for minimisation without
derivatives', Prentice-Hall.

Brown, K.M. and Dennis, J.E. (1972), 'Derivative free
analogues of the Levenberg-Marquardt and Gauss algorithms
for nonlinear least squares approximation, Num. Math., 18,
pp289-297.

Brinkworth, B.J.(1972), 'Solar Energy for Man', Compton.

Caputo, R.S.(1975), 'An initial study of solar power plants
using a distributed network of point focussing
collectors', JPL report 900-724, Caltech, California.

Carden, P.O.(1977), 'Energy corradiation using the reversible
ammonia reaction', Solar Energy, 19, pp365-378.

Carden, P.O. (1978a), 'Steering a field of mirrors using a
computer based controller', Solar Energy, 20, pp343-355.

Carden, P.O.(1978b), 'Solar Power for remote areas', ISES
symposium, Perth.

Carden, P.O. and Williams, O.M.(1978), 'The efficiencies of
thermochemical energy transfer', International Journal of

Energy research, Vol 2, pp389-406.

Chung, D.H.(1977), 'Four design principles get the most out of microprocessor systems', Electronics pp102-110.

Clarke, H.L.(1950), 'Sun follower for V-2 rockets', Electronics, October, pp71-73.

Cohen, E. et al(1964), 'Calculation of wind forces and pressures on antennas', N.Y. Academy of Science, Annals, 116, pp161-221.

Davenport et al(1975), 'The structural and environmental effects of wind on buildings and structures', Dept of Mechanical Engineering, Monash University.

Derr, J.H. et al(1975), 'Predicting the reliability of systems using complex MOS/LSI devices in automotive applications', Proceedings of the Annual Reliability and Maintainability Symposium, pp366-371.

Dibble, D. and Nagaraja Rao, C.R.(1966), 'An inexpensive solar pointing control', J. Sci. Instrum., 43, p588.

Dixon, L.C. (Ed) (1976), 'Optimisation in Action', Academic.

Draper, N.R. and Smith, H(1968), 'Applied Regression Analysis', Wiley.

Dubberley, A. Private Communication.

Duffie, J.A. and Beckman, W.A.(1974), 'Solar Energy Thermal Processes', Wiley, New York.

Dummer, G.W.A.(1970), 'Electronic Components, Past, Present and Future', Electronic Components, Oct.

Easton, C.R. et al(1976), 'Collector field design for a central receiver solar thermal power plant', Joint Conference of the American section of ISES, and the Solar Energy Society of Canada, Inc., Winnipeg, Manitoba, Canada, pp374-384.

Edwards, B.P.(1978a), 'Shading and Spacing in Paraboloidal Collector arrays', Solar Energy, 21, 5, pp435-439.

Edwards, B.P.(1978b), 'Computer based sun following system', Solar Energy, 21, 6, pp491-496.

Electricity Supply Association of Australia (1977), 'The electricity supply industry in Australia, Year 1975-76'.

Electronics(1977), International Newsletter section, Nov 10.

Electronics and Power(1978), Vol 24, 3, p178.

Fourakis, E. and Severson, A.M.(1977), 'Low profile heliostat

design for solar central receiver system', Solar Energy 19, pp349-356.

Francia(1968), 'Pilot plants of solar steam generating stations', Solar energy 12, pp51-64.

Fujii, S. and Gomi, M.(1976), 'A note on the two-dimensional cylinder wake', Journal of Fluids Engineering, 98, series 1, 2, pp318-320.

General Electric(1972), SCR manual, Fifth edition, New York.

Gervais, R.L. et al(1976), 'A central receiver solar system applicable to central power stations', Joint Conference of the American section of ISES, and the Solar Energy Society of Canada, Inc., Winnipeg, Manitoba, Canada. pp325-335.

Grant, E.L. and Ireson, W.G.(1960), 'Principles of Engineering Economy', Fourth Edition, Ronald, New York.

Greenbaum, I.(1954), 'Observed and Theoretical Values of Astronomical Refraction at low altitudes', Astronom. J., 59, pp17-19.

Grouchko, D.(1971), 'Operations Research and Reliability', NATO Conference(1969), Gordon and Breach.

Hart, J.F.(1968), 'Computer Approximations', Wiley.

Hastings, C.(1955), 'Approximations for digital computers',
Princeton, N.J.

Hodges, D.A.(1976), 'Trends in Computer Hardware Technology',
Computer Design, February 1976, pp77-85.

Hughes, R.O.(1977), 'The sun tracking control of solar
collectors using high performance step motors', Sixth
Annual Symposium on Incremental Motion Control Systems and
Devices, Illinois, May 1977.

IAU(1965), 'The construction of large telescopes; IAU
symposium No 27, Tucson Arizona, Crawford, D.C.(Ed),
Academic 1966.

ITT(1973), 'Reference data for radio engineers', 5th Ed,
Howard and Sams.

Jackson, L.A. and Stern, J.R.(1977), 'Optical fibre systems
for the civil communications network', Optics and Laser
Technology, pp233-240.

Jayant, N.S.(1967), 'Data communication through the
atmospheric burst error channel', IEEE Trans Com Tech, Vol
COM-15, 3, pp.383-389.

Kao, C.K. and Goell, J.E.(1976), 'Design process for fibre
optic systems follows familiar rules', Electronics,

September 16, pp113-116.

Kaplan, G.H. et al(1976), 'Almanac for Computers, 1977', USNO Circular 155, October 1(1976).

Kowalik, J. and Osborne, M.R.(1968), 'Methods for Unconstrained Optimisation problems', Elsevier.

Kratky, K.W.(1978), 'The area of intersection of n equal circular discs', J. Phys. A, 11, 6, pp1017-1024.

Lauffenburger, H.A.(1977), 'A reliability comparison of semiconductor and microcircuit technologies', NBS Special Publication 400-42, US Dept of Commerce.

Lill, S.A.(1976), 'A survey of methods for minimising sums of squares of nonlinear functions', in L.C.Dixon(Ed), 'Optimisation in action', Academic.

Lof, G and Duffie, J.A.(1963), 'Optimisation of focussing solar collector design', Journal of engineering for power, 85, pp221-228.

Lucas, P. and Knight, L.(1976), 'Observed failure rates of electronic components in computer systems', Microelectronics and Reliability, 15, pp239-243.

Mosher, D.M. et al(1977), 'The advantages of sun tracking for

planar silicon solar cells', *Solar Energy*, 19, pp91-97.

Muska, W.M.(1975), 'Detection taps for single fibre optical data bus', Topical meeting on Optical Fibre Transmission, Williamsburg, Va.

McClelland, W.J. and Preston, T.(1907), 'Spherical Trigonometry', McMillan.

Oetzel, G.N. and Pierce, E.T(1969), 'VHF technique for locating lightning', *Radio Science*, 4, 3, pp199-202.

Paltridge, G.W. and Proctor, D.(1976), 'Monthly mean solar radiation statistics for Australia', *Solar Energy* 18,3,pp235-243.

Peattie, C.G. et al(1974), 'Elements of Semiconductor Device Reliability', *Proc IEEE*, 62, 2, pp149-168.

Perry, R.H.(1973), 'Chemical Engineers handbook', Fifth Ed, McGraw-Hill.

Powell, J.C. et al(1974), 'Dynamic conversion of Solar generated heat to Electricity', Honeywell Inc. and Black and Veatch, for NASA Lewis, NASA CR-134724.

Robinson, N.B.(1966), 'Solar Radiation', Elsevier.

Rubanovich, I.M. (1967), 'Objective estimation of the accuracy of the reflecting surfaces of the paraboloidal concentrators of high temperature solar devices', *Geliotekhnika* 3, 6, pp26-33.

Sakurai, T. et al (1964), 'Construction of a large solar furnace', *Solar Energy* 8, 4, pp117-126.

Sawyer, J.G. et al (1972), 'Causes of shutdown in ammonia plants' *Ammonia Plant Safety Vol 14*, Am. Inst of Chem. Eng.

Schlichting, H. (1960), 'Boundary Layer Theory', Fourth Ed, McGraw-Hill.

Scruton, C. (1969), 'Some considerations of wind effects on large structures', in Mar, J.W. (Ed), 'Structures Technology for large Radio and Radar Telescope Systems, MIT press, pp65-88.

Shaner, W.W. and Wilson, H.S. (1975), 'Cost of paraboloidal collectors for solar to thermal electric conversion', *Solar Energy* 17, pp351-358.

Sherlock, R.H. (1947), 'Gust factors for the design of buildings', *Inter. Assoc. Bridge and Struct. Eng. Vol 8*.

Simiu, E and Lozier, D.W. (1975), 'The buffeting of tall

structures by strong winds', NBS Building Science series 74, US Govt printing office, Washington.

Stickley, R.A. et al(1974), 'Solar Power array for the concentration of energy', Semi-Annual Progress Report, NSF-RA-N-74-090.

Sumner, C.J. and Patterson, G.(1969), 'A sun tracking instrument stand', Solar Energy 12, pp537-542.

Teplyakov, D.I.(1973), 'Optical and energetic aspects of radiation concentration in high temperature solar units', Geliotekhnika, 9, 2, pp21-28.

Teplyakov, D.I. and Poluektov, V.P.(1968), 'Similar generalisation in studies of the angular defocussing regimes of paraboloidal solar devices', Geliotekhnika, 4, 2, pp36-42.

Thaler, G.J. and Brown, R.G.(1960), 'Analysis and design of feedback control systems', McGraw-Hill.

UN(1977) United Nations statistical yearbook.

US Dept of Defence(1974), Military Standardisation Handbook, 'Reliability Prediction of Electronic Equipment', MIL-HDBK 217-B.

Vant-Hull, L.L.(1976), 'Development of the solar tower program in the united states', Proc Society of Photo-Optical Instrumentation engineers, Vol 85, 'Optics in Solar Energy Utilisation 2', Aug 24-25(1976), San Diego CA.

Vant-Hull, L.L.(1976), 'Methods for estimating total flux in the direct solar beam at any time', Joint Conference of the American section of ISES, and the Solar Energy Society of Canada, Inc., Winnipeg, Manitoba, Canada, pp369-375.

Vant-Hull, L.L. and Easton, C.R.(1975), 'Solar Thermal Power Systems based on Optical Transmission', Final Report, NSF-RA-N-75-288.

Vickery, B.J., 'On the reliability of gust loading factors', in: 'Wind loads on buildings and structures', NBS Building Science series 30, US Govt Printing Office, Washington.

Weiss, G.H.(1978), 'Heat losses from Absorbers', Dept of Engineering Physics Technical Publication SR-46.

Whittingham, H.E.(1964), 'Extreme Wind Gusts in Australia', Bureau of Meteorology Bulletin 46.

Williams, O.M.(1978), 'Thermochemical Energy Transport Costs for a distributed Solar Power Plant', Solar Energy, 20, pp333-342.

Williams, O.M. and Carden, P.O.(1978), 'Energy storage efficiency for the ammonia/nitrogen-hydrogen thermochemical energy transfer system', International journal of energy research.

Williamson, H.(1972), 'Hidden line plotting program' Communications of the ACM, 15, 2, pp100-103.

Zakhidov, R.A.(1965), 'Calculation of the energy distribution in the radiation field of reflector type solar energy devices', Geliotekhnika, 1, 5, pp11-18.

Zakhidov, R.A.(1977), 'Analysis and Classification of concentrating system design methods', Geliotekhnika, 13, 4, pp3-13.

Zakhidov, R.A. and Teplyakov, D.I.(1966), 'Power characteristics of concentrator type solar devices under field tracking conditions', Geliotekhnika, 2, 4, pp35-43.

Zakhidov, R.A. and Vainer, A.A.(1974), 'Distribution of radiation produced by a paraboloidal concentrator', Geliotekhnika 10, 3, pp34-40.

APPENDIX A

PROGRAM FOR CALCULATING SHADING

A.1 INTRODUCTION

In this appendix we describe the operation of the program which calculates the amount of shading experienced by a paraboloid mirror in an array, as required for the calculations in chapter 3. We begin by demonstrating how the presence of other collectors in the array is handled mathematically and then describe how the hidden line plotting program HIDE(Williamson, 1972) is used to evaluate the contour surrounding the illuminated part (or parts) of the shaded mirror. Two simple cases are used to illustrate the problems that arise.

A.2 SHADING CALCULATIONS

To calculate the fraction of the aperture of the shaded mirror which is illuminated, the following procedure is pursued. The mirror field is constructed as an array of points in the XY plane. These points are the positions of each mirror pedestal, and represent the layout of the mirrors on the ground.

The array of points is projected onto an inclined plane normal to the sun's rays, and the coordinates of this projected array are reexpressed in coordinates referred to this inclined plane, the x-axis being the intersection of the inclined plane and the horizontal, and the y-coordinate increasing with height above the ground. This last fact ensures that all the mirrors which are closer to the sun than the shaded mirror are easily determined, as they will have y values which are smaller than the y value of the shaded mirror.

As all mirrors track the sun, the shape of the aperture is unchanged on the inclined plane, and the aperture is assumed to be circular. Thus all the mirrors which might shade the shaded mirror are those mirrors with centres within one mirror diameter of the shaded mirror's centre. The mirrors which satisfy these two requirements, viz being closer to the sun than the shaded mirror, and being within one diameter of the centre of the shaded mirror, are called the shading mirrors. The procedure to evaluate the amount of shading at an instant is as follows. Starting with the shading mirror closest to the sun (the lowest y value of the shading mirrors), the upper boundary of the shadow cast by the mirror is evaluated. This boundary is called the visual maximum contour. The contour representing the lower boundary of the shadow, or visual minimum contour, is also evaluated. Then the shading mirror with the next lowest y value is considered, and a new visual maximum and visual minimum contour evaluated which respectively represent the upper and

lower boundary of the combined shadow for the two mirrors. This procedure is repeated until all the shading mirrors have been considered, and the final visual maximum and visual minimum contours represent the upper and lower boundaries of the total shadow cast by all the shading mirrors. Once this procedure has been completed, the contour which is the outline of the unshaded part of the shaded mirror can be evaluated. The area inside the contour is evaluated using Green's theorem in the plane.

A.3 IMPLEMENTATION.

The program HIDE was designed to produce a two-dimensional representation of a surface by plotting segments of a succession of curves, each curve being plotted where it is not hidden by any of the curves previously plotted. This characteristic is used to evaluate the upper and lower boundaries of the shadows cast by all the shading mirrors.

A.3.1 Details.

Firstly HIDE requires that each curve to be plotted has x increasing through the set of points which define the curve. Hence a circle can only be plotted by plotting two semicircles, (being the upper and lower halves of the circle)

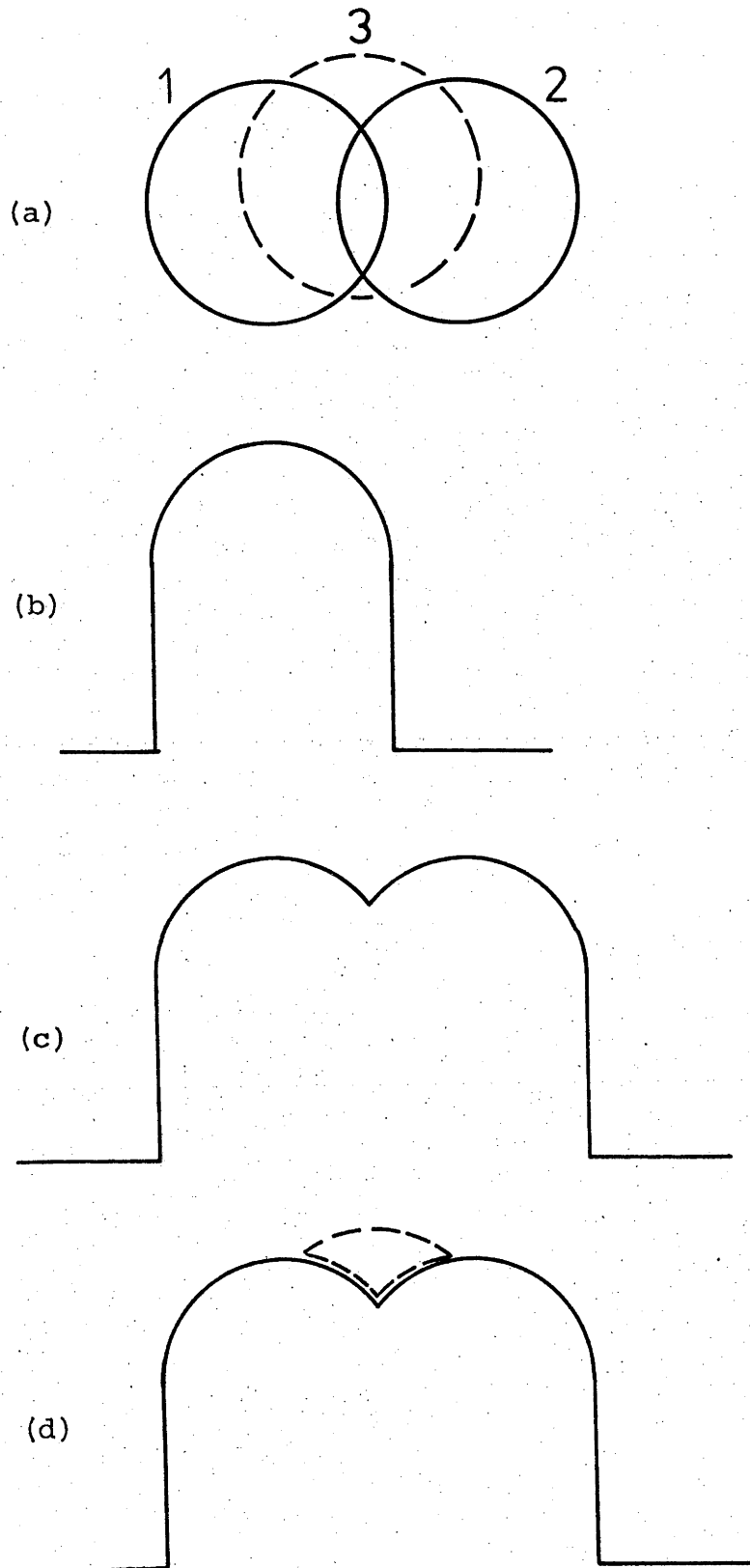


Figure A1.

(a) Full circles: Shading mirrors

Dashed circle: Shaded mirror

(b) Visual maximum contour (or upper shadow boundary) after considering mirror 1.

(c) Visual maximum contour after considering mirrors 1 and 2.

(d) Dashed line is the contour surrounding one illuminated area of mirror 3.

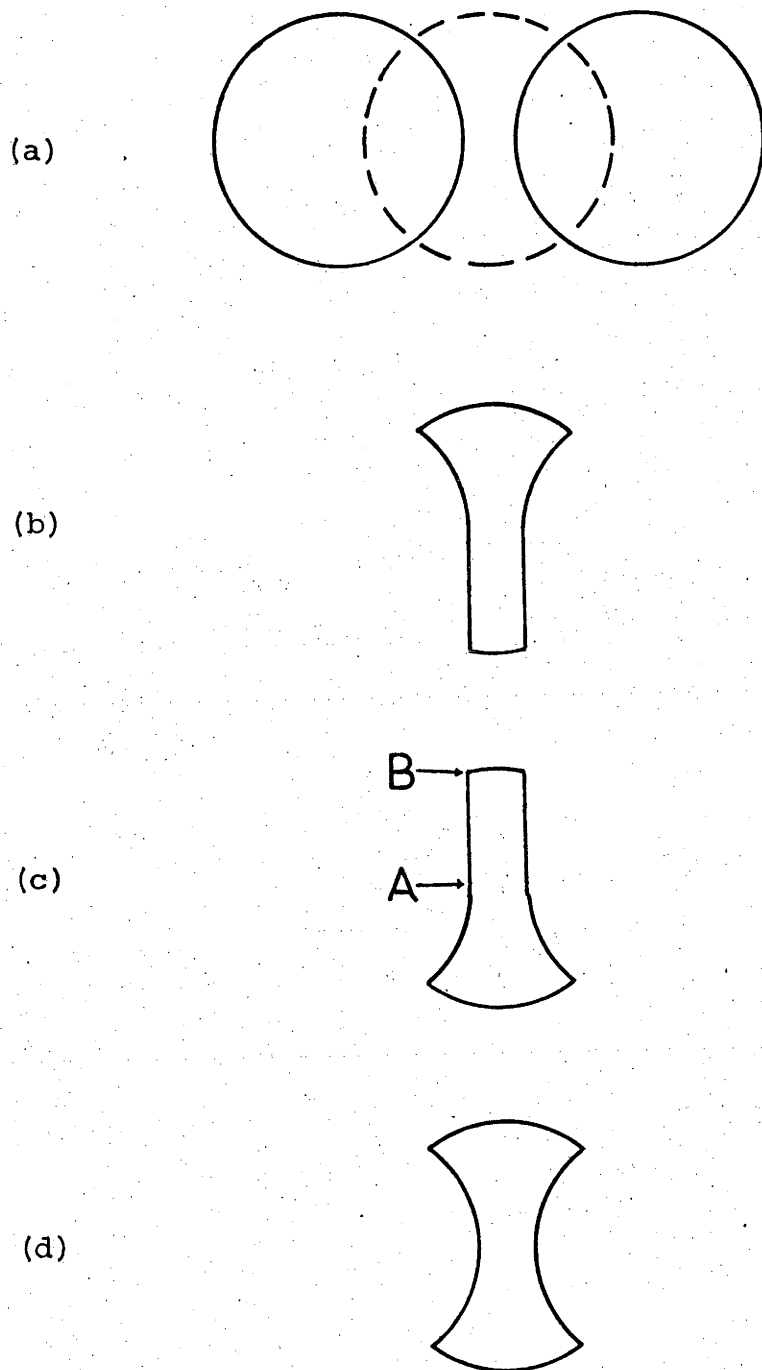


Figure A2

(a) Full circles: Shading mirrors.

Dashed circle: Shaded mirror.

(b), (c) Contours equivalent to the dashed contour in figure A1(d)

(d) Resultant contour outlining the illuminated portion of the shaded mirror in figure A2(a).

between points which are larger than usual. These occur for example between points A and B in figure A2(c). By detecting these points, the two contours in figures A2(b) and A2(c) are joined to form a contour as in figure A2(d).

The area enclosed by the contour is evaluated using Green's theorem in the plane, viz:

$$\int_R dx dy = 0.5 \int_C (x dy - y dx) \quad (A.1)$$

A.4 AFTERTHOUGHT.

A paper by Kratky (1978) on the area of intersections of equal diameter circular discs may be of interest if faster calculations are desired.

APPENDIX B

ANALYSIS OF CAMPBELL-STOKES SUNSHINE RECORDS FOR GRIFFITH (1975).

B.1 INTRODUCTION

At present the only available statistics on beam radiation are daily totals of sunshine, as measured on the Campbell-Stokes sunshine recorder. Statistics which offer higher time resolution are not available, and such statistics would be useful for the design of solar power plants, particularly those which involve tracking or high temperature operation.

B.2 THE RECORDS

Campbell-Stokes records of beam radiation are available for a large number of years, and a substantial number of localities. To obtain some results in the shortest possible time records for 1975 were borrowed from the CSIRO station at Griffith. The year 1975 was chosen for two reasons, firstly the rainfall for 1975 was within 6% of the average, and secondly 2800 hours of sunshine were recorded, which is within 10% of the average. It is hoped that with these average gross statistics, the higher resolution statistics obtained in this

study will also be representative.

B.3 THE INSTRUMENT.

The Campbell-Stokes recorder consists of a spherical glass ball, which focusses the sun's radiation onto a cardboard record sheet mounted on a spherical surface a few cm from the ball. When the sun is shining a track is burnt in the cardboard. The threshold of the instrument has been extensively studied by Bider(1958), (though unfortunately the paper is in german). This threshold varies throughout the year, and also depends on whether the sun is rising or setting. The threshold of the instrument depends also upon the interpretation of the records; the threshold for a completely burned through track (denoted B in later figures) being higher than the threshold for a mere single mark (denoted C-St).

TABLE B.1. Threshold of the Instrument (Wm^{-2}) (Bider 1958).

	Winter	Spring/Autumn	Summer	Year	Average
C-St	220/200	260/210	190/180	220/200	210
B	320/270	290/260	290/250	300/260	280

Where the first figure is the threshold for sunrise, and the second figure for sunset.

Bider also tabulates the elevation of the sun at the time when the recorder indicates sunrise and sunset (for cloudless sunrises/sets). This also varies with the season,

the average elevation for 'sunrise' being recorded as 4.7 degrees, and the average elevation for 'sunset' being 4.2 degrees. For the completely burnt through tracks the elevations are 7.8 and 7.3 degrees respectively.

B.4 METHOD OF DATA REDUCTION.

The records were attached to the bed of the engineering physics string digitiser using a thin sheet of Mylar and two or three bar magnets. The Mylar protected the records from damage, and the bar magnets were a flexible attachment scheme which held the variable shape (and often warped) records secure and flat.

The hour marks on the records and the starts and stops of the sunshine periods were digitised. The times of the starts and stops were linearly interpolated between adjacent hour marks. At Griffith the record cards are changed during the day and the time of this change was also recorded. Because of this changeover, each record card is an incomplete record of two days and a program combined the records to give a complete account of the sunshine for each day.

Substantial interpretation was required to evaluate the records as there is a gradation in record burns from a thin scorch to a complete burn through the record. The person digitising attempted to adhere to a uniform strategy of using only burnt through marks. Thus the threshold of the derived records is around 280Wm^{-2} , but this threshold has both yearly and hysterical variations. The shortest burst of sunshine

detectable was considered to be around 1 minute.

B.5 RESULTS.

1737 sunshine bursts were recorded from the 364 days analysed. Of these bursts 1187 were shorter than half an hour and 900 were less than 12 minutes.

The amount of energy contained in a specific sunshine burst length domain is shown in figure B.1, in histogram form with a step size of half an hour. From this figure it is seen that significant energy is contained in short bursts. The data in figure B.1 has been integrated and in figure B.2 is shown the amount of energy contained in bursts longer than a certain length, and in figure B.3 for bursts shorter than a certain length. Another point of interest is the symmetry of cloud cover over the day as cloud cover is often assumed to be constant. The number of times the sun was shining at a specific time of the day is plotted in figure B.4. In figures B.5 and B.6 data is presented which has direct bearing on the guidance and control system design. Firstly it is known that some form of anticipation by the guidance and control scheme is required to roughly locate the solar collector so it is in a position to absorb energy. It is shown in figure B.5 that an anticipation of the sun's position at only one point, eg sunrise, would not be very effective, as the sun appears at times which are spread fairly evenly over the day. Secondly, if one designs a guidance and control scheme which uses the sun's radiation to determine the sun's direction, then a

procedure must be followed when the sun disappears. This procedure depends upon the time till the likely reappearance of the sun. It is shown in figure B.6 that the reappearance is likely after some 10-15 minutes and failing that, after around 12 hours.

B.6 USES OF THE DATA.

B.6.1 The Value Of Low Response Time.

The elapsed time from the appearance of the sun till when the collector is following the sun to the required accuracy is called the response time. Sophisticated computer based systems will be capable of reducing this time to nothing, by predicting the sun's position and positioning the collector in readiness, and the benefit of such a system (which determines the allowable cost of the system) can be calculated from the product of this response time and the number of sunshine bursts. From the above data, the number of bursts is a function of the length of the burst, and for bursts longer than 10 minutes, there are approximately 1000 bursts each year.

B.6.2 Focal Receiver Performance.

The sequence of sunshine bursts can be combined with suitable time constants to determine losses in the focal receiver subsystem.

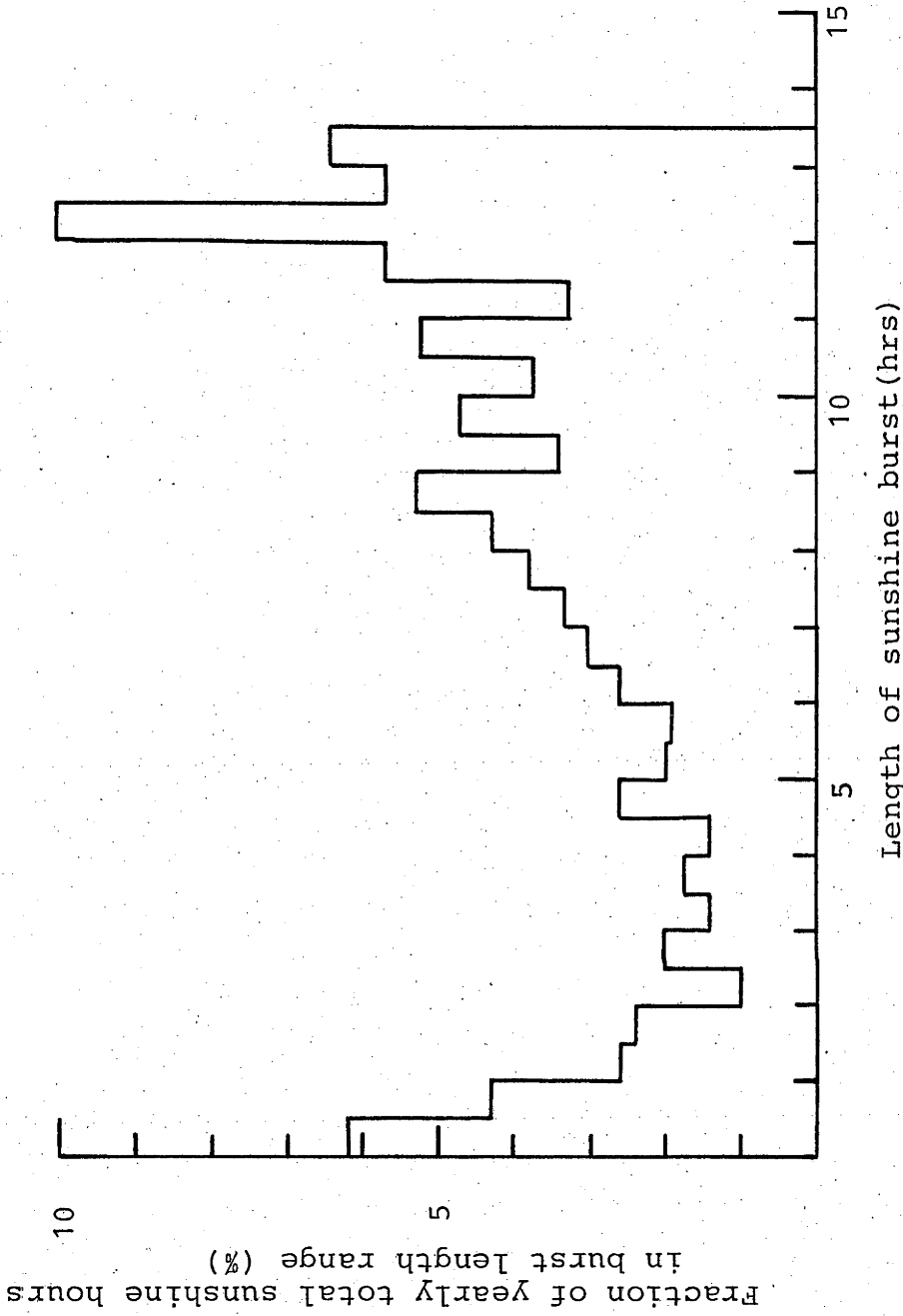


Figure B.1 Fraction of sunshine hours contained in sunshine bursts of a specific lengths. Histogram step size is 30 minutes.

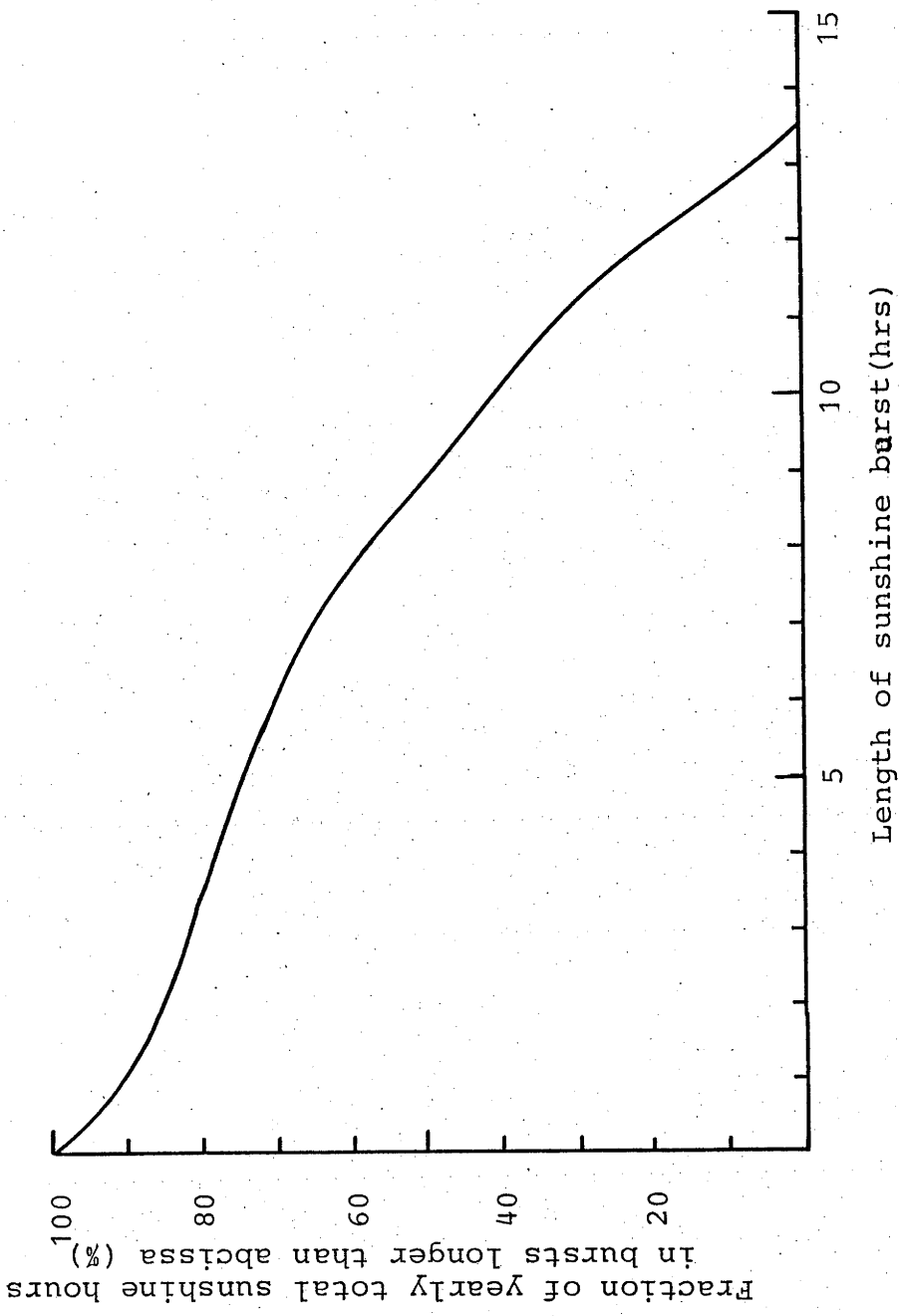


Figure B.2 Fraction of sunshine hours contained in sunshine bursts longer than a specific length.

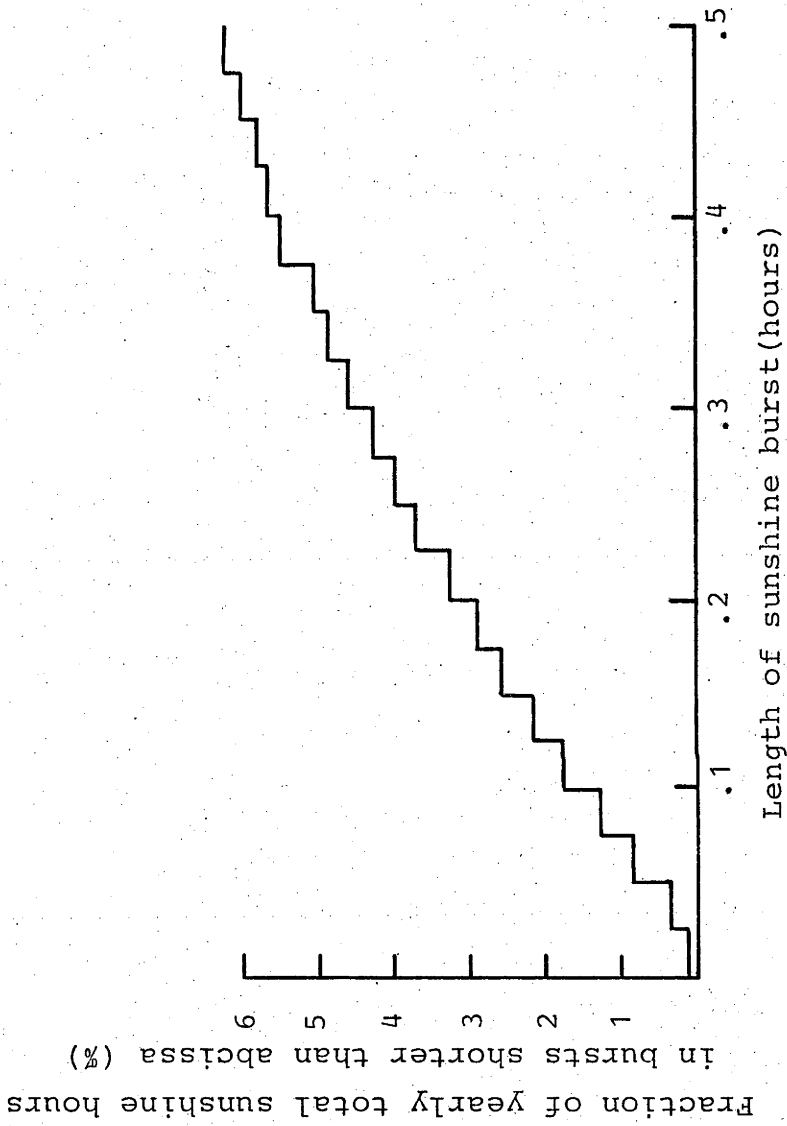
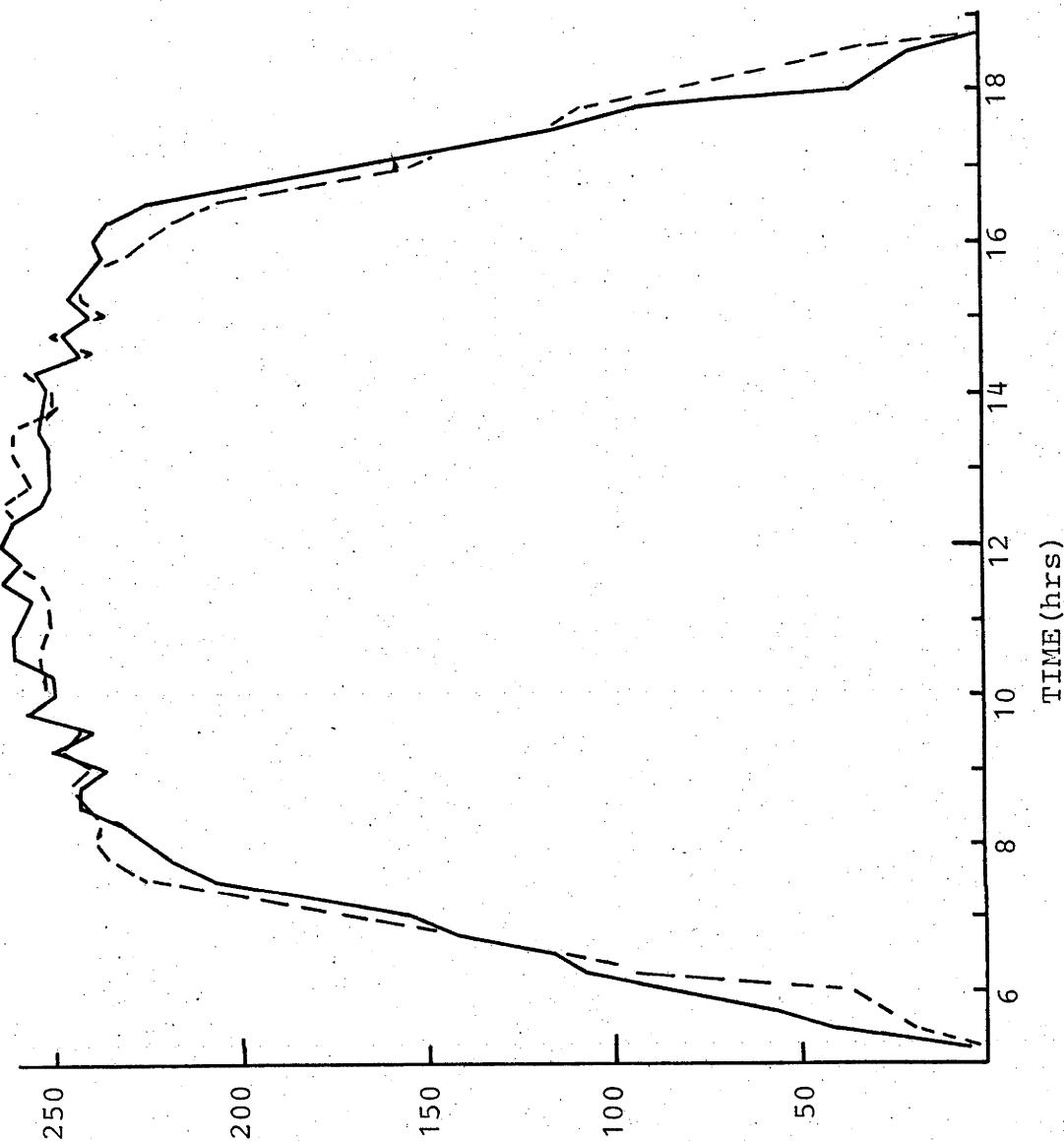


Figure B.3 Fraction of sunshine hours contained in sunshine bursts shorter than a specific length. Histogram step size is 1.5 minutes.



Number of occasions on which sun was out at time.

Figure B.4 The number of occasions on which sunshine was recorded at a specific time of day. The dashed line is the reflection through midday of the unbroken line. The unbroken line is the data which corresponds to the abscissa.

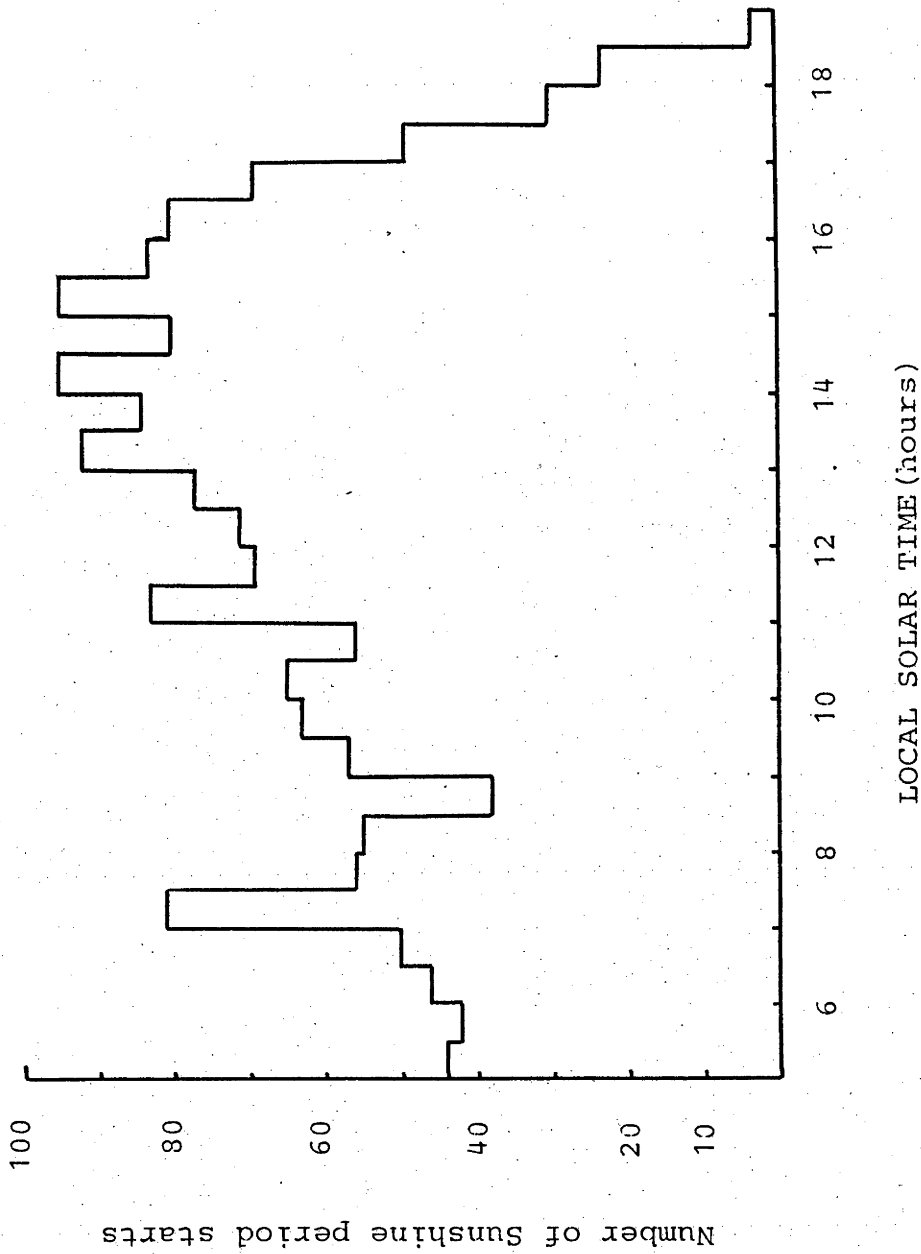


Figure B.5 A histogram of the time when the sun appears is shown.

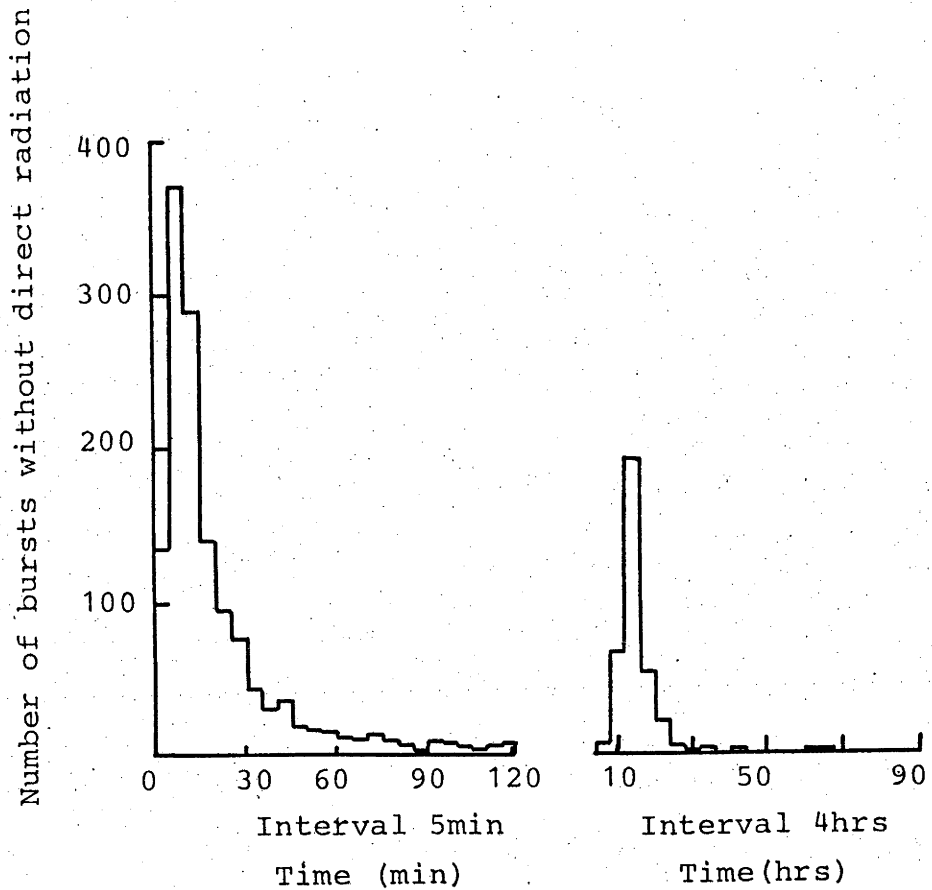


Figure B.6 This figure shows the length of the darkness periods. The left hand graph covers bursts from 0-2hrs, with a histogram step size of 5 minutes, and the right hand graph covers bursts from 2-90hours, with a histogram step size of 4 hours.

TECHNICAL NOTE

Shading and spacing in paraboloidal collector arrays

B. P. EDWARDS

Department of Engineering Physics, Research School of Physical Sciences, Australian National University,
Canberra, A.C.T., Australia

(Received 20 February 1978; revision accepted 1 June 1978)

1. INTRODUCTION

The cost of a solar energy collector is determined primarily by its aperture, while the cost of the energy collected depends on both the collector cost and the amount of energy passing through the aperture. One way to decrease the cost of solar energy is to decrease the amount of shading the aperture experiences, and if one increases the amount of energy collected by 1 per cent, then, all else remaining equal, the energy collected will be 1 per cent cheaper. This paper evaluates the variations in losses due to shading as a function of spacing for square arrays. It is not realistic to increase the spacing between collectors sufficiently to completely eliminate shading caused by adjacent collectors, as several costs increase with increased spacing. These costs are dependent upon the links between the mirrors and the central control/power plant, which in turn depend upon the system used to control the mirrors, and the system used to collect the energy from the mirrors. In this paper the work of Williams[1] on energy transfer costs is used in conjunction with the shading calculations to evaluate the optimum spacing for collector arrays. In addition the minor costs of the links for both communication and supplying power to the collectors for movement are considered.

Williams has noted that some change in technology is needed to reduce the installation costs for pipe networks. The effect of such a change is considered in this paper by varying parameter values in the pipe cost formulation used by Williams, and studying the effects of such variations.

2. SYSTEM UNDER STUDY

The system studied is an array of collectors with circular apertures, each collector being mounted on a fixed pedestal. The pedestals are laid out in a rectangular grid of square section.

The energy transfer scheme used in this paper is the NH_3 scheme of Carden[2]. System pressure is 300 atm, and the mass fraction of dissociation occurring at the collectors is 0.6. As in the study of Williams[1] it is assumed that the thermal energy contained by the gases coming out of the heat exchanger at slightly above ambient cannot be recovered. Thus the variation in energy collection with spacing is limited to the extra pumping power and the effects of shading. An advantage of this thermochemical transfer scheme is its fast response to radiation input. Alternative schemes, such as the transfer of sensible heat, require a period to warm up the network of pipes. Also the thermochemical scheme, because of the high pressures involved, has only a small receiver mass operating at high temperature, and thus energy is received at the central plant within a short period of the mirrors being illuminated. Hence early morning radiation is in fact useable energy, and does not simply make up heat leaks for this transfer scheme. It is assumed that storage is provided for the thermochemical reactants at the central plant, and the total plant produces a constant power output.

The collector array further involves links for the distribution of power to the actuators on the collectors and communication links for control, in addition to the pipes required for energy transfer. The costs of the three types of links in the array, viz. power, energy transfer and communication, are combined into a single formulation representing the cost of the network.

3. SHADING CALCULATIONS

3.1 General

The shading of one mirror deep inside the array is representative of the shading of the whole array due to the symmetry of the array and thus a calculation of the amount of shading experienced by a single mirror is all that is necessary. This is accomplished by determining the boundary of the illuminated part (or parts) of the mirror for many occasions during the year, and then evaluating the average amount of shading. The mirror chosen as being representative of the field is called the shaded mirror. The pseudo 3-dimensional plotting program HIDE[3] has been modified to calculate the set of points which define this contour. In calculating the shading, it is assumed that the shadow cast by each of the collectors which shade the shaded mirror is identical to the shadow cast by the aperture, i.e. the effect of the pedestal and support structure is not included.

The array studied is as shown in Fig. 1. A square array with 49 collectors was used in the calculations, with the shaded collector being the furthest from the sun in one corner of the array. This array was big enough to include all collectors which might shade the collector in the corner of the array. The spacing in the array is described by the ground cover ratio g , which is the ratio of the total aperture area to the area of ground occupied by the collectors.

The fraction of the aperture illuminated is calculated at 40 points over each day, and for 20 equispaced days over the year. The fraction is then combined with the intensity of direct radiation to give the energy collected over a year. This is then divided by the aperture of the collector to give $E_A(g)$ ($\text{Whr}/(\text{m}^2 \text{yr})$), the energy collected by the collector over a year, for each square metre of aperture. When g is zero, the separation is infinite and the collected energy is a maximum and the illumination function $f(g)$ describes the ratio:

$$f(g) = E_A(g)/E_A(0). \quad (1)$$

Values for $f(g)$ have been calculated for the square array of Fig. 1, and the orientation of the array, as determined by the direction of the array reference with respect to North, has been varied to determine the best orientation.

Only a fraction of the energy which passes through the collector is available for conversion from thermal energy to electrical energy at the central plant. A collection efficiency factor, η_c , quantifies this fraction, and includes the efficiency of the thermochemical energy transfer process, the quality of the alignment and optics, the reflectivity of the collector and so on. This factor does not include pumping losses, and is not a function of spacing. The energy available at the central station (E_F) is therefore:

$$E_F = \eta_c f(g) E_A(0) \text{ Whr}/(\text{m}^2 \text{yr}). \quad (2)$$

No energy collection is considered below 5 degrees elevation for two reasons. Firstly, direct radiation at these elevations is variable, and not conducive to simple modelling, and secondly, the direct radiation from the sun decreases near the horizon, and this reduces the relative importance of shading. The values are calculated for two latitudes, 25 S and 35 S.

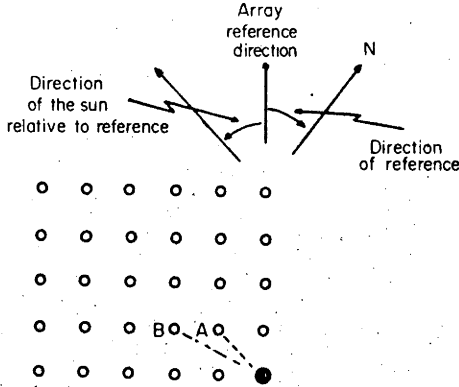


Fig. 1. Layout of the rectangular array, indicating the collector under consideration (or shaded collector), black dot; the shading collectors, circles; and the array reference direction (applicable to the Southern Hemisphere).

3.2 Direct radiation model

Vant-Hull[4] studies several tabulations of the direct clear sky radiation intensity as a function of solar elevation. He considers only the model of Allen (1964) to be appropriate for calculations concerning solar power stations. The following calculations assume Allen's model with an atmospheric water content of 14.4 mm, and a pressure of 760 mm Hg. The sun's position was calculated using standard equations as given by Brinkworth[5], with a sinusoidal variation in declination.

3.3 Cloud effects

The values derived for $f(g)$ will only hold in the presence of cloud cover if the variation in cloud cover has no regular daily or seasonal variation. Data from specific sites will need to be examined before more exact calculations can be made, and thus the following calculations strictly apply only to areas where cloud cover is relatively constant throughout the year.

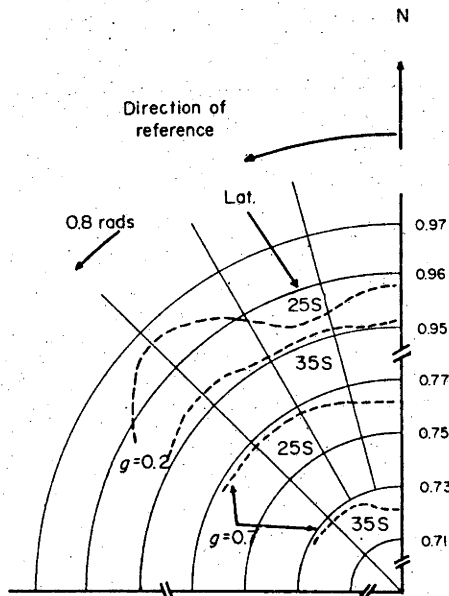


Fig. 2. The function $f(g)$ as a function of the orientation of the direction of the array pattern. The function is the ratio of the annual energy entering an aperture for ground cover ratio g to the annual energy entering an aperture when g is zero. The orientation is expressed by the angle between North and the direction of the array reference indicated in Fig. 1.

3.4 Results

The effect of changing the orientation of the array on the illumination function $f(g)$ is shown on polar scales in Fig. 2 for rectangular arrays at latitudes 25 S and 35 S. Shading is minimised with the direction of the array reference 0.8rad from North.

Figure 3 gives further information for this direction of the array reference. Note that at small ground cover ratios, the effect of shading is pronounced near the equinox, which is when the sun rises in line with the collector A in Fig. 1. The function $f(g)$ is plotted for a rectangular array in Fig. 4, for the same array reference direction as Fig. 3.

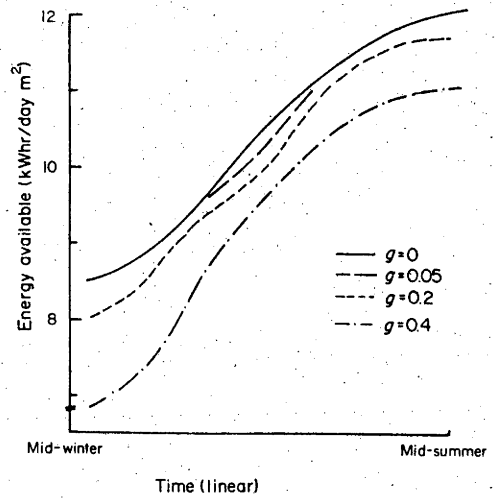


Fig. 3. Energy entering a m^2 of aperture per day as a function of the time of year. The array reference direction is 0.8 radians West of North. The curves are for four different ground cover ratios, as indicated. Latitude 35 S.

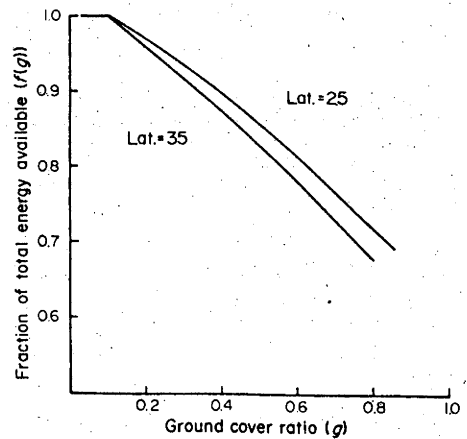


Fig. 4. The reduction in energy collection due to mutual shading. $f(g)$ is shown here as a function of ground cover ratio. The array reference direction is 0.8 rad West of North.

4. COSTS INVOLVED IN SPACING

4.1 Cost of energy transfer

The cost of installed pipe per unit length (C_m) is assumed to be given by an expression of the form[1]:

$$C_m = B_1 + B_2 d^2 \quad (\$/m^{-1}) \quad (3)$$

where B_1 and B_2 are cost parameters, and d is the internal diameter of the pipe. The cost of energy transfer is given by the

sum of the cost of the pipe links (C_n), derived from eqn (3), and the cost of the equipment and energy required to circulate the energy transfer fluid. The cost of pumping equipment is determined by the peak pumping power requirement (w_p) (W), and the capital cost of pumping equipment per installed watt (I_p , \$/W). The cost of the energy required for pumping can be determined either by the peak power demand, or by the energy consumed, or by a combination of the two, depending upon the utility's charging policy. In this study it is assumed that the cost is determined by the energy consumed, and the cost of the energy transfer network (C_p) may be expressed in terms of the capacity factor of the pump (S) and the effective capital cost of solar electricity generating plant (I_p), which includes both the installed capital cost and an amount which when invested at standard interest rates will provide for running costs. Thus the cost of the energy transfer network may be expressed:

$$C_p = C_n + Sw_p I_e + w_p I_p \quad (\$) \quad (4)$$

4.2 Cost of the communication and power links

Dubberley[6] has provided tables of costs for the installation of telephone line equipment. These tables indicate that the cost of a communication network is related only to the total length of line, and is directly proportional to the total length. We can expect a similar result for power cables, and the cost of both these items can be included in (3), simply by adjusting B_1 .

4.3 Cost of energy collectors

The cost of the solar energy collectors is assumed to be, for a given diameter, proportional to the area of the aperture, and is costed at C_c (\$/m²).

5. TRADEOFF BETWEEN ENERGY COLLECTION AND SPACING

The energy collected by each m² of aperture has already been given (2), and the total cost related to that m² is the sum of the costs of collector, pipe links, power and communication links. The cost of storage, and the other elements of the central power plant do not affect the calculations since they are invariant with g . The variation of pipe diameter in the pipe links is not a factor in either the collection of energy or the cost of collectors, and so the selection of the pipe diameters can be accomplished independently of these considerations. This is accomplished in Section 5.1. The optimum spacing is then determined as a function of the variables in Section 5.2.

5.1 Minimum pipe network costs

The minimum cost is derived in an identical manner to Williams[1], with two minor differences. Firstly, the installed capital cost of electricity I_e , is in fact the sum of two components, the cost of the pipe links (C_p), and the cost of other items (C_f), which are not affected by the pipe diameters. The value of I_e is then given by:

$$I_e = (C_p + C_f)/W_0 \quad (\$/W) \quad (5)$$

where W_0 is the electrical output of the power station. Secondly, we consider variable power input to each collector. We assume that the flow rate is controlled so that the amount of dissociation in the focal receiver is held constant. This ensures that the compositions in the feed and return pipes are constant. That is, the mass flow rate is proportional to the product ($P(t)$) of the instantaneous illumination function and the instantaneous solar flux. Thus S , in eqn (10), is determined by:

$$S = \int P^3(t) dt/P^3 \quad (6)$$

where P is the peak value of $P(t)$. S is evaluated at the same time as $f(g)$ is calculated, and is likewise a function of spacing. Typically, S is in the range 0.15-0.2.

To first order, these equations yield the same expression for minimum cost given by Williams, with the minor change that the installed capital cost of electricity in his equation is replaced by

the expression

$$I_p + SC_f/W_0 \quad (\$/W) \quad (7)$$

In subsequent calculations it is assumed that the efficiency of the collector in converting the incident radiation into thermochemical energy is 0.8. Variations in this value, however, have little effect on all the subsequent evaluations.

5.2 Spacing.

The objective of solar power plant design is to minimise the cost of energy. The average thermal power produced by the array is given by $E_F/8760$ (W m⁻²), and thus the capital cost of the power is given by:

$$C = (8760/E_F)(C_c + C'_p) \quad (\$/W) \quad (8)$$

where C'_p is the minimum cost of the network for each m² of aperture. In the following figures, an array of collectors with a total aperture area of approximately 150,000 m² is coupled to a storage facility, and the combination supplies the central boiler with some 42 η_c MWt on a continuous basis. The value of η_c was taken as 0.65, and thus the available thermal energy from this array is 27 MWt. The collector diameter used was 5 m, and so approximately 7500 collectors are involved. The cost of the network and the collectors is given as a function of ground cover ratio in Fig. 5. The worth of evaluating optimum spacing (g_0) is demonstrated in the figure. The effect of the variable B_1 and collector cost on both cost of the network and collectors and g_0 is shown in Figs. 6 and 7. Increasing collector cost is coupled with lower ground cover ratios and greater utilisation of the collector area (higher $f(g)$). Increasing B_1 leads to higher ground cover ratios as the costs of connecting mirrors increases. Note that a reduction in B_1 from 32 \$/m to 10 \$/m involves a corresponding increase of 5 per cent in $f(g)$, and the consequent reduction in the necessary collector area will lower plant costs.

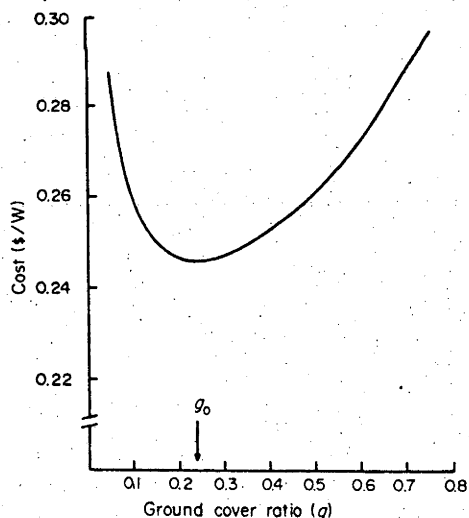


Fig. 5. Variation of costs and spacing. Capital costs due to the collectors and the network linking the array. The optimum spacing (g_0) is arrowed. $C_c = 50$ \$m⁻²; $B_1 = 10$ \$m⁻¹; $B_2 = 0.663 \times 10^4$ \$m⁻²; $D = 5$ m.

6. OTHER NETWORK COST FORMULATIONS

If we consider that the network is constructed of links whose cost is not a function of capacity, or only a very weak function of capacity, then we may take the cost of the collectors and network to be given by:

$$C = (8760/E_F)(C_c + 2.25B_1/Dg^{0.5}) \quad (9)$$

from which it is clear that the value of g which minimises this cost (g_0) is solely a function of the dimensionless variable

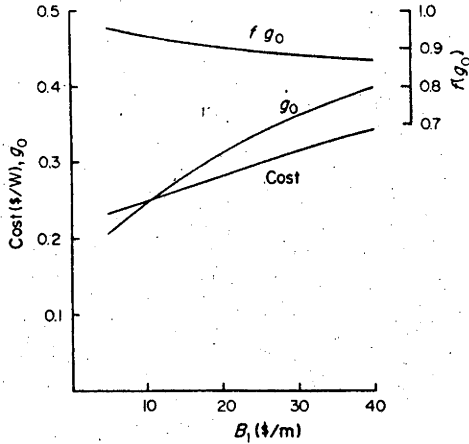


Fig. 6. Variation of costs with B_1 . Capital costs of both the network links and the collectors. $B_2 = 0.663 \times 10^4 \text{ \$m}^{-3}$; $C_c = 50 \text{ \$m}^{-2}$; $D = 5 \text{ m}$.

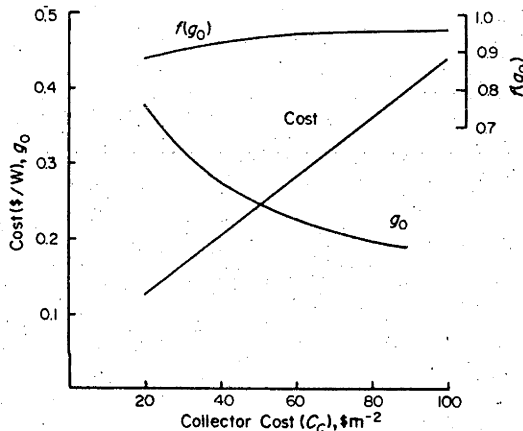


Fig. 7. Variation of costs with C_c . Capital costs due to both the network costs and collector costs. $B_1 = 10 \text{ \$m}^{-1}$; $B_2 = 0.663 \times 10^4 \text{ \$m}^{-3}$; $D = 5 \text{ m}$.

$B_1/(DC_c)$, for a given $f(g)$. The values of g_0 are given as a function of $B_1/(DC_c)$ in Fig. 8. We note that as B_1 approximates the cost per unit length of pipe, and two pipes are required in a thermochemical energy transfer link, eqn (9) gives the costs for a network whose pipe cost is $2B_1$ $\text{\$/m}$.

7. CONCLUSION

This paper has demonstrated the importance of the cost per unit length (B_1) of the links between collectors in an array, be they pipes, cables or both. This value determines the optimum spacing, and the network costs can contribute significantly to the total cost of electricity. As stated by Williams[1], a different installation technique is required to overcome the high cost of pipe installation as estimated by Black and Veatch[7]. This cost was presumably determined by the number of footings and pipe joints, as telephone cable installed in trenches costs only 1 $\text{\$/m}$ [6], while installed 0.5 in. pipe costs 32 $\text{\$/m}$ [7]. There is an advantage in being able to reel out the pipes in unlimited lengths, with minimal attention to footing, as is done for cables, and this would be possible if tubes up to 6 mm OD were employed. Carden[2] has shown that such tubes are appropriate for thermochemical systems employing high pressure gases and liquids. Using the same trench, or footing, for both pipes and cables would also save money.

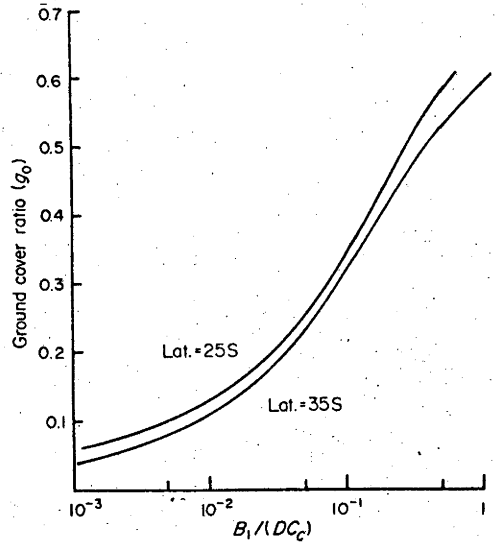


Fig. 8. Ground cover ratio (g_0) required to minimise installed costs for the alternative network cost formula of Section 6.

The possibility of manufacturing and installing pipes in such a way as to reduce B_2 has not been considered. For pipes rated at 300 atm, the value of B_2 of $6630 \text{ \$m}^{-3}$ corresponds to a cost of 370 $\text{\$/ton}$ for the steel involved. For this reason it seems unlikely B_2 could be reduced.

This optimisation has application to any distributed system where energy is to be transferred to a central point, and negligible energy is lost in transit. For example, Caputo[8] suggests a scheme where a Brayton engine and generator is located at each collector and energy is transferred in the form of electricity to the central plant by aluminium cables. He estimates that these cables cost 32 $\text{\$/m}$ (1974 $\text{\$/m}$) to buy and install, of which 90 per cent is installation cost. The optimum ground cover ratio for this situation can be determined from Fig. 8 with B_1 at 16 $\text{\$/m}$.

The question arises as to whether there is a collector layout which collects energy more efficiently than the above layouts. Williams studies a pipe layout for a rectangular (square) array and considers it 'reasonable' because the cost of piping per collector is very nearly proportional to the spacing of collectors. It is probable that for most arrays the cost of the pipe/communication network is nearly proportional to the minimum length between collectors, the trunk lines having a minimal effect. To collect energy as efficiently as possible, we must therefore minimise the minimum length between collectors and also minimise the shading. The latter requires long distances between collectors which shade each other. These two apparently conflicting requirements are compatible, as the distance which principally determines shading is the East-West distance, and the minimum distance between collectors can be the North-South distance. Thus an array with North-South rows of collectors close together, with the rows relatively far apart in the East-West direction may satisfy both requirements. Analysis of such a layout will require the formulation of cost estimates for piping for such an array. It is unfortunate that neither Williams[1] nor Caputo[8] considered piping costs in the light of shading. The following estimates show the possible savings of such a scheme.

For a square array at latitude 35, a ground cover ratio of 0.13 would give an illumination factor of 0.98. The pipe and communication costs for this layout would be approximately proportional to the pipe length per collector (L), which for g of 0.13 is $2.46D$ m. A rectangular layout was constructed with the North-South distance between mirrors (the minimum distance between mirrors) being $1.48D$. To attain the same illumination factor of 0.98, the East-West distance was set at $4.44D$. The pipe length per collector for this layout is only $1.48D$. Thus a simple layout change has reduced the costs due to B_1 by 40 per cent. Whether the costs due to B_2 have increased enough to nullify this ad-

vantage depends upon the values of B_1 and B_2 . Certainly at current values the costs due to B_1 are dominant. This area needs further study, but this is not warranted until more work is done on realistic pipe cost formulations.

NOMENCLATURE

B_1, B_2	parameters in the pipe cost formulation (3)
C_c	collector cost (\$/m)
C_m	cost of installed pipe
C_n	cost of installed pipe network
C_p	cost of energy transfer
d	pipe internal diameter
D	collector aperture diameter
E	annual energy collected
$f(g)$	illumination function, defined in (1)
g	ground cover ratio
I_e	capital cost of electricity
I_p	capital cost of installed pumping equipment
L	minimum distance between collectors
$P(t)$	product of instantaneous solar flux and illumination function
S	pump capacity factor
w	pumping power

W	power station electrical output
η_c	collection efficiency

REFERENCES

1. O. Williams, Thermochemical energy transport costs for a distributed solar power plant. *Solar Energy* 20(4), 333-342 (1978).
2. P. O. Carden, Energy corradiation using the reversible ammonia reaction. *Solar Energy* 19, 365-378 (1977).
3. H. Williamson, Hidden line plotting program. *Communications of the ACM*, 15(2), 100-103 (1972).
4. L. L. Vant-Hull, Methods for estimating total flux in the direct solar beam at any time. *Joint Conf. Am. Section ISES and Solar Energy Soc. Canada* (1976).
5. B. J. Brinkworth, *Solar Energy for Man*. Compton, Chicago (1972).
6. A. Dubberley, Private communication.
7. Black and Veatch, and Honeywell Inc., Dynamic conversion of solar generated heat to electricity. *Monthly Technical Narrative* No. 4, for NASA Lewis, NASA CR-134724 (1974).
8. R. S. Caputo, An initial study of solar power plants using a distributed network of point focussing collectors. *JPL Tech. Rep.* 900-724, Caltech, California (1975).

APPENDIX D

CALIBRATION CONSTANT DETERMINATION

D.1 GENERAL

This appendix describes the determination of the calibration constants of the sun tracker mounted on the solar energy platform. This sun tracker mimics the actions of a collector in following the sun. The method used is identically the method (c) described in section 5.4.2.2 of the thesis. Typical results of the procedure are given.

D.2 DESCRIPTION OF THE SUN TRACKER.

The sun tracker is based on a nominally alt-azimuth mount. The two actuators used are both printed circuit motors driving the sun tracker through a gearbox reduction of 400 000. Actuator displacements are determined from an encoder disc mounted on the output shaft of the printed circuit motor. This disc has ten holes evenly spaced around the perimeter and these holes are detected by a lamp and phototransistor combination. The resolution is thus some 1.5microradians. The displacements are recorded by two up/down counters which count the pulses from the lamp

phototransistor combination. An analogue servo amplifier controls the motors using a sun sensor and positions the sun tracker so that the sun sensor is near null at all times. The precise details of the sensor and servo are not of interest here, it is sufficient to say that actuator nonlinearities cause considerable deviations from the sensor null. This topic will be raised again later.

D.3 OPERATION OF CALIBRATION PROCEDURE.

The counters and servo were switched on. A crystal controlled clock was synchronised with the telephone time service. Both the time and the counters were sampled simultaneously, the time being required to calculate the sun's position in the sky and the counters giving the actuator displacements. Data was taken at intervals over the sunshine hours.

The data, consisting of the time and counter readings, was input to a program which evaluated the calibration constants. The best estimate for the calibration constants was calculated using the procedure outlined in chapter 5, and using the same Levenberg-Marquardt algorithm as used for the simulations. The position of the sun was calculated using polynomial approximations provided by the US Naval Observatory Circular number 155, (Kaplan(1976)). Refraction corrections were made using the data and method of Greenbaum(1954).

The calibration constants calculated were the actuator displacement zero points and two angles which describe the orientation of the azimuth axis. The coordinates used for this measurement are directly analogous to latitude and longitude.

D.4 TYPICAL RESULTS.

A determination of the calibration constants was made using data taken on 10 Aug 77. The derived constants of interest are those describing the fixed axis orientation, which was nominally vertical. The calculated 'longitude' of the fixed axis relative to Canberra's longitude was $.002\text{rad}$, and the calculated 'latitude' of the axis was $-.619\text{rad}$ (cf Canberra $-.616\text{rad}$). Thus the fixed axis was within a few mrad of the vertical position. The resulting differences between the actuator displacements as recorded by the counters, and the displacements calculated using the derived calibration constants and the known sun position are shown in figure D.1. These differences can be attributed to the ability of the servo/sun sensor combination to maintain a sensor null. The lower speeds of the elevation actuator resulted in more severe hunting due to actuator friction, and this could be the reason for the larger differences encountered for the elevation axis. These mechanical sources of following error clearly contribute an rms error of some $.3\text{mrad}$. It is possible there is a trend in the azimuth error differences, however, little can be inferred from D.1.

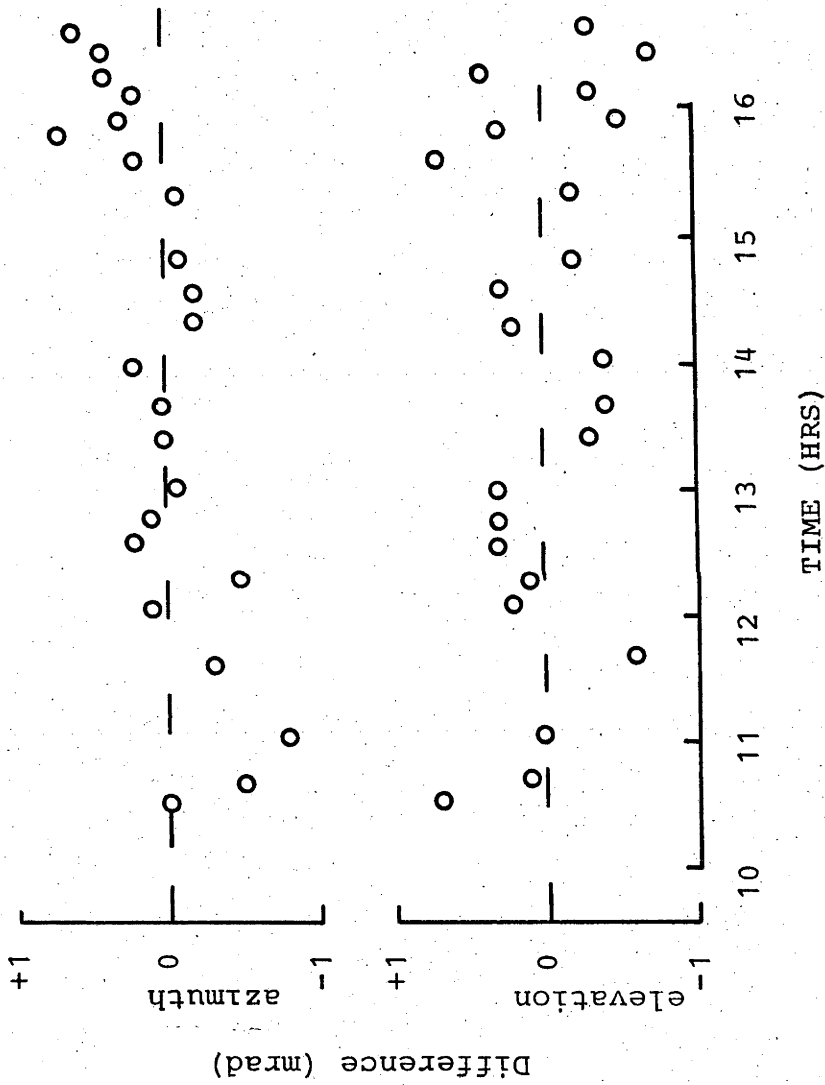


Figure D.1 Difference between the position of the actuators as measured by counters, and the position of the sun as predicted using the calculated calibration constants. Data taken on 10 Aug 77. Adjacent buildings prevent any data acquisition before 10:35 am during winter.

APPENDIX E

SOLAR ENERGY Vol 21, No 6, pp491-496.

COMPUTER BASED SUN FOLLOWING SYSTEM

B.P.Edwards

Dept of Engineering Physics,
Research School of Physical Sciences,
Australian National University,
Canberra, A.C.T., Australia.

Abstract

This paper is a design study of a computer based system which controls a large number of paraboloidal collectors for sunfollowing operation. The system operates with the computer changing the speeds of each of the collector actuators in the field at regular intervals over the day. It is assumed that each collector requires individual attention in the calculation of appropriate speeds. Sources of following error within the system are evaluated, and for specific data rates over the communication link between the central controller and the field of collectors, the variables within the system are chosen to minimise the following error. Accurate sunfollowing is shown to require a data output from the central controller of only 500bit/sec for 10 000 collectors.

Further a computer based learning procedure which is functionally equivalent to an alignment process is detailed. This procedure is implemented by collecting data from each collector in the field. Accurate 'alignment' of a 10 000 collector field is shown to require data collection by the central controller at a rate of only 500 bit/sec for a single day. No new technology is required to accommodate the data rates mentioned.

1.0 INTRODUCTION

Considerable interest has been developed recently in solar thermal power generation, with most attention being paid to the 'central receiver' (or power tower) concept[1,3], and to the distributed system[2,4]. Each approach requires the sun's path to be followed across the sky by a large number of heliostats for the former, or collectors, for the latter. Current designs for solar energy power plants[3] employ angle encoders on the collector actuators and misalignment sensors for feedback and thus following accuracy. In this paper the following situation, as proposed by Carden[5], is considered. A system for following a specific path across the sky is constructed with a central controller issuing speed commands to the collector actuators at regular intervals. The collector actuators maintain this 'command speed' precisely in between commands. The path of the sun is thus approximated by the collector's motion as a series of straight line segments. By communicating speed commands more frequently to each collector, tracking error can be reduced, but only at the expense of an increased data rate between the central controller and the field of collectors. It is assumed that all collectors require unique speed commands, and with this assumption the communication requirements of the data link connecting the field of mirrors to the central controller are considered in terms of the tracking error allowable for a direct sun tracking system. Both error and data rate are functions of variables within the control system, and these variables are evaluated for each data rate. It is shown that

for accurate continuous sun following to within 2mrad the output data rate from the central controller is only 500bit/sec for 10 000 mirrors. This presents no barrier to the implementation of this system.

A further feature of the Carden system is that an adaptive controller will be able to learn certain parameters which govern the behaviour of the tracker, in particular such a controller may deduce the pointing direction of the fixed axis, and also the relative direction of the other axis, the rotational axis. This constitutes a measurement of how the mirror is aligned. An alignment procedure will thus be no longer necessary and this will reduce the installation cost of the tracker. With this skill a central controller will be able to train itself to point each collector in an array in the same direction, even though initially all the collectors in the array were not identically oriented. The accuracy with which the parameters are learnt depends on the variables within the system, and in particular on the data transfer over the communication link. The variables in a possible system are calculated to minimise the data rate required to perform the procedure. The amount of information required for this 'alignment' process for a system of 10 000 collectors can be gathered in one day at a continuous data rate of 500bit/sec by this method.

2.0 GENERAL DESCRIPTION OF SYSTEM UNDER STUDY.

In this paper we confine discussion to a distributed system consisting of a large number of paraboloidal collectors, (in this study 10 000), each with its own focus. All the collectors are aligned, but the errors in the alignment are larger than the allowable following error. Thus each collector requires individual attention. An actuator on each axis of the collector enables each collector to track the sun directly. The class of collectors with orthogonal axes will be considered, which includes both the altitude-azimuth and equatorial systems. The paper assumes that the fixed axis of the collector is in the vertical plane. Each collector can communicate in either direction with the central controller.

Each collector has a sun sensor which gives signals related to the tracking error. In this case the type studied is as in [5], where photosensitive elements are located in the penumbra cast by an alignment bar. These devices have photosensitive elements which are small compared to the width of the penumbra, and this ensures a steep slope in the output against tracking error curve. This factor reduces the effects of gain drift in the photosensitive elements.

The collector actuators are designed so that a short time after the receipt of a speed command they behave as if they had changed to the correct speed instantaneously, and no errors are accumulated. These characteristics enable a central controller to determine the angular position of the two actuators and thus the pointing direction of the collector by using knowledge of previous speed commands, and the initial

position of the collector. The central controller can direct the collector to follow any path in the sky by giving the actuators new speed commands at intervals. In this system the interval between speed commands is maintained constant, and is called the command time (t_c).

The method of determining alignment utilises the tracking error information (derived from the sun sensor) to ascertain the initial position and alignment of the collector.

Basically this is done by the following method. The collector acts as a well behaved function, transforming the input which is the angular position of the actuators, generated by the speed commands from the central controller, into an output, a pointing direction. This well behaved function is determined as a function of collector parameters such as the alignment of axes. Conversely with knowledge of the output, the pointing direction, and input, one may compute the values of these collector parameters. To gain knowledge of the output, the sun sensor is interrogated, and when the collector crosses the sun, the collector pointing direction is known, as it is the direction of the sun. The time and position when each crossing occurs are called the fix position and fix time respectively, and there will be a set of fix times and positions for each coordinate. These 'fixes' constitute the output data. The mathematical process followed is to use a trial set of parameters to generate a trial set of output data from the known input data. This trial output set is compared with the true output set, viz the corresponding known position of the sun. The trial parameters are then

varied until a satisfactory correlation is obtained between the trial output set, and the true output set. This is called the correlation process. We will consider a method for gathering the required data in section 5.5.

3.0 IMPLICATIONS OF THE SYSTEM WITH REGARD TO COST.

The use of more complex control generates the possibility of a cost reduction. The simplest physical arrangement for anticipating the sun's position would be to align all the mirror collectors identically. This alignment measurement would need to be of the order of milliradians, and would need to be checked regularly, an expensive process. To overcome this expense, the present system enables the collectors to be installed with little attention to alignment, and their actual alignment determined accurately after installation. This alignment may be repeated at regular intervals, and thus one can allow for foundation subsidence.

The number of parameters which determine the collector's behaviour, previously confined to parameters related to alignment, may be increased. For example, it may prove cheaper to employ nonpositive drives such as belts, friction drives or winches, and in this case drive ratios may vary from collector to collector and may even vary gradually with time. There may also be other parameters which vary as a result of using some cheaper manufacturing method. Provided that one can still express the pointing direction of the mirror as a well behaved function of the set of collector parameters and

the actuator displacements, then functional complexity and intelligence in the controller could permit such cost saving possibilities without sacrificing the ability of the tracking scheme.

4.0 DIGITISATION

The extra intelligence and sophisticated communication link in the proposed system will certainly reduce maintenance, and will allow randomly orientated fixed axes. The economies of this flexible system depend upon the costs, one of which is the communication link. The flow of information over the link is estimated to help determine the feasibility of the scheme. This flow of information demands digitisation of data to preserve accuracy and minimise costs, and this causes certain discretisation errors.

The sun sensor described in section 2 has photosensitive elements substantially smaller than the sun's penumbra, and providing that the error is smaller than half the angle subtended by the sun, gives analog signals varying very nearly linearly with the pointing error. These error signals are digitised into a binary number of n_s bits, and the full intensity of the sun gives a sample of $2^{n_s} - 1$. Thus the maximum error of the device at small tracking errors (under 5mrad) is:

$$\Delta\theta_s = \Omega / (2(2^{n_s} - 1)) \quad (1)$$

where Ω is the solar diameter.

It is considered necessary to collect three pieces of information from the sun sensor, the third piece being a representation of the intensity of the sun, which determines the validity of the two error signals.

The command speeds to the actuators are also digitised and only one of a set of discrete speeds is possible. There are $(n_m + 1)$ bits in the speed command, the extra bit being the direction of the speed, and the minimum speed change is given by [5]:

$$\Delta\omega = \pi / (T 2^{n_m}) \quad (2)$$

Where T is the traverse time, the time to traverse π rads.

The data rate over the communication link between the central controller and the field of collectors can be divided into two parts, the motor speed commands leaving the central controller, and the feedback information returning from each collector to the central controller. As each collector requires unique attention, each message to a collector needs an identifier, which in this case is a binary number. For 10 000 collectors, 14 bits are required for this identifier, and these 14 bits are attached to each message.

Thus the data rate for the speed commands is:

$$R_m = 10000 (14 + 2(n_m + 1)) / t_c \quad (\text{bits/sec}) \quad (3)$$

5.0 DETERMINATION OF POINTING ACCURACY.

The sources of error during sun following are:

1. The segmented straight line approximation to the sun's path.
2. The discretization of motor speeds.
3. The accuracy of determination of the collector parameters referred to in section 3.

The determination of the parameters is carried out by the correlation routine described in section 3. The inaccuracy due to this correlation routine determination is considered in detail in section 5.5.

5.1 Errors Due To Segmented Line Fit.

The path of the sun was assumed to be given by the equations derived for a uniformly rotating earth, with the declination of the sun varying sinusoidally with time, as given by Brinkworth[6].

The tracking errors in this section come from two sources, firstly, the errors produced by approximating the sun's curved path as a series of straight line segments, and secondly because of the collector falling behind the sun due to the sun's high azimuthal velocity near zenith. This high velocity has a maximum of [6]:

$$\phi(\max) = k \cos(d) / \sin(B-d) \quad (4)$$

where $\Delta\phi$ and $\Delta\theta$ are the errors in azimuth and altitude respectively, and θ is the altitude angle.

The variation of maximum error over the day with variations in both t_c and the parameter (B-d) is shown in figure 2. Although the length t_c of the command time has most effect on $\Delta\theta_1$, the phase relationship between the succession of command intervals and the functions describing θ and ϕ with time is also important. Thus in figure 2, $\Delta\theta_1$ vs t_c is represented by a zone in some cases rather than a specific curve, the exact position within the zone being dependent on the phase.

For subsequent studies in this paper the latitude is fixed at -33 degrees, with nominal alt-azimuth collectors. In this case the minimum value of the parameter (B-d) is 10 degrees, and the appropriate curve from Figure 2 gives the maximum error due to the curvature of the sun's path. This situation is identical to many other situations, for example the consideration of a site at latitude -23 degrees, where the fixed axis of the nominal alt-azimuth collector has been tilted South through 10 degrees. The minimum value of (B-d) is vital in the calculations of maximum error. The latitude of the collector is not independently important.

5.2 Motor Speed Discretization Error

The discretization of motor speed commands causes a second degradation in accuracy. In general it is impossible to arrive at a specific position after a certain period of motion, because one is forced to choose a speed which is

slightly in error with respect to the desired speed. The positioning error at the end of a time t_c is called the discretization error and is given by[5]:

$$\Delta\theta_2 = \Delta\omega(t_c/2) \quad (6)$$

In subsequent studies one hour is selected as a suitable traverse time (T), for use in the above equation.

5.3 Error Due To The Correlation Process.

In order to implement sun following the computer requires knowledge of the sun's position, and knowledge of the response of the collector to speed commands in terms of pointing direction. This knowledge involves the collector parameters, e.g., the pointing direction of the fixed axis, the initial pointing direction, and so on. To show the flexibility of the system, and the possibility of cost reductions, seven parameters in all were considered, including two angles to describe the lean of the fixed axis, two angles to describe the initial position of the collector, two numbers to describe the two gearbox ratios, and a final parameter describing the angle between the two axes of rotation. These parameters relate the alignment and construction of the tracker to the local true alt-az frame.

The accuracy of sunfollowing depends upon the accuracy of determination of the tracker parameters, which in turn depends upon both the accuracy of the fixes collected and the

number of fixes. The ratio of the pointing error due to imperfect knowledge of the collector parameters to the fix error is important, and is termed the 'error ratio'. It was found to be independent of fix error, which is to be expected, and its value was derived for several circumstances using a series of simulation runs. From a statistical point of view one realizes that the correlation process must be carried out over the full range of the input and output variables, i.e. over a minimum length of one day. With a typical set of parameters, an artificial set of fix positions for one day was created with a specific fix error. A minimisation routine then evaluated a tracker parameter vector which correlated best with this artificial set of fixes. Knowing the original set of parameters used to generate the artificial set of fixes, one can then calculate the pointing error due solely to the inaccuracies in the determination of the estimated set of parameters. The error ratio is then calculated. The error ratio decreases as the number of fixes increases, and this variation is shown in Figure 3, where the error ratio has been plotted against the number of fixes in each set of fixes. The dashed line in this figure indicates the variation encountered in the error ratio. These variations are getting large when 20 fixes are used in the calculation. The contribution to pointing error is given by the product of the error ratio (r) as given in figure 3, and the fix error ($\Delta\theta_f$), viz:

$$\Delta\theta_3 = r(\Delta\theta_f) \quad (7)$$

The fix error depends upon the system used to collect the fixes, and will be evaluated in a section 5.5 for a possible system.

5.4 Combination Of Error Causes (1) And (2).

This combination will represent the total pointing error if the pointing error due to cause (3) is relatively small. The total error is obtained by arithmetic addition for simplicity. This error is given by:

$$\Delta\theta_4 = \Delta\theta_1 + \Delta\theta_2 \quad (8)$$

where $\Delta\theta_1$ is given in figure 2 with $(B-d)=10$ degrees, and $\Delta\theta_2$ is given in equation (6). This equation ignores the effects of output shaft backlash, which can be included simply when a suitable value is known. The data rate necessary to achieve this pointing error is given in equation (3). Both $\Delta\theta_4$ and R_m are functions of n_m and t_c , and for a particular R_m , there is a combination of n_m and t_c which minimises $\Delta\theta_4$. Equations (3) and (8) are combined in figure 4 to show these variables as functions of data rate. The values of t_c and n_m required for this minimum are also shown. Clearly with quite low data rates, pointing error due to these two causes can be made small for the situation considered.

5.5 Determination Of The Error (3).

The error $\Delta\theta_4$ is the following error of the computer controlled follower, provided that the controller knows the tracker parameters precisely. By monitoring the sun sensor data the controller can evaluate $\Delta\theta_3$, which is the following error due to imperfections in the knowledge of the collector parameters. If the controller finds $\Delta\theta_3$ has increased over a period, then the correlation process described in section 3 can be used to reestablish the controller's accurate knowledge of the parameters. The minimum value of $\Delta\theta_3$ which can be obtained as a result of monitoring the sun sensor information over a single cloudfree day is evaluated in this section as a function of the data rate of sun sensor information.

Equation (7) relates the error $\Delta\theta_3$ to the product of the error ratio and the fix error. The fixes are obtained by monitoring the sun sensor information at the start and end of each command time, and interpolating from this information when and where the collector and the sun were aligned. Thus the number of fixes accumulated is equivalent to the number of command times during daylight, which determines r , and the minimum error of this interpolation is limited by the sensor discretization error, equation (1), and the size of the output drive backlash(B), and hence:

$$\Delta\theta_f = \Delta\theta_s + B \quad (9)$$

The data rates during this process consists of the motor speed commands from the central controller to the collectors, as given in equation 3, and the sun sensor information (in the opposite direction), the data rate for the latter being given by:

$$R_s = 10000(14+3n_s)/t_c \quad (10)$$

In minimising $\Delta\theta_f$ algebraically, it is found that the optimum value for n_s is a function only of B , and is not influenced by the value of the data rate (R_s). The value of this optimum value is given implicitly in equation (11).

$$3.2 \times 10^{-3} (14+3n_s)/2^{n_s} = B \quad (11)$$

For a backlash of 1.6mrad the optimum value of n_s is 6, while decreasing the value of backlash to .14mrad increases the optimum value of n_s to 10. In figure 5, B is taken as .5mrad for which the optimum value of n_s is 8. In this figure the minimum value of $\Delta\theta_3$ obtained for a specific data rate is plotted against R_s . The value of t_c necessary to obtain the minimum $\Delta\theta_3$ is also shown. The effect of employing a non-optimum value of n_s (of 4) increases the minimum error by some 36%. Considering that halving n_s causes a substantial change in $\Delta\theta_s$, using optimum values cannot be considered crucial.

During the fix collection process the following error must be acceptably (eg 1mrad), and thus t_c is limited to around 750secs, from figure 4. Thus R_s is determined with a decision

on the value of n_s . Selecting n_s to minimise $\Delta\theta_3$ does not seem viable, as this implies a sun sensor accuracy of 10^{-5} rads, which would be difficult to achieve. Reducing n_s to 4 maintains $\Delta\theta_3$ substantially smaller than $\Delta\theta_4$, however the accuracy required of the sun sensor is now only .3mrad, a more realistic figure. The data rate (R_s) with t_c at 750 seconds is only 350bits/sec. One could decrease n_s further, however it seems reasonable to maintain $\Delta\theta_3$ small compared to $\Delta\theta_4$, as this will enable changes in the tracker parameters to be easily detected, as well as permitting more accurate following.

It is however, not necessary to use all the fixes collected to determine the collector parameters. In fact computation time for the correlation process is directly proportional to the number of fixes, and a saving can be accomplished by using a small number of fixes. For the number of collector parameters considered here, around 25 fixes are needed to evaluate the collector parameters without wide variations in r , and thus $\Delta\theta_3$. A few values for $\Delta\theta_3$ with varying n_s are given in Table 1, contrasting the small increases in $\Delta\theta_3$ with the large reduction in computation time between using 25 and 58 fixes (some 50%).

6.0 DISCUSSION.

The possibility of implementing the above scheme depends on two factors, the ability of the communication network to handle the necessary data rates, and the ability of the

central controller to perform the required computation. The data rates calculated in this paper show that the former is no barrier, twisted pairs as used in standard telephone installations being easily capable of the figures mentioned. The computation can be divided into two major items. The first item is the necessity to calculate speeds for every one of the collectors each command time, and thus each calculation must only take t_c seconds divided by the number of collectors. For $t_c = 750$ secs, the central controller has 75ms to calculate the command speeds for each collector. The calculation itself is not a demanding one, and the fact that the calculation will be carried out some 500000 times a day should encourage work on developing a fast implementation of the calculation and thus meet the 75ms constraint. The second item is the computation required for the correlation process, for which every night is available. Using the non-specialised program to develop figure 3, 700 such correlations could be performed each night, and there is no doubt that this number could be increased. Thus one could perform a correlation for every collector once every fortnight.

The above discussion on the ease of implementation of the scheme does not consider the cost and the benefits. The cost includes a central controller/computer, and a communication network. To offset this cost, we have a system which will improve the collector's collecting efficiency, due to the capability of anticipating the sun's position. Minimal foundations are required for the collectors, and no field adjustments or alignment is required. Further, the central

controller can minimise weather damage by suitable pointing of the collector in adverse conditions. Finally, maintenance and downtime costs will be reduced, both by the capability of the system to recognise breakdowns more quickly, and by anticipating breakdowns. Test routines applied via the communication network will also reduce repair times.

An experimental system utilising the correlation process to determine the tracker parameters is currently under construction and should be operating shortly. Field tests of this system will be published at a later date.

ACKNOWLEDGEMENT

The author wishes to thank Dr P.O.Cardon, Head of the Energy Conversion group, for stimulating his interest in the study of tracking schemes and in particular for his critical comments on the manuscript.

7.0 NOMENCLATURE

- T - traverse time required of the actuators, or time to complete 180 degrees(seconds).
- t_c - the interval between speed commands, or command time(seconds).
- n_s - the number of bits in each sun sensor sample.
- n_m - the number of bits in the magnitude of the

actuator speed command.

R - the data rate to be expected over the communication link between the field of trackers and the central controller (bits/sec).

TABLE 1

n_s	expected $\Delta\theta_3$ (mrad)	
	25 fixes	58 fixes
2	.58	.44
4	.23	.18
8	.15	.11

8.0 REFERENCES

1. Vant-Hull, L.L and Hildebrandt, A.F., 'A Central Receiver Solar system applicable to Central power stations',
Solar Energy Vol 18, pp31-39 (1976).
2. Carden, P.O., 'Energy corradiation using the reversible ammonia reaction',
Solar Energy, 19, pp365-378 (1977).
3. Gervais, R.L. et al, 'A central receiver solar system applicable to central power stations',
Joint conference of the American section of ISES and the Solar Energy Society of Canada, Inc.,
pp325-335, 1976.
4. Caputo, R.S., 'An initial study of solar power plants using a distributed network of point focussing collectors',
JPL Technical Report 900-724, Caltech,
California (1975).
5. Carden, P.O., 'Steering a field of mirrors using a shared computer based controller',
ISES conference, Los Angeles (1975).
6. Brinkworth, B.J., 'Solar Energy for man',
Compton (1972).

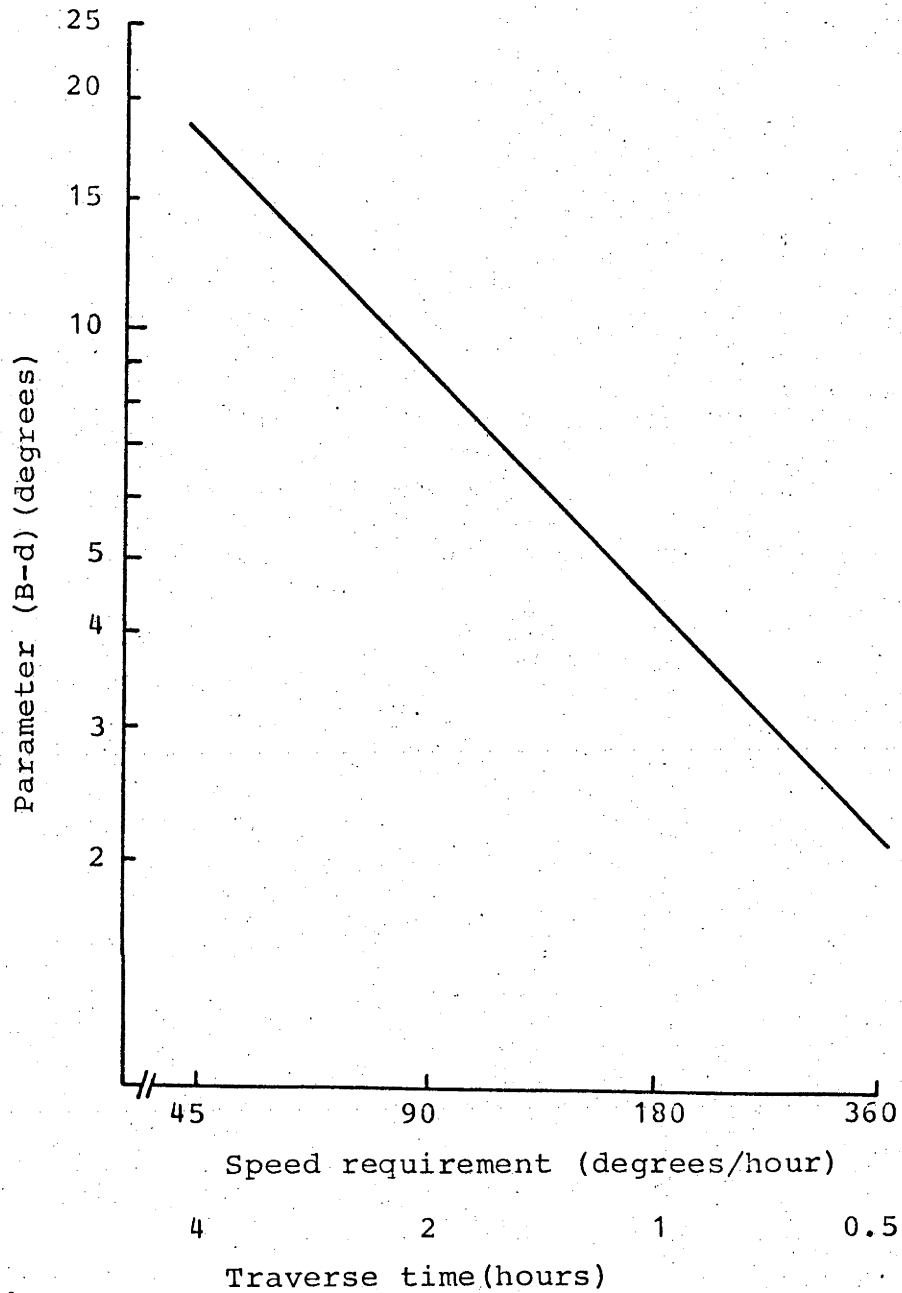


Figure 1. Variation of the maximum speed required of the azimuth drive with the minimum value of (B-d) experienced by the tracker during the year. The parameter (B-d) is the minimum angle between the azimuth (fixed) axis and the sun, measured in the vertical N-S plane.

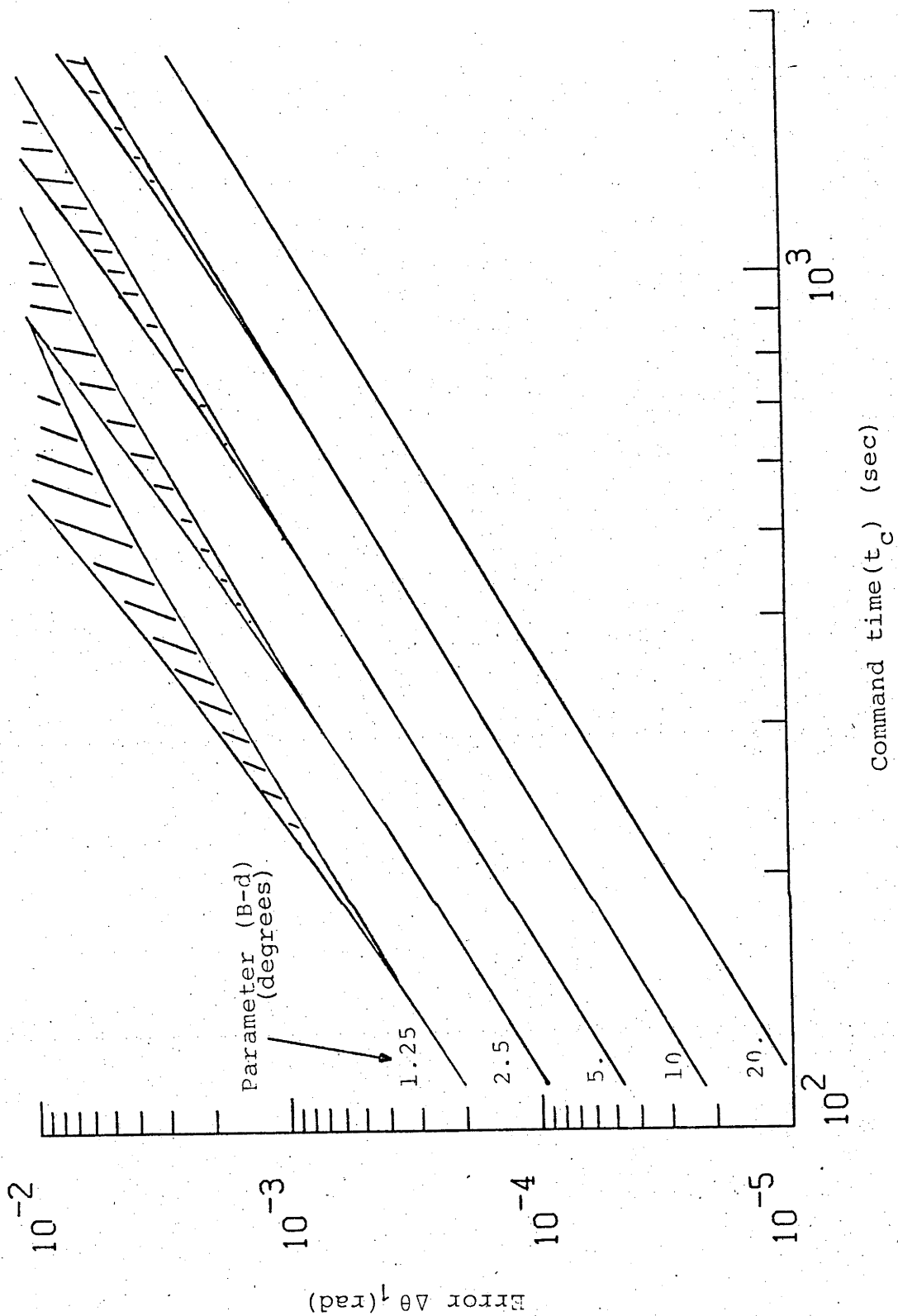


Figure 2. Variation of the maximum error ($\Delta\theta_1$) over the year between the segmented line approximation and the sun's path. The dashed region occurs due to the dependence of $\Delta\theta_1$ on the phase relationship between the speed change times and midday

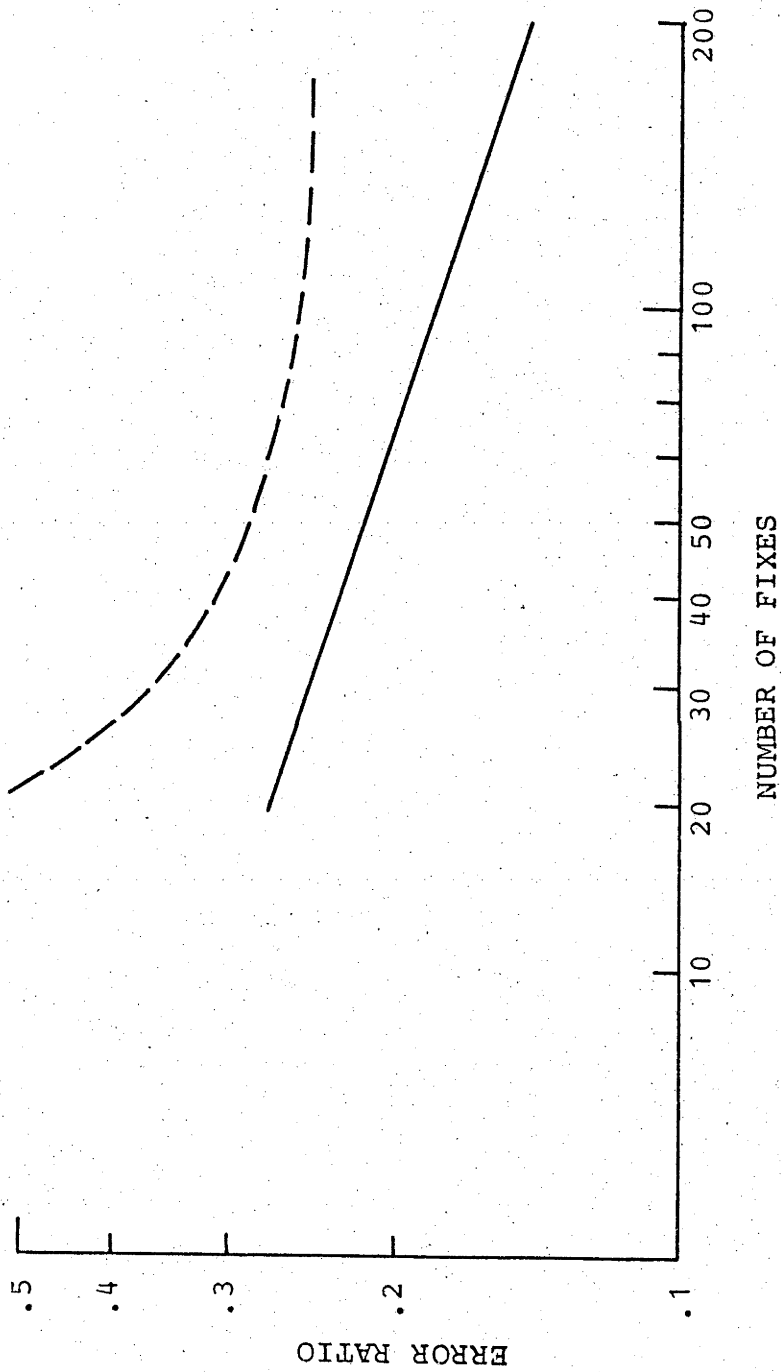


Figure 3. Error ratio for the correlation process as a function of the number of fixes in each coordinate used in the correlation. The unbroken line is the expected value of the ratio, while the broken line indicates the upper boundary of the points used in determining the full line

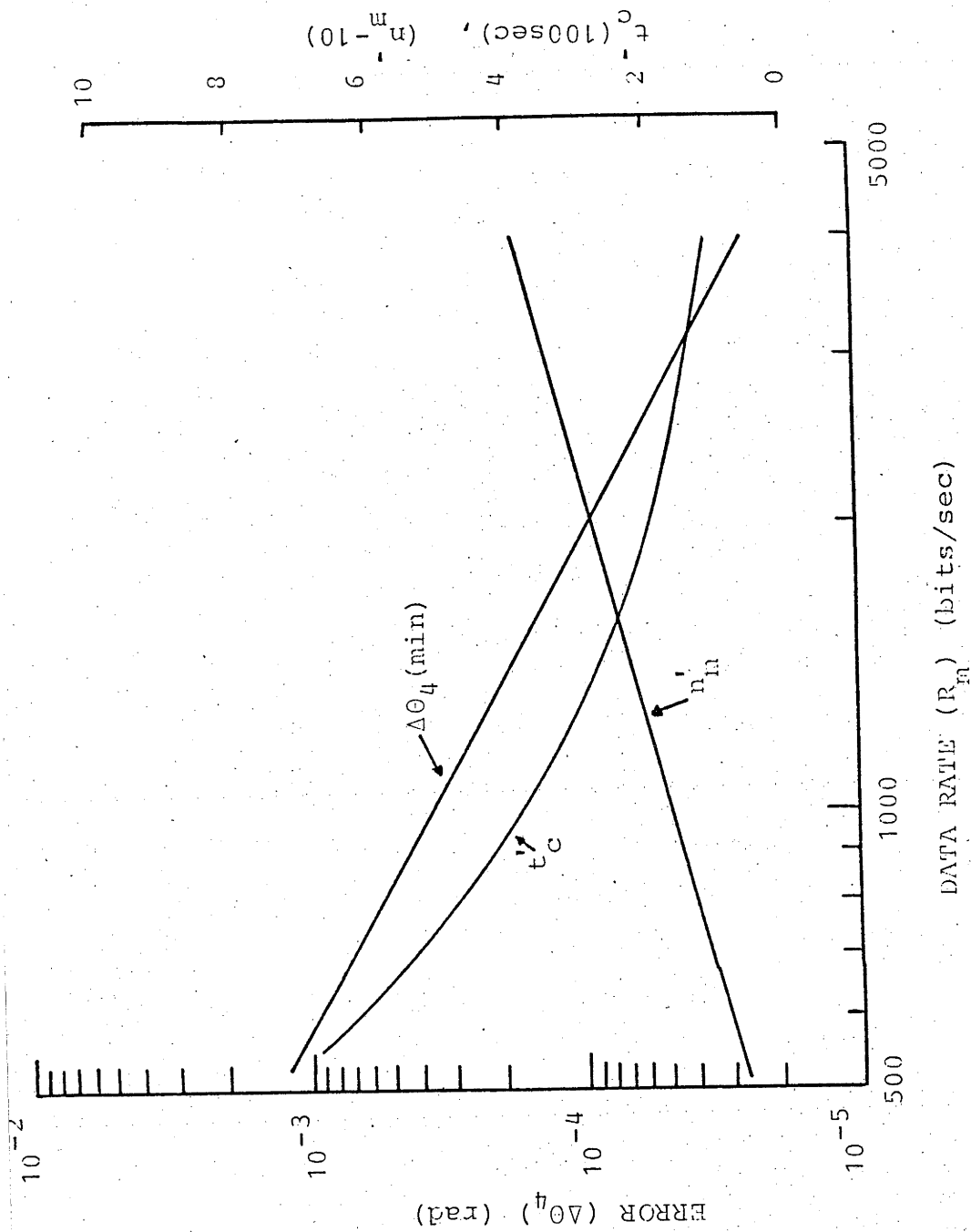


Figure 4. Combination of error causes (1) and (2).

Maximum pointing error over a year for a specific data rate.

t'_c and n'_m are the values of t_c and n_m which minimise $\Delta\theta_4$ for a particular R_m .

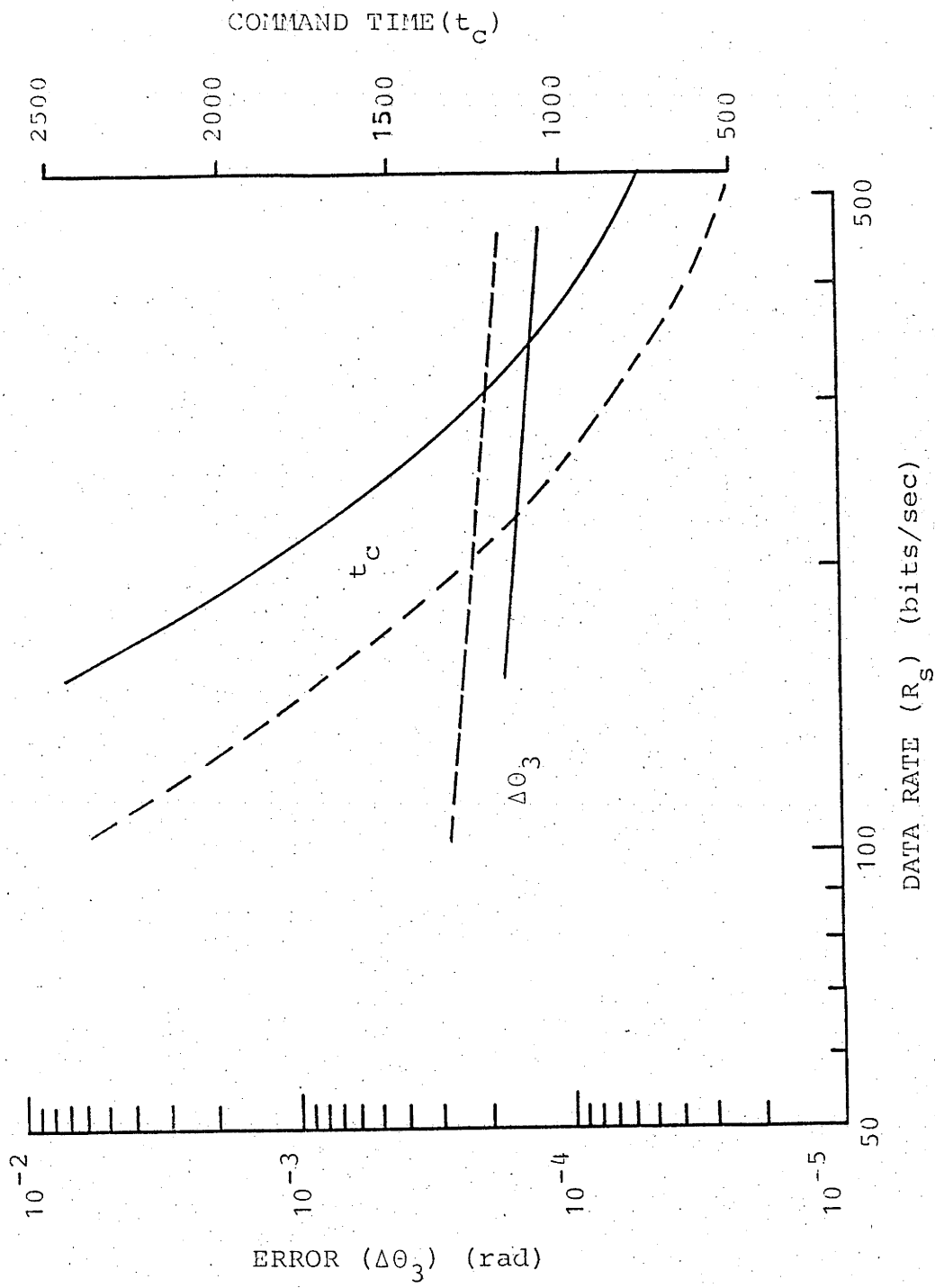


Figure 5. Minimum error $\Delta\theta_3$ as a function of R_s . The dashed lines show the effect of choosing $n_s=4$ instead of the optimum value of $n_s=8$.

APPENDIX F

DEVICES FOR FEEDBACK IN SUNTRACKING
SYSTEMS

Energy Conversion Technical Report No. 20

by

B. P. Edwards

December 1978

DEPARTMENT OF ENGINEERING PHYSICS,
Research School of Physical Sciences,
The Australian National University,
Canberra, A.C.T. 2600
Australia

Abstract

The design and operation of feedback devices used in servo loops for aiming equipment at the sun is discussed. In particular the stability of the devices with respect to gain changes in the photosensitive elements used in the devices is analysed. The construction of a simple feedback device, and the construction of an experimental rig which can test device stability to better than $.1\text{mrad}$, is described. The stability of the simple feedback device is shown to be no better than $.5\text{mrad}$. A bibliography of extant designs for feedback devices is given.

<u>CONTENTS</u>		<u>Page</u>
20.1	Introduction	1
20.2	Historical	3
20.3	Theory of Operation	4
20.4	Validity of Output Signal and Acquisition Range	9
20.5	Construction	11
20.6	Performance of Design	14
20.7	Stability of Sun Sensor	19
20.8	Discussion	20
20.9	Conclusion	20
20.10	Acknowledgements	21
20.11	References	21
20.12	Bibliography	22

20.0 DEVICES FOR FEEDBACK IN SUN TRACKING SYSTEMS.

20.1 Introduction

In this report we consider sensors whose output signal is related to the angle between the axis of the sensor and a beam of radiation. We are particularly interested in 'sun sensors' where the beam of radiation comes from the sun, and the sensors are used as a feedback device in a servo loop whose purpose is to align equipment with the sun, as shown in figure 20.1.

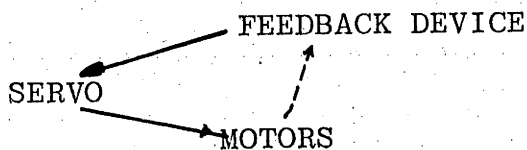


Figure 20.1 The sun sensor can be used as a feedback device where motors are controlled by a servo loop enclosing the sun sensor.

The terms 'feedback device' and 'sun sensor' are used interchangeably here. In the case of the sun the beam of radiation is distributed over some 9mrad, and the aligned position is a repeatable attitude with respect to this distribution. The degree of misalignment is called the sun following error.

Each sun sensor gives an output signal to indicate the sun following error in each axis. The sun sensor may also give a signal to indicate the validity of the error data, a situation which, for example, may be required to indicate the sun is not shining.

The sensor must be constructed so that the aligned position, corresponding to a target point on the sun, does not vary. Important variables which affect stability are temperature, which may reach 80C, and the varying intensity of the sun.

The output signal for a typical sun sensor is shown in figure 20.2.

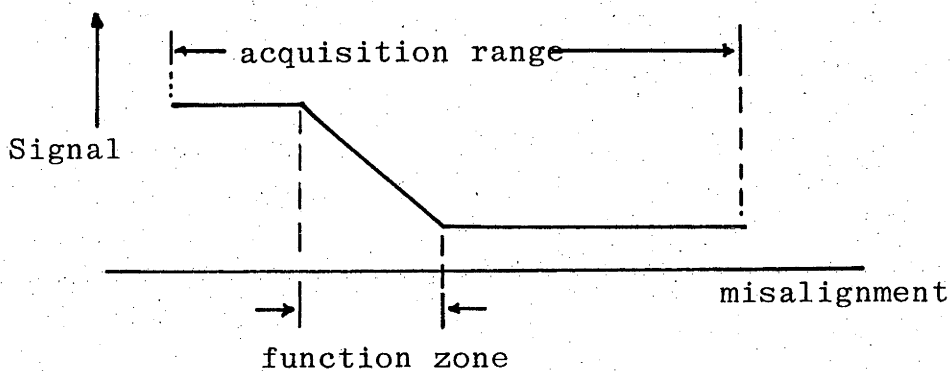


Figure 20.2 Typical output signal of a sun sensor as a function of misalignment. Over the acquisition range information on misalignment can be obtained from the output signal, and over the function zone, the misalignment is a true function of the output signal.

In this figure we illustrate the acquisition range of the sun sensor, over which meaningful error information can be obtained from the sun sensor signals, and the function zone, where the sun following error can be expressed as a true function of the sun sensor signal.

20.2 Historical

Extant designs (see bibliography) for sun sensors are in general cumbersome due to the only recent development of small photosensitive elements, in comparison to the bulky phototubes and resistors. Regardless of the type of photosensitive elements used, however, most rely on sensing the position of a shadow, and the operation of these devices is discussed in the next section.

A sun sensor design not using this principle which caught the author's eye was that of Moore and Amand (1957), where a single photovoltaic cell was used most elegantly. The operation of the device is shown in figure 20.3. A semicircular shutter is rotated at 60revs/sec by a synchronous motor, and the signal from the photovoltaic cell examined for a component whose frequency is 60Hz.

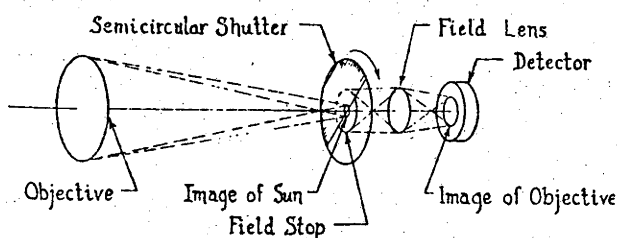


Figure 20.3 Schematic of Moore design.

If the image of the sun is off centre in any direction, this component is non-zero, and the magnitude of the component is related to the sun following error, and the phase of the

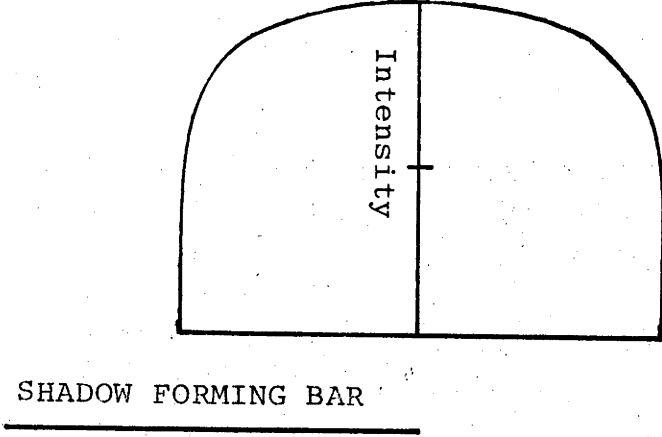
component gives the direction of the sun following error. AC servo motors are coupled to the signal to drive the equipment to null the 60Hz component. While the solution is elegant, the author feels cheaper designs are possible.

20.3 Theory Of Operation.

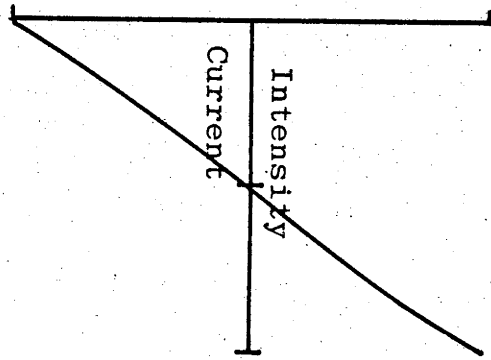
Most known feedback devices sense the edge of a shadow formed by some member, and this is usually achieved by placing photosensitive elements in positions such that at alignment these elements will be centred on the sun's penumbra. Misalignment of the device will cause variations in the outputs of the photosensitive elements. In the simplest form one would have, in each coordinate direction, a bar forming a shadow where the bar extends at right angles to the misalignment to be detected. The following analysis of the response of such a device gives insight into its capability.

Figure 20.4(a) plots the relative intensity of the sun's radiation at a wavelength of 800nm against radial distance from the centre of the sun (Robinson 1966). The radial distance is measured in solar diameters, and the wavelength of 800nm has been chosen as it coincides with the peak response of a typical photosensitive element, a phototransistor (BPX 70). The bar producing the shadow, shown schematically below Figure 20.4(a), then integrates this radiation to produce behind the bar an intensity profile as in Figure 20.4(b).

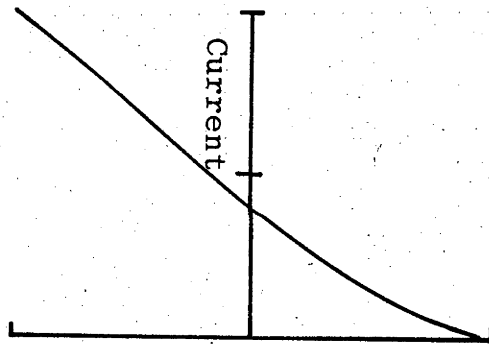
(a)



(b)



(c)



(d)

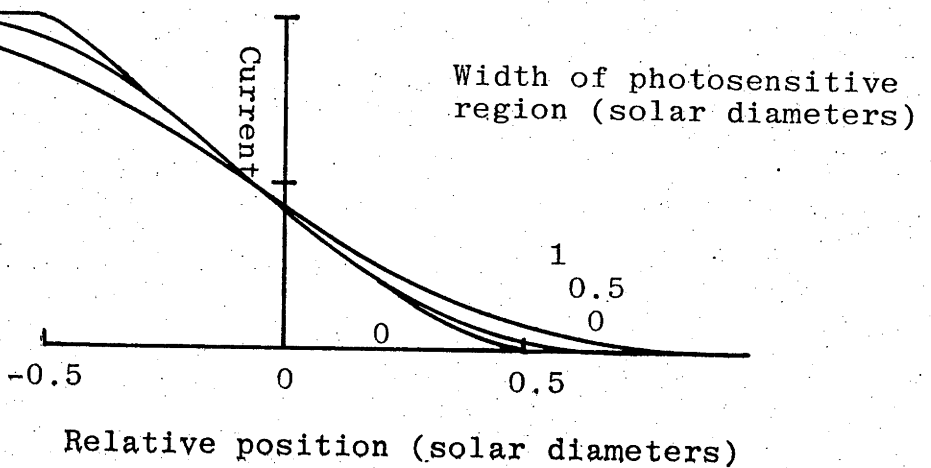


Figure 20.4 Response of sensors in shadow sensor. All ordinates are relative. Abcissae the same in all cases.
 (a) Intensity of the sun.
 (b) Intensity gradation across penumbra.
 (c) Resultant current through point size BPX 70.
 (d) Resultant current as a function of the width of the photosensitive element in the penumbra.

Only the response in the penumbra is shown, as there is no variation outside the penumbra. The phototransistor has a response to light intensity such that, at constant collector-emitter voltage, collector current varies as intensity to the power 1.3 (Phillips 1974). Thus a point size phototransistor, placed at different positions across the penumbra, would produce a collector current as shown in Fig 20.4(c). Note that when the sensor indicates it is pointing at the centre of the sun, the position generally used as the aligned position, the output current is 0.4 the maximum. However for some feedback devices the phototransistor is not sufficiently small to be considered as a point. Figure 20.4(d) shows the effect of using phototransistors of finite dimensions, whose response then depends on the integral of the intensity over the width of the photosensitive region. The width of the sensitive area is expressed in terms of the width of the solar penumbra.

Curves similar to 20.4(d) will be obtained for almost any photosensitive element. The main point to be observed is the decreasing slope of the curve with increasing width of the element.

By placing a small aperture above the photosensitive element the photosensitive width can be reduced, however this will reduce the acquisition range.

The photosensitive elements used in these devices to sense the intensity behind the shadow forming bar divide into two groups on the basis of size. If the distance between the shadow bar and the photosensitive element is around 30 cm,

then while phototransistors and photodiodes are smaller than the width of the penumbra, photoconductive cells, photovoltaics and phototubes are substantially larger.

Feedback devices in general employ one element on either side of the anticipated image or shadow of the sun as shown in figure 20.5, and alignment is defined as occurring when the signals from the two elements are equal. This approach balances the effects of drift in the photosensitive elements and thus reduces the movement of the target point on the sun with which the aligned position corresponds. To cause any variations in the aiming point the gains of the photosensitive elements must drift differently.

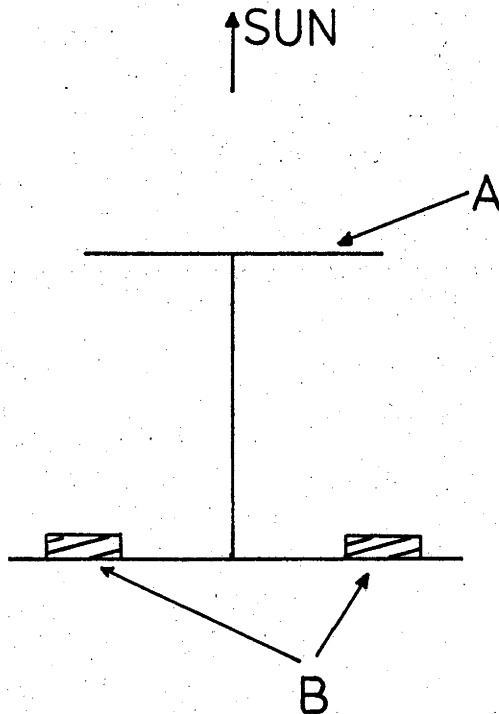


Figure 20.5 Simple shadow sensing feedback device.
A Shadow forming bar.
B Photosensitive elements.

We analyse this by assuming that initially the gains are identical, and that the output signal is linear over a range ψ (the function zone). The ratio of gains, γ , is related to the movement of the aiming point β by:

$$\gamma = \frac{\tan(\psi/2 + \beta)}{\tan(\psi/2 - \beta)} \quad (20.1)$$

Representative values of these quantities are given below.

γ	.5	.8	.9	1.1	1.2	1.5
β/ψ	.17	.055	.026	.023	.045	.1
$\psi = \Omega, \beta$ (mrad)	1.6	.5	.24	.21	.42	.93

where Ω is the sun's diameter.

Thus it is clear that devices with small ψ are less sensitive to gain changes.

A comparison between feedback devices employing relatively large photosensitive elements and those employing phototransistors must take account of the use of these devices. As mentioned before, this is for a servo system where the device is to be continually aligned as accurately as possible with a repeatable position on the sun. While devices with large photosensitive elements have a larger function zone where the error signal increases with sun following error, this is not a great advantage, for if the system is not pointing near the sun, only the direction of the error is of importance. A factor that is important is the stability of

the aligned position. It is in the aligned position that devices with small photosensitive elements exhibit a steeper slope in the error signal against misalignment curve, and this steeper slope will reduce the effects of differential gain drift in the photosensitive elements. In this respect, photodiodes and phototransistors have the potential for greater stability for moderately sized sun sensors.

20.4 Validity Of Output Signal And Acquisition Range.

One problem experienced with sun-tracking servos is the tendency of the servo system to track the brightest point in the sky, be it the sun or otherwise. To prevent this, a simple expedient is to employ the fact that the sun is in general far brighter than other sources. If the intensity of the object being tracked is less than a certain value, then the error signal is gated to zero to prevent any unwanted response from the servo system.

With photosensitive elements suitably placed in the penumbra of a shadow bar, as in figure 20.5, that signal can be provided by the sum of the outputs from the two photosensitive elements. However with phototransistors, it is difficult to place them correctly, resulting either in the sum of the two signals peaking around alignment if the phototransistors are too far apart, or the sum dipping if they are too close together. To bypass this alignment problem one can dedicate one phototransistor to measuring the solar intensity by placing it fully exposed to the sun.

For large misalignments, the signal from the element exposed to the sun will decrease with increasing misalignment according to the cosin rule, until the signal is so low that the servo system cannot distinguish whether the signal is due to the sun at a large misalignment angle, or due to some less intense source overhead, such as the bright edge of a cloud. Thus an intensity is set below which the servo should take no action, and this defines the acquisition range. At the expense of additional elements, or the construction of specially lensed elements, the cosin law response could be avoided, and the sun's presence detected unambiguously at large misalignments.

It has been more usual to construct a feedback device with a shield around the device shown in Figure 20.5. This arrangement is shown in Figure 20.6, (Dibble and Nagaraja Rao, 1966).

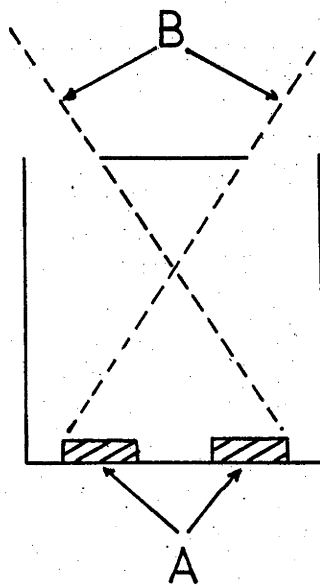


Figure 20.6 Acquisition range(B) of shielded device. The 'A's are the photosensitive elements.

In this case the detection of the sun at large misalignment angles is limited by the geometry of the device.

20.5 Construction

The precursor to the preferred design is by Carden(1978). His design employs a shadow disc, with three photosensitive elements equally spaced around the circular penumbra. Phototransistors are used, and the geometry is such that the photosensitive area is narrow compared to the penumbra. The disadvantage of this geometry is that firstly, the orthogonal components of the error signal are not obvious, and difficult to obtain except under certain conditions, and secondly, if this problem is overcome by using four phototransistors, then a problem still exists that signals produced at large angles of misalignment may be ambiguously interpreted. Hence a new geometric arrangement was sought which facilitated the use of the information provided by three sensing elements.

It was felt that drift could be cancelled by balancing a single photosensitive element in a penumbra, (one half of the arrangement in figure 20.5) against some fraction of the output signal from a photosensitive element that is fully exposed to the sun. Such a situation is reasonable provided that the output signal is proportional to some power of intensity. For the chosen photosensitive elements, BP X70 phototransistors, this was ostensibly the case (Phillips, 1974).

The sensor constructed is shown in figure 20.7, and consists of an aluminium T-piece, with a top cap.

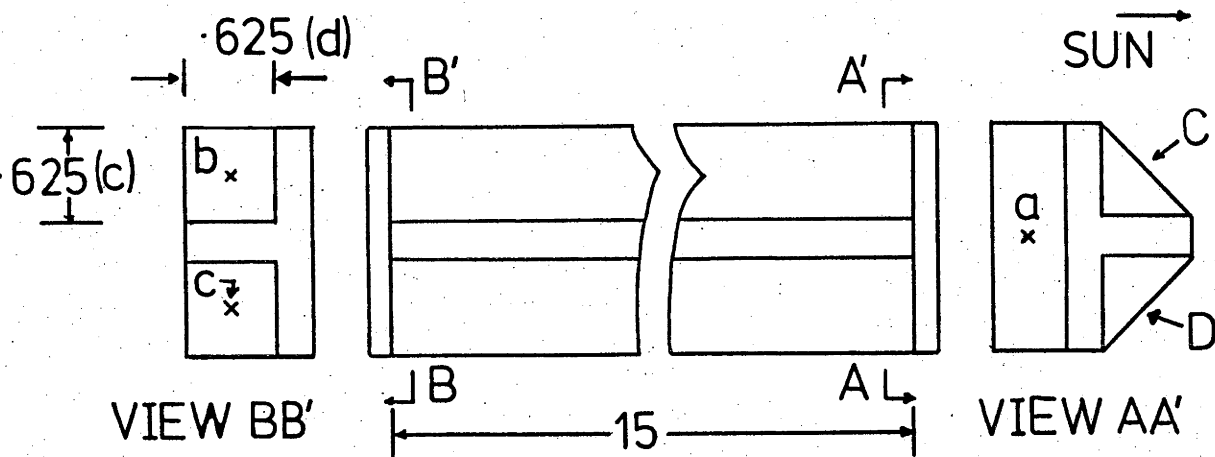


Figure 20.7 Plan of feedback device.
 a,b,c: positions of phototransistors. (c),(d),C,D: see text.
 Dimensions in inches.

The extrusion is milled so that dimensions c and d are equal, ensuring that the lines C and D across the edges of the T-piece are at right angles. The dimensions are chosen so that the width of the sensitive area of the phototransistors placed at (b) and (c) is narrower than the penumbra, and the width is about one-fifth that of the penumbra in the design. Extending the top cap produces a suitable position for the location at (a) of a third photosensitive element to detect the unhindered intensity of the sun.

The operation of the device is as follows. To each of the phototransistors the edges of the T-piece and the top cap divide the sky up into two regions, one of which is visible to

the phototransistor, and one of which is not. As an example, in the azimuth coordinate of an azimuth-elevation system, the plane dividing the two regions (defined by the edges of the T-piece and the top cap), would be vertical. If the sun is fully in the region which is visible to the phototransistor, a signal commensurate with the intensity of the sun will result. Conversely, if the sun is fully in the region not visible to the phototransistor, a signal commensurate with darkness will result. The results of the comparison of the signal from the phototransistor at (b) or (c) with a fraction of the signal from the phototransistor at (a) determine which way each actuator should move to align the equipment.

The photosensitive elements, in the current version, are BPX 70 phototransistors, chosen for their wide angle response. This response is effectively $\cos\theta$. These phototransistors are operated as shown in Fig 20.8, as under open base operation, when exposed to sunlight, collector current readily approaches the recommended maximum.

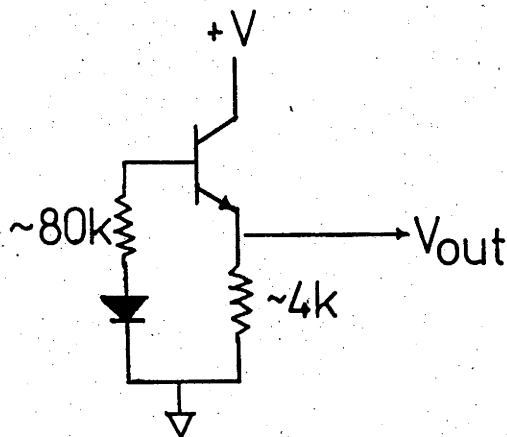


Figure 20.8 Phototransistor circuit.

The diode should yield some temperature stability.

This device is easily adapted to simple servo operation, with the photosensitive element (a) providing an intensity indication, and photosensitive elements (b) and (c), when combined with (a), giving signals related to alignment. The performance of the device at large misalignment angles could be improved by simply tilting sensors (b) and (c) outward, however this would be detrimental to the balancing of the response of (a) and (b), and (a) and (c).

The advantage of this device lies in its simple construction. The simple phototransistor used has an angle between half sensitivity directions of 120 degrees, which enables the sun to be detected unambiguously at sun following errors up to about 75 degrees. Also the alignment in the azimuth coordinate is detectable at large sun following errors in the elevation coordinate. Response of the device at small sun following errors in both coordinates, is identical to that in figure 20.4(d), with the width of the photosensitive element corresponding to 0.4 of the penumbra. Of course if one coordinate has a large sun following error, then at the sensing element in the other coordinate, the size of the penumbra is reduced and the response then corresponds to that of a relatively wide photosensitive element.

20.6 Performance Of Design

To test the above sensor a simple servo was constructed, as shown in figure 20.9.

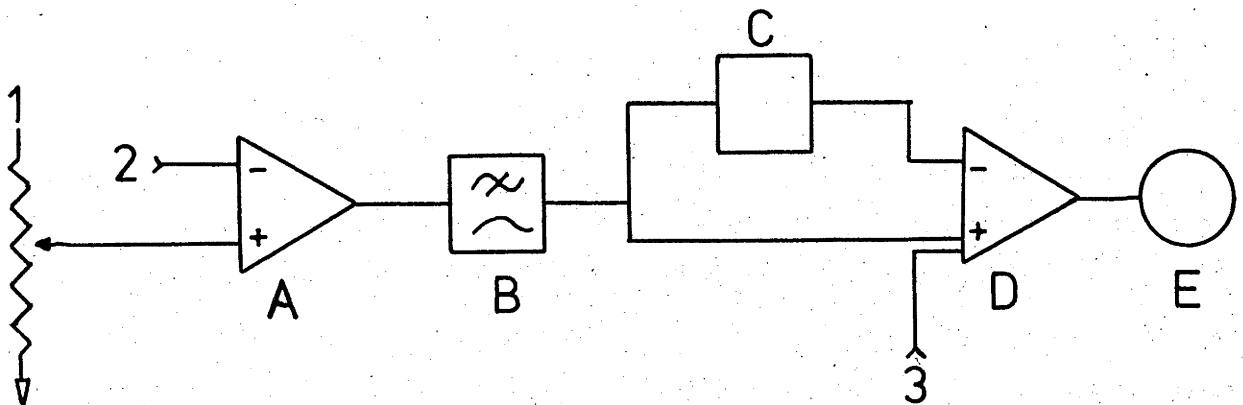


Figure 20.9 Block diagram of servo system.

- (1) Signal representing solar intensity,
- (2) Signal from phototransistor in penumbra,
- (3) Input to null velocity error.
- (A) Voltage amplifier, gain=60.
- (B) Low pass filter,
- (C) Differentiator,
- (D) Summing amplifier,
- (E) Motors.

With the overall voltage gain of sixty, the steady state error at a typical speed would be near $.2\text{mrad}$. The extra input (3) was operated manually to null the input error voltage and eliminate this velocity error, and the input error voltage could be monitored to achieve this null. The amplitude of the error voltage oscillations was near $.01$ volts peak to peak, which was due to the motors being operated near stall, and corresponded to angular error oscillations of 0.03 mrad. Thus the feedback device was aligned on a continuous basis.

To test the motion of the sun relative to the feedback device, and thus the feedback device stability, a long pinhole camera was constructed, and fixed relative to the feedback device.

The arrangement of the mount, sun sensor and pinhole camera is shown in figure 20.10.

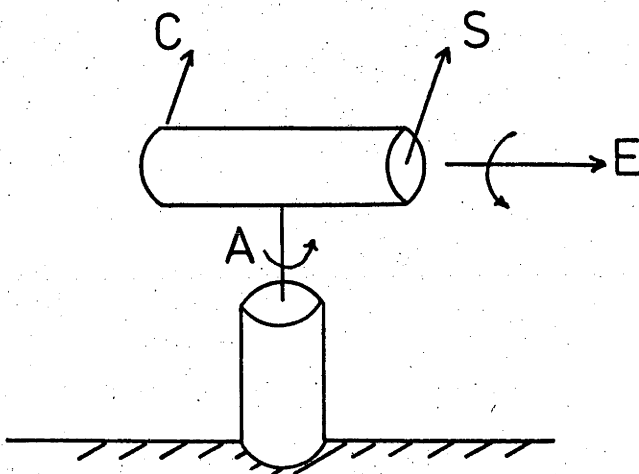


Figure 20.10 Arrangement of equipment on mount.
(C) pinhole camera, (S) sun sensor, (E) elevation axis, (A) azimuth axis.

The elevation axis has a mounting flange on both ends. The feedback device is mounted on one end, and the pinhole camera on the other.

The use of this mount raises one problem, that the misalignment signal in the elevation axis is affected by misalignment in the azimuth direction. This effect is fortunately small, and it can be shown that the maximum effect occurs for an elevation of 45degrees, when the false

misalignment error in elevation ($\Delta\theta$) produced by the misalignment in azimuth ($\Delta\phi$), is given to order $\Delta\phi^2$ by:

$$\Delta\theta = 0.25 (\Delta\phi)^2 \quad (20.2)$$

Thus for small $\Delta\phi$, even up to 30degrees, the effect of azimuth pointing error on the elevation misalignment signal is small.

The pinhole camera used is shown in figure 20.11. A 2.5in OD Aluminium tube is used to hold a .020in hole 75in away from a ground glass viewing screen.

The operation of the pinhole camera system to determine the relative position of the sun is as follows. The double axis micrometer assembly controls the position of a disc which is marginally smaller than the sun's image. The observer positions this disc so that the part of the sun's image which is visible is an annulus of even width. This annulus is thin, and the positioning process can be accomplished to some .005in. The position of the sun's image, relative to the tracking mount, can then be read off the the micrometer barrels. Thus the pinhole camera, with the micrometer assembly, can detect a relative motion of the sun's image of less than .1mrad. Deflections of the tube due to its weight are important, and deflections of the tube affected measurements of the sun's position by some .5mrad between the horizontal and vertical positions of the camera. These deflections are solely a function of the cosin of elevation, and affect the elevation axis only.

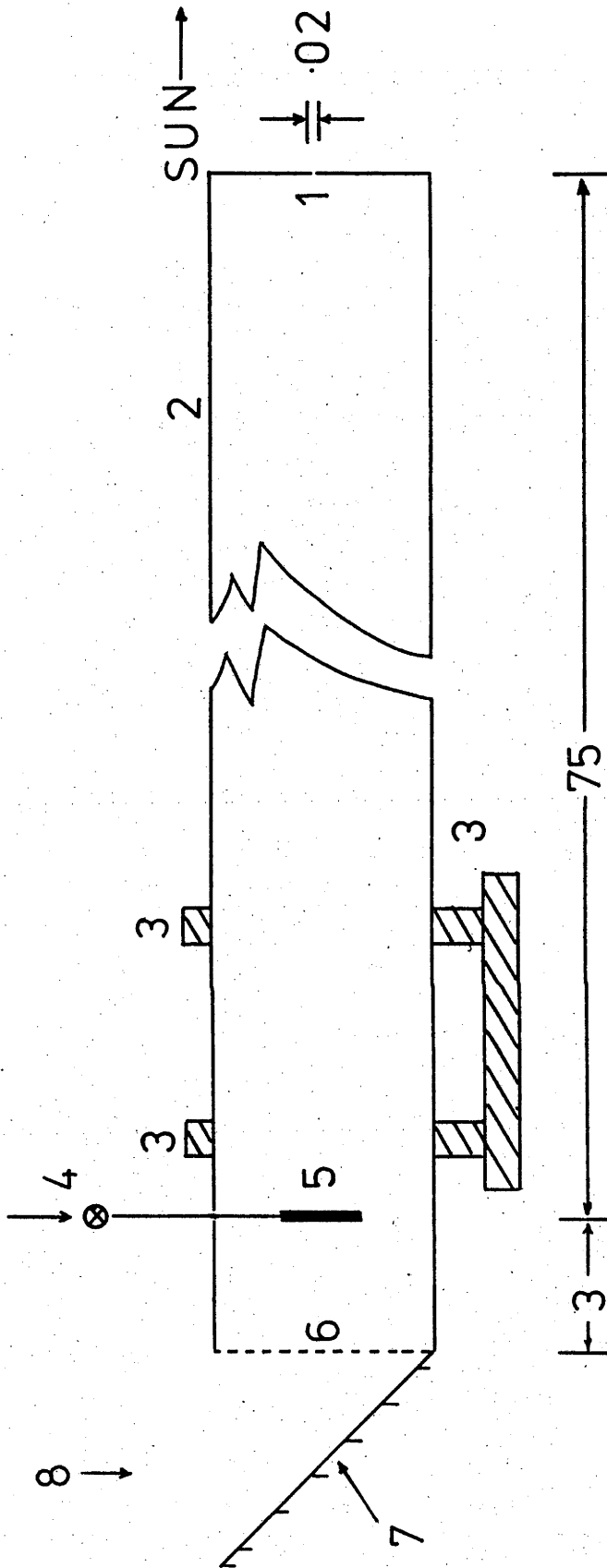


Figure 20.11 Pinhole camera schematic, Dimensions in inches.

(1) pinhole, (2) Al tube, 2.5in OD, (3) Mounting webs, (4) 2 axis micrometer positioning system, (5) Occulting disc, (6) ground glass screen, (7) mirror, (8) viewing direction.

20.7 Stability Of Sun Sensor.

The results of a days monitoring are shown in figure 20.12.

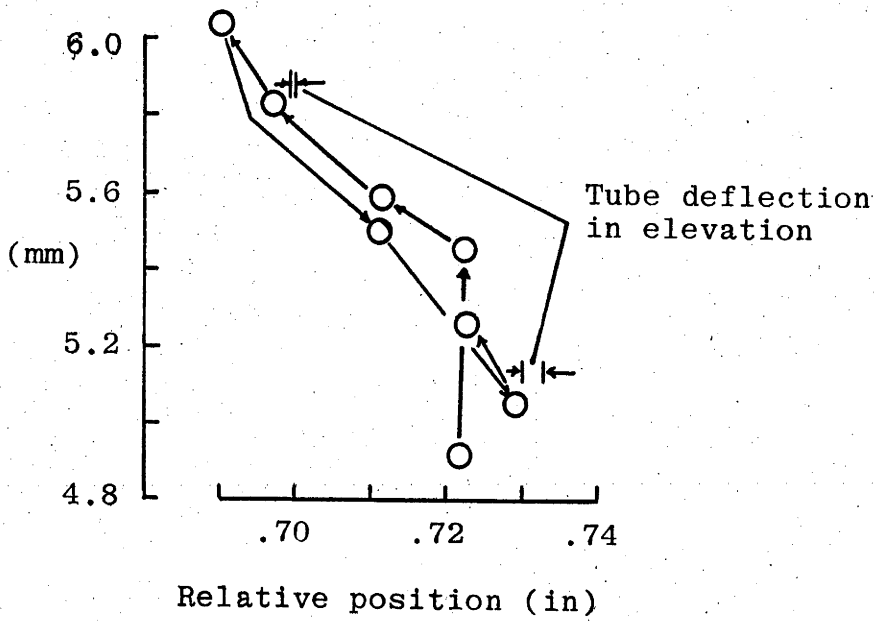


Figure 20.12 Relative motion of sun's image over a days sun following. Note one axis is in mm, and one axis is in inches.

1.9mm, or .075in is equivalent to 1mrad.

The magnitude of the corrections required to allow for the deflection of the tube are indicated. The loop of the graph is the relative position of the sun's image, with the bottom right hand corner being both the start and finish of the test, at around 30 degrees elevation, and the top left hand corner of the loop being the middle of the test at 70 degrees elevation, around midday. Both axes suffer a similar lack of stability of around .5mrad between elevations 30 and 70 degrees. Clearly the sun sensor suffers from a balancing

problem, and stability has been compromised.

20.8 Discussion

A series of tests were made using both stacks of neutral density filters, and also a penumbra to vary intensity, and in both cases the output signal appeared to be a power of intensity. The resolution of the problem may lie in the fact that the phototransistor in the totally exposed position collects more diffuse radiation than the phototransistor in the penumbra, and this may be the crucial lack of balance. If this is the case, then a shield will be necessary as even the arrangement of 20.5 suffers lack of balance in this respect if the elevation axis is considered near the horizon. This will unfortunately reduce the acquisition range, however, this is less important than stability. It is recommended that future sensors are symmetrical, i.e. with photosensitive elements on both sides of a shadow bar, at least as in figure 20.5. The installation of a shield would also be appropriate.

20.9 Conclusion

More tests are required to ascertain whether diffuse radiation is the problem, and the experimental setup described is ideal for the task. A removable shield could be used to alter the amount of diffuse radiation received by each photosensitive element, and the movement of the aligned position monitored. This test could be repeated on both sunny

and cloudy days to measure the sensitivity of the device to different amounts of diffuse radiation.

20.10 Acknowledgements.

I am indebted to the master, Bob Whelan, for transforming the idea of the pinhole camera into an operational concern. His manifestation of the idea exceeded the original specifications, thanks to his incorporation of the micrometer assembly.

20.11 References

Carden, P.O.(1978) 'Steering a field of mirrors using a shared computer based controller' Solar Energy 20, pp343-355.

Moore, J G and Amand, P St, 'A guidance system for a solar furnace', Solar Energy 1, 4, pp27-29, 1957.

Dibble, D and Nagaraja Rao, C R, (1966), 'An inexpensive solar pointing control', J. Scient. Instrum. 43,588.

Phillips Data Handbook (1974), 'Semiconductor and Integrated Circuits' Part 4b, December.

Robinson, N. (Ed), (1966) 'Solar Radiation' Elsevier, New York.

20.12 Bibliography

Badinov, I Ya, 'A three stage photoelectric transistor tracking system', Planetary and Space Science, 11, pp971-982, 1963.

Clark, H L, 'Sun follower for V-2 rockets', Electronics, Oct 1950, pp71-73.

Egorov, A V, et al, 'Sensors in the automatic control system of a solar power installation', Geliotekhnika, 4, 4, pp7-10, 1968.

Gliberman, A Ya and Burmistrova, L V, 'Use of silicon photocells in solar orientation sensors', Geliotekhnika, 9, 3, pp7-15, 1973.

Harihan, T A, 'Simple sun follower assembly', Rev Sci Instrum, 37, pp1078-1080, 1966.

Laszlo, T S et al, 'A guiding system for solar furnaces' Solar Energy 2, 1, pp18-20, 1958.

Schweiger, R N, and Laszlo, T S, 'A simple guidance system for solar furnaces', Solar Energy 11, 2, pp85-86, 1967.

Simonyants, A A, et al, 'Design of a tracking system for a solar-energy installation', Geliotekhnika, 12, 1, pp22-26, 1976.

Sumner, C J and Patterson G, 'A sun tracking radiation instrument stand', Solar Energy 12, pp537-542, 1969.

Note: I am certain the claims made for the control accuracy of this instrument in the hourangle coordinate do not match the operational accuracy, due to a design deficiency related to the non-balance of the hourangle sensor.

Vasil'ev, I G, and Shapov, A I, Planetary and Space Science, 11, pp93-98, 1963.

APPENDIX G

AERODYNAMIC DAMPING COEFFICIENT OF COLLECTOR

The damping of the collector is likely to be dominated by aerodynamic damping, as the collector is a large, relatively light structure. Structural damping of a completely welded structure is small. Here we calculate an approximation for the aerodynamic damping by modelling the collector as a plate, of area A , and mass M , over which the wind velocity (\bar{V}) is constant. The wind force on the plate is given by:

$$F = \frac{1}{2} \rho C_D A (\bar{V} + \dot{x})^2$$

where \dot{x} is the velocity of the plate.

To first order, the time varying component of the drag force is:

$$F' = \rho C_D A \bar{V} \dot{x}$$

Using the general equation for damped oscillations, viz:

$$M\ddot{x} + 2 \zeta f M \dot{x} + M f^2 x = 0$$

where ζ is the damping coefficient and f the natural frequency, in rads/sec, we have:

$$\zeta = \frac{1 \rho C_D A \bar{V}}{4 \pi f M}$$

where f is the natural frequency in Hz.

For a notional aperture of 10 square metres, the mass of the mirror is estimated at 180kg. Thus for $C_D = 1$, $\rho = 1.2\text{kg/m}^3$, and $\bar{V}=5\text{m/s}$,

$$\zeta = .026/f$$

At lower wind velocities the damping will be correspondingly lower.

APPENDIX H

A SUN FOLLOWING SCHEME:

OPERATION OF THE CARDEN/McMURTRIE/WHYTE LEGACY

B. P. EDWARDS

JULY 1977

Energy Conversion Technical Report No. 14

Energy Conversion Group
Department of Engineering Physics

Initial feelings (Carden, 1978a) were that following the sun using real time information on the sun following error would be accomplished by a servo loop which relied upon the intelligence of the central control rather than that at the local control. The central control would control all collectors by time multiplexing itself. In this report the aspects of time multiplexing are not considered, only the aspects related to the control of one collector are considered. Local control intelligence would be limited to obedience to positional change requests and to sun sensor information transmission. For full information on the proposed scheme, the reader is referred to Carden(1978a).

14.1 Operation Of Tracking Servo: General.

The operating procedure of the servo loop was as follows. The central control would interrogate the sun sensor of a particular collector at discrete times, evenly spaced, and, after a fixed number of interrogations, would analyse the accrued sun sensor data for information on the position of the sun, and adjust the speed of the actuators appropriately. The interval between the actuator speed adjustments is maintained constant, and called the command interval(t_c). The length of the command interval determines the time the central control can dedicate to each calculation of the speed commands for each collector. It was anticipated that this time would be of the order of 100's of seconds. The events within the control loop are shown in figure 14.1.

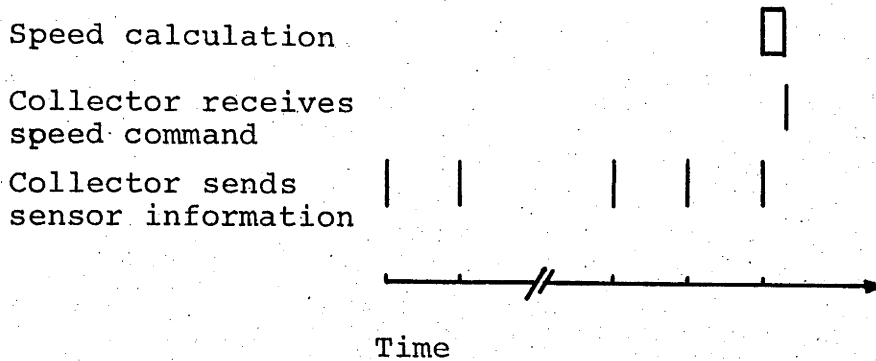


Figure 14.1 Time sequence of communication, sun sensor data gathering, motor speed calculation and motor speed command transmission with reference to one mirror only.

14.2 Particulars Of The System.

To transfer the sun sensor information from each collector to the central control, and to transfer motor speed commands to the collectors, the values are transmitted in binary. It is assumed that the sun sensor is of the type suggested by Carden(1978a), where the error signal is related to the error as shown in figure 14.2. Binary transmission of the error transforms the ramp into a staircase, and the maximum possible error in the transmitted data is given by:

$$\Delta\theta = \frac{1}{2} \Omega / 2^{n_s} \quad (14.1)$$

where Ω is the solar diameter.

n_s is the number of bits in the binary representation.

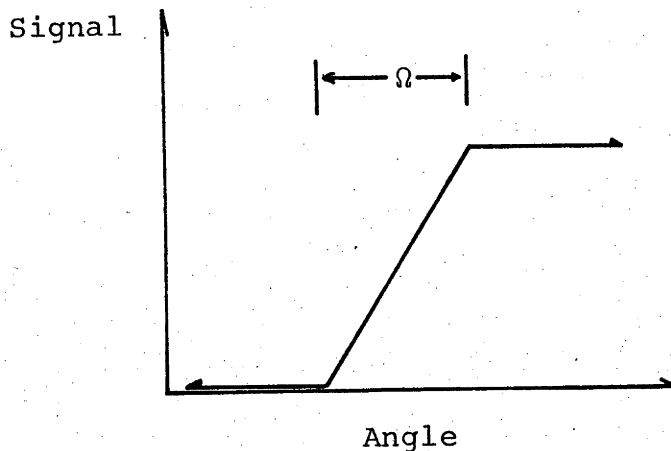


Figure 14.2 Response of sun sensor.
 Ω is the sun's angular diameter.

The local control has sufficient intelligence to maintain the requested actuator speed precisely, without accumulating errors. Thus after a time t_c with speed command ω , the position of the actuator will have changed by precisely ωt_c units. Because of this behaviour the central control can maintain awareness of the actuator position by integrating the speed commands.

14.3 Operation Of The Servo: Detail.

For energy collection purposes it is desired that the sun following error oscillates around zero. Thus the actuator position will slightly overshoot the position of the sun at the end of each command interval, and the sun following will proceed in a zig-zag fashion, as shown for one axis in figure 14.3. Also shown in figure 14.3 is another expected characteristic of this tracking system, that initially the overshoot will be large, and then die away to a small value.

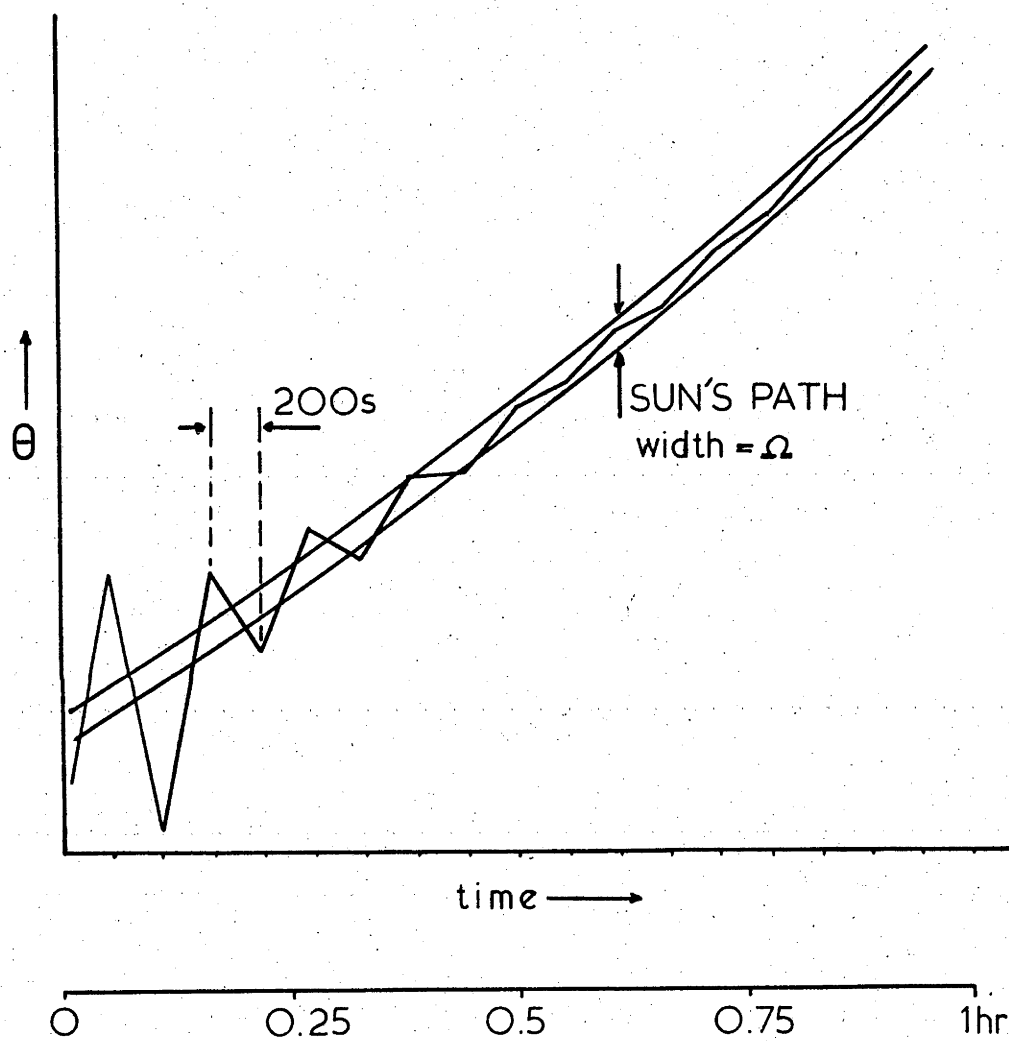


Figure 14.3 Simulated performance of computer controlled sun follower.

Both axes operate identically, and the discussion which follows refers to the operation of one of the axes.

On each occasion when the sun's position can be inferred from the sun sensor data, the position is recorded. After a period of tracking, the position of the sun will be known at a series of instants. This information on the sun's position is extrapolated to predict the future position of the sun, and actuator speeds are calculated to ensure an overshoot of the sun's position.

The combination of the past history of the sun's position and the current sensor information to provide appropriate actuator speeds presents many possibilities. The servo system being operated here is of course identical to that of section 5.7 of my thesis, and the use of the current sensor information corresponds to DC gain, while the use of past history information corresponds to integral gain. To produce low oscillation amplitudes, the DC gain must be low.

There are thus three processes involved. Firstly the sun sensor data must be analysed for information on the sun's position, program SUNFIX. Secondly, the information on the sun's position must be analysed to predict the position of the sun at future time, (program PRDICT), and thirdly, an appropriate overshoot must be calculated. This overshoot will be large if the past history is sparse, and small if the past history is well known. The combination of the current estimated relative position, the estimated future position of the sun, and the overshoot gives the command speed for the next interval.

If the past history information on the sun's position is exceedingly poor, then no curve fit can be attempted, and only the current time sun sensor information can be used, viz DC gain.

A flowchart of the operations is shown in figure 14.4.

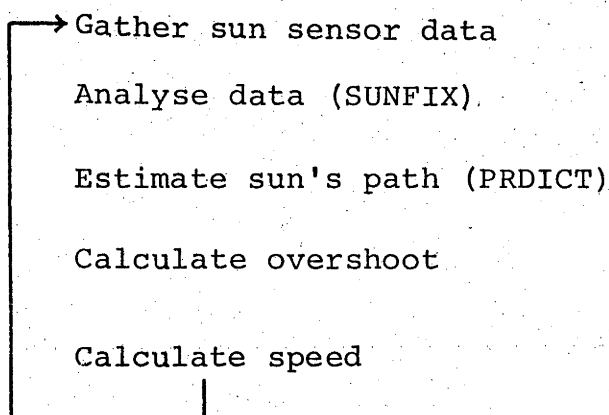


Figure 14.4 Flowchart of servo operation. Names in brackets are the names of the respective programs which perform the functions.

14.4 Procedure SUNFIX.

The time when information on the sun's position can be obtained is called a fix time. The position of the sun at that time is called the fix position. In general the event is called a fix. The nature of the sun sensor gives rise to two types of fixes, 'slow', and 'fast' fixes, so called because they occur when the collector position crosses the sun's position either slowly, or quickly.

(a) 'fast' fixes.

Typical sun sensor data for a fast fix, where the data for maximum negative and positive error is 0 and 7 respectively, would be:

Data sample number	0	1	2	3	4	5
Sun sensor data	0	0	7	7	7	7

The information from this on the sun's position is restricted to knowing that at some time between samples 1 and 2 the sun's position coincided with that of the collector. In the case of this information, the position of the sun at the midpoint in time between samples 1 and 2, is estimated to be that of the collector at that time. The maximum possible error in this estimation is given by the product of half the time between samples and the relative speed of the collector and the sun. For fast fixes this relative speed is usually high, and so we estimate the maximum possible error by:

$$\Delta\theta_f = \omega_m t_s / 2 \quad (14.2)$$

where ω_m is the maximum speed of the collector, and t_s is the interval between sun sensor data samples.

(b) 'slow' fix.

A typical set of sun sensor data received in this case would be:

Sample number	0	1	2	3	4
Sun sensor data	0	0	5	7	7

At sample 2, the sun's relative position is determinable, and the error in the estimation of the sun's position is the maximum possible error in the sun sensor information, which is given by:

$$\Delta\theta_s = 1/2 \quad \Omega/2^s \quad (14.3)$$

This calculation of the sun's position was found to be sometimes in error. The source of this error was traced to thin high cloud, which increased the apparent diameter of the sun, altering the slope of the sun sensor response curve in figure 14.2. Thus fixes of the above form were treated as fast fixes, where the only information gleaned is that a fix occurs between samples 1 and 2.

A slow fix was only recorded if samples were of the form:

Sample number	0	1	2	3	4
Sun sensor data	0	1	4	7	7

where the fix position can be interpolated between samples 1 and 2. Such a procedure is independent of the slope of the sun sensor response, though the slope must be constant with time, and the possible error in the fix, which is identical to

that given above, is affected.

14.5 Program PRDICT.

The past history of the sun's position was fitted to a curve, using least squares methods to minimise the effect of errors in the past history. The type of curve used under various conditions is itemised in the next section. The position of the sun is estimated at both the current time and the current time plus t_c seconds.

14.5.1 Curve Fitting To Past History. -

(a) Two or less fixes - No curve fit, no prediction of the sun's position. The extrapolation errors in a linear fit to two inexact points can be large.

(b) 3 fixes. Linear least squares fit provided that the last command interval contained a fix.

(c) 4 or more fixes. Parabolic least squares fit provided that the last fix occurred more recently than three command intervals previous to current time. No more than 10 of the previous fixes were used in this fit.

14.5.2 Overshoot Program. -

In general overshoot was calculated to be one third of the current estimated relative position, though it was never allowed less than a particular quantity which was a user defined variable. In later diagrams this variable was 4mrad. If the sun's path was not crossed in the previous interval, indicating some source of error in the prediction process, the overshoot was increased by a factor of 10.

It is possible to use the errors in the fixes, and the times of the fixes, to estimate statistically the possible errors in the predicted position of the sun. The calculation of this possible error is given in standard texts, eg Draper and Smith(1968), however, the computation is complex, and the author felt the simple rules above more than adequate.

14.6 Simulation Tests.

The results of a simulation program embodying the above principles have already been given in figure 14.3.

14.7 Hardware Used In Experiments.

A diagram of the hardware used is given in figure 14.5.

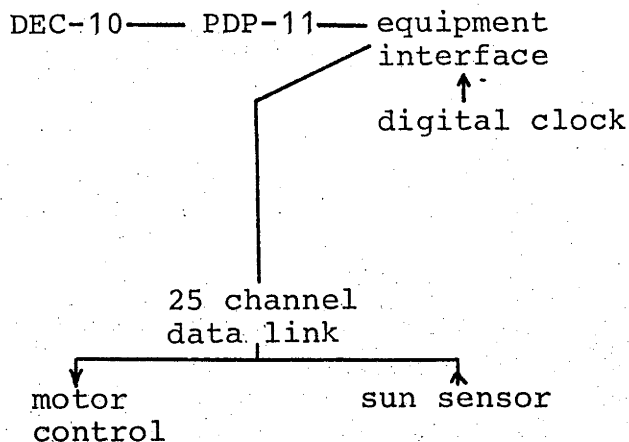


Figure 14.5 Hardware used in servo implementation. The DEC-10 machine is the item directly controlled by the programs, and as such is analogous to the central control.

A DEC-10 machine performed all the calculations, and the PDP-11 served solely as an interface.

The interface has been described (McMurtrie, 1974b), and was modified by the author to include buffers for the digital clock information.

The digital clock, a Systron Donner, was synchronised with the telephone time service, and the oscillator in the clock was adjusted by comparison with VNG radio.

The 25 channel data link (McMurtrie, 1974b), proved to be unreliable and was modified to make it truly differential, in contrast to its original construction. Further, protection boxes with fuses and interference suppressors were incorporated to reduce damage from electrical interference.

The analogue to digital conversion and transmission of information has been described by McMurtrie (1974a). The frequency response of this unit was modified to reduce its

susceptibility to noise. Further problems were encountered due to zero output being recorded if the input voltage was high.

The actuator control boxes (McMurtrie, 1974b) were notoriously unreliable, and the mean time between failures was estimated by the author to be of the order of hours. In addition, continuous 'tuning' of the boxes was necessary. The inability of the units to recover from a stalled motor resulted in loss of positional information for the central control. Stability had to be further sacrificed by modifications to prevent stalling.

14.8 Results.

Despite these problems, the system was run successfully for short periods, and a typical run yielded results as shown for one of the two axes in figure 14.6. In this diagram the command time was 200 seconds, and ten sensor samples were taken between each speed adjustment. Successful operation shows that there are no problems in implementing this scheme.

14.9 Discussion.

There are two features of the above system. Firstly, the intelligence required at each collector is small, being restricted to obedience to motor speed commands and response to requests for sun sensor information.

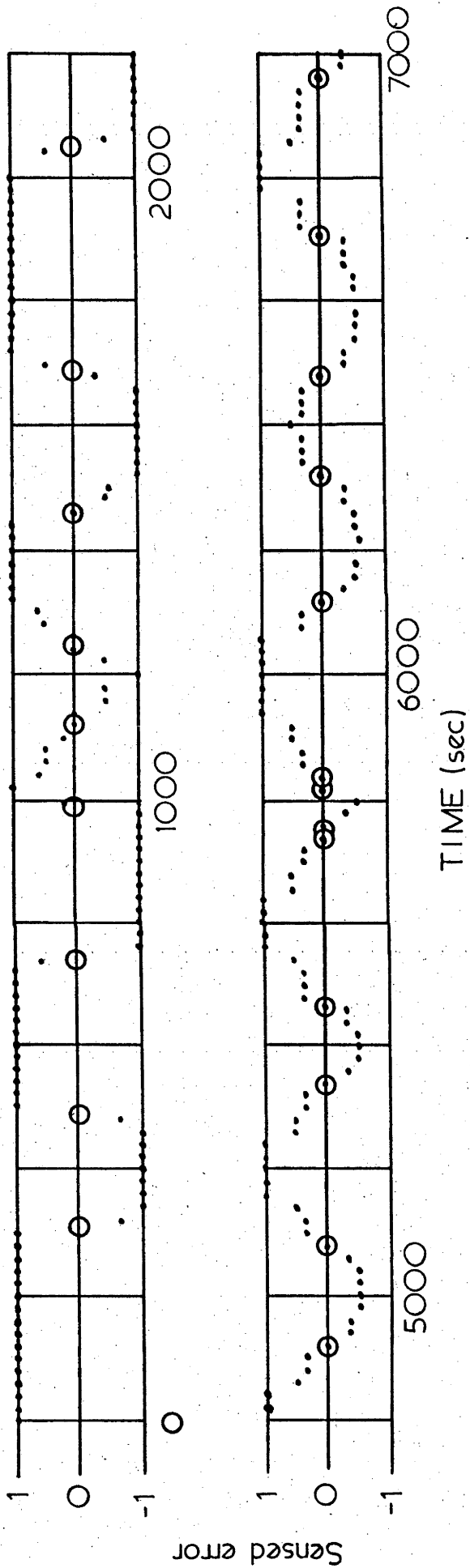


Figure 14.6 Performance under computer control. The graphs are azimuth pointing error vs time. The errors are presented as points representing the sampled responses of the sun sensor, and therefore the ordinate must be interpreted in conjunction with figure 14.2. The vertical bars are the instants at which the motor speed was changed, at intervals of 200seconds. The upper graph shows the performance at and immediately following the first crossing of the sun. The lower graph begins 4800secs after the beginning of the upper graph and shows the final stable performance. The calculated fix points are circled. The minimum overshoot in this case was 4mrad.

Secondly, the central station has continuous awareness of the position of the collector. These features require the central computer to perform a large number of calculations which mimic the action of a sun following servo, involve a reasonable load on the data link (see Edwards, 1978a), and result in a relatively long response time, with accurate tracking not achieved until 3-5 command intervals after the first crossing of the sun. A simpler way to achieve these features is to provide the intelligence for the tracking servo at the local control, and to interrogate the local control when the central control desires awareness of collector position. In chapter 5 of the thesis it is shown that the achievement of both these features is not a difficult proposition with microprocessors at each local control. Such a scheme minimises response time, reduces the calculation capacity of the central machine, reduces the load on the data link, all with negligible cost increase. This solution seems preferable, particularly in the light of the calculations in chapter five on wind gust deflections, where it is shown that low bandwidth control loops, such as the one above, require higher rigidity collectors than higher bandwidth control.

14.10 REFERENCES

Carden P O(1978a), 'Steering a field of mirrors using a shared computer based controller', Solar Energy 20, pp343-355.

Edwards B P(197X), Ph D thesis, Dept of Engineering Physics.

McMurtrie R L (1974a), 'Solar Interface Mk 1', En-Con Technical Report No 5.

McMurtrie R L (1974b), 'Analogue to digital Conversion of sun sensor data from a sun tracking device', En-Con Technical Report No 6.

Draper N R and Smith H, 'Applied Regression Analysis', Wiley.(1968)